

ELUCIDATING THE IMPACT OF PYRUVATE KINASE ON CYSTINE METABOLISM  
AND FERROPTOSIS IN PANCREATIC CANCER

By

Elliot Michael Ensink

A DISSERTATION

Submitted to  
Michigan State University  
in partial fulfillment of the requirements  
for the degree of

Genetics – Doctor of Philosophy

2023

## ABSTRACT

Pancreatic ductal adenocarcinoma (PDAC) is an aggressive cancer with high mortality and limited efficacious therapeutic options. PDAC cells undergo metabolic alterations to survive within a nutrient-depleted tumor microenvironment. One critical metabolic shift in PDAC cells occurs through altered isoform expression of the glycolytic enzyme, pyruvate kinase (PK). Pancreatic cancer cells preferentially switch from the constitutively active pyruvate kinase muscle 1 isoform (PKM1) to the allosterically regulated pyruvate kinase muscle isoform 2 isoform (PKM2). Overexpression of PKM2 in PDAC produces a profound reprogramming of many metabolic pathways including glucose and glutamine metabolism, but little is known about the impact on cysteine metabolism. Cysteine metabolism is critical for supporting survival through its role in defense against ferroptosis, a non-apoptotic iron-dependent form of cell death characterized by unchecked lipid peroxidation. Exploiting this cell death mechanism has enormous potential for treating PDAC cells that are vulnerable to cystine starvation.

To improve our understanding of the metabolic adaptations that cancer cells depend on for survival and proliferation, we generated PKM2 knockout (KO) human PDAC cells. We evaluated PKM2KO cell tolerance of low cystine environments, sensitivity to compounds known to induce ferroptosis, and expression of ferroptosis related proteins. Fascinatingly, PKM2KO cells demonstrate a remarkable resistance to cystine starvation mediated ferroptosis. This response to cystine starvation was found to be caused by decreased PK activity, rather than an isoform specific effect. We further utilized stable isotope tracing to evaluate the impact of glucose and glutamine reprogramming in PKM2KO cells. PKM2KO cells demonstrate a dependence on

glutamine metabolism to support antioxidant defenses against lipid peroxidation. This is attributed primarily to increased glutamine flux through the malate aspartate shuttle and utilization of ME1 to produce NADPH. Lastly, we found that ferroptosis could be synergistically induced by the combination of PKM2 activation with TEPP-46 and cystine starvation with imidazole ketone erastin (IKE) *in vitro*. Preliminary investigations *in vivo* show strong potential for this drug combination as a novel and effective therapy for PDAC.

This work is dedicated to my wife Andrea  
Ensink. Without her elegance, grace, and  
faithful love and support this work would not  
have been possible.

## ACKNOWLEDGEMENTS

### Lunt Lab

I am enormously grateful to my mentor Dr. Sophia Lunt who took me on as a student back in 2016. As a dual degree student, I have many other responsibilities in medical school and clinical rotations outside of the lab and I am thankful for her patience over the years and consistent guidance and support. I am especially grateful for her willingness to allow me to explore new ideas independently while also challenging my ideas and keeping me on the right track. Thanks to the former members of the Lunt lab, Dr. Shao Thing Teoh, Dr. Marty Ogrodzinski, Dr. Deanna Broadwater, Dr. Lei Yu, Galloway Thurston, Anmol Pardal, and Che Yang, who helped my progress early on in graduate studies. A special thank you to Shao and Marty for their work in developing the metabolomics methodology described in Chapter 4 and for equipping me with the skills to work independently and improve our techniques. Additional thanks to Shao for bringing me into his board gaming group. I must thank Lei for her work on pyruvate kinase that laid the foundation for my own project. Thank you to Galloway Thurston and Anmol Pardal for taking time away from medical school to engage in research and assist in my projects. I must also thank the current Lunt lab members: Dr. Hyllana Medeiros, Tessa Jordan, and Amir Roshanzadeh. Hyllana is instrumental in caring for the animals we use in the lab, and I would not have been able to do my *in vivo* experiments without her. A special thank you to Tessa for eagerly contributing to the work described in this thesis, and for continuing on the project after me.

### Guidance Committee

I would like to thank my guidance committee members, Dr. Bill Henry, Dr. Hua

Xiao, and Dr. Karen Liby. I greatly appreciate the time and effort you have invested in evaluating my work and progress over the years. Each one of you brought a unique perspective and your questions and insights have stayed with me as I developed this project and will continue to shape my scientific progress going forward.

### **Biochemistry Personnel**

I am very thankful for the support staff within the Biochemistry building. The staff of the biochemistry store, Deanna Ely, Nichole Daly, and others who were always helpful in acquiring the reagents and supplies we needed. Thank you to Mary Thompson for her work ensuring our product orders arrive smoothly. Thank you to Leslie Thompson for organizing events and helping me when I locked myself out of the lab. Thank you to Ron Dunn who persistently worked to stop the ceiling from dumping water into our lab when others had shrugged it off. Lastly an enormous thank you to Kaillathe Padmanabhan (Pappan). Pappan always warmly and genuinely greeted me with kindness. Pappan taught me the value of stopping what I was doing for a moment and just appreciating a brief moment of human connection. Pappan also rescued data I thought was lost on a corrupted flash drive and helped with many other technical difficulties.

### **Genetics and Genome Sciences Personnel**

I would also like to thank the genetics and genome sciences program personnel. Thank you to Dr. Cathy Ernst and Claire Vielle for directing the program and a special thank you to Alaina Burghardt for coordinating the many administrative questions that have come up throughout the course of my training.

### **DO/PhD Program Personnel**

I am thankful for the DO/PhD program administration and students. The dual

degree program is a long marathon and each of you has helped make it feel like a large family. In particular I would like to thank Dr. Justin McCormick and Bethany Heinlen for bringing me into the program and administering it in the first years of my training. I would also like to thank Dr. Brian Schutte for taking on the role of director and taking the time to invest in mentoring me through my training. A huge thank you to Michelle Volker for tirelessly caring for the students, planning events, and answering so many questions over the years.

### **Collaborators and Supporters**

Over the course of my training, I have had the opportunity to collaborate with many researchers and clinicians including Dr. Dan Isaac, Dr. Neal Hammer, Dr. Nils Halberg, Dr. Jamie Bernard, and Dr. Yibin Deng. I am especially thankful to Dr. Dan Isaac for bringing a clinical and translational perspective to my projects, giving me clinical enrichment experiences in his practice, and for helping us expand our cancer metabolism research into prostate cancer models. I am also thankful for Dr. Eran Andrechek and Dr. Kathleen Gallo for consistently running the Cancer Research Network seminar series, stimulating discussion among the students and faculty, and striving to connect researchers with local clinicians to improve the translational aspect of our work. Thank you to Mass Spectrometry Core facility, specifically: Tony Schillmiller, Lijun Chen, and Dan Jones for your patient training and helpful guidance for my metabolomics experiments. Thank you to the vet staff and administrative staff of the campus animal resources team. Thank you to Dr. Arjun Krishnana for giving me an appreciation for statistics and how to use them properly unlike anyone else before. Thank you to BioRender.com for enabling beautiful figure creation tools. Thank you to VectorBuilder

for saving me weeks of cloning time. Lastly, I must thank the Aitch Foundation and in particular Lauren Aitch who funded my research for a year and is committed to supporting young investigators trying to make a difference in cancer patient outcomes.

### **Friends and family**

Finally, I want to express a heartfelt gratitude for the love and support my family has given me over the years. First, I must thank my wife Andrea Ensink to whom this thesis is dedicated. Pursuing the career of a physician scientist requires enormous time commitment and sacrifice. Thank you to Andrea who has borne that sacrifice and gracefully stood by my side despite many long hours away from home. I cannot emphasize enough how important her role is in my daily functioning and ability to carry on this work. Thank you also to my baby boy Russell who was born in the midst of my graduate studies; you have been a radiant beam of joy in the midst of many dark days. Next, I have deep gratitude for my parents Bob and Karen Ensink. You have shown such love and dedication to me over the years in a way that can never be truly repaid. You fed my appetite for science and learning from a very early age and consistently provided support and resources to help me along this path. Thank you also to my sister Elizabeth Ensink who has provided me with excellent advice and camaraderie over the years. Thank you to my grandparents, especially John Buiters, who always supported me and was an inspirational source to always ask questions and engage in learning. I am also thankful for the support of my father and mother-in-law Dan and Carol Monsma, brothers-in-law Austin VanPutten, Joe Monsma and Justin Hiemstra, and sisters-in-law, Natalie Hiemstra, Lydia Monsma, and Madelyn Monsma. I am also thankful to many mentors I have had in my personal life: Pastor Haak, Pastor Kleyn, Pastor Langerak, Pastor Griess,

Pastor Kortus, Dr. Brian Haab, Dr. Nate Lanning, and Dr. Brendan Looyenga. Each of you helped shape who I am today and kept me on the right path. I would also like to thank my close circle of friends who have been my closest companions since my youth. In particular I would like to thank Alex Poortinga, Chad Rutgers, Erik Moelker, and Solomon Bosman. Each of you has been closer than a brother to me and have provided me with a breath of fresh air outside of academia.

In conclusion, I would like to express my sincere gratitude for the opportunity and privilege to engage in cancer research and clinical training. There are many others who have helped me along the way in this journey who are not named here, yet each one of you has helped in small ways and large to contribute to my progress.

## TABLE OF CONTENTS

LIST OF ABBREVIATIONS .....	xii
CHAPTER 1: INTRODUCTION - THE METABOLISM OF PANCREATIC CANCER AND IMPLICATIONS FOR TARGETED THERAPY .....	1
Pancreatic Cancer .....	1
Cancer Metabolism and Implications for PDAC.....	5
Metabolic Mechanisms of Ferroptosis and Implications for PDAC .....	13
Clinical Applications of Targeted Metabolic Therapies in PDAC .....	24
The Role of Pyruvate Kinase in PDAC Metabolism.....	27
CHAPTER 2: CYSTEINE CATABOLISM AND THE SERINE BIOSYNTHESIS PATHWAY SUPPORT PYRUVATE PRODUCTION DURING PYRUVATE KINASE KNOCKDOWN IN PANCREATIC CANCER CELLS .....	34
Preface.....	34
Introduction.....	34
Results .....	37
Discussion.....	48
Conclusions.....	52
Acknowledgements .....	52
Author Contributions.....	53
Materials and Methods .....	53
CHAPTER 3: PYRUVATE KINASE ACTIVITY REGULATES CYSTINE STARVATION INDUCED FERROPTOSIS THROUGH MALIC ENZYME 1 IN PANCREATIC CANCER CELLS.....	58
Preface.....	58
Abstract.....	58
Introduction.....	59
Results .....	61
Discussion.....	91
Methods .....	97
CHAPTER 4: MEASURING THE NUTRIENT METABOLISM OF ADHERENT CELLS IN CULTURE .....	109
Preface.....	109
Introduction.....	109
Materials.....	113
Methods .....	115
CHAPTER 5: APPLICATIONS OF METABOLOMICS TECHNIQUES AND CONTRIBUTIONS TO SCIENCE.....	135
Preface.....	135
Tryptophan Metabolism in the Malignant Transformation of Mammary Epithelial Cells .....	135
Quantification of glutamate released by <i>S. aureus</i> Ggt from reduced and oxidized glutathione.....	139
Other co-authored papers: .....	143

CHAPTER 6: CONCLUSIONS AND FUTURE DIRECTIONS .....	144
Conclusions.....	144
Future Directions.....	145
REFERENCES.....	152
APPENDIX A: SUPPLEMENTARY DATA IN SUPPORT OF CHAPTER 2.....	176
APPENDIX B: SUPPLEMENTARY DATA IN SUPPORT OF CHAPTER 3.....	189

## LIST OF ABBREVIATIONS

μl – Microliter

μm – Micrometer

μM – Micromolar

μmol – Micromole

2/3-PG – 2/3-Phosphoglycerate

3-NPH – 3-Nitrophenylhydrazine

5-FU – 5-fluorouracil

6MP – 6-mercaptopurine

AA – Arachidonic acid

ALOX – Arachidonic lipoyxygenase

Arg – Arginine

ASCL4 – Acyl-CoA synthetase long-chain family member 4

ATP – Adenosine triphosphate

BH4 – Tetrahydrobiopterin

BHT – Butylated hydroxytoluene

BRCA1 – Breast cancer gene 1

BRCA2 – Breast cancer gene 2

BSO – Buthionine sulfoximine

CA – Cancer antigen

Cas9 – Caspase 9

CD – Cluster of differentiation

CDKN2A – Cyclin dependent kinase inhibitor 2A

CI – Complex I  
CIII – Complex III  
CoA – Coenzyme A  
CoQ10 – Coenzyme Q10  
CRISPR – Clustered regularly interspaced short palindromic repeats  
Cys – Cystine  
DFO – Deferoxamine  
DHFR – Dihydrofolate reductase  
DHODH – Dihydroorotate dehydrogenase  
DMEM – Dulbecco's modified eagle medium  
DM-Mal – Dimethyl malate  
dMMR – Deficient DNA mismatch repair  
DM-Suc – Dimethyl succinate  
DM- $\alpha$ kg – Dimethyl  $\alpha$ -ketoglutarate  
Dox – Doxycycline  
EDC – 1-ethyl-3(3-(dimethylamino)propyl) carbodiimide  
EGFR – Epidermal growth factor receptor  
ERK2 – Extracellular signal-regulated kinase 2  
ETC – Electron transport chain  
FBP – Fructose-1,6-bisphosphate  
FER – Ferrostatin-1  
Fig – Figure  
FOLFIRINOX – 5-Fluorouracil, leucovorin, irinotecan, and oxaliplatin

FSP1 – Ferroptosis suppressor protein 1

G6PD – Glucose-6-phosphate dehydrogenase

GC – Gas chromatography

GCH1 – GTP cyclohydrolase 1

GCLC – Glutamate cysteine ligase catalytic subunit

GCLM – Glutamate cysteine ligase modifier subunit

GGT –  $\gamma$ -glutamyl transpeptidase

Gis – glutathione import system

Gln – Glutamine

GLS – glutaminase

Glu – Glutamate

Gly – Glycine

GOT1 – Glutamate oxaloacetate transaminase 1

GOT2 – Glutamate oxaloacetate transaminase 2

GPX4 – Glutathione peroxidase 4

GSH – Reduced glutathione

GSH-EE – Reduced glutathione ethyl ester

GSSG – Oxidized glutathione

GTP – Guanosine triphosphate

H2DCFDA – 2',7'-dichlorodihydrofluorescein diacetate

HD – Histidine aspartate

HDDC3 – HD domain-containing protein 3

HFD – High fat diet

His – Histidine

hnRNP – Heterogeneous nuclear ribonuclear protein

HPLC – High performance liquid chromatography

IKE – Imidazole ketone erastin

Ile – Isoleucine

KD – Knockdown

KO – Knockout

KPC – K-ras<sup>LSL.G12D/+</sup>; p53<sup>R172H/+</sup>; PdxCre

KRAS – Kirsten rat sarcoma viral oncogene homolog

LC - Liquid chromatography

LC-MS - Liquid chromatography-mass spectrometry

LC-MS/MS – Liquid chromatography tandem mass spectrometry

LDHB – Lactate dehydrogenase B

Leu – Leucine

LOX – Lipoxygenase

LPCAT3 – Lysophosphatidylcholine acyltransferase 3

Lys – Lysine

M – Mass

ME1 – Malic enzyme 1

ME1i – Malic enzyme1 inhibitor

ME2 - Malic enzyme 2

MEF – Mouse embryonic fibroblasts

MESH1 – Metazoan SpoT Homolog 1, encoded by HDDC3

Met – Methionine

mL – Milliliter

mm – Millimeter

mM – Millimolar

MS – Mass spectrometer

MSI-H – high microsatellite instability

mtDNA – mitochondrial DNA

mTORC1 – Mechanistic target of rapamycin complex 1

N – Sample size

Nab-Paclitaxel – Nanoparticle albumin-bound paclitaxel

NAC – N-acetylcysteine

NANS - N-Acetylneuraminase synthase

NCOA4 – Nuclear receptor coactivator 4

NEC – Necrostatin-1S

NETs – Pancreatic neuroendocrine tumors

nm – Nanometer

nM – Nanomolar

NOX – NADPH oxidase

NPL - N-acetylneuraminase pyruvate lyase

NPL – N-acetylneuraminase pyruvate lyase

NRF2 – nuclear factor (erythroid-derived 2)-like 2

NSG – NOD scid gamma

P/S – Penicillin and streptomycin

PALB-2 – partner and localizer of BRCA2

PC - Pyruvate carboxylase

PDAC – Pancreatic ductal adenocarcinoma

PE – Phosphatidylethanolamine

PEP – Phosphoenolpyruvate

PEPCK-M – Mitochondrial phosphoenolpyruvate carboxykinase

Phe – Phenylalanine

PHGDH – Phosphoglycerate dehydrogenase

PIPES – PiperazineN,N-bis (2-ethanesulfonic acid)

PK – Pyruvate kinase

PKM1 – Pyruvate kinase muscle isoform 1

PKM2 – Pyruvate kinase muscle isoform 2

PLS-DA – Partial least squares-discriminant analysis

POR – Cytochrome P450 oxidoreductase

PPP – Pentose phosphate pathway

PRPP – Phosphoribosyl pyrophosphate

p-val – p value

REDOX – Reduction/Oxidation

ROS – Reactive oxygen species

RSL3 – Ras selective lethal 3

S. aureus – Staphylococcus Aureus

SAICAR – serine and succinyl-5-aminoimidazole-4-carboxamide-1-ribose 5'-phosphate

SDH – Serine dehydratase

Ser – Serine

SHMT – Serine hydroxymethyltransferase

SLC – Solute carrier

SMAD4 – Small mothers against decapentaplegic family member 4

T3 – Thyroid hormone

TCA – Tricarboxylic acid

Thr – Threonine

Treg – Regulatory T cell

TRO – Trolox

Trp – Tryptophan

Tyr – Tyrosine

U – Uniform

Val – Valine

Vec – Vector

Veh – Vehicle

WT – Wild-type

X<sub>c</sub><sup>-</sup> - System X<sub>c</sub><sup>-</sup> consisting of xCT (SLC7A11) and SLC3A2

xCT – SLC7A11, component of system X<sub>c</sub><sup>-</sup> cystine/glutamate antiporter

ZVAD – Z-VAD-FMK

## **CHAPTER 1: INTRODUCTION - THE METABOLISM OF PANCREATIC CANCER AND IMPLICATIONS FOR TARGETED THERAPY**

### **Pancreatic Cancer**

Over the last several decades, researchers and clinicians have made remarkable progress in improving outcomes for patients suffering from several cancer types including lung, breast, prostate, and colon cancer.<sup>1</sup> In sharp contrast, the mortality and incidence rates of pancreatic cancer have increased among men and women since the late 1990's.<sup>1</sup> Pancreatic cancer is only the 10<sup>th</sup> most common cancer type in men and 8<sup>th</sup> most common type in women; however, it remains the 4<sup>th</sup> leading cause of cancer deaths in both men and women.<sup>1</sup> Further, investigators project pancreatic cancer to become the second leading cause of cancer-related deaths by 2030.<sup>2</sup> The vast majority (90%+) of pancreatic cancer arises from the exocrine tissue of the pancreas, leading to pancreatic ductal adenocarcinoma (PDAC).<sup>1</sup> While the less common pancreatic neuroendocrine tumors (NETs) have a better prognosis and younger median age of diagnosis, the much more common PDAC has a 5 year survival rate of approximately 12%, which translates to a dismal median survival time of 10-12 months from the time of diagnosis.<sup>1,3</sup>

The poor prognosis of pancreatic cancer is largely due to limited diagnostic and therapeutic options as well as the absence of signs and symptoms until advanced disease is present. Pancreatic cancer cells are capable of silently progressing and producing metastatic cells before clinical symptoms or predictive biomarkers can be detected.<sup>4</sup> The pancreas sits deep in the abdominal cavity making it inaccessible for routine exams that are possible for other tumor types such as colon, breast, and prostate. No reliable biomarker or imaging test has been approved for screening of asymptomatic

individuals.<sup>1,5</sup> Only serum carbohydrate antigen (CA) 19-9 has been approved, but it has limited sensitivity and specificity and very poor predictive value in an asymptomatic patient due to high degree of false positives from diseases such as pancreatitis, acute cholangitis, and liver cirrhosis.<sup>5</sup> Pancreatic tumors produce metastatic cells early in the disease process and disseminate in a disease process that may take place over 2 decades.<sup>6,7</sup> Given these limitations in diagnosis, 48.2% of cases have already metastasized to distant sites at time of diagnosis while only 13% of cases represent localized disease at the time of diagnosis.<sup>8</sup> There are few modifiable risk factors for pancreatic cancer including tobacco smoke and excess body weight. Patient age, family history of pancreatic cancer, medical history of chronic pancreatitis, type 2 diabetes, Lynch syndrome, or inherited mutations in breast cancer gene 1 or 2 (BRCA1 or BRCA2) also increase risk.<sup>1</sup> Therefore, other than smoking cessation and improving metabolic health, there is no clear prevention strategy for pancreatic cancer.

In addition to the limitations in diagnosis, new combinatorial and immunotherapy treatment strategies have largely failed to create a lasting impact in this disease.<sup>4,9</sup> The current standard of care consists first of selecting patients who are eligible for pancreaticoduodenectomy (Whipple procedure), but only about 15-20% of patients are eligible for this procedure.<sup>10,11</sup> This procedure offers improved survival outcomes, boosting the 5-year survival rate to 25%, but clearly there is much room for improvement.<sup>3</sup> Following surgical resection, adjuvant chemotherapy can further improve outcomes but is varied in approach and ability to complete the regimen based on patient performance status.<sup>3</sup> Recently, strategies investigating neoadjuvant chemotherapy (treatment before surgical intervention) have also shown some improvements in survival outcomes and the

ability to identify tumors that will respond well to surgical resection.<sup>3</sup> For those patients ineligible for surgical resection, there exists two main chemotherapy regimens: gemcitabine in combination with nanoparticle albumin-bound paclitaxel (nab-paclitaxel) or the multi-drug combination of 5-fluorouracil, leucovorin, irinotecan, and oxaliplatin (FOLFIRINOX).<sup>3</sup> Unfortunately, these chemotherapy strategies are associated with a high degree of chemoresistance over time.<sup>3,12</sup> Second-line therapies are varied dependent on patient factors. Some patients with BRCA1/2 mutations or partner and localizer of BRCA2 (PALB-2) mutated disease show improved response to gemcitabine and cisplatin, but this treatment is associated with a high degree of hematologic toxicities.<sup>3</sup> The poly-ADP ribose polymerase (PARP) inhibitor, Olaparib, is effective in BRCA mutated patients who haven't progressed on platinum based chemotherapy regimens.<sup>13</sup> Rarely, pancreatic cancer patients are deficient in DNA mismatch repair (dMMR) with high microsatellite instability (MSI-H) and show improved survival using the immune checkpoint inhibitor Pembrolizumab.<sup>14</sup> Other advances in immunotherapeutic interventions for pancreatic cancer have not been successful due to poor immunogenicity and highly immunosuppressive microenvironment of the pancreatic tumor.<sup>9</sup>

Although diagnostic and therapeutic strategies are severely limited, there is a surprisingly high understanding of the biology driving pancreatic cancer. PDAC is typically characterized by mutations in four genes in the majority of patients. These genes include activation of the Kirsten rat sarcoma viral oncogene homolog (Kras) proto-oncogene in over 90% of patients, and the loss of the tumor suppressors cyclin dependent kinase inhibitor 2A (CDKN2A), p53, and small mothers against decapentaplegic family member 4 (SMAD4) in 95%, 50-75%, and 55% of patients respectively.<sup>15-17</sup> Given the high rate of

KRAS mutation, targeting this oncogene is an obvious candidate for therapy; however, efforts to target this protein have been challenging and largely unfruitful for the last four decades.<sup>18</sup> Recently, new progress has been made in targeting KRAS<sup>G12C</sup> mutations that allow for locking KRAS into an inactive conformation.<sup>18–22</sup> However, the KRAS<sup>G12C</sup> mutations only represent about 1% of all KRAS mutations in PDAC compared to the much more common KRAS<sup>G12D</sup> mutations. Targeted therapies for this particular mutation are currently under investigation and there is exciting progress that a new KRAS<sup>G12D</sup> inhibitor, MRTX1133, works cooperatively with immune cell function to eliminate pancreatic tumors.<sup>23</sup>

An additional complexity to pancreatic tumors is the fibrotic deposition and accumulation of extracellular matrix components, specifically hyaluronic acid, in a reaction known as desmoplasia.<sup>24,25</sup> The KRAS mutations driving pancreatic cancer progression also regulate tumor cell signaling to stromal cells and contribute to desmoplasia.<sup>26,27</sup> Desmoplasia decreases blood perfusion to the tumor, leading to hypoxia and limiting drug delivery, and increases cancer cell motility.<sup>28–32</sup> This dense fibrotic environment is thought to contribute to aggressive tumor biology.<sup>33,34</sup> However, other more recent studies suggest that fibrosis actually plays a protective role and restrains growth, suggesting more work needs to be done to understand the heterogeneity and complexity of the pancreatic tumor microenvironment.<sup>7,35,36</sup> Additionally, the desmoplastic reaction has typically been thought to create an immunosuppressive environment that restricts T cell infiltration.<sup>37</sup> However, recent studies have identified significant variation in PDAC subgroups consisting of different cellular composition and distributions of CD4<sup>+</sup> and CD8<sup>+</sup> T cells, regulatory T cells (Treg),

and M1 versus M2 polarized macrophages resulting in either immunosuppressive or immune rich cytotoxic environments.<sup>36,38</sup> Therefore, there is a complex cross-talk between tumor, stromal, and immune cells generating heterogeneity within the tumor and between patients. Regardless of this heterogeneity, overall efforts at implementing immunotherapy strategies have failed to demonstrate strong efficacy suggesting that overall the PDAC tumor microenvironment (TME) prevents an effective adaptive immune response.<sup>39</sup> Ongoing clinical trials will hopefully reveal further insight into the immune landscape of pancreatic cancer and results in better targeted therapies. In summary, pancreatic cancer cells exist in a complex TME that creates a niche for persistent cells to grow and produce advanced tumors while remaining clinically silent and resisting our best efforts to selectively target them.

Despite the disappointing current standard of care, I have been encouraged by the fact that the 5 year survival rate doubled from 6% in 2013,<sup>40</sup> when I began studying pancreatic cancer as young undergraduate researcher, to approximately 12% in 2023.<sup>1</sup> There is still a long road ahead to eliminating the devastating effects of this disease, but the continued efforts of many teams of dedicated researchers and clinicians working together will persevere to make long term improvements for patients with pancreatic cancer. It has been an honor to play a small role in this while working in the Lunt lab, by addressing changes in pancreatic cancer metabolism and identifying new vulnerabilities for targeted therapy.

### **Cancer Metabolism and Implications for PDAC**

In the absence of reliable and effective treatment strategies for PDAC, alternative avenues are desperately needed. Targeting cancer metabolism is a promising candidate

for alternative strategies rich with potential targets for intervention. Early in the 20<sup>th</sup> century, Nobel laureate Dr. Otto Warburg made a critical discovery that tumor tissues exhibit increased lactate production compared to normal tissue, even in aerobic conditions.<sup>41</sup> Warburg further went on to show that this “aerobic glycolysis” is a common feature of tumors (Fig. 1.1).<sup>42,43</sup> Aerobic glycolysis is often eponymously referred to as “the Warburg Effect” to this day, and has become arguably the most well-known metabolic feature of cancer.

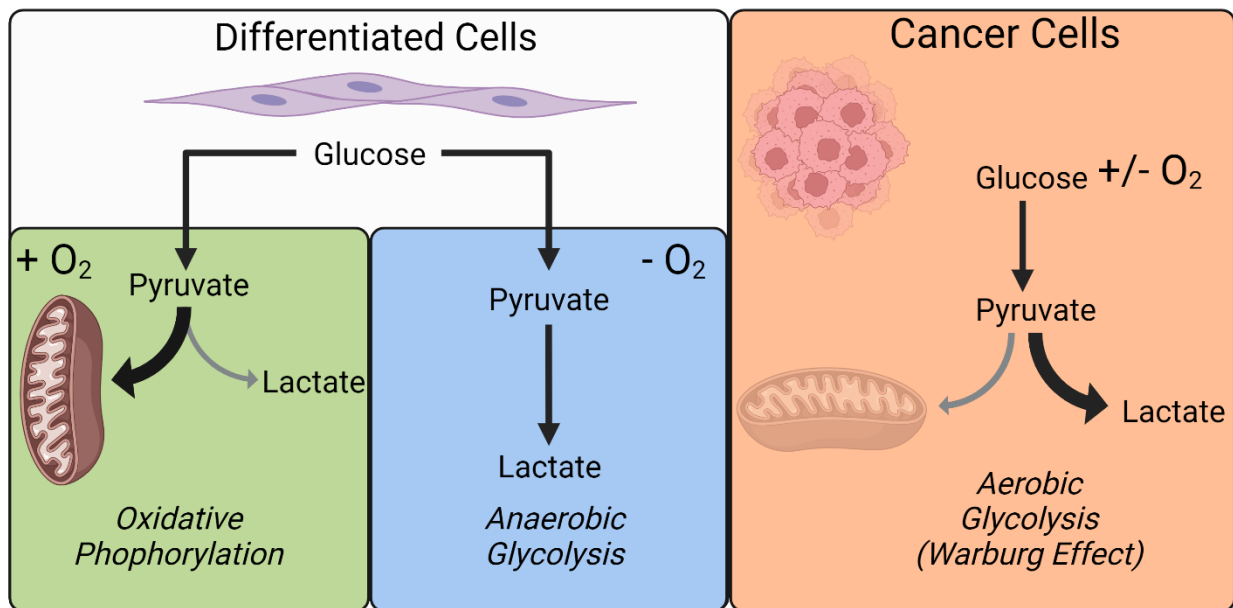


**Figure 1.1 Cancer cells demonstrate aerobic glycolysis.**

Differentiated cells consume glucose and produce pyruvate through glycolysis. When oxygen is present, pyruvate is transported to the mitochondria and further metabolized through oxidative phosphorylation. When oxygen is absent, pyruvate is fermented to lactate. In contrast, cancer cells will preferentially ferment glucose derived pyruvate into lactate even in the presence of oxygen in a process known as aerobic glycolysis or the Warburg Effect.

Warburg laid a foundational understanding of cancer metabolism that has been critical to the work of cancer researchers. Later in the 20<sup>th</sup> century the identification of the structure of DNA and genetic sequencing technologies shifted the focus of cancer to a genetic rather than a metabolic disease.<sup>44</sup> Despite major discoveries in the mutations in the oncogenes and tumor suppressors that drive tumorigenesis, a genetic focus alone has failed to yield definitive cures for cancer. Now, another 50 years later, metabolism has risen again to the mainstream of cancer research in an ongoing effort to conquer the devastating impacts cancer has on humanity. Many critical metabolic pathways that support cancer have been well characterized (Fig.1.2), but there remain many open questions about tumor heterogeneity and context specific metabolic effects.

Warburg's original hypothesis was that cancer cells had defective mitochondria or impaired oxidative metabolism and thus needed to rely on the less efficient glycolysis for adenosine triphosphate (ATP) production. However, later work by Warburg and others demonstrated active respiration in cancer cells, indicating that enhanced glucose uptake and fermentation to lactate was not at the expense of cellular respiration.<sup>45</sup> More recent work has shown the importance of mitochondrial function and cellular respiration within cancer cells and demonstrated ongoing glucose oxidation using <sup>13</sup>C tracing experiments.<sup>46-49</sup> Clinicians have also taken advantage of the Warburg effect by employing the commonly used diagnostic imaging procedure known as a positron emission tomography (PET) scan. PET scans detect tumors that exhibit the Warburg effect by using fluorodeoxyglucose (<sup>18</sup>F-FDG), a positron emitting radiotracer analog of glucose, which accumulates in highly glycolytic tissues and radiolabels otherwise difficult to detect tumors.<sup>50</sup>

Despite strong evidence of this metabolic reprogramming, there remains some controversy over why cancer cells engage these metabolic behaviors and what environmental and genetic contexts alter this effect. There are several explanations for why cancer cells utilize this less efficient metabolism including: rapid ATP synthesis in glycolysis, promoting flux into biosynthetic pathways, enhancing disruption of microenvironmental tissue architecture and immune cell evasion, and allowing for signal transduction through ROS and chromatin modulation.<sup>51</sup> There is evidence for the validity of each of these proposals, yet open questions remain. For example, per unit of glucose, aerobic glycolysis is substantially less efficient compared to oxidative phosphorylation in the mitochondria.<sup>43,52</sup> However, aerobic glycolysis is approximately 10-100 times faster than mitochondrial respiration and can produce equivalent ATP in the same amount of time with increased glucose uptake and utilization.<sup>53</sup> Yet the ATP demands of the proliferating cell likely do not require this capacity, and other non-aerobic glycolysis strategies for rapid ATP production such as creatine kinases or adenylate kinase could be utilized by cancer as well. Therefore, rapid ATP production cannot be the sole explanation for why cancer cells prefer increased glucose uptake and lactate fermentation. Similarly, another common proposal to explain the Warburg Effect is an adaptation to increase biosynthetic requirements to produce another cancer cell during division. In this model, excess glucose derived carbon is used for de novo synthesis of lipids, amino acids, and nucleotides, as well as the production of the reducing equivalent NADPH through increased flux in the oxidative pentose phosphate pathway (PPP).<sup>43,54–</sup>  
<sup>57</sup> Similarly, the fermentation of pyruvate produced by glycolysis to lactate by lactate dehydrogenase regenerates NAD<sup>+</sup> to maintain active glycolysis.<sup>58</sup> This explanation

makes intuitive sense; however, recent work demonstrates that cells use up to 10% of their proteome and 50% of all metabolic genes to produce the machinery required for glycolysis.<sup>59</sup> Thus, the cost to produce the proteins to increase aerobic glycolysis would equal or even outweigh the cost to produce proteins for biosynthesis of other molecules.<sup>43</sup> There remains additional open questions regarding why oncogenes specifically program this type of metabolic activity. Therefore, ongoing research is still required to identify the metabolic underpinnings that drive the Warburg effect and support cancer survival and proliferation.

Over the 100 years following Warburg's initial discovery, there have been many improvements to our understanding of cellular respiration and the metabolic reprogramming within cancer cells.<sup>43,60</sup> In their pivotal paper in 2000, Hanahan and Weinberg defined a set of hallmarks of cancer including: sustaining proliferative signaling, evading growth suppressors, activating invasion and metastasis, enabling replicative immortality, inducing angiogenesis, and resisting cell death.<sup>61</sup> A decade later, these hallmarks were updated with enabling characteristics and emerging hallmarks including deregulating cellular metabolism.<sup>62</sup> Most recently, it has been concluded that the deregulation of cellular metabolism (more commonly thought of as reprogramming of cellular metabolism) has been sufficiently validated to be definitively included as a hallmark of cancer.<sup>63</sup> Indeed, the oncogene and tumor suppressor mutations that drive cancer growth also contribute to metabolic signaling networks.<sup>64</sup> Pancreatic cancer is no exception to these observations. As described in the previous section, the desmoplastic reaction in the pancreatic tumor microenvironment creates a harsh nutrient deprived and hypoxic environment.<sup>65,66</sup> Given the low nutrient stress these cells are under, targeting of

the metabolic adaptations needed to survive this environment represent promising novel strategies for treating pancreatic cancer. In their excellent review, Halbrook and Lyssiotis, thoroughly review this topic.<sup>4</sup> Recent studies have found a high degree of metabolic and genetic heterogeneity in pancreatic cancer cells both *in vitro* and *in vivo*, highlighting the challenge in treating this disease.<sup>67-74</sup> However, there are common features especially when considering the oncogene *KRAS*. *KRAS*, which is mutated in the vast majority of PDAC drives a particular metabolic reprogramming.

*KRAS* promotes increased expression of the glucose transporter, GLUT1, and hexokinase (HK) to enable elevated glucose scavenging in a scarce environment.<sup>75</sup> There is an additional glycolytic enzyme, pyruvate kinase, that plays a particularly important role in cancer and will be discussed extensively in the following section due to its relevance to the broader scope of this thesis. Interestingly, there is evidence that *KRAS* decouples glucose and glutamine metabolism.<sup>76</sup> *KRAS* alters glucose flux into aerobic glycolysis, pentose phosphate pathway, and the hexosamine pathway while increasing glutamine flux for anaplerosis into the TCA cycle and maintaining redox balance.<sup>75,77</sup> Glutamine serves in this redox role through its contribution to glutathione, a major defense metabolite against ROS, and generation of NADPH, a higher energy molecule used for redox balance and biosynthesis of lipids.<sup>77-79</sup> *KRAS* promotes a unique pathway for NADPH production in pancreatic cancer by utilizing GOT2, GO1, and ME1.<sup>77</sup> PDAC cells use glutamine to derive aspartate through a series of reactions within the mitochondria. Aspartate is then transferred to the cytosol by the malate aspartate shuttle and converted back to oxaloacetate, then malate, and finally to pyruvate through malic enzyme 1 to produce NADPH (Fig.1.2). This pathway is not used in normal cells that instead rely on

glutamate dehydrogenase (GLUD1) to convert glutamine derived glutamate into  $\alpha$ -ketoglutarate.<sup>77</sup> Other work has also shown that KRAS activates nuclear factor (erythroid-derived 2)-like 2 (NRF2) to signal cellular ROS detoxification programs.<sup>80-84</sup> Additionally, KRAS activates expression of the cystine/glutamate antiporter (xCT) to preserve intracellular redox balance.<sup>85</sup> However, it is important to keep in mind the experimental model systems used to derive evidence for these metabolic pathways. *In vitro* models demonstrate high levels of glutamine metabolism for mitochondrial oxidative phosphorylation (perhaps in part due to artificially high nutrient concentrations in culture media), however in *in vivo* models, glucose metabolism dominates.<sup>86-89</sup> Therefore, while glucose and glutamine metabolism play fundamental roles in fueling pancreatic cancer cell growth, one must be careful to understand the environmental contexts in which these pathways are most critical.

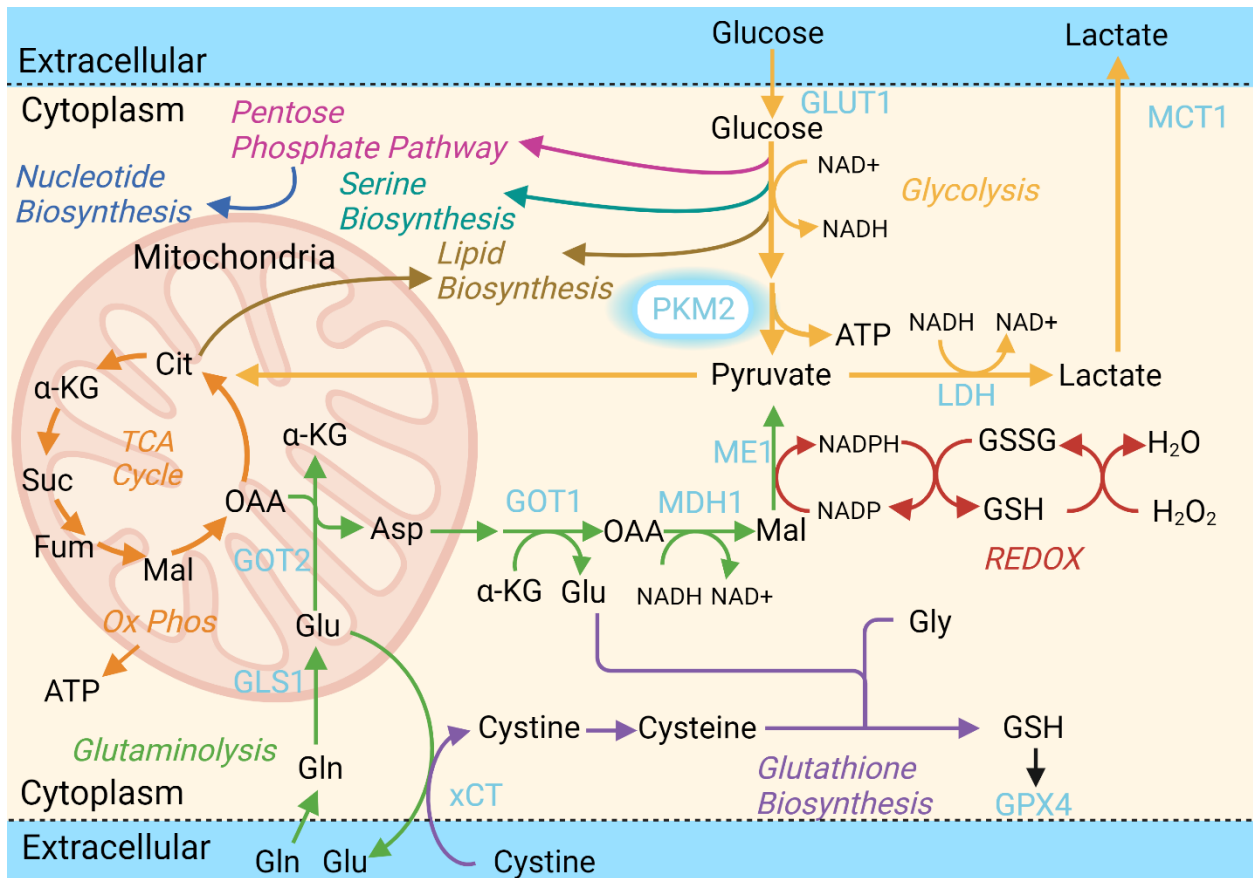


**Figure 1.2 Metabolic reprogramming in PDAC.**

Decreased activity of PKM2 promotes shunting of glucose carbon into biosynthetic pathways including the PPP and nucleotide, serine, and lipid biosynthesis. Pyruvate is fermented to lactate and secreted into the extracellular environment. Glutaminolysis is increased for anaplerosis and enhanced NADPH production through a series of reactions involving GLS1, GOT2, GOT1, MDH1, and ME1. Cystine is acquired through the antiporter xCT in exchange for glutamate secretion. Cystine is used along with glutamate and glycine for glutathione synthesis.

In addition to glucose and glutamine metabolism changes, PDAC cells also alter metabolic scavenging and recycling pathways such as autophagy.<sup>90–92</sup> These cells also

elevate macropinocytosis to harvest extracellular proteins.<sup>93-95</sup> Stromal stellate cells in the PDAC TME secrete alanine, which is imported by PDAC cells for anaplerosis.<sup>96</sup> Most cells use tryptophan metabolism as the primary source for NAD<sup>+</sup> synthesis; however, PDAC cells rely on nicotinamide phosphoribosyltransferase (NAMPT) to produce nicotinamide mononucleotide as the precursor for NAD<sup>+</sup>.<sup>97,98</sup> Most recently, uridine was discovered to be a critical fuel source for ribose production which fascinatingly is used for cellular reducing potential rather than nucleotide metabolism.<sup>99</sup>

Altogether, many diverse groups have uncovered a variety of metabolic mechanisms that contribute to the survival and progression of pancreatic cancer cells in a complex and harsh microenvironment. Yet many open questions remain about the tumor heterogeneity and environmental factors that drive these metabolic behaviors and the feasibility of targeting these highly adaptable pathways.

### **Metabolic Mechanisms of Ferroptosis and Implications for PDAC**

The goal of targeted metabolic therapy involves selectively blocking critical metabolic pathways to starve cancer cells of essential resources and induce cell death or at least stop growth and metastasis. With this goal in mind, an emerging fervor has grown over a particular form of cell death, known as ferroptosis. Ferroptosis is a non-apoptotic, non-necroptotic form of cell death characterized by unchecked lipid peroxidation propagated by intracellular iron.<sup>100</sup> Ferroptosis is fundamentally an aberrant metabolic process and can be triggered by interrupting the metabolic defenses cells rely upon. The various metabolic pathways involved are reviewed in an excellent summary by Zheng and Conrad in 2020, and the highlights will be discussed here.<sup>101</sup> As this is a newly emerging field, there are many contradictory findings that indicate a high degree of specificity to

environmental context and cancer type. Nevertheless, ferroptosis has been thoroughly demonstrated *in vitro* and *in vivo* in a variety of human cancers, including PDAC, as well as neurodegenerative conditions such as Alzheimer's disease and stroke.<sup>102–104</sup>

Over the last decade, the mechanism of ferroptosis has been refined, yet there are many open questions regarding the various contexts that produce ferroptosis.<sup>105</sup> The term ferroptosis was first coined in 2012 by Dixon et al. in their investigation of the mechanisms of cell death caused by compounds targeting the RAS oncogene.<sup>106</sup> Although this definition was formalized in recent years, there are early reports that match descriptions of ferroptosis that trace back to the mid-20<sup>th</sup> century.<sup>101</sup> Early investigations revealed a connection between what we now know as ferroptosis and cystine metabolism. Cystine, the oxidized dimer of cysteine, was identified as a necessary resource for cancer cells and its removal induced a unique morphology.<sup>107</sup> Additionally, reduced glutathione (GSH), which is synthesized from cysteine, was found to promote cell growth.<sup>108</sup> Withdrawal of cystine caused cell death following GSH depletion that could be ameliorated by the antioxidant vitamin E.<sup>109</sup> Further connections were made by the observation of liver necrosis in rats starved of vitamin E and cystine which could be rescued by supplying selenium (now known to be a critical trace element for glutathione peroxidase (GPX4), the inhibitor of lipid peroxides.<sup>110–112</sup> The connection between lipid peroxidation and iron was made when it was discovered that mice injected with iron dextran formed lipid peroxidation in adipose tissue which could be exacerbated by unsaturated fat and inhibited by vitamin E.<sup>113</sup> Later discoveries about the mechanism of ferroptosis were made by work completed in the Stockwell and other labs by characterizing compounds that were synthetically lethal to cells with mutant RAS (HRAS, KRAS, or BRAF).<sup>114–116</sup> One

compound, named erastin, was found to induce cell death without DNA fragmentation or caspase activation.<sup>114</sup> Another compound, RSL3, was later found to induce cell death in a similar manner, and that death could be inhibited by chelating iron.<sup>115,116</sup> These compounds induced a morphologically distinct form of cell death that caused reduced mitochondrial volume with increased membrane density. Importantly the dying cells were absent of characteristic features such as chromatin condensation seen in apoptosis, organelle swelling and membrane rupture in necroptosis, or double membrane vesicles in autophagy.<sup>106,115</sup> The mechanism of erastin was then determined to be mediated through accumulation of lipid peroxidation, modulation of voltage dependent anion channel (VDAC) 2 and 3, and the targeting of the sodium independent cystine/glutamate antiporter, system  $x_C^-$ .<sup>106</sup> System  $x_C^-$  exists as a heterodimer of SLC7A11 (xCT) and SLC3A2 (also known as 4F2hc, CD98hc) and is the main source of cystine acquisition in cancer cells.<sup>117,118</sup> The system  $x_C^-$  antiporter was already known for its importance to neurons metabolism as it was found that high glutamate levels induce toxicity and death in brain cells by competitive inhibition with system  $x_C^-$ .<sup>119,120</sup> Blockade of system  $x_C^-$  had also previously been shown to inhibit glutathione synthesis due to limiting access to cysteine.<sup>121,122</sup> Erastin was demonstrated to eliminate uptake of cystine, while RSL3 had no effect on this process.<sup>106</sup> The loss of glutathione along with decreased availability or function of the associated protein, GPX4 are now known to be hallmark features of ferroptosis.<sup>102,123,124</sup> Indeed, the mechanism of action of RSL3 was later determined to be irreversible antagonism of GPX4.<sup>125</sup> Recent years have seen the identification and development of several ferroptosis inducing compounds, but nearly all operate on the core principle of blocking cystine acquisition or inhibiting lipid peroxidation defense

proteins.<sup>100</sup> Interestingly, direct depletion of GSH by blocking biosynthesis with buthionine sulfoximine (BSO) does not directly lead to ferroptosis in all circumstances, indicating that there may be additional triggers needed to begin the lipid peroxidation cascade.<sup>100,125–127</sup> Similarly, although ferroptotic cell death is attributed to ROS accumulation in the form of lipid peroxidation propagated by iron, the precise role of iron remains under investigation.

At the core function of ferroptosis, the lipid peroxidation reaction chemistry can be explained by the Fenton reaction with iron (Fig.1.3A).<sup>128</sup> Iron is an essential trace element for basic cellular function and cancer cells have an increased demand for iron.<sup>129</sup> In normal physiology, iron is bound in the plasma by transferrin which binds to the transferrin receptor 1 (TFRC) on cell membranes.<sup>129</sup> TFRC is brought into the cell where it is degraded within endosomes and lysosomes to release the iron into labile iron pools or to be bound by intracellular ferritin (Fig.1.3B).<sup>129–131</sup> The autophagic degradation of ferritin to release iron is known as ferritinophagy and is regulated by nuclear receptor coactivator 4 (NCOA4).<sup>132,133</sup> Ferritinophagy releases iron from the lysosome and provides a source of iron for lipid peroxide propagation.<sup>134</sup> Before the lipid peroxidation cascade can begin, an initiating event (such as oxidative metabolism in the mitochondria or the action of oxidoreductases) produces a lipid radical on a polyunsaturated fatty acid (PUFA) acyl chain. This radical then combines with molecular oxygen to produce a lipidperoxyl radical. The lipidperoxyl radical continues the chain reaction by abstracting a hydrogen atom from another lipid yielding a lipid peroxide and another lipid radical. This chain reaction then rapidly propagates by auto initiation through the Fenton reaction in which the lipid peroxide reacts with ferrous (reduced) iron ( $\text{Fe}^{2+}$ ) to produce ferric iron ( $\text{Fe}^{3+}$ ), a hydroxide ion, and a lipid peroxyl radical.<sup>135,136</sup> These lipid peroxyl radicals create additional lipid

radicals to react with oxygen. This cascading process can be terminated by radical trapping agents such as endogenous vitamin E, exogenous ferrostatin-1, or through GPX4 mediated elimination of lipid peroxides (Fig. 1.3A).<sup>137</sup> The subcellular location of the lipid peroxidation appears to be predominantly in the endoplasmic reticulum. Mitochondria, lysosomes, and Golgi can also initiate and amplify lipid peroxidation under cystine starvation (Fig.1.3B).<sup>105,138</sup>

GPX4 is the central inhibitor of lipid peroxidation, and thus ferroptosis. There are 3 other GPX4 independent pathways for preventing ferroptosis including: ferroptosis suppressor protein 1 (FSP1)/coenzyme Q10 (CoQ<sub>10</sub>), dihydroorotate dehydrogenase (DHODH), and guanosine triphosphate (GTP) cyclohydrolase 1 (GCH1) / tetrahydrobiopterin (BH<sub>4</sub>).<sup>105</sup> FSP1 regenerates the reduced form of CoQ<sub>10</sub> found in the mitochondria and cell membrane.<sup>139–141</sup> GCH1 produces the lipophilic antioxidant BH<sub>4</sub> which functions similarly to CoQ<sub>10</sub>.<sup>142,143</sup> DHODH functions in a similar manner as FSP1 to reduce mitochondrial CoQ<sub>10</sub> (Fig.1.3B).<sup>144</sup>

In addition to iron metabolism and initiating oxidative stress, lipid metabolism also appears to be a critical element of ferroptosis. PUFAs are sensitive to lipid peroxidation and are essential for the cascade leading to ferroptosis.<sup>145</sup> Beyond ferroptosis lipid peroxides are used in normal physiology as potent signaling molecules to stimulate cell survival and proliferation.<sup>136</sup> Phosphatidylethanolamine (PE) containing arachidonic acid (AA) is the key phospholipid that undergoes peroxidation in ferroptosis.<sup>146</sup> Lipoxygenases (LOX) were shown to regulate erastin induced ferroptosis, but not GPX4 induced ferroptosis, and silencing of arachidonate lipoxygenase 15B (ALOX15B) or ALOXE3 rescues erastin-induced ferroptosis.<sup>146</sup> Similarly, acyl-coenzyme A (CoA) synthetase long

chain family member 4 (ACSL4) and lysophosphatidylcholine acyltransferase (LPCAT3) were identified as enablers of ferroptosis.<sup>147,148</sup> However, ACSL4 knockout dramatically improves sensitivity to RSL3, but not erastin. Additional work demonstrates that LOX are not essential for ferroptosis but can play a role in its initiation.<sup>149</sup>

The initiation of lipid peroxidation and subsequent ferroptosis can occur through several ways; most commonly, the reaction between reduced iron ( $\text{Fe}^{2+}$ ) and hydrogen peroxide is used to explain this process. However, ferroptosis cannot be explained by simple Fenton chemistry alone as hydrogen peroxide induced death is unique from ferroptosis.<sup>106</sup> Instead, there is evidence that hydroperoxyl radicals formed from iron containing enzymes such as NADPH oxidases (NOX), cytochrome P450 oxidoreductases (POR), and the electron transport chain (ETC) complexes I and III (CI/CIII) may be responsible.<sup>106,137</sup> Interestingly, the early work describing ferroptosis demonstrated that osteosarcoma cells incapable of producing ETC-dependent ROS due to depletion of mitochondrial DNA (mtDNA) showed similar sensitivity to erastin as those with WT mtDNA.<sup>106</sup> Instead, the source of ROS was attributed to NOX enzymes that produce superoxide from NADPH and are upregulated in RAS mutant tumors. NOX inhibition suppressed ferroptosis induced by erastin.<sup>106,150</sup> Additionally, inhibition of the PPP enzyme glucose-6-phosphate dehydrogenase (G6PD) prevented erastin induced ferroptosis.<sup>106</sup> This finding is counter-intuitive as NADPH is typically viewed as reducing power for antioxidant responses. Further work has demonstrated that NADPH levels can be used as a biomarker for ferroptosis sensitivity where elevated levels of NADPH predict resistance to ferroptosis and low NADPH levels predict sensitivity to ferroptosis.<sup>151</sup> Additionally, other researchers have found that Metazoan SpoT Homolog 1, encoded by

HDDC3 (MESH1) regulates NADPH levels and that loss of MESH1 depletes NADPH levels and sensitizes cells to erastin induced ferroptosis.<sup>152</sup>

Recent work now shows that mitochondria do play role in ferroptosis.<sup>153,154</sup> Specifically, in mouse embryonic fibroblasts (MEFs) starved of cystine, the removal of glutamine decreased mitochondrial membrane potential, decreased lipid peroxidation, and eliminated ferroptosis under cystine starvation. Further, adding back cell permeable analogs of TCA cycle intermediates re-sensitized the cells to ferroptosis.<sup>153,154</sup> This has led to the model that active mitochondria will lead to rapid exhaustion of GSH by GPX4 under cystine starvation, while less active mitochondria will have diminished ferroptosis.<sup>153,155</sup> However, GPX4 inhibition is able to potently induce ferroptosis regardless of mitochondrial function.<sup>153,155</sup> The precise role of glutamine metabolism and mitochondrial function in pancreatic cancer remains under investigation as recent work has shown that glutamine starvation may actually induce ferroptosis in some circumstances.<sup>156</sup> This will be discussed extensively in Chapter 3. More complexity is further introduced by the observation that inhibiting individual enzymes or the entire ETC has variable effects on ferroptosis depending on the cell line and environmental contexts.<sup>101,106,138,153,157–160</sup>

While ferroptosis occurs independent of autophagy, there are overlapping regulators of ferroptosis and autophagy including SLC7A11, GPX4, NCOA4, NRF2, p53, and ACSL4.<sup>161</sup> For example, NCOA4 promotes the autophagic breakdown of ferritin which increases the availability of labile iron which can propagate lipid peroxides.<sup>162,163</sup> Additionally, the autophagy inhibitor bafilomycin A1 can inhibit ferroptosis under some circumstances but not universally.<sup>126,162,164</sup> However, core autophagy genes, such as

ATG7, are rarely found to be involved in ferroptosis.<sup>137,165</sup>

The p53 and mechanistic target of rapamycin complex 1 (mTORC1) pathways both influence ferroptosis. mTORC1 can inhibit ferroptosis by coupling cystine availability with GPX4 protein synthesis to prioritize oxidative stress defense.<sup>166</sup> On the other hand, others have shown that mTORC1 can promote ferroptosis in fibrosarcoma cells under cystine starvation by diverting cysteine away from GSH synthesis.<sup>167</sup> p53 has similar controversial findings regarding its role in ferroptosis as either a promoter or suppressor.<sup>137,168–172</sup> It is possible for both to be true due to differences in cells lines and method of ferroptosis induction. Thus, these context dependent and contradictory findings create an environment in which it is difficult to make strong conclusions about the implications for inducing ferroptosis as a mechanism for treating cancer patients. One should always read papers carefully and keep in mind the precise methodology used to produce each conclusion.

Attempts to make a universal network of ferroptosis have been challenging, unlike apoptosis and necroptosis, due to the highly variable nature of ferroptosis.<sup>157</sup> Some components seem to be more important in particular types of ferroptosis induction methods, for example ACSL4 is important in mediating ferroptosis under direct GPX4 inhibition but not cystine starvation or erastin treatment.<sup>157</sup> Despite a few commonalities under different circumstances, there are no universal proteins that will always be involved to cause unchecked iron mediated lipid peroxide propagation and cell death.<sup>137</sup> The highly context dependent nature of ferroptosis has led to the recent development of a flexible model for ferroptosis where no one factor or single unifying signaling pathway is necessary and different configurations of defense strategies, environmental conditions,

and initiating factors are involved to induce ferroptosis.<sup>137</sup> Therefore, ferroptosis represents an exciting field with many open questions and enormous potential for developing targeted metabolic therapies directed at cancer cells and beyond.

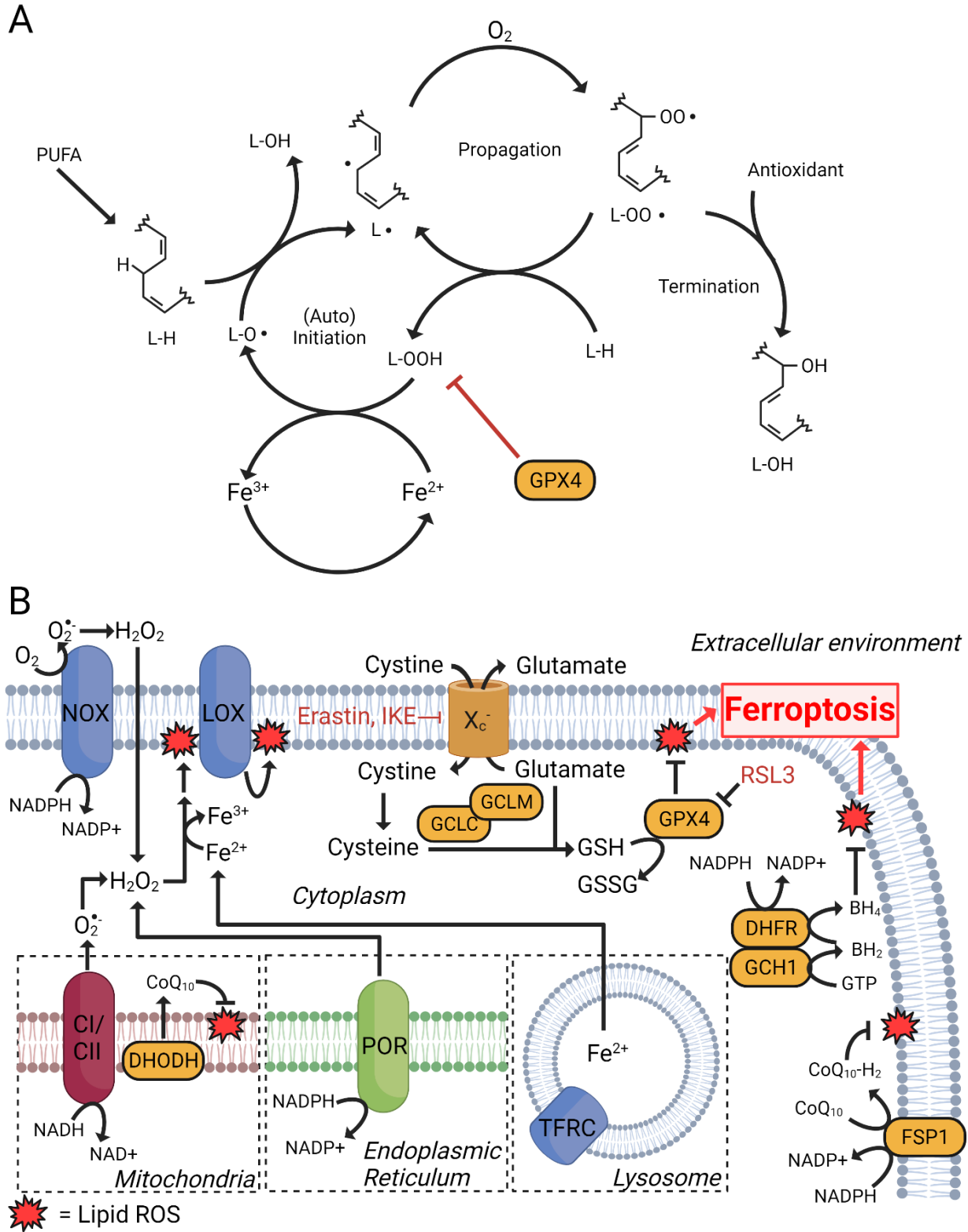


### Figure 1.3 (cont'd)

and termination. The process begins by a lipid radical ( $L\cdot$ ) forming on a polyunsaturated fatty acid (PUFA) acyl chain which combines with oxygen to form a lipid peroxy radical ( $L-OO\cdot$ ). The  $L-OO\cdot$  abstracts a hydrogen atom from another  $L\cdot$  and a lipid peroxide ( $L-OOH$ ). Once this process begins, a chain reaction can propagate through auto initiation by the reaction of  $L-OOH$  with reduced iron to form a new lipid alkoxyl radical ( $L-O\cdot$ ) which can produce an additional  $L\cdot$ . The process is terminated by radical trapping agents or antioxidants that reduce  $L-OO\cdot$  to lipid alcohols ( $L-OH$ ). The action of glutathione peroxidase 4 (GPX4) eliminates lipid peroxides limiting the propagation and cascade towards ferroptosis. **B.** Key elements of the ferroptosis mechanism. NADPH oxidase (NOX), and lipoxygenase (LOX) are sources of lipid peroxidation. Mitochondrial complex 1 and 3 (CI and CIII) and cytochrome P450 oxidoreductase in the endoplasmic reticulum are additional sources of lipid peroxides. Iron brought into the cell and released from the lysosome contributes to radical formation and lipid peroxidation propagation. Cystine is imported through System  $X_c^-$  and reduced to cysteine. Cysteine, along with glutamate and glycine, is used for glutathione synthesis through glutamate cysteine ligase modifier and catalytic proteins (GCLM and GCLC). Glutathione is used by GPX4 to eliminate lipid peroxides. Dihydroorotate dehydrogenase (DHODH) and ferroptosis suppressor protein 1 (FSP1) reduce  $CoQ_{10}$  which eliminates reactive oxygen species (ROS). GTP cyclohydrolase 1 (GCH1) and dihydrofolate reductase (DHFR) work to produce tetrahydrobiopterin ( $BH_4$ ) which eliminates ROS. Figure was adapted from Dixon & Pratt, 2023.<sup>137</sup>

## **Clinical Applications of Targeted Metabolic Therapies in PDAC**

There is a long history of metabolic therapies employed to treat cancer. In the mid-20th century, Dr. Sidney Farber famously discovered the dependency of acute lymphoblastic leukemia cells on folate metabolism. The subsequent development of aminopterin and later methotrexate were among the first “anti-metabolites” to be used in cancer therapy.<sup>173,174</sup> Since then, many metabolic therapies have been introduced that are still used today and many more are currently under investigation in clinical trials. A brief overview of examples of metabolic therapies include: asparaginase to limit asparagine acquisition, 5-fluorouracil (5-FU) to block thymidylate synthase, methotrexate to block dihydrofolate reductase (DHFR), leflunomide to block DHODH, 6-mercaptopurine (6MP) which blocks phosphoribosyl pyrophosphate (PRPP) amidotransferase, metformin which blocks mitochondrial complex I, AZD3965 which inhibits lactate export through monocarboxylate transporter 1 (MCT1), ivosidenib to block mutant isocitrate dehydrogenase 1 (IDH1), PEG-BCT-100 to deplete circulating arginine, CPI-613 to block pyruvate dehydrogenase/ $\alpha$ -ketoglutarate dehydrogenase, CB839 to block glutaminase (GLS), and many others (Fig.1.4).<sup>174</sup>

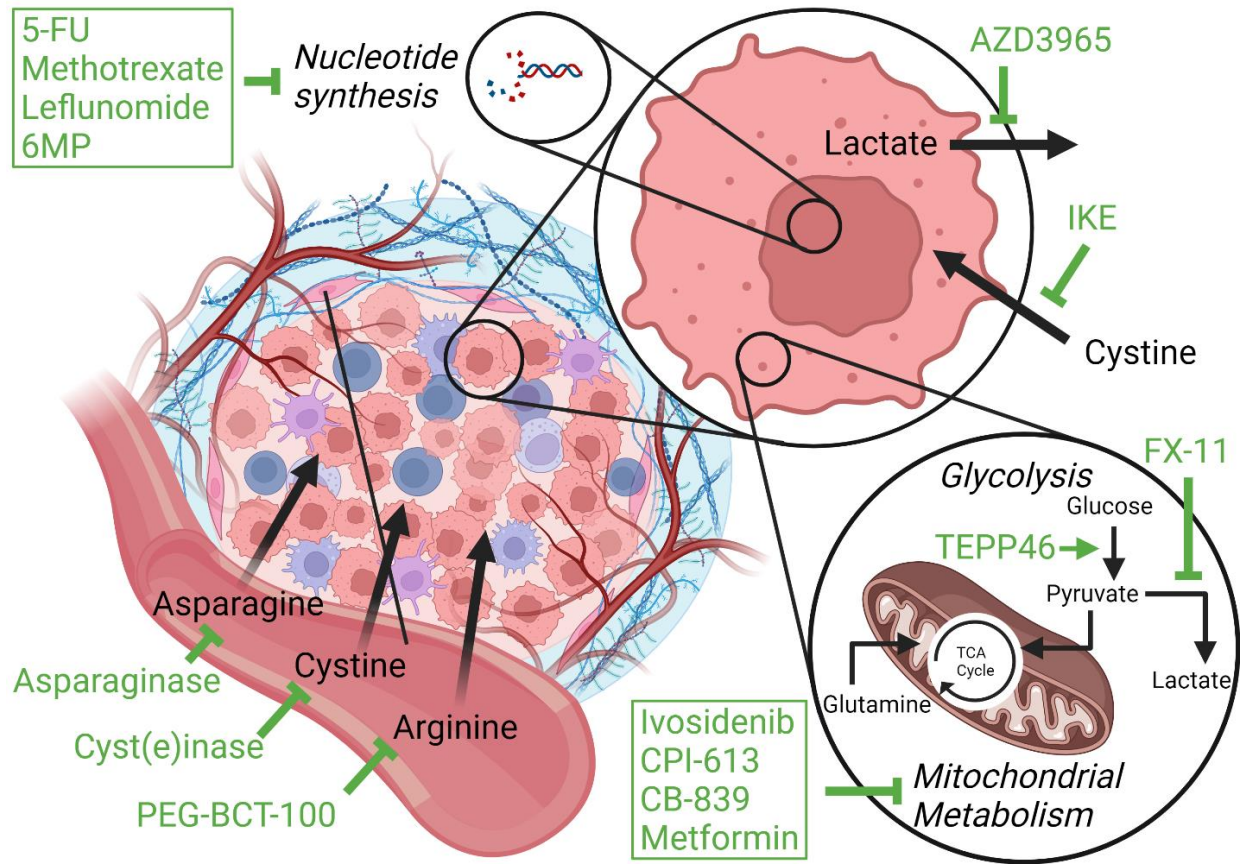


**Figure 1.4 Overview of metabolic therapies in cancer.**

5-fluorouracil (5-FU) to blocks thymidylate synthase. Methotrexate blocks DHFR. leflunomide block DHODH. 6MP blocks PRPP amidotransferase. Asparaginase breaks down asparagine. Cyst(e)inase breaks down cystine/cysteine. IKE blocks cystine uptake. PEG-BCT-100 breaks down arginine. Metformin inhibits mitochondrial complex I. AZD3965 inhibits lactate export through monocarboxylate transporter 1. Ivosidenib inhibits mutant IDH1. CPI-613 inhibits pyruvate dehydrogenase/ $\alpha$ -ketoglutarate dehydrogenase. CB839 inhibits GLS. FX-11 inhibits lactate dehydrogenase. TEPP46 activates PKM2.

The efficacy of a particular metabolic therapy is dependent on the type of cancer and tumor microenvironment conditions. For example, the glutaminase inhibitor CB839 is effective at eliminating proliferation and glutamine metabolism of cultured A549 lung cancer cells *in vitro*, yet A549 subcutaneous xenografts show limited glutamine metabolism and response to CB839 *in vivo*. The difference in glutaminase efficacy has been shown to be at least in part due to artificially high levels of cystine in culture media.<sup>89</sup> The difference in environmental conditions between experimental approaches may also explain the lack of robust results from targeting glutamine metabolism in cancer patients.<sup>175,176</sup> Therefore discrepancy between *in vitro* and *in vivo* conditions should be strongly considered when evaluating the potential for targeted metabolic therapy. Differences in environmental context may also explain why both pharmacologic activators and inhibitors of pyruvate kinase M2 have both been shown to decrease tumor growth, which will be discussed more extensively in the next section.<sup>177–180</sup>

Combinatorial metabolic therapies represent a successful approach to treating cancer by taking advantage of the multiple metabolic dependencies of cancer cells and limiting the cancer cell's ability to flexibly reprogram their metabolism in response to a single insult. For example, a common therapy for pancreatic cancer involves the combination of nab-paclitaxel (a microtubule stabilizer) and gemcitabine (inhibits nucleotide synthesis). This dual pronged approach takes advantage of the increased demand for PDAC cells to synthesize new nucleotides as well as increased macropinocytosis to acquire extracellular protein (such as albumin) which brings in the bound paclitaxel payload.<sup>4</sup> However, as discussed previously, resistance quickly develops pointing to the need for better therapies. In another example, the combination of the pyruvate kinase M2 activator,

TEPP-46 with the lactate dehydrogenase inhibitor FX-11 demonstrate synergistic reduction of pancreatic tumor growth and represents promising potential for future clinical trials.<sup>181</sup> Our lab has also collaborated on the development of combinatorial metabolic therapies in prostate cancer, which will briefly be discussed in Chapter 5.

Inducing ferroptosis in pancreatic cancer also shows promising potential. Agents such as imidazole ketone erastin (IKE) can block cystine uptake and induce ferroptosis in cancer cells.<sup>182</sup> This was also recently demonstrated *in vivo* using the engineered enzyme cyst(e)inase that depletes plasma and tumor levels of cysteine/cystine and induces ferroptosis in a mouse model of PDAC.<sup>126</sup> Cyst(e)inase represents exciting progress towards a ferroptosis inducing metabolic therapy, yet there is much room for active investigation in this field. In the next section, I will introduce my research focus on pyruvate kinase and its role in ferroptosis in PDAC.

### **The Role of Pyruvate Kinase in PDAC Metabolism**

As discussed previously, many metabolic changes contribute to the Warburg Effect and pancreatic cancer development. One change that is particularly important for supporting these changes is the glycolytic enzyme pyruvate kinase (PK). PK catalyzes the final step in glycolysis by converting phosphoenol pyruvate (PEP) to pyruvate along with the transfer of a phosphate group to ADP producing ATP (Fig. 1.5).

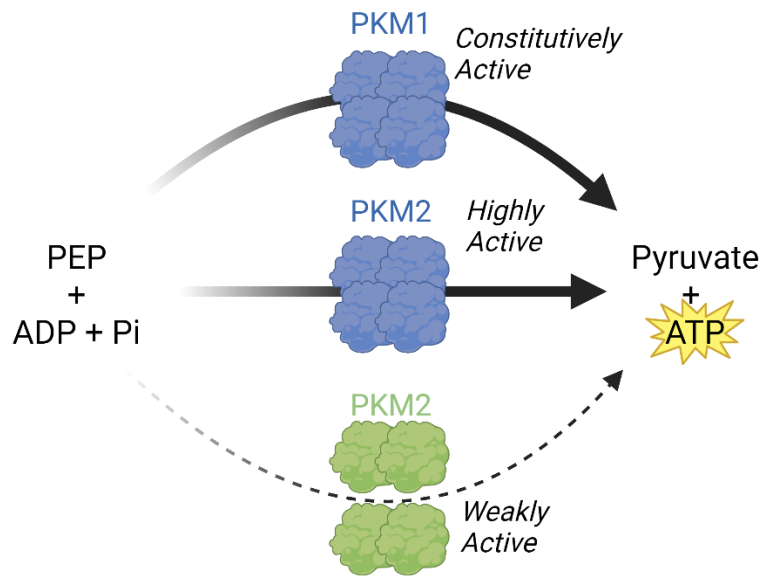


**Figure 1.5 Mechanism of PKM1 and PKM2.**

Both PKM1 and PKM2 catalyze the conversion of PEP and ADP to Pyruvate and ATP. PKM1 forms a constitutively active tetramer. PKM2 has additional regulatory domains that allow it to exist as a highly active tetramer or a weakly active dimer.

In humans, four isoforms of pyruvate kinase exist encoded on 2 separate genes.<sup>183</sup> The PKLR gene encodes PKL, expressed in the liver and kidneys, and PKR, expressed in erythrocytes.<sup>44</sup> The PKM gene encodes the PKM1 and PKM2 isoforms through mutually exclusive alternative isoform splicing of exon 9 and exon 10, respectively (Fig. 1.6).<sup>44</sup> The PKM2 isoform is expressed during embryogenesis, tissue regeneration, and in most cancer cells whereas PKM1 is expressed in brain cells, mature sperm, and cardiac, skeletal, and smooth muscle cells.<sup>44,184–186</sup> The mechanism by which cancer cells select for PKM2 expression has been well characterized. The alternative splicing mechanism that regulates inclusion of either exon 9 to produce PKM1 or exon 10 to

produce PKM2 is under the control of three heterogeneous nuclear ribonuclear proteins (hnRNP): polypyrimidine tract binding protein 1 (PTB, also known as hnRNP I), hnRNP A1, and hnRNP A2 heterogeneous riboproteins.<sup>187–189</sup> These riboproteins are under the regulation of CMYC which is commonly overexpressed in cancer cells including pancreatic cancer.<sup>188,190,191</sup> As mentioned above, KRAS activation is nearly universal in PDAC and CMYC is activated downstream of KRAS, thus connecting KRAS and PKM2 expression in pancreatic cancer (Fig. 1.6).<sup>76,191</sup>

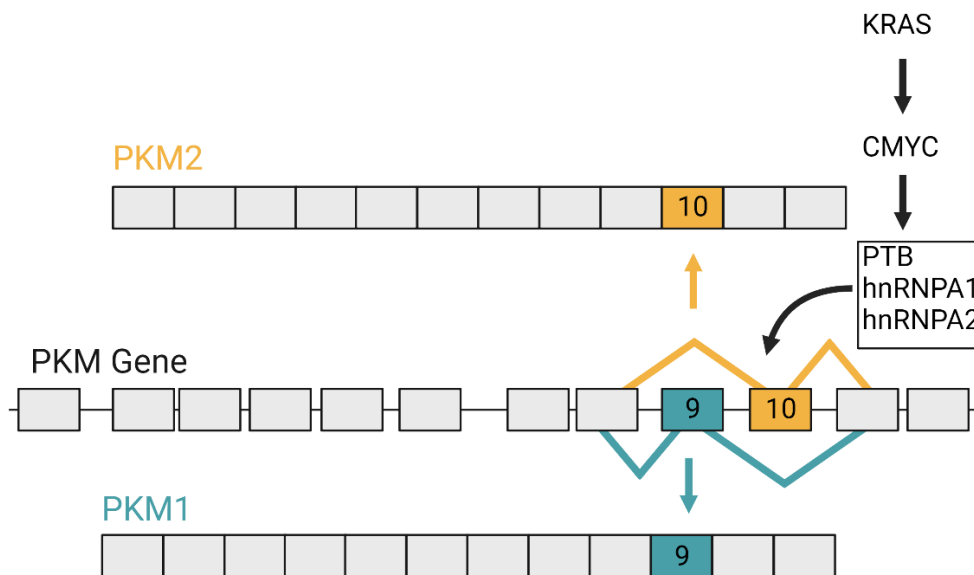


**Figure 1.6 Alternative splicing regulation of PKM1 and PKM2 cancer.**

PKM1 and PKM2 are produced by mutually exclusive alternative splicing of exons 9 and 10 respectively. Oncogenic activation of CMYC leads to upregulation of heterogeneous nuclear ribonuclear proteins PTB, A1, and A2 which promote inclusion of exon 10 to produce PKM2.

Each PKM isoform has the identical catalytic function and only differs by 22 amino acids.<sup>192</sup> However, this small difference produces a profound change in the regulatory

domains. PKM1 exists as a constitutively active tetramer while PKM2 exists as either an inactive dimer or active tetramer.<sup>193</sup> The altered amino acid sequence in PKM2 creates an allosteric regulatory domain that allows for binding of fructose-1,6-bisphosphate (FBP), a metabolite upstream in glycolysis. FBP stabilizes the tetramer form of PKM2 and activates the enzyme in a feed forward mechanism.<sup>193,194</sup> In addition to FBP, serine, succinyl-5-aminoimidazole-4-carboxamide-1-ribose 5'-phosphate (SAICAR), and histidine also promote the active tetramer form of PKM2.<sup>195-197</sup> On the other hand, cysteine, phenylalanine, alanine, tryptophan, thyroid hormone (T3), ATP, oxidative stress, and phospho-tyrosine signaling can inhibit tetramer formation and decrease the activity of PKM2.<sup>44,187,198-202</sup> (Fig. 1.7)

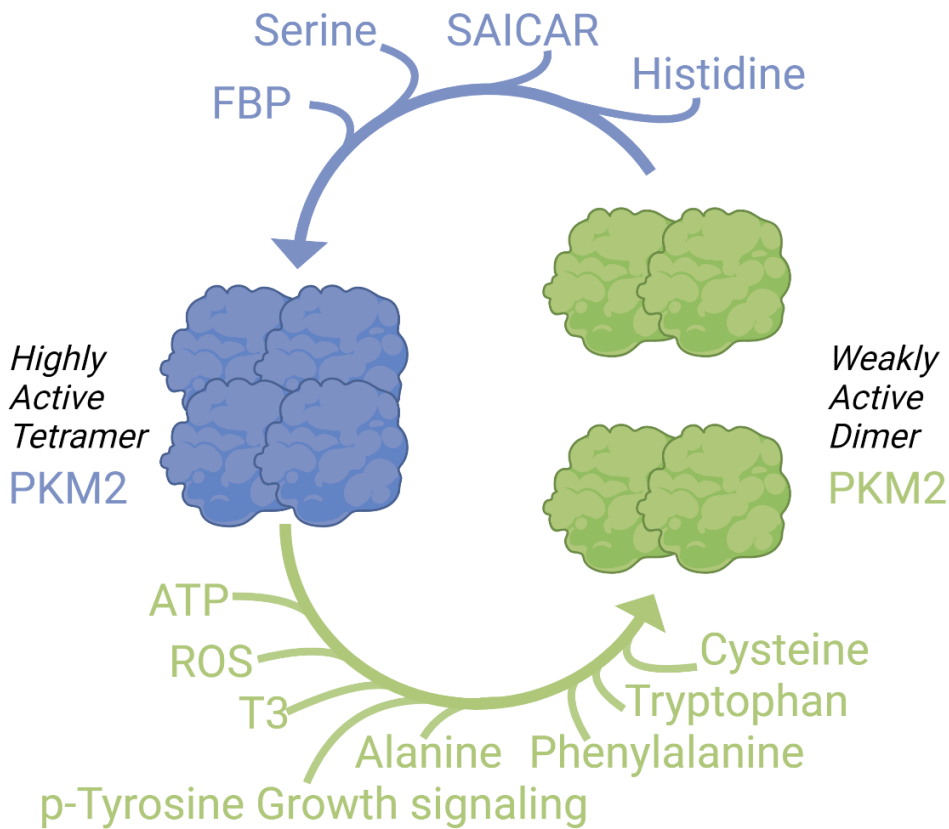


**Figure 1.7 Regulation of PKM2 activity.**

### Figure 1.7 (cont'd)

PKM2 is highly active in a tetrameric form and weakly active as a dimer. FBP, serine, SAICAR, and histidine promote activation of PKM2 by stabilizing the tetramer form. ATP, oxidative stress (ROS), T3, alanine, phenylalanine, tryptophan, cysteine, and phosphotyrosine growth signaling promote inhibition of PKM2 activity by destabilizing the tetramer form to produce the dimer form.

Interestingly, the metabolic reprogramming of cancer cells appears to be promoted through reduced PK enzymatic activity. Decreased PK activity allows for diversion of glycolytic intermediates into biosynthetic routes such as the PPP, serine biosynthesis, antioxidant response, and nucleotide production.<sup>201,203–205</sup> Decreased PK activity appears to be a survival response for pancreatic cancer cells growing in the low glucose conditions of the pancreatic TME.<sup>206</sup> Further, activation of PK activity by forcing over expression of PKM1 represses tumor growth.<sup>207,208</sup> To this end, several PKM2 activators, such as TEPP-46, have been developed and have demonstrated their ability to suppress tumor growth.<sup>177–179</sup> On the other hand, PKM2 inhibitors have also been identified, including Shikonin and compound 3k. Inhibition of PKM2 with these compounds disrupts metabolism, inhibits proliferation *in vitro* and suppresses tumor growth *in vivo*.<sup>179,180</sup> There is also evidence that inhibition of PKM2 activity overcomes chemoresistance and provides synergistic action when combined with chemotherapeutics such as gemcitabine, cisplatin, 5-FU, and docetaxel.<sup>179</sup> It is somewhat curious that both activation and inhibition of PKM2 can contribute to decreased tumor growth. These findings suggest that, while cancer cells preferentially inhibit PKM2 activity to promote growth, it is the flexibility of PKM2's activity

that critically allows cells to adaptively respond to energetic and biosynthetic demands.<sup>44</sup> Heterogeneous PKM2 and PKM1 expression within tumors has been reported, suggesting a potential role of metabolic cooperation between cells with varying degrees of PK activity and expression.<sup>207,209</sup> With this in mind, it is important to note that although PKM2 is nearly always present in cancer cells, it is not essential or required for tumorigenesis or tumor growth in a variety of tumor types.<sup>210-212</sup> Indeed, PKM1 expression may actually be advantageous to tumors under some circumstances and create subset of persistent cells within the tumor.<sup>207,213</sup> Interestingly, tumors produced from cells lacking PKM2 continue to undergo aerobic glycolysis and produce lactate, suggesting that sub-populations of non-proliferating cells that retain PKM1 may be responsible for lactate production.<sup>207</sup> Proliferating cells have been shown to use this lactate as metabolic fuel, creating a symbiotic heterogeneous environment within the tumor.<sup>214-217</sup> It has been argued that the loss of highly active PKM1 expression may be more important than retention of PKM2.<sup>207</sup> Further, tumor cells can sustain a low PK active state through repression of exon 9 to inhibit PKM1 expression without relying on PKM2.<sup>207</sup> This fact will be important to consider in the light evidence presented from our work in Chapter 3, that demonstrates that the activity of PK rather than isoform specificity is the important factor that influences ferroptosis.

In addition to the metabolic role of PKM2, there are controversial reports that PKM2 (but not PKM1) can translocate into the nucleus and influence gene expression.<sup>187</sup> Reportedly, epidermal growth factor receptor (EGFR) activated extracellular signal-regulated kinase 2 (ERK2) binds directly to PKM2 promoting its import to the nucleus.<sup>218</sup> PKM2 then acts as a coactivator of  $\beta$ -catenin to induce CMYC expression which

reciprocally influences PKM2 expression in a positive feedback loop as well as inducing increased expression of other metabolic genes such as GLUT1 and LDHA, thus regulating the Warburg Effect.<sup>187,218–222</sup> These studies suggest PKM2 functions as a protein kinase by using PEP as a phosphate donor to phosphorylate targets including Stat3, histone H3, and ERK1/2.<sup>187,218,223,224</sup> However, the fact that tumors can progress without the presence of PKM2 suggests that a transcriptional role of PKM2 in cancer progression is limited.<sup>44,209,225</sup> Additionally, recent work has shown a lack of evidence for this activity and points to contaminating ATP dependent protein kinases making PKM2's role as a transcription factor unlikely.<sup>226</sup> It is only the dimeric (less active) form of PKM2 that reportedly can translocate into the nucleus to effect this change.<sup>187</sup> Therefore it is difficult to deconvolute the influence of the reprogrammed metabolic effects on gene expression from purely PKM2 dependent gene expression modulation. Overall, the evidence suggests that it is the metabolic effects of PKM2 that provide the critical advantage for cancer cells.

Given that cancer cells function with low PK activity, there remain open questions on what additional metabolic pathways cells rely on to produce pyruvate and supply glucose derived carbon to the TCA cycle. In the next chapter, I will discuss how our lab began to address this question and how this laid the preliminary groundwork for the major focus of my subsequent research.

## CHAPTER 2: CYSTEINE CATABOLISM AND THE SERINE BIOSYNTHESIS PATHWAY SUPPORT PYRUVATE PRODUCTION DURING PYRUVATE KINASE KNOCKDOWN IN PANCREATIC CANCER CELLS

### Preface

This chapter is a modified version of a previously published article:

Lei Yu, Shao Thing Teoh, **Elliot Ensink**, Martin P. Ogrodzinski, Che Yang, Ana I. Vazquez, and Sophia Y. Lunt. Cysteine catabolism and the serine biosynthesis pathway support pyruvate production during pyruvate kinase knockdown in pancreatic cancer cells. *Cancer & Metabolism* **7**, 13 (2019)

This work was the primary project of the former postdoctoral researcher, Lei Yu, in the Lunt lab. In my first 2 years in the Lunt lab, I was able to contribute to the methodology, experiment design, and writing for this project which laid the foundation for my future project that will be discussed in Chapter 3.

### Introduction

Pancreatic ductal adenocarcinoma (PDAC) is a devastating disease with < 10% of patients surviving beyond 5 years after diagnosis.<sup>227</sup> It is currently the fourth leading cause of cancer-related death in western countries and is expected to be the second leading cause by 2030.<sup>228</sup> Currently, treatment options for pancreatic cancer patients include surgical resection, radiation therapy, and/or systemic chemotherapy.<sup>229,230</sup> However, current therapies often fail because most patients are diagnosed at advanced stages. Given the poor outlook for PDAC patients, it is critical to improve our understanding of pancreatic cancer cells to design improved treatment strategies.

Reprogramming cancer metabolism is recognized as a hallmark of cancer.<sup>62</sup> Many

tumor cells exhibit the “Warburg effect,” fermenting glucose to lactate even in the presence of abundant oxygen.<sup>42,58</sup> Indeed, pancreatic cancer cells rewire metabolism to utilize a wide range of nutrients including glucose, extracellular proteins, and various amino acids to support survival and proliferation.<sup>231–233</sup> Targeting metabolic pathways specifically upregulated in PDAC cells may be a promising direction for therapy.<sup>234</sup>

Altered metabolism in cancer cells is supported in part by the expression of a specific isoform of pyruvate kinase (PK), a glycolytic enzyme which catalyzes the conversion of phosphoenolpyruvate (PEP) and ADP into pyruvate and ATP.<sup>235</sup> Pyruvate kinase has four isoforms (L, R, M1, and M2) encoded by two genes.<sup>44</sup> The PKLR gene encodes PKL and PKR, and the PKM gene encodes PKM1 and PKM2 through alternative splicing of exons 9 and 10, respectively.<sup>183</sup> PKL is mainly expressed in the liver, kidney, and small intestine and PKR in erythrocytes.<sup>236,237</sup> PKM1 is mainly expressed in differentiated tissues such as muscle, heart, and brain, whereas PKM2 is expressed in various adult tissues and many proliferating cells, including embryonic and tumor cells.<sup>44,236–238</sup> Generally, expression of PKM1 and PKM2 is mutually exclusive in a given cell type, and loss of PKM2 leads to compensatory expression of PKM1.<sup>205</sup> PKM2 is highly expressed in a variety of human cancer cells, including pancreatic cancer cells.<sup>239</sup> PKM2 has been reported to promote proliferation, migration, invasion, and tumorigenesis in pancreatic cancer.<sup>240–242</sup> However, there are conflicting reports regarding the expression of PKM2 and overall patient survival: some studies show that PKM2 expression is associated with worse overall survival of pancreatic cancer patients<sup>240,243,244</sup>, while others show improved overall survival<sup>245</sup>, and still others show no effect on overall survival.<sup>246,247</sup> A recent study demonstrated that expression of PKM1, but not PKM2, promotes small-

cell lung cancer cell growth.<sup>213</sup> Other studies reported that PKM2 is dispensable for leukemia, liver cancer, colon cancer, lymphoma, lung cancer, and pancreatic cancer.<sup>209–212,225</sup>

Given the controversial roles of pyruvate kinase in cancer, we investigated the function of PKM1/2 for pancreatic cancer in PDAC cells derived from a KrasG12D<sup>-/-</sup>; p53<sup>-/-</sup> pancreatic mouse model. Our results demonstrate that knockdown of PKM2 results in expression of PKM1 and does not affect pancreatic cancer cell proliferation. Additionally, pancreatic cancer cells are able to proliferate even with concurrent knockdown of both PKM1 and PKM2 isoforms. Further, they are able to produce pyruvate from glucose with knockdown of both PKM1 and PKM2 isoforms. We explored the contributions of alternative pathways to pyruvate production, such as the serine biosynthesis pathway and the sialic acid pathway during PKM1/2 knockdown. Knockout of phosphoglycerate dehydrogenase (PHGDH), the rate-limiting enzyme in the serine biosynthesis pathway, decreased pyruvate production from glucose in PKM1/2 knockdown cells. However, knockout of N-acetylneuraminase pyruvate lyase (NPL), which can convert phosphoenolpyruvate to pyruvate in the sialic acid pathway, did not decrease pyruvate production from glucose. Using multiple isotopically labeled precursors, we discovered that glucose contributes to only ~ 40% of intracellular pyruvate, and amino acid cysteine contributes ~ 20% of intracellular pyruvate in these cells. The relatively low contribution of glucose to pyruvate in combination with alternative sources for pyruvate generation may explain the minimal impact of PKM1/2 knockdown on pancreatic cancer cell proliferation.

## **Results**

### **PKM2 and PKM1/2 knockdown do not decrease pancreatic cancer cell proliferation**

To study the role of pyruvate kinase in pancreatic cancer proliferation, we characterized PDAC cell lines (A13M2-1 and A13M13) derived from a *Kras*<sup>G12D</sup>/-; *p53*<sup>-/-</sup> mouse pancreatic tumor.<sup>248</sup> A13M2-1 contains a doxycycline inducible hairpin that knocks down ~ 85% of PKM2 expression after 7 days of doxycycline treatment. Knockdown of PKM2 does not arrest proliferation of PDAC cells (Fig. 2.1A). Consistent with previous reports<sup>210</sup>, knockdown of PKM2 in PDACs induced PKM1 expression (Fig. 2.1A). Since PKM1 expression may compensate for PKM2 knockdown, we further knocked down both PKM1 and PKM2 expression in the A13M13 cell line, which contains a doxycycline-inducible short hairpin RNA (shRNA) that knocks down ~ 85% of both PKM1 and PKM2 after 7-day doxycycline treatment (Fig. 2.1B and A.1A). Unexpectedly, knockdown of both M1 and M2 isoforms still does not affect PDAC cell proliferation (Fig. 2.1B). To ensure that PKL or PKR expression was not induced after PKM1/2 knockdown, we probed the expression of PKL/R in PDAC cells. Western blot results indicated that there is no PKL/R expressed in A13M13 cells (Fig. A.1B). We also measured intracellular metabolites levels following knockdown of both M1 and M2 isoforms in A13M13 PDAC cells (Fig. 2.1C). Knockdown of PKM1/2 greatly elevated upstream intermediates of glycolysis, such as 2/3-phosphoglycerate (2/3-PG) and phosphoenolpyruvate (Fig. 2.1C). This is consistent with decreased glycolytic flux through PK, indicating that PK is the rate-limiting step in glycolysis during PKM knockdown. Pyruvate levels were unchanged, but downstream intermediate lactate was significantly decreased with PKM1/2 knockdown. We further performed <sup>13</sup>C-glucose labeling experiments to determine how glucose is

processed through different metabolic pathways. Surprisingly, PDACs with PKM1/2 knockdown are able to generate proportionally similar amounts of  $^{13}\text{C}$ -labeled pyruvate (Fig. 2.1D). Approximately 60% of pyruvate and 90% of lactate and alanine were labeled in PDAC cells with PKM1/ 2 knockdown, indicating that pyruvate can still be made from glucose despite targeting a key glycolytic enzyme.

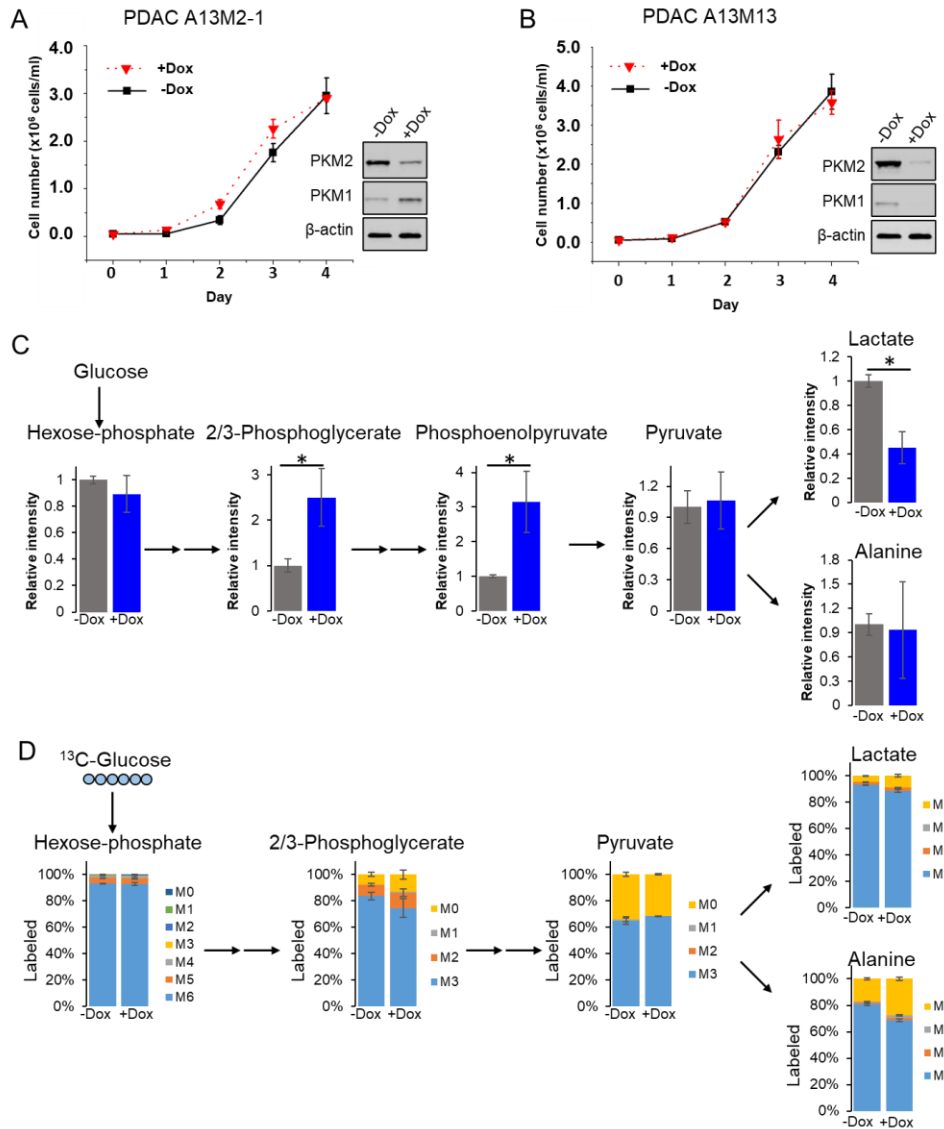


**Figure 2.1 PKM2 and PKM1/2 knockdown do not decrease proliferation of pancreatic cancer cells.**

### **Figure 2.1 (cont'd)**

**A, B.** PDACs proliferate at the same rate with (+Dox) or without (-Dox) PKM1/2 knockdown. Proliferation was assessed by counting cell numbers in triplicates for 4 days following 7 days of vehicle (-Dox) or 1 µg/ml doxycycline (+Dox) treatment to maximize PKM2 or PKM1/2 knockdown. Western blot confirms PKM1/2 knockdown in PDACs after 7 days of vehicle (-Dox) or doxycycline (+Dox) treatment. **C.** Relative intracellular metabolites levels are represented by peak intensities and are displayed relative to -Dox averages. **D.** <sup>13</sup>C-glucose labeling of intracellular metabolites for 24 h in A13M13 PDAC cells with vehicle (-Dox) or PKM1/2 knockdown (+Dox). The y-axis for all graphs is the percent labeling of indicated <sup>13</sup>C-isotopologue.

### **Serine biosynthesis pathway is upregulated in PDACs following PKM1/2 knockdown**

While PKM1/2 knockdown does not decrease PDAC cell proliferation (Fig. 2.1B), it does impact cellular metabolism. PDACs displayed different intracellular metabolic profiles upon PKM1/2 knockdown (Fig. 2.2A). As expected, PKM1/2 knockdown causes an accumulation of glycolytic intermediates upstream of pyruvate, including fructose 1,6-bisphosphate (FBP), 2/3-PG, and PEP. In addition, serine biosynthesis pathway intermediates phosphoserine and serine were vastly elevated. In contrast, many other amino acids were decreased in PKM1/2 knockdown cells (Fig. 2.2A). Further investigation with <sup>13</sup>C-glucose labeling studies showed that glucose flux to serine is upregulated in PDACs with PKM1/2 knockdown (Fig. 2.2B). Since serine can be converted to pyruvate via the action of serine dehydratase<sup>249,250</sup>, we postulated that the

serine biosynthesis pathway may be one way to circumvent PKM1/2 knockdown in pancreatic cancer cells (Fig. 2.2C).

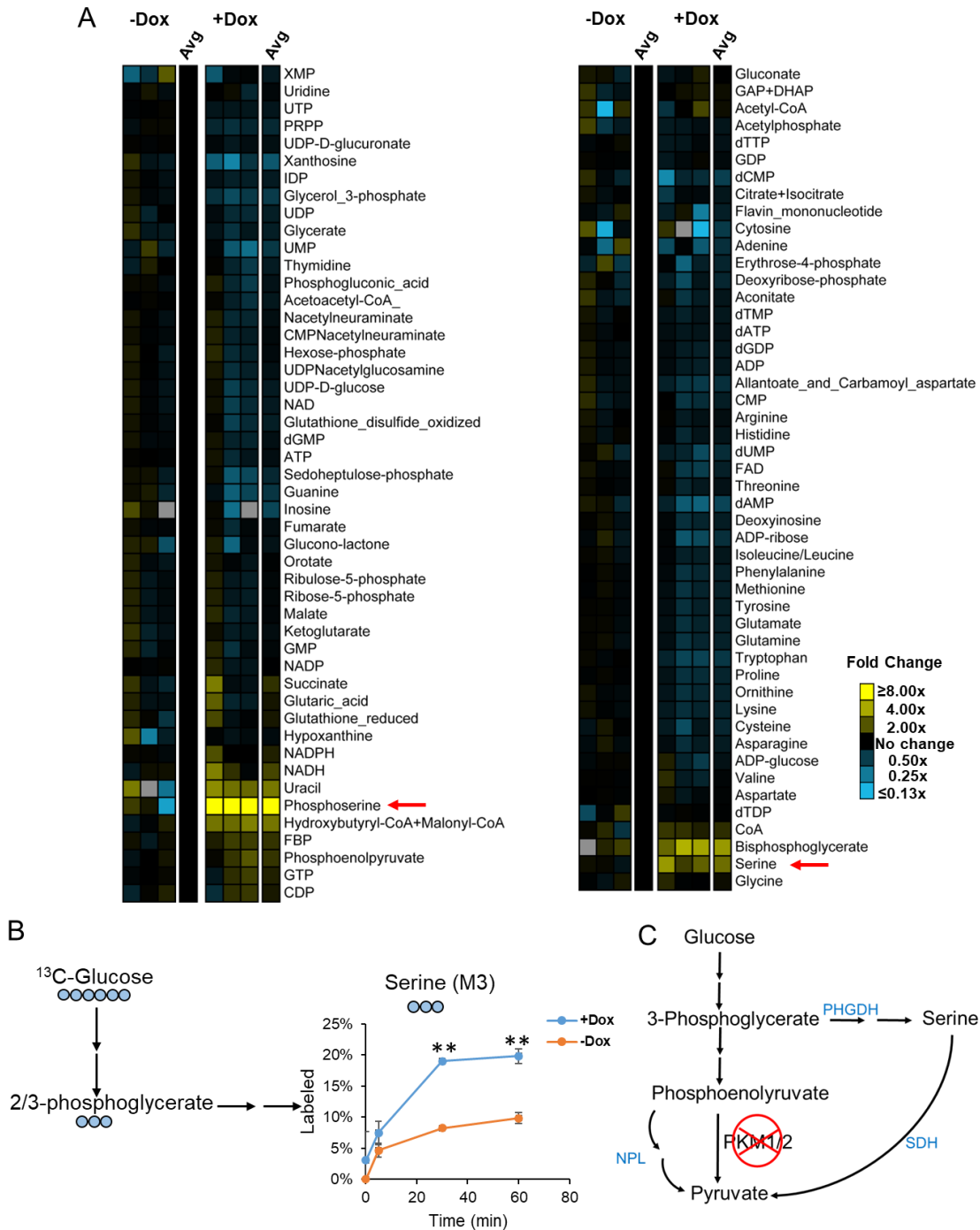


**Figure 2.2** Pancreatic cancer cells upregulate the serine biosynthesis pathway following PKM1/2 knockdown.

## Figure 2.2 (cont'd)

**A.** Pool sizes of intracellular metabolites in PDAC cells treated with (+Dox) or without (-Dox) PKM1/2 knockdown were detected using UPLC-MS/MS. **B.**  $^{13}\text{C}$ -Glucose flux to serine is upregulated in A13M13 PDAC cells with PKM1/2 knockdown (+Dox). **C.** Metabolic pathways that may generate pyruvate from upstream glycolytic intermediates during PKM knockdown.

### **PHGDH knockout depletes intracellular serine and decreases pyruvate production**

It is possible that cells bypass PKM1/2 knockdown and convert glucose to pyruvate through the serine biosynthesis pathway (Fig. 2.2C). To explore this possibility, we targeted the serine biosynthesis pathway by deleting phosphoglycerate dehydrogenase (PHGDH), the rate-limiting enzyme in this pathway. PHGDH converts  $\text{NAD}^+$  and 3-phosphoglycerate to  $\text{NADH}$  and 3-phosphohydroxypyruvate.<sup>251–253</sup> We deleted PHGDH using CRISPR/Cas9 gene editing technology. We successfully generated PHGDH knockout (KO) PDAC populations and single cell clones, as confirmed by Western blotting (Figure A.2F) and DNA sequencing (Figure A.3). We find that PHGDH KO does not affect PDAC population cell proliferation following PKM1/2 knockdown (Fig. 2.3A and A.2A–E). We also measured the levels of serine in PHGDH KO clone cells. As expected, knocking out PHGDH significantly decreased serine levels (Fig. 2.3B). We also find that PHGDH KO indeed led to reduced pyruvate levels (Fig. 2.3B). Interestingly, PHGDH KO resulted in decreased levels of upstream glycolytic intermediates 2/3-PG and PEP (Fig. 2.3B), suggesting that targeting the serine biosynthesis pathway may downregulate glycolysis. We further performed  $^{13}\text{C}$ -glucose labeling and confirmed that knockout of PHGDH

abolished serine and glycine production from  $^{13}\text{C}$ -glucose as indicated by loss of M3 and M2 labeling in serine and glycine, respectively (Fig. 2.3C). Additionally, the fraction of M3-labeled pyruvate from  $^{13}\text{C}$ -glucose was slightly decreased, indicating that the serine biosynthesis pathway indeed contributes to pyruvate production during PKM1/2 knockdown.

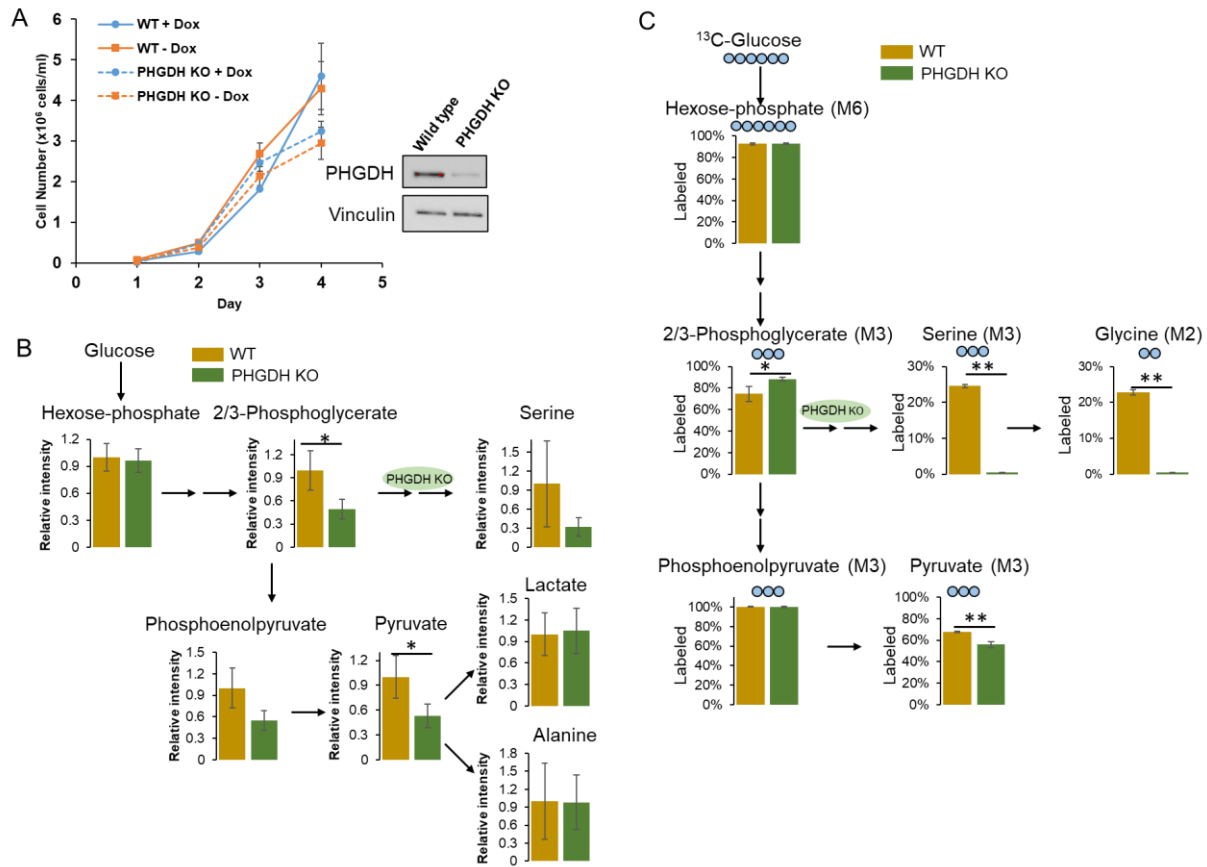


**Figure 2.3 PHGDH knockout depletes intracellular serine, slightly decreases pyruvate generation, but does not affect cell proliferation.**

**A.** Proliferation rates of wild-type A13M13 (PHGDH WT) or PHGDH knockout (PHGDH KO) populations of PDACs with vehicle (-Dox) or PKM1/2 knockdown (+Dox). Cell counts were measured daily (n = 3) after vehicle or doxycycline treatment. Western blot confirms PHGDH knockout in PDACs. **B.** Relative intracellular metabolites levels are represented

### **Figure 2.3 (cont'd)**

by peak intensities and are displayed relative to WT metabolite intensity averages. Cells are collected after 7 days of doxycycline treatment. Values are the average of three biological replicates. Error bars represent standard deviation. **C.**  $^{13}\text{C}$ -Glucose labeling of intracellular metabolites for 24 h in WT and PHGDH KO PDAC clone P24 cells with PKM1/2 knockdown. The y-axis for all graphs is the percent labeling of indicated full labeled  $^{13}\text{C}$ -isotopologue.

### **PHGDH/NPL dual knockout does not impact cell growth rate and pyruvate generation**

Since  $^{13}\text{C}$ -glucose still contributes to a significant fraction of labeled pyruvate in PHGDH KO cells with PKM1/2 knockdown (Fig. 2.3C), we investigated whether the sialic acid pathway contributes to producing pyruvate from upstream glycolytic intermediates (Fig. 2.2C). N-acetylneuraminase synthase (NANS) produces N-acetylneuraminic acid (sialic acid) from N-acetylmannosamine and PEP, while N-acetylneuraminase pyruvate lyase (NPL) catalyzes the degradation of sialic acid into N-acetylmannosamine and pyruvate<sup>254,255</sup>; hence, this pathway could potentially bypass pyruvate kinase to convert glucose-derived phosphoenolpyruvate into pyruvate. To test this possibility, we generated NPL knockout PDAC cells by using CRISPR/Cas9. NPL knockout PDAC clones can proliferate as well as wild-type PDAC cells following PKM1/2 knockdown (Fig. A.4A). Since it is possible that cells use the serine biosynthesis pathway for pyruvate generation during NPL knockout, we further generated PHGDH/NPL dual knockout (dual KO) PDAC cells by using CRISPR/Cas9 (Fig. A.5), as confirmed by sequencing (Fig. A.6). We find

that dual KO cells do not suffer loss of proliferative ability with PKM1/2 knockdown (Fig. 2.4A). We further investigated the metabolic impacts in PHGDH/NPL dual KO cells using  $^{13}\text{C}$ -glucose labeling. Glucose can still be converted into pyruvate in wild-type and dual KO cells following PKM1/2 knockdown (Fig. 2.4B). Although N-acetylneuraminic acid is labeled by  $^{13}\text{C}$ -glucose after 24 h (Fig. A.1C), it was not labeled in either wild-type or PHGDH/NPL dual KO cells after 60 min, indicating that  $^{13}\text{C}$ -glucose did not go through the sialic acid pathway to generate labeled pyruvate in this experiment.

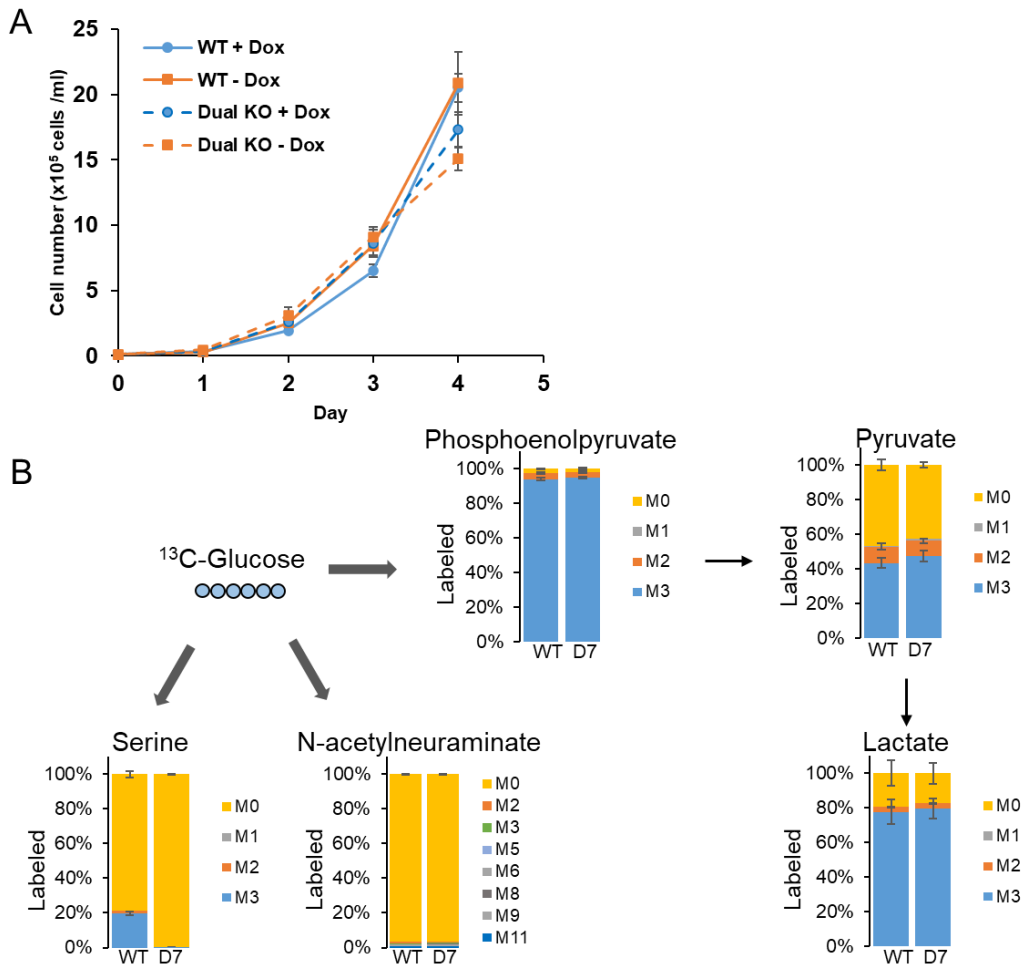


**Figure 2.4 PHGDH and NPL dual KO does not impact growth rate and pyruvate generation from glucose.**

**A.** Average proliferation rates of 3 PHGDH/ NPL dual knockouts (dual KO) clones or WT

## Figure 2.4 (cont'd)

PDACs with vehicle (-Dox) or PKM1/2 knockdown (+Dox). Cell counts were measured daily (n = 3). **B.**  $^{13}\text{C}$ -Glucose labeling of intracellular metabolites for 60 min in wild-type (WT) or PHGDH/NPL dual knockout clone D7 cells with PKM1/2 knockdown for 60 min. The y-axis for all graphs is the percent labeling of indicated  $^{13}\text{C}$ -isotopologue.

### Other sources of pyruvate

A significant fraction of pyruvate remains unlabeled even after incubation with  $^{13}\text{C}$ -glucose for 24 h in both wildtype and PHGDH KO cell lines with or without PKM1/2 knockdown (Fig. 2.3C). This suggests that pyruvate can be generated from sources other than glucose in these cell lines. Potential pathways that can generate pyruvate during PKM1/2 knockdown are shown in Fig. 2.5a. Studies of pyruvate metabolism demonstrate that anaplerotic pyruvate entry by pyruvate carboxylase (PC) in the mitochondria will generate oxaloacetate, which can produce phosphoenolpyruvate through mitochondrial phosphoenolpyruvate carboxykinase (PEPCK-M). PEP is then transported out of the mitochondrial matrix by an anion transporter into the cytosol. Cytosolic malate also can be converted to pyruvate through malic enzyme. To determine whether PC, PEPCK-M, or malic enzyme actively contribute to pyruvate production in PDAC cells, we characterized  $^{13}\text{C}$ -glutamine labeling in dual KO cells. While a large proportion of citrate (~ 60%) and malate (~ 80%) were labeled from  $^{13}\text{C}$ -glutamine, the downstream metabolites of pyruvate—lactate and alanine— remained virtually unlabeled (Fig. 2.5B). These results suggest that glutamine-derived TCA cycle intermediates are not converted into pyruvate in these cells. We further extended the labeling time and showed that

pyruvate, alanine, and lactate are not labeled by  $^{13}\text{C}$ -glutamine even after 24 h (Fig. 2.13A). Pyruvate can also be produced from several other amino acids. Serine can be converted to pyruvate by serine dehydratase. Threonine can be cleaved to yield glycine<sup>256</sup>, which is converted to serine by serine hydroxymethyltransferase (SHMT) and then converted to pyruvate by serine dehydratase. Tryptophan catabolism via the kynurenine pathway yields alanine<sup>257</sup>, which can be converted to pyruvate via transamination. Cysteine may also be catabolized to yield pyruvate and inorganic bisulfite<sup>258</sup>. We further investigated pyruvate generation from amino acids by using  $^{13}\text{C}$ -serine,  $^{13}\text{C}$ -tryptophan,  $^{13}\text{C}$ -threonine, and  $^{13}\text{C}$ -cysteine tracers (Fig. A.7). Surprisingly, we find that  $^{13}\text{C}$ -serine has negligible contribution to pyruvate and lactate labeling (Fig. 2.5C and A.7D). On the other hand, cysteine contributes to an unexpectedly large proportion (~ 20%) of pyruvate in dual KO cells (Fig. 2.5D). Cysteine has not been previously reported as a major source of pyruvate production in PDAC cells. WT PDAC cells also produce labeled pyruvate (~ 10%) from  $^{13}\text{C}$ -cysteine (Fig. A.8), indicating that these cells generally produce pyruvate from cysteine. The lower production of pyruvate from cysteine in WT cells (~ 10%) compared to PHGDH/NPL dual KO cells (~ 20%) is likely due to the dual KO cells having impaired pyruvate production through other pathways (e.g., serine biosynthesis pathway) and requiring a larger proportion of pyruvate production from cysteine. Other amino acids did not significantly contribute to the production of pyruvate (Fig. 2.5D). To better understand the sources of pyruvate, we performed a multi-tracer experiment in PHGDH/NPL dual KO cells. Cells were cultured with 1,2- $^{13}\text{C}$ -glucose, 5- $^{13}\text{C}$ -glutamine, and U- $^{13}\text{C}$ -cysteine for 60 min (Fig. 2.6). Approximately 40% of pyruvate is generated from glucose, as 20% of labeled pyruvate

(M2) and 20% of unlabeled pyruvate (M0) comes from 1,2-<sup>13</sup>C-glucose. Consistent with the lack of alanine and lactate labeling from <sup>13</sup>C-glutamine (Fig. 2.5B), pyruvate, alanine, and lactate were not labeled by <sup>13</sup>C-glutamine in this multitracer experiment. Interestingly, 20% of labeled pyruvate (M3) comes from <sup>13</sup>C-cysteine.

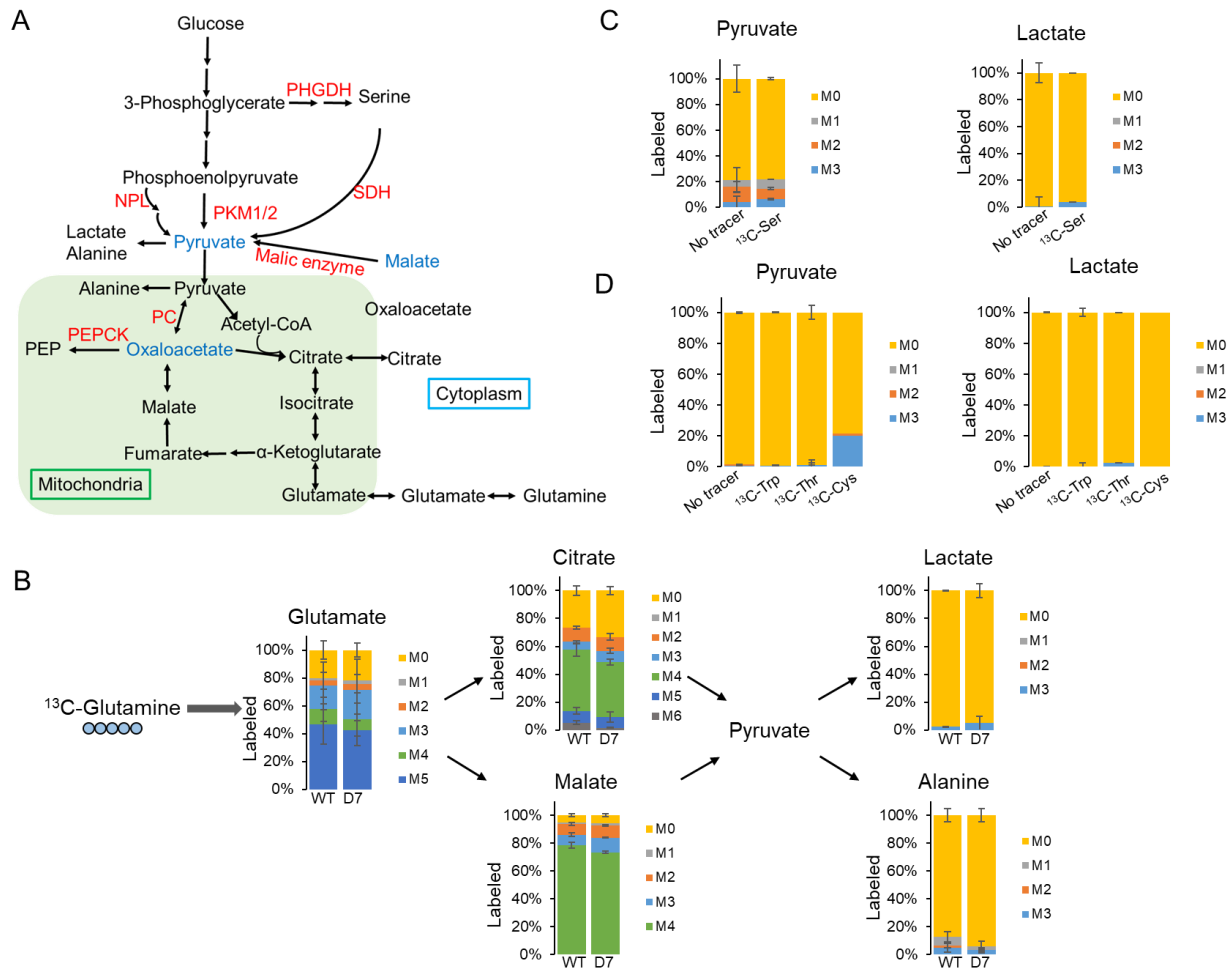


**Figure 2.5 Investigation of additional pathways for pyruvate generation.**

**A.** Metabolic pathways that may generate pyruvate from other intermediates during PKM1/2 knockdown. **B.** <sup>13</sup>C-Glutamine labeling of intracellular metabolites for 60 min in WT and PHGDH/NPL dual KO D7 PDAC cells with PKM1/2 knockdown. **C.** <sup>13</sup>C-Serine labeling of intracellular metabolites for 60 min in PHGDH/NPL dual KO D7 PDAC cells

## Figure 2.5 (cont'd)

with PKM1/2 knockdown. **D.**  $^{13}\text{C}$ -Tryptophan,  $^{13}\text{C}$ -threonine, and  $^{13}\text{C}$ -cysteine labeling of intracellular metabolites for 60 min in PHGDH/NPL dual KO D7 PDAC cells with PKM1/2 knockdown. The y-axis for all graphs is the percent labeling of indicated  $^{13}\text{C}$ -isotopologue.

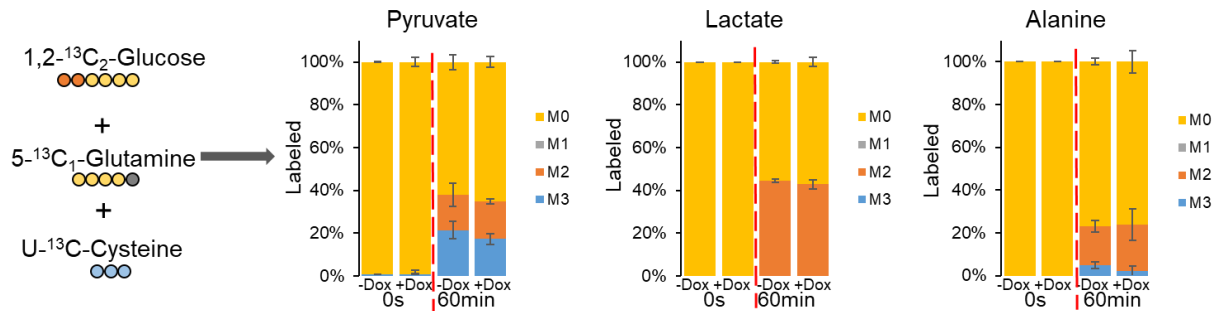


## Figure 2.6 Cysteine contributes to pyruvate production in PDAC cells.

Labeling with multiple tracers shows that ~ 20% of pyruvate is generated from cysteine. Multi-tracer of 1,2- $^{13}\text{C}_2$ -glucose, 5- $^{13}\text{C}_1$ -glutamine, and  $^{13}\text{C}$ -cysteine labeling of intracellular metabolites in PHGDH/NPL dual knockout D7 PDAC cells following with vehicle (-Dox) or PKM1/2 knockdown (+Dox). The y-axis for all graphs is the percent labeling of indicated  $^{13}\text{C}$ -isotopologue.

## Discussion

In this study, we demonstrate that pancreatic cancer cells can rewire their metabolism and continue to proliferate during PKM1/2 knockdown. PKM2 in cancer has been studied since the early twenty-first century, but its roles remain controversial. High expression of PKM2 is correlated with poor prognosis in pancreatic cancer patients<sup>240,243,244</sup>, and suppression of PKM2 expression resulted in decreased cell survival.<sup>240,259</sup> On the contrary, our results, like other published studies investigating

PKM2 function in pancreatic cancer<sup>206,210</sup>, showed that knockdown of PKM2 expression has no effect on PDAC cell proliferation. Similar results were observed in other cancer models, including breast cancer<sup>207</sup>, hepatocellular carcinoma<sup>209</sup>, colon cancer<sup>211</sup>, and leukemia<sup>225</sup>. Differences between our results and published reports may be due to incomplete knockout of PKM1/2 in our cells; despite ~ 85% depletion in PKM1/ 2 expression, a small fraction of PKM1/2 may be enough for maintaining pyruvate production. Complete knockout of PKM1/2 did not yield any surviving clones in multiple experiments, indicating a small amount of PKM1/2 is likely essential for in vitro survival of these cells. The impact of pyruvate kinase on cancer cell proliferation is likely dependent on the context of each cancer cell, including genetic makeup, mutations, and the microenvironment.

We find that downregulation of PKM1/2 expression does not impact pyruvate production in PDAC cells. However, we do observe rewiring of metabolism following PKM1/2 knockdown: there is accumulation of upstream glycolytic intermediates, consistent with previous reports.<sup>186,212,259</sup> We further find that PKM1/2 knockdown causes an increase in serine biosynthesis intermediates. This may be due to an accumulation of upstream glycolytic intermediates causing increased flux through the serine biosynthesis pathway. Knockout of PHGDH, the rate-limiting enzyme in the serine biosynthesis pathway, decreases pyruvate production as indicated by both pyruvate levels (Fig. 2.3B) and pyruvate labeling from <sup>13</sup>C-glucose (Fig. 2.3C). Thus, our data suggests that the serine biosynthesis pathway contributes to the production of pyruvate from glucose during PKM1/2 knockdown. However, since addition of <sup>13</sup>C-serine to the media does not result in pyruvate labeling (Fig. 2.5C), serine imported from the media does not appear to be

directly converted into pyruvate. It is possible that flux through the serine biosynthesis pathway may have a regulatory effect on pyruvate production since serine is an allosteric activator of PKM2.<sup>196</sup> Despite reports that suppression of PHGDH can impair cancer cell proliferation<sup>252,253,260</sup>, we find that PHGDH deletion does not attenuate cell proliferation in PDAC cells. This may be related to the fact that <sup>13</sup>C-glucose-derived serine comprises only a small fraction of overall serine; most serine remained unlabeled after 24 h (Fig. 2.3C) and presumably originated from the culture media. This data agrees with another study that shows the majority of intracellular serine is obtained extracellularly in T cells.<sup>261</sup> Finally, we note that PHGDH KO results in accumulation of nucleotide intermediates (PRPP, UMP, UTP, UDP, dUMP, dTMP, dTTP, and ATP), TCA cycle intermediates (αketoglutarate, fumarate, and citrate/isocitrate), and many amino acids (Fig. A.9), indicating that PHGDH deletion causes glucose flux to be shunted to nucleotides, the TCA cycle, and amino acid biosynthesis.

During PKM1/2 knockdown, cell growth is supported in part by alternative pathways that generate pyruvate, including breakdown of exogenous amino acids. We explored the breakdown of cysteine, serine, glutamine, tryptophan, and threonine into pyruvate. Cysteine is a key sulfur-containing semi-essential amino acid which plays important functions in redox homeostasis, protein function, and metabolism.<sup>262</sup> Interestingly, our results show that about 20% of pyruvate came from <sup>13</sup>C-cysteine (Fig. 2.6). This is an unexpectedly high fraction since cysteine has not been previously reported as a major source of intracellular pyruvate in PDAC cells. WT PDAC cells also generate pyruvate from <sup>13</sup>C-cysteine (Fig. A.7), indicating that this is a general pathway of cysteine production in these cells. The higher fraction of cysteine-derived pyruvate in PHGDH/NPL

dual KO cells (~20%; Fig. 2.6) compared to WT cells (~ 10%; Fig. A.8) may be due to the dual KO cells having impaired pyruvate production through other pathways (e.g., serine biosynthesis pathway) and hence requiring a larger proportion of pyruvate generation from cysteine. We also observed a trend toward decreased cysteine pools in the WT cells upon PKM knockdown (Fig. 2.2A) which may be indicative of cysteine utilization to produce pyruvate, supporting the notion that cysteine is a major source of pyruvate in PDAC cells. The labeled pyruvate from  $^{13}\text{C}$ -cysteine is not further converted to lactate or alanine, as indicated by the absence of M3 lactate labeling in either metabolite (Fig. 2.6). Since lactate is produced in the cytosol, and alanine is predominantly produced in the mitochondria, this data may suggest that cysteine is converted to pyruvate within another cellular compartment that is distinct from either the cytosol or mitochondria. The dependence on cysteine is a potential metabolic adaptation for pyruvate generation in PDAC cells. Glutamine is another potential source of pyruvate that we investigated. As the most abundant amino acid in plasma, upregulated glutamine metabolism has been found in several cancer types.<sup>234</sup> Once transported into mitochondria, glutamine serves as a carbon source for the production of fatty acids, nucleotides, and TCA cycle intermediates, and up to 60% of glutamine has been reported to be used for generating lactate and alanine. In our study, glutamine does not contribute to pyruvate generation in PDACs (Fig. 2.5B and A.7A), despite their dependence on glutamine for proliferation (Fig. A.10). Tryptophan and threonine can also be converted to pyruvate, but this was not observed in our cells (Fig. 2.5D and A.7B-C). Thus, our results show that ~40% of pyruvate is generated from glucose and ~ 20% of pyruvate is generated from cysteine. For our labeling experiments, we used DMEM formulated without pyruvate and dialyzed

FBS that does not contain low molecular weight compounds like amino acids. We further checked the media by LC-MS/MS and confirmed that both dialyzed FBS and DMEM contain negligible amounts of pyruvate (Fig. A.11). It is possible that the remaining unlabeled portion of pyruvate is produced from amino acids released by degradation of serum proteins in the media, as macropinocytosis and extracellular protein scavenging has been observed in pancreatic cancer cells.<sup>93,94,263</sup> Since the cells produce pyruvate from cysteine, cystine in the media—which can be imported via xCT and subsequently converted to cysteine intracellularly—may also contribute to the unlabeled portion of pyruvate.

### **Conclusions**

Pancreatic cancer cells rewire their metabolism during pyruvate kinase knockdown. The serine biosynthesis pathway enables some conversion of glucose to pyruvate during pyruvate kinase knockdown; however, since direct conversion of serine to pyruvate was not observed, it appears that the serine pathway contributes to pyruvate generation through a potentially regulatory mechanism. We also find that a surprisingly large percentage of intracellular pyruvate comes from cysteine. Our study reveals the resilience of PDAC cells to pyruvate kinase knockdown, underscoring the metabolic flexibility of these cells to overcome environmental perturbation and maintain proliferation.

### **Acknowledgements**

We thank Talya Dayton and Tyler Jacks for sharing the A13M2-1 and M13 cell lines. We thank the Michigan State University RTSF Mass Spectrometry and Metabolomics Core for helpful technical assistance. We also thank Deanna Broadwater for critical reading of this manuscript.

## **Author Contributions**

SYL and LY conceived and designed the study. LY carried out the experiments, performed the data analysis, and wrote the manuscript. CY performed the experiments. EE performed experiments and assisted with data analysis. STT and MO assisted with the data analysis. LY, STT, EE, MO, CY, AIV, and SYL wrote and revised the manuscript. All authors read and approved the final manuscript.

## **Materials and Methods**

### **Cell culture**

A13M2-1 and A13M13 cell lines were derived from  $Kras^{G12D/-}; p53^{-/-}$  pancreatic mouse tumor and contain doxycycline-inducible hairpins that target PKM2 or both PKM1 and PKM2, respectively.<sup>248,264</sup> Cells were cultured in Dulbecco's modified eagle medium (DMEM) (Fisher Scientific, MT10017CV) without sodium pyruvate, supplemented with 10% fetal bovine serum (FBS), 1% penicillin and streptomycin (P/S), and 1% glutamine and cultured in a humidified incubator with 5% CO<sub>2</sub> at 37 °C. For cells infected with inducible vectors, doxycycline aqueous solution (1 mg/ml as stock solution) was added at the time of plating at a final concentration of 1 µg/ml. Cells were passaged in doxycycline-containing media for 7 days to maximize knockdown of PKM1/2 before experiments were conducted.

### **Cell proliferation assay**

The cells were seeded at 25,000 per well in 6-well plates in normal cell growth medium. Cell counts were obtained using a Cellometer Auto T4 Cell Counter (Nexcelom).

### **Gene knockout by CRISPR/Cas9 gene editing**

We used CRISPR/Cas9-mediated genome editing to achieve gene knockout with

lentivirus-mediated gene expression.<sup>265</sup> Dual-guide RNAs targeting PHGDH or NPL gene were designed by CRISPR DESIGN (<http://crispr.mit.edu/>) and set just before the protospacer adjacent motif (PAM), a DNA sequence immediately following the Cas9-targeted DNA sequence. All the specific target sequences were amplified and cloned into lentiviral vectors and verified by DNA sequencing. CRISPR gene editing plasmid vectors with gRNA and Cas9 co-expression were acquired from VectorBuilder. The VSVG plasmid was a gift from Bob Weinberg (Addgene plasmid # 8454; <http://n2t.net/addgene:8454>; RRID: Addgene 8454). The psPAX2 plasmid was a gift from Didier Trono (Addgene plasmid # 12260; <http://n2t.net/addgene:12260>; RRID: Addgene 12260). To produce lentivirus, HEK293T cells seeded in 10-cm plates were transfected with 10.0 µg lentivirus plasmids, 0.5 µg VSVG, and 5.0 µg psPAX2 plasmids. The following morning, fresh DMEM with 15% FBS and 1% P/S was added, and cells were grown for another 48 h to generate virus. For transduction with lentivirus, the A13M13 cells ( $1 \times 10^5$  cells) were seeded in 10-cm plates and the supernatant of transfected HEK293T was collected and passed through 0.45 micron PVDF syringe filter. Five milliliters of the viral supernatant and 5 ml of fresh media were added to recipient A13M13 cell plates with polybrene (Fisher Scientific, TR1003G) at final concentration of 4 µg/ml. The cells were cultured for 24 h followed by adding fresh DMEM medium supplemented with 10% FBS and treated for 10 days with 10 µg/ml blasticidin (Fisher Scientific, A1113903) for selection. The blasticidin selected cells were then resuspended to a concentration of 5 cells/ml and seeded 1 cell/well on 96-well plates. Surviving clones were expanded and analyzed for successful gene knockout. Genomic DNA was extracted using DNeasy Blood and Tissue Kit (Qiagen) to check for successful gene editing. Dual

gRNAs for PHGDH knockout plasmid vector are 5'-CGGGCTCAGC CCTCCGACCC-3' and 5'-GGTGCTCCCTACCAAGCC GT-3'. Dual gRNAs for NPL knockout plasmid vector are 5'- GAGCGTCTCTGAACGTCGCC-3' and 5'-CGTGGG AGCACTAAACGTGA-3'. To address PHGDH/NPL dual knockout, we designed a plasmid vector containing gRNAs for both PHGDH and NPL. The gRNAs are 5'-CGTGGG AGCACTAAACGTGA-3' (targeting PHGDH) and 5'- CGGGCTCAGCCCTCCGACCC-3' (targeting NPL). The sequence for scramble control plasmid with blasticidin selection maker is 5'-GCACTACCAGAGCTAACTCA-3'.

### **Western blot analysis**

Cell lysis and Western blot analysis were carried out according to standard protocols. The following dilutions of primary commercial antibodies were used as probes: 1: 1000 dilution of anti-PKM1 (Cell Signaling Technology, 7067S), 1:1000 dilution of anti-PKM2 (Cell Signaling 4053S), 1:1000 dilution of  $\beta$ -actin (13E5) (Cell Signaling Technology, 4970S), 1:10000 dilution of anti-vinculin (E1E9V) (Cell Signaling Technology, 13901S), 1:1000 dilution of anti-GAPDH (Cell Signaling Technology, 5174S), and 1:1000 dilution of anti-PHGDH (Cell Signaling Technology, 13428S). Primary antibodies were diluted in 5% non-fat milk and incubated overnight at 4 °C. Secondary antibodies (Cell Signaling Technology, 7074S) were diluted in 5% non-fat milk at a dilution of 1:1000 and incubated at room temperature for 1 h.

### **Metabolomic profiling and stable isotope labeling**

For metabolite quantification, cells were seeded in triplicates ( $n = 3$ ) in 6-well plates with DMEM supplemented with 10% FBS and 1% PS. For stable isotope labeling, media was switched to labeling media containing appropriate tracer, 25 mM [U- $^{13}$ C<sub>6</sub>]-glucose, 5

mM [U-<sup>13</sup>C<sub>5</sub>]-glutamine, 2 mM [U-<sup>13</sup>C<sub>3</sub>]-serine, 2 mM [U-<sup>13</sup>C<sub>3</sub>]-cysteine, 3.5 mM [U-<sup>13</sup>C<sub>11</sub>]-tryptophan, 7.2 mM [U-<sup>13</sup>C<sub>4</sub>]-threonine, 25 mM [1,2-<sup>13</sup>C<sub>2</sub>]-glucose, or 5 mM [5-<sup>13</sup>C<sub>1</sub>]-glutamine (all from Cambridge Isotopes Laboratories, Inc). Samples collected at T = 0 (unlabeled), 5 min, 30 min, 60 min, 120 min, and 24 h after starting the experiment. Metabolite extraction was performed as described previously.<sup>266</sup> Protein left from the extraction was dissolved in 0.2 M potassium hydroxide aqueous solution overnight, then quantified using Pierce BCA Protein Assay Kit (Fisher Scientific, PI23225). Dried metabolite extracts were resuspended in HPLC-grade water containing 1 μM 1, 4-piperazinediethanesulfonic acid (PIPES; Sigma Aldrich, P6757) as an internal standard. To normalize sample concentrations, samples were resuspended at volumes corresponding to their protein quantification values. For amino acid analysis, 20 μL of resuspended sample was added to 80 μL methanol and derivatized with 10 μL triethylamine and 2 μL benzyl chloroformate. For pyruvate, lactate, and citrate analysis, 20 μL of resuspended sample was added to a mixture of 20 μL of 250 mM 3-nitrophenylhydrazine (3-NPH) in 50% methanol, 20 μL of 150 mM 1-ethyl-3-(3-dimethylaminopropyl) carbodiimide HCl (EDC) in methanol, and 20 μL of 7.5% pyridine in methanol and allowed to react at 30 °C for 30 min.<sup>267</sup> After this reaction, 16 μL of 2 mg/ml butylated hydroxytoluene (BHT) in methanol was quickly added to these solutions, which were then diluted with 104 μL of water. Samples with and without derivatization were transferred to HPLC vials for analysis. LC-MS/MS analysis was performed with ion-pairing reverse phase chromatography using an Ascentis Express column (C18, 5 cm × 2.1 mm, 2.7 μm, Sigma-Aldrich) for separation and a Waters Xevo TQ-S triple quadrupole mass spectrometer operated in negative mode as mass analyzer. LC parameters were

described previously.<sup>266</sup> Peak processing was performed in MAVEN.<sup>268</sup> Isotope labeling data was corrected for the natural abundance of different isotopes using IsoCor.<sup>269</sup> Heat maps were generated using Cluster and exported using Java Treeview.<sup>270,271</sup>

### **Statistical analysis**

Statistical analysis was performed using a two-tailed Student's t test. Experiments were performed in triplicates and all data are displayed as the mean values  $\pm$  standard error. Statistically significant differences ( $p$ -value) are marked with asterisks (\* $p < 0.05$ , \*\* $p < 0.01$ )

# CHAPTER 3: PYRUVATE KINASE ACTIVITY REGULATES CYSTINE STARVATION INDUCED FERROPTOSIS THROUGH MALIC ENZYME 1 IN PANCREATIC CANCER CELLS

## **Preface**

This section is a modified version of the article which will be submitted for publication in 09/2023:

Elliot Ensink, Tessa Jordan, Hyllana C D Medeiros, Galloway Thurston, Anmol Pardal, Lei Yu, and Sophia Y. Lunt. Pyruvate Kinase Activity Regulates Cystine Starvation Induced Ferroptosis through Malic Enzyme 1 in Pancreatic Cancer (2023)

## **Abstract**

Pancreatic ductal adenocarcinoma (PDAC) is an aggressive cancer with high mortality and limited efficacious therapeutic options. PDAC cells undergo metabolic alterations to survive within a nutrient-depleted tumor microenvironment. One critical metabolic shift in PDAC cells occurs through altered isoform expression of the glycolytic enzyme, pyruvate kinase (PK). Pancreatic cancer cells preferentially upregulate pyruvate kinase muscle isoform 2 isoform (PKM2). PKM2 expression reprograms many metabolic pathways, but little is known about its impact on cystine metabolism. Cystine metabolism is critical for supporting survival through its role in defense against ferroptosis, a non-apoptotic iron-dependent form of cell death characterized by unchecked lipid peroxidation. To improve our understanding of the role of PKM2 in cystine metabolism and ferroptosis in PDAC, we generated PKM2 knockout (KO) human PDAC cells. Fascinatingly, PKM2KO cells demonstrate a remarkable resistance to cystine starvation

mediated ferroptosis. This resistance to ferroptosis is caused by decreased PK activity, rather than an isoform-specific effect. We further utilized stable isotope tracing to evaluate the impact of glucose and glutamine reprogramming in PKM2KO cells. PKM2KO cells depend on glutamine metabolism to support antioxidant defenses against lipid peroxidation, primarily by increased glutamine flux through the malate aspartate shuttle and utilization of ME1 to produce NADPH. Ferroptosis can be synergistically induced by the combination of PKM2 activation and inhibition of the cystine/glutamate antiporter in vitro. Proof-of-concept in vivo experiments demonstrate the efficacy of this mechanism as a novel treatment strategy for PDAC.

## **Introduction**

Pancreatic ductal adenocarcinoma (PDAC) is a devastating disease with a poor prognosis due to limited diagnostic and therapeutic options. PDAC cells are capable of silently progressing and producing metastatic cells before clinical symptoms present or predictive biomarkers can be detected.<sup>4,272</sup> Pancreatic cancer is currently the fourth leading cause of cancer deaths in the United States and is projected to become the second leading cause by 2030.<sup>1,2</sup> Disappointingly, recent advances in combinatorial chemotherapy and targeted immunotherapy have failed to significantly improve pancreatic cancer patient outcomes.<sup>4,9</sup>

Disrupting reprogrammed PDAC metabolism is a promising new strategy to improve treatment and survival of PDAC patients.<sup>273,274</sup> In the nutrient starved tumor microenvironment, tumor cells undergo genetic and cellular alterations to reprogram their metabolism.<sup>62</sup> One adaptation is differential isoform expression of the glycolytic enzyme pyruvate kinase (PK). PDAC cells preferentially switch from the constitutively active PK

muscle 1 isoform (PKM1) to the allosterically regulated PK muscle 2 isoform (PKM2).<sup>44,187,207</sup> The shift to PKM2 contributes to increased glucose consumption and lactate secretion even in the presence of oxygen, a phenomenon known as the Warburg effect.<sup>42,43,58,186</sup> Overexpression of PKM2 in PDAC enables rapid proliferation and survival in low glucose conditions by diverting glucose carbon into biosynthetic precursors and altering glutamine metabolism.<sup>78,205,206,213,275</sup> Glutamine supplies cancer cells with a critical fuel supply for mitochondrial tricarboxylic acid (TCA) cycle and non-essential amino acid production in a process known as anaplerosis when glucose is limited or utilized for other purposes.<sup>78,276</sup> The shift in PK isoform expression produces a profound reprogramming of complex networks of metabolic pathways, many of which are not well understood, including cysteine metabolism.

Cysteine is critical for cell survival given its dual role in protein synthesis and as a precursor for the tripeptide glutathione and coenzyme A to defend against the elevated reactive oxygen species (ROS) in PDAC.<sup>126,277</sup> Healthy cells utilize circulating cysteine or cysteine biosynthesis to fulfill these roles, but cancer cells depend on exogenous cystine, the oxidized dimer of cysteine.<sup>278</sup> Cystine is acquired predominantly through the cystine/glutamate antiporter (system X<sub>C</sub><sup>-</sup>) which is a heterodimer of SLC7A11 (also known as xCT) and SLC3A2, and is overexpressed in many cancer cells.<sup>279</sup> Depletion of extracellular cystine leads to a loss of intracellular glutathione supply and accumulation of oxidative damage to membrane lipids.<sup>126,277,278,280</sup> Uncontrolled lipid peroxidation propagates by reacting with ferrous iron and producing hydroxyl radicals leading to a form of cell death known as ferroptosis.<sup>106,280</sup> Ferroptosis is fundamentally a product of aberrant metabolic behavior including changes in central carbon metabolism such as increased

mitochondrial glutaminolysis and increased dependence on glucose flux through the pentose phosphate pathway to generate NADPH.<sup>153,182,281</sup> However, the impact of PKM2 on ferroptosis in PDAC remains poorly characterized. Previous work in our lab demonstrated that PDAC cells use cysteine catabolism to support pyruvate production during PKM2 knockdown.<sup>282</sup> Additionally, current evidence suggests PKM2 in its inactive dimeric form reprograms central carbon metabolism to increase supply of precursors for biosynthesis of nucleotides and antioxidant defense.<sup>184,201,202,259,283</sup> To further elucidate reprogrammed PDAC metabolism, we investigated the mechanisms by which PK impacts cysteine, glucose, and glutamine metabolism in PDAC cells under nutrient restricted conditions.

Herein, we demonstrate that PKM2 knockout (PKM2KO) in PDAC cells is associated with increased defense against cystine starvation induced ferroptosis. This effect is mediated by decreased PK activity, reprogramming of glutamine metabolism, and utilization of malic enzyme 1 (ME1) to produce NADPH, a critical reducing agent for protection against ROS. Further, we identify that activation of PK leads to increased ferroptosis and demonstrate a proof-of-concept that the combination of cystine starvation and PKM2 activation is a novel and efficacious strategy for treating PDAC.

## **Results**

### **PKM2KO enhances PDAC survival during cystine starvation induced ferroptosis**

To evaluate the impact of PKM2 on cysteine metabolism, we generated human PDAC cell lines that lack PKM2 expression. We selected 2 human PDAC cell lines, AsPC1 and Panc1, due to their sensitivity to cystine starvation.<sup>126</sup> Using lentiviral clustered regularly interspaced short palindromic repeats (CRISPR)/caspase 9 (cas9) gene editing

technology to target the PKM2 specific exon 10, we selectively knocked out (KO) PKM2 (Fig. 3.1A). Deletion of exon 10 led to complete loss of PKM2 expression and low level re-expression of PKM1 in all successfully generated clones (Fig. 3.1B).

We first evaluated the tolerance of PKM2KO cells to low nutrient stress by assessing the viability of PKM2KO cells in response to depleting each of the individual amino acids typically included in Dulbecco's Modified Eagle Medium (DMEM). This produced significant differences in survival between controls and PKM2KO clones under starvation of several amino acids (Figs. 3.1C & B.1A). The most dramatic and consistent difference was the increased viability of all PKM2KO clones under cystine starvation, the most restrictive condition for the respective control cell lines. Morphologic examination of these cells revealed distinct cell volume shrinkage and membrane blistering in the control cells, characteristic of ferroptosis morphology<sup>103</sup>, and retention of normal morphology in the PKM2KO cells (Figs. 3.1D & B.1B). We then used DMEM containing approximate physiologic levels of glucose (5 mM) and glutamine (1 mM) and either 200  $\mu$ M cystine (supraphysiologic) or 0  $\mu$ M cystine (starvation).<sup>66,88</sup> Under cystine starvation, the PKM2KO cells had significantly higher viability compared to the PKM2 expressing controls when evaluated using the AlamarBlue and trypan blue viability assay (Figs. 3.1E-F & B.1C) confirming the reproducibility of this effect and independence from changes in reducing power production alone. To further ensure that the enhanced viability of PKM2KO cells was not simply an artifact of the vector introduced in the control cells, we evaluated the parental wild-type (WT) AsPC1 and Panc1 cells and observed nearly identical sensitivity to cystine starvation as the control cells and significantly lower viability compared to the PKM2KO cells (Fig. B.1D-E). We then exposed the AsPC1 and Panc1 PKM2KO cells to

a range of cystine concentrations and found that the significant increase in viability in PKM2KO cells occurs as cystine concentrations reach 10  $\mu$ M or lower (Figs. 3.1G and B.1F). Cystine starvation resulted in dramatic inhibition of cell proliferation in the AsPC1 and Panc1 control and PKM2KO cell lines (Fig. 3.1H-I), indicating that despite the enhanced viability of PKM2KO cells, they are not actively dividing in this environment. Together, these results suggest that cells that are not expressing PKM2 may represent a sub-population of cells able to persist under stressful low nutrient conditions and allow for tumor survival.<sup>207</sup>

Next, we examined the mechanism of cell death occurring in the control cells under cystine starvation. Under cystine starvation, co-treatment of the AsPC1 and Panc1 cells with the ferroptosis inhibitors ferrostatin-1 (a lipid peroxide inhibitor, FER), trolox (a vitamin E derivative and lipophilic antioxidant; TRO), and deferoxamine (an iron chelator; DFO) significantly restored viability in control cells (Figs. 3.1J & B.1G) with little effect on the PKM2KO clones. These results indicate that the control cells are undergoing ferroptosis while the PKM2KO clones are resistant. Importantly, co-treatment with Z-VAD-FMK (an apoptosis inhibitor; ZVAD) and Necrostatin-1S (a necroptosis inhibitor; NEC) had no significant effect on viability indicating that cell death is not occurring through either apoptosis or necroptosis (Figs. 3.1J & B.1G). Given that ferroptosis is characterized by an accumulation of unchecked lipid peroxidation, we next measured the ratio of oxidized to reduced lipids using the C11-BODIPY probe, which detects lipid peroxides by shifting from red (~590 nm) to green (~510 nm) emission when oxidized. Consistently, PKM2KO cells did not increase in lipid peroxidation compared to the significantly elevated levels in the control cells, which can be quenched by ferrostatin-1 (Figs. 3.1K-L & B.1J-K). AsPC1

and Panc1 PKM2KO cells also have significantly lower general ROS accumulation as measured by the 2',7'-dichlorodihydrofluorescein diacetate (H2DCFDA) probe, a general detector of ROS (Fig. B.1H-I). These observations support the conclusion that PKM2KO in PDAC cells enhances their resistance to cystine starvation induced ferroptosis.

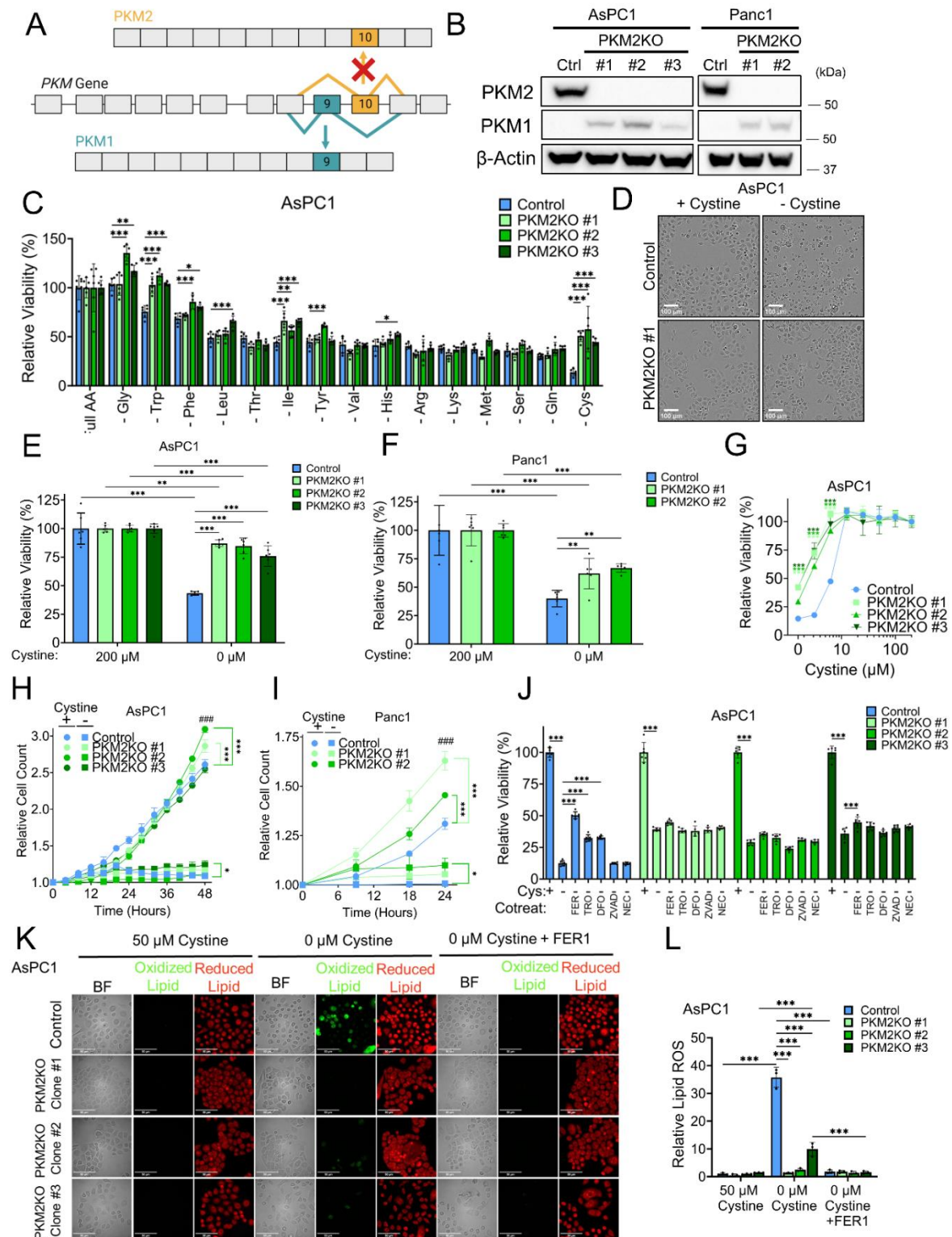


**Figure 3.1** PKM2KO enhances PDAC survival during cystine starvation induced ferroptosis.

### Figure 3.1 (cont'd)

**A.** Schematic view of mutually exclusive alternative splicing of *PKM* to produce PKM1 or PKM2. Targeting of exon 10 by CRISPR deletes PKM2 expression. **B.** Western blot of PKM1 and PKM2 in AsPC1 and Panc1 control cells and PKM2KO clones. **C.** Relative viabilities of AsPC1 control and PKM2KO clones #1-3 in DMEM without each individual amino acid as shown. Significance was assessed by two-way ANOVA and Tukey test. \* $p < 0.05$ , \*\*\* $p < 0.001$ . **D.** Brightfield microscopy images of AsPC1 control and PKM2KO cells under either 200  $\mu\text{M}$  (+) or 0  $\mu\text{M}$  (-) cystine conditions. Scale bar = 100  $\mu\text{m}$ . **E, F.** Relative viabilities of AsPC1 (**E**) and Panc1 (**F**) control and PKM2KO clones under 200  $\mu\text{M}$  or 0  $\mu\text{M}$  cystine. Significance was assessed by two-way ANOVA and Tukey test. \*\* $p < 0.01$ , \*\*\* $p < 0.001$ . **G.** Relative viabilities of AsPC1 control and PKM2KO clones under a range of cystine concentrations from 200  $\mu\text{M}$  to 0  $\mu\text{M}$ . Significance was assessed by two-way ANOVA and Dunnett test. \* $p < 0.05$ . **H, I.** Proliferation analysis using Incucyte cell counts of both AsPC1 (**H**) and Panc1 (**I**) control and their respective PKM2KO clones under 200  $\mu\text{M}$  (+) or 0  $\mu\text{M}$  (-) cystine. Significance was assessed by two-way ANOVA and Tukey test. Comparison between Control and PKM2KO cells at endpoint: \* $p < 0.05$ , \*\*\* $p < 0.001$ . Comparison between 200 and 0  $\mu\text{M}$  cystine conditions for each cell line at endpoint: ### $p < 0.001$ . **J.** Relative viabilities of AsPC1 control and PKM2KO cells under 50  $\mu\text{M}$  cystine (+) and 0  $\mu\text{M}$  cystine (-) co-treated with 5  $\mu\text{M}$  ferrostatin-1 (FER), 100  $\mu\text{M}$  trolox (TRO), 100  $\mu\text{M}$  deferoxamine (DFO), 50  $\mu\text{M}$  Z-VAD-FMK (ZVAD), or 10  $\mu\text{M}$  necrostatin-1S (NEC). Significance by two-way ANOVA. \* $p < 0.05$ , \*\*\* $p < 0.001$ . Multiple hypothesis correction by Tukey test. **K.** Representative brightfield and fluorescent images of AsPC1 cell lipid peroxidation quantified in panel **L**. Scale bar = 50  $\mu\text{m}$ . **L.** Relative lipid

### **Figure 3.1 (cont'd)**

peroxidation of AsPC1 control and PKM2KO cells under 50  $\mu$ M cystine, 0  $\mu$ M cystine, and 0  $\mu$ M cystine with 5  $\mu$ M FER1, visualized by C11-BODIPY.

### **Pyruvate kinase activity dictates response to cystine starvation induced ferroptosis in PDAC cells**

We next sought to explain how PKM2KO cells have enhanced survival under cystine starvation. Given that the PKM2KO cells re-express PKM1, it could be either the loss of PKM2, the gain of PKM1, or some other factor that is driving the difference in viability. To address these possibilities, we used lentiviral vectors to overexpress PKM1 in the control cells and re-introduce PKM2 expression in the PKM2KO cells for both AsPC1 and Panc1 (Fig. B.2A). Evaluation of the response to cystine starvation revealed that neither re-expression of PKM1 nor PKM2 altered the viability (Fig. B.2B-E). However, we observed that the control cells in which PKM1 was overexpressed continued to express PKM2 and similarly the PKM2KO cells with PKM2 re-expressed continue to also express PKM1 at a low level indicating that the re-expression of either PK isoform does not restore cells to their original state (Fig. B.2A). Thus, the total dosage and activity of PK is likely different with respect to their parental cell lines. We then hypothesized that the difference in cystine starvation survival is due to differences in total PK activity. We found that the activity of PK in AsPC1 PKM2KO cells had consistently lower overall PK activity regardless of cystine availability, despite expressing PKM1 at low levels, whereas the control cells decreased their PK activity in response to 0  $\mu$ M cystine (Figs. 3.2A & B.2F), consistent with PKM2's response to oxidative stress.<sup>284</sup> We then tested whether

modulation of PK activity would influence viability under 0  $\mu$ M cystine. By treating cells with compound 3k, a potent and specific PKM2 antagonist (Fig. 3.2B), we were able to dramatically restore viability in four different WT PDAC cell lines (AsPC1, Panc1, MiaPaCa2, and BxPC3) under 0  $\mu$ M cystine (Fig. 3.2C-F). Additionally, co-treatment of imidazole ketone erastin (IKE)<sup>182</sup>, a potent inhibitor of xCT, with compound 3k restored viability in the majority of WT PDAC cell lines tested (Fig. B.2H-K), demonstrating that decreased PK activity can improve resistance to cystine starvation induced ferroptosis. To further confirm our hypothesis, we combined IKE treatment with TEPP-46, a potent and selective PKM2 allosteric agonist (Fig. 3.2B). The combination treatment synergistically and significantly decreased viability in a concentration dependent manner in each cell line tested except BxPC3 (Fig. 3.2G-N). Interestingly, BxPC3 retains residual PKM1 expression suggesting that this cell line likely has reprogrammed glycolytic activity relative to the other WT cells (Fig. B.2G). Overexpression of PKM1 in the control cells does significantly increase PK activity but did not further inhibit viability likely because they are already maximally inhibited by cystine starvation (Fig. B.2L-M). PKM2 re-expression significantly increased PK activity under cystine replete conditions, but not under cystine starvation (Fig. B.2N-O). We further evaluated the mechanism of cell death caused by co-treatment of IKE and TEPP-46 and found that ferrostatin-1 but not Z-VAD-FMK nor necrostatin-1S was able to restore viability, indicating that TEPP-46 is working with IKE to induce ferroptosis specifically (Fig. B.2P-S). Together, these observations present compelling evidence that PK activity dictates the response to cystine starvation induced ferroptosis.

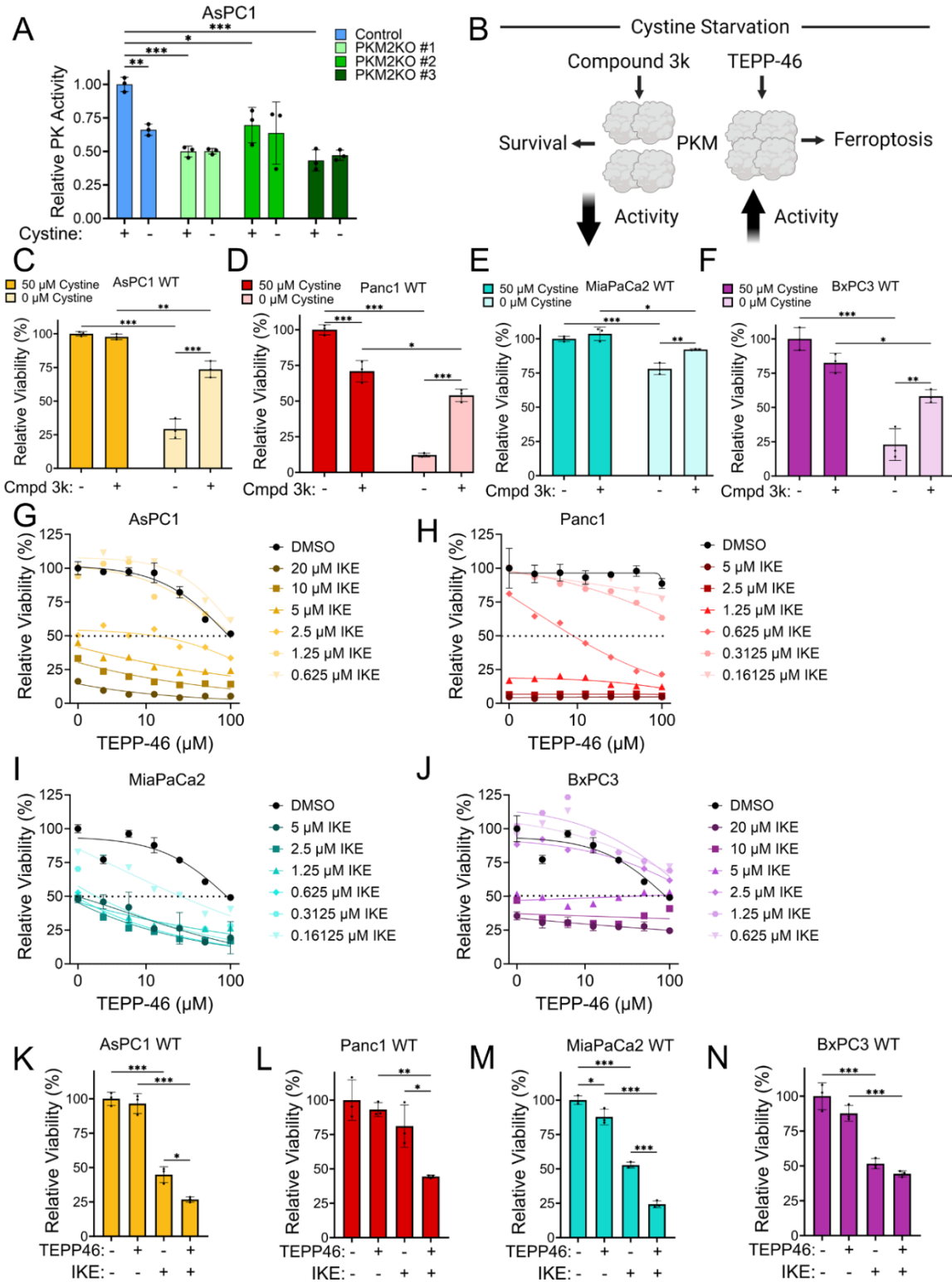


**Figure 3.2 Pyruvate kinase activity dictates response to cystine starvation induced ferroptosis in PDAC cells.**

### Figure 3.2 (cont'd)

**A.** Relative PK activity in AsPC1 control and PKM2KO cells under 50  $\mu\text{M}$  (+) and 0 (-)  $\mu\text{M}$  cystine. Significance was assessed by two-way ANOVA. \* $p < 0.05$ , \*\*\* $p < 0.001$ . Multiple hypothesis correction by Tukey test. **B.** Schematic showing TEPP-46 promoting the formation of the active tetrameric form of PKM2 and compound 3k inhibiting tetramer formation, producing the less active dimeric form of PKM2. **C-F.** Relative viabilities at 50  $\mu\text{M}$  and 0  $\mu\text{M}$  cystine with (+) or without (-) treatment of 10  $\mu\text{M}$  compound 3k in WT cells: AsPC1 (**C**), Panc1 (**D**), MiaPaCa2 (**E**), and BxPC3 (**F**). Significance was assessed by two-way ANOVA. \* $p < 0.05$ , \*\* $p < 0.01$ , \*\*\* $p < 0.001$ . Multiple hypothesis correction by Tukey test. **G-J.** The effect of IKE and TEPP-46 combination treatment in the range of the indicated concentrations in AsPC1 WT cells (**G**), Panc1 WT cells (**H**), MiaPaCa2 WT cells (**I**), and BxPC3 WT cells (**J**). **K.** Relative viability of AsPC1 WT cells with (+) or without (-) treatment with 5  $\mu\text{M}$  IKE and 12.5  $\mu\text{M}$  TEPP-46. **L.** Relative viability of Panc1 WT cells with (+) or without (-) treatment with 0.625  $\mu\text{M}$  IKE and 12.5  $\mu\text{M}$  TEPP-46. **M.** Relative viability of MiaPaCa2 WT cells with (+) or without (-) treatment with 0.625  $\mu\text{M}$  IKE and 12.5  $\mu\text{M}$  TEPP-46. **N.** Relative viability of BxPC3 WT cells with (+) or without (-) treatment with 5  $\mu\text{M}$  IKE and 12.5  $\mu\text{M}$  TEPP-46. For **K-N**, significance was assessed by two-way ANOVA. \* $p < 0.05$ , \*\* $p < 0.01$ , \*\*\* $p < 0.001$ . Multiple hypothesis correction by Tukey test.

## **PDAC PKM2KO enhanced defense against ferroptosis is specific to cystine starvation**

To further investigate the mechanism contributing to ferroptosis resistance in the PKM2KO cells, we evaluated the expression of two key protective proteins: xCT and glutathione peroxidase 4 (GPX4). xCT is the transporter by which cancer cells acquire nearly all of their cystine and GPX4 is primarily responsible for quenching lipid peroxides (Fig. 3.3A).<sup>118</sup> Under cystine starvation, AsPC1 control cells increase xCT to a greater extent than PKM2KO cells, while Panc1 control and PKM2KO cells have similar expression (Figs. 3.3B & B.3A). Both AsPC1 and Panc1 control cells have decreased GPX4 expression under cystine starvation, but PKM2KO cells retain equivocal expression of GPX4 (Figs. 3.3B & B.3A). This suggests that the presence of PKM2 may modulate expression of these genes through a yet to be determined mechanism.

We further explored the difference in ferroptosis defense between control and PKM2KO cells by evaluating their response to IKE (targets xCT) and Ras selective lethal 3 (RSL3, targets GPX4) (Fig. 3.3A).<sup>118</sup> Both AsPC1 and Panc1 PKM2KO cells demonstrate a significantly high degree of resistance to IKE compared to controls; however, these same cells have equivalent or enhanced sensitivity to RSL3 (Fig. 3.3C-F). Control cells treated with IKE were significantly rescued by co-treatment with ferrostatin-1, trolox, or deferoxamine but not Z-VAD-FMK or necrostatin-1S, while the PKM2KO clones show little to no response to these rescue agents (Figs. 3.3G-H & B.3B). Additionally, all AsPC1 cells show strong sensitivity to RSL3 that can only be rescued by ferroptosis inhibitors, while Panc1 cells show limited sensitivity to RSL3 (Fig. B.3C-E). AsPC1 PKM2KO cells show decreased lipid peroxidation under IKE and equivalent lipid

peroxidation under RSL3 compared to control cells (Fig. B.3F). This suggests that PK is not uniformly responsible for providing defense against all routes to ferroptosis, but rather specifically influences the metabolic reprogramming that occurs under cystine starvation and the subsequent propensity towards ferroptosis.

We next investigated whether this difference in IKE sensitivity would have the same effect on control and PKM2KO cells *in vivo*. We generated xenograft tumors in mice using AsPC1 control and PKM2KO cells. PKM2KO tumors had significantly lower tumor growth compared to the control (Fig. 3.3I). IKE treatment produced a significant decrease in tumor volume in the PKM2 expressing control tumors in contrast to the limited response in the PKM2KO tumors (Fig. 3.3I). Therefore, PKM2KO in PDAC provides resistance to cystine starvation mediated cell death *in vitro* and *in vivo*.

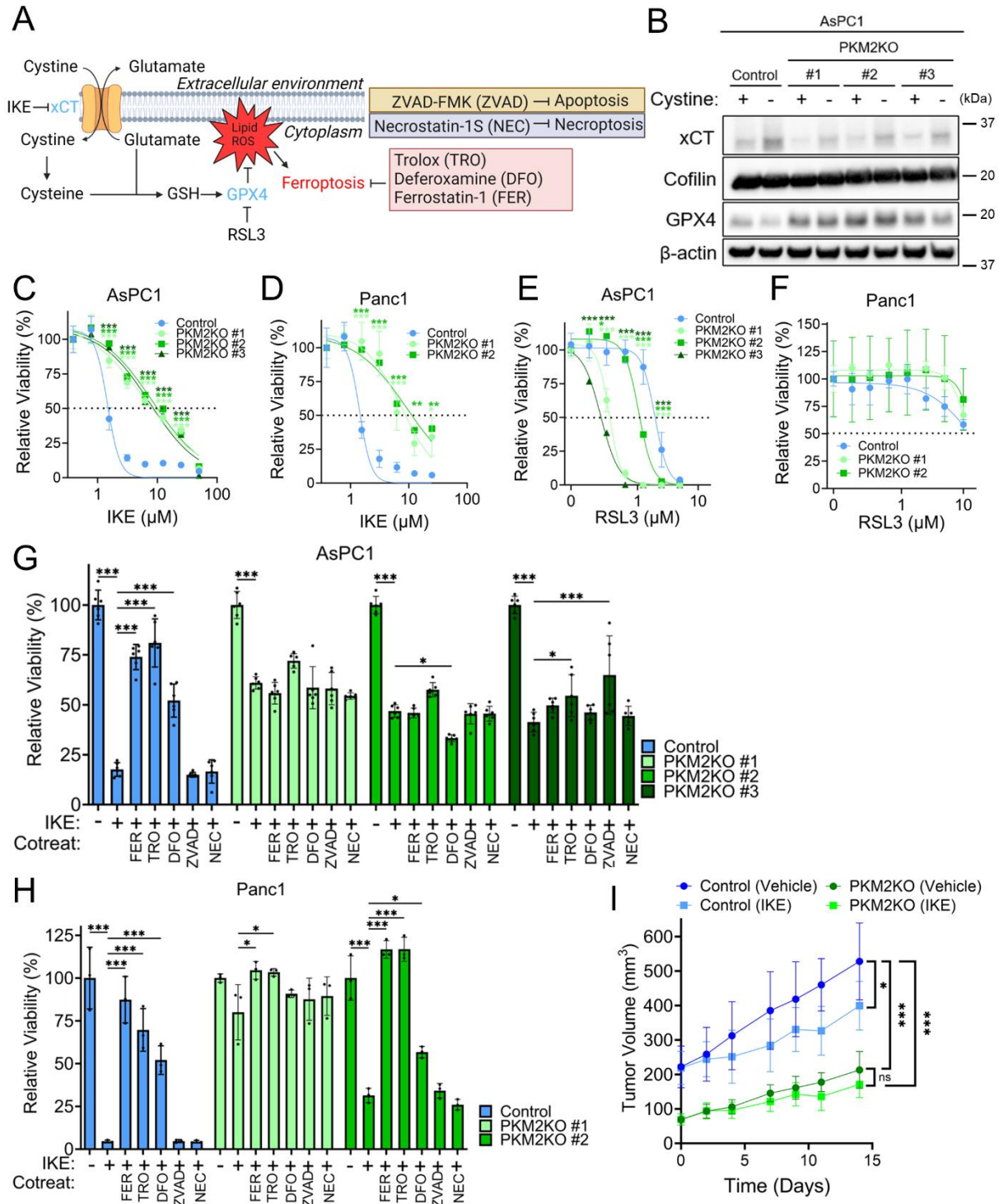


**Figure 3.3 PDAC PKM2KO enhanced defense against ferroptosis is specific to cystine starvation.**

### Figure 3.3 (cont'd)

**A.** Schematic of the mechanism of ferroptosis, the defense proteins xCT and GPX4 (the targets of imidazole ketone erastin (IKE) and Ras selective lethal 3 (RSL3), respectively), and the ferroptosis, apoptosis, and necroptosis inhibitors used in the study. **B.** Western blot of xCT and GPX4 expression in AsPC1 control and PKM2KO cells under 50  $\mu$ M (+) and 0  $\mu$ M (-) cystine. **C-D.** Concentration dependent response in viability of AsPC1 (**C**) and Panc1 (**D**) control and PKM2KO clones to a range of IKE concentrations from 50-0  $\mu$ M. **E-F.** Concentration dependent viability responses of AsPC1 (**E**) and Panc1 (**F**) control and PKM2KO clones to a range of RSL3 concentrations from 10-0  $\mu$ M. For **C-F**, significance was assessed by two-way ANOVA. \* $p$ <0.05, \*\*\* $p$ <0.01, \*\*\*\* $p$ <0.001. Multiple hypothesis correction by the Dunnett test. **G, H.** Relative viabilities of AsPC1 (**G**) and Panc1 (**H**) control and PKM2KO cells under 50  $\mu$ M cystine with 5  $\mu$ M IKE (+) co-treated with 5  $\mu$ M ferrostatin-1 (FER), 100  $\mu$ M trolox (TRO), 100  $\mu$ M deferoxamine (DFO), 50  $\mu$ M Z-VAD-FMK (ZVAD), or 10  $\mu$ M necrostatin-1S (NEC). Significance was assessed by two-way ANOVA. \* $p$ <0.05, \*\*\*\* $p$ <0.001. Multiple hypothesis correction by Tukey test. **I.** Growth of xenograft tumors produced from AsPC1 control and PKM2KO cells treated with vehicle control or 50 mg/kg IKE. Significance was assessed by two-way ANOVA at end point. \* $p$ <0.05, \*\*\*\* $p$ <0.001, ns = non-significant. Multiple hypothesis correction by Tukey test.

## **PDAC PKM2KO cells exhibit increased glutamine anaplerosis and decreased glucose metabolism under cystine starvation**

PKM isoform selection is known to cause reprogramming in the overall metabolic activity within cancer cells, including both glucose and glutamine metabolism.<sup>78,205,206,213,275</sup> To evaluate changes in metabolic pathways under low cystine conditions that may explain the survival advantage in PKM2KO cells, we performed targeted mass-spectrometry and stable isotope tracing. Using  $^{13}\text{C}_{1,2}$ -glucose, we traced the flow of glucose-derived carbon through glycolysis and into the TCA cycle. The abundance of labeled hexose-phosphate is equivalent between control and PKM2KO cells under high and low cystine conditions (Figs. 3.4A, B.4A, & B.5A). Downstream lactate production is significantly higher in control cells, which is consistent with PKM2's influence on the Warburg effect.<sup>218,220</sup> However, labeled lactate production significantly decreases under cystine starvation (Figs. 3.4B, B.4C, & B.5C). Glucose-derived carbon entry into the TCA cycle intermediates is also lower under cystine starvation, consistent with the observation that PK activity is decreased under these conditions (Figs. 3.4C-F, B.4D-G & B.5D-G).

Given the decrease in glucose metabolism under cystine starvation, we next investigated glutamine metabolism. KRAS mutated PDAC cells rely on glutamine,<sup>76,77,285</sup> and glutaminolysis contributes to ferroptosis.<sup>153</sup> Given this connection, we hypothesized that PKM2 expression alters glutamine metabolism and promotes ferroptosis. Using uniformly (U) labeled U- $^{13}\text{C}_5$ -glutamine as a tracer, we found that the breakdown of glutamine into glutamate is slightly decreased in PKM2KO cells and under cystine starvation (Figs. 3.4G and B.4L). PKM2KO cells also secrete significantly lower glutamate than the PKM2 expressing controls (Figs. 3.4H and B.4M). Additionally, PKM2KO cells

have significantly lower production of  $\alpha$ -ketoglutarate from glutamine while having equivalent amounts of malate and succinate production downstream in the TCA cycle (Figs. 3.4I-J, B.4N-Q, & B.5K-N). We also observe that PKM2KO cells have increased glutamine contribution to glutathione (Fig. 3.4L) and the amino acids aspartate and proline (Figs. 3.4K & B.4R-T). Asparagine synthesis from glutamine is significantly lower in PKM2KO cells under high cystine but increases under cystine starvation (Fig. B.4S). Importantly, we did not observe increased glucose contributions to aspartate in the PKM2KO cells (Fig. B.4H), suggesting that there is a specific utilization of glutamine for production of these amino acids. Under cystine starvation, supplementation with aspartate, asparagine, glutamate, and proline produced no change in viability compared to cystine starvation alone and did not alter the difference in viability between control and PKM2KO cells (Fig. B.6H). This suggests that the ability of the PKM2KO cells to increase production of amino acids from glutamine is not essential for improving cellular defense against ferroptosis. Together, these observations show that under cystine starvation, there is metabolic reprogramming away from glucose metabolism with a persistent reliance on glutamine metabolism, and that the absence of PKM2 influences how glucose and glutamine are metabolized.

Decreased PK activity has been linked to increased flux through the pentose phosphate pathway (PPP), an important pathway for generating NADPH.<sup>201</sup> Since NADPH is a critical reducing agent for reducing glutathione (GSH) and defending against lipid peroxidation, this raises the possibility that utilization of the PPP is more active in the PKM2KO cells under low cystine stress. To address this, we used the  $^{13}\text{C}_{1,2}$ -glucose tracer to take advantage of the fact that flux through the PPP results in the loss of the first

carbon. Subsequent re-entry into glycolysis would result in mass +1 (M1) labeling, while flux directly through glycolysis will produce M2 labeling downstream. We observe that M1 labeling in ribose-5-phosphate and ribulose-5-phosphate is actually decreased under cystine starvation, though the result was not significant (Figs. B.4J-K & B.5I-J). Further, there were no significant differences between control and PKM2KO cells. We did observe significantly more M1 isotopologue hexose-phosphate in one AsPC1 PKM2KO clone, but no consistent or significant trend in the other cells (Figs. B.4I & B.5H). This suggests that differential utilization of the PPP is likely not a major driver for explaining the difference in defense against ferroptosis between PKM2KO cells and PKM2 expressing cells.

Glutathione (GSH) is a critical antioxidant defense molecule, synthesized from cysteine, glycine, and glutamate.<sup>135</sup> As expected, we observed GSH synthesized from glutamate plummets under cystine starvation, likely due to rapid consumption for quenching lipid peroxides and the lack of new cysteine to synthesize more (Fig. B.6A-D). Although the pool of GSH is extremely low, we do observe significantly increased GSH in two of the AsPC1 PKM2KO clones under cystine starvation, but this effect was not seen in the Panc1 cells (Figs. 3.4L and B.6B, D). To further explore potential differences in GSH synthesis, we co-treated the control and PKM2KO cells with buthionine sulfoximine (BSO), an inhibitor of glutathione synthesis that does not induce ferroptosis.<sup>126,127</sup> We observed a minor decrease in viability with BSO treatment that can be restored by co-treatment with ferrostatin-1 in AsPC1 cells but not Panc1 cells (Fig. B.6E-G). Under cystine starvation, BSO treatment does not alter viability of either control or PKM2KO cells, indicating that inhibition of GSH synthesis cannot further alter ferroptosis when environmental cystine is removed. These results suggest that there are some minor

differences in GSH synthetic capabilities between control and PKM2KO cells, but the ability to synthesize GSH is likely not the major contributor to the difference in ability to defend against ferroptosis. Altogether, this data suggests a complex utilization of glutamine metabolism by PKM2KO cells to support defense against cystine starvation induced ferroptosis.



### Figure 3.4 (cont'd)

**A-F.** Stable isotope tracing of  $^{13}\text{C}_{1,2}$ -glucose under 50  $\mu\text{M}$  (+) and 0  $\mu\text{M}$  (-) cystine for 4 hours in AsPC1 control and PKM2KO clone #1 to produce M+2 labeled hexose-phosphate (**A**), lactate (**B**), citrate (**C**),  $\alpha$ -ketoglutarate (**D**), malate (**E**), and aspartate (**F**). **G-K** Stable isotope tracing of  $^{13}\text{C}_5$ -glutamine under 50  $\mu\text{M}$  (+) and 0  $\mu\text{M}$  (-) cystine for 24 hours in AsPC1 control and PKM2KO clone #1 to produce M+5 labeled glutamate (**G**), secreted glutamate (**H**),  $\alpha$ -ketoglutarate (**I**), glutathione (**L**), and M+4 labeled malate (**J**), and aspartate (**K**). Significance was assessed by two-way ANOVA. \* $p < 0.05$ , \*\* $p < 0.01$ , \*\*\* $p < 0.001$ . Multiple hypothesis correction by Tukey test.

### Glutamine is required for PKM2KO PDAC cell defense against cystine starvation induced ferroptosis

Glutamine metabolism is an important component of ferroptosis.<sup>153</sup> Given the difference in glutamine metabolism in the PKM2KO cells, we tested whether environmental glutamine availability would influence cell survival. We found that complete removal of glutamine significantly enhances the viability of the control cells under cystine starvation, while the PKM2KO cells have reduced viability when glutamine is removed under cystine starvation induced by IKE treatment (Fig. 3.5A-B). The difference in viability under cystine starvation between PKM2KO and control cells is present with glutamine levels as low as 250  $\mu\text{M}$ , but complete removal of glutamine reverse this effect (Figs. 3.5C & B.7A, D-F). Glutamine metabolism can also be inhibited by the glutaminase inhibitor CB-839.<sup>286,287</sup> Treatment with CB-839 significantly decreases the viability of PKM2KO cells, but has a more muted effect on the control cells (Fig. B.7B). In contrast, under

cystine starvation, CB-839 restores viability in the control cells (Fig. B.7B). We further observe that removal of glutamine eliminates the increased lipid peroxidation observed in control cells under 0  $\mu$ M cystine conditions and that glutamine removal causes no significant increase in lipid ROS in either control or PKM2KO cells compared to replete media conditions (Fig. 3.5D). We next evaluated whether simultaneous glutamine and cystine starvation would alter expression of the ferroptosis defense proteins, xCT and GPX4. When both environmental glutamine and cystine are removed, we no longer observe the increase in xCT or decrease in GPX4 under cystine starvation alone, indicating that either the stressful stimuli promoting their expression is absent or the presence of glutamine is required to promote expression (Fig. 3.5E-F). Together, these results support the conclusion that altered glutamine metabolism in PKM2KO cells is in part responsible for the differential ferroptosis response under cystine starvation conditions.

Glutamine anaplerosis is an important metabolic process for replenishing resources required for the TCA cycle to function in the low nutrient conditions of the PDAC tumor microenvironment<sup>78,276</sup> and is influenced by PK enzyme activity.<sup>206,288</sup> To address whether metabolites downstream of glutaminolysis would influence ferroptosis, we grew the AsPC1 and Panc1 PKM2KO cells in the absence of cystine and co-treated the cells with cell permeable dimethyl  $\alpha$ -ketoglutarate (DM- $\alpha$ kg), dimethyl succinate (DM-Suc), and dimethyl malate (DM-Mal) at concentrations shown to increase ferroptosis under cystine starvation.<sup>153</sup> In the AsPC1 cells, the addition of DM- $\alpha$ kg or DM-Suc did not change viability. Fascinatingly, the addition of malate significantly restored viability to these cells (Fig. 3.5G-I & B.7C). Even more surprisingly, when environmental glutamine is removed,

we observe the same trend where DM- $\alpha$ kg and DM-Suc do not affect viability, and treatment with DM-Mal further increases viability (Figs. 3.5G-I & B.7C). The AsPC1 PKM2KO cells have worse viability when environmental glutamine is removed, yet the addition of DM- $\alpha$ kg or DM-Mal, but not DM-Suc, rescues viability loss caused by glutamine removal (Fig. 3.5G-I & B.7C). Treatment with DM-Mal also restores viability when glutamine metabolism is blocked by CB-839 (Fig. B.7B). While this effect is prominent in the AsPC1 cells, we do not observe the same effect in Panc1. The viability of Panc1 cells under cystine starvation is restored by DM- $\alpha$ kg, but further decreased when DM-Suc and DM-Mal are supplemented (Fig. B.7D-F). To confirm that the rescue by malate is not an artifact of higher concentration of malate, we also find that using a lower concentration of DM-Mal (8 mM) is sufficient to cause the same changes in the AsPC1 and Panc1 PKM2KO cells (Fig. B.7G-H). Supplementation with DM- $\alpha$ kg and DM-Suc produce little change under cystine and glutamine replete conditions, but DM-Mal supplementation consistently increases viability (Fig. B.7I-O). Collectively, our data presents strong evidence that PK plays a key role in altering ferroptosis by reprogramming glutamine metabolism and suggests that under low PK activity, cells utilize enhanced glutamine metabolism under low cystine conditions for survival.

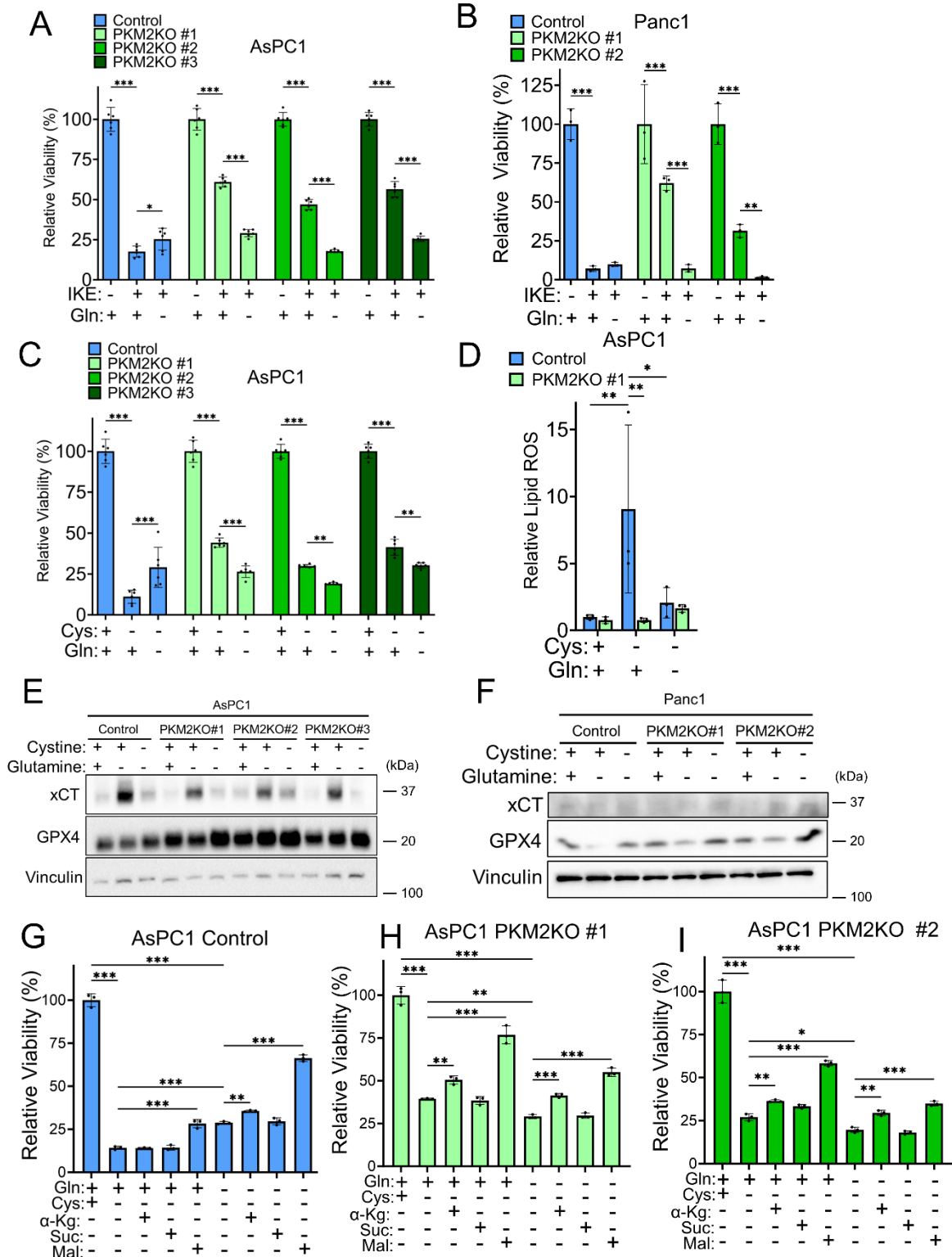


**Figure 3.5** Glutamine is required for PKM2KO PDAC cell defense against cystine starvation induced ferroptosis.

### Figure 3.5 (cont'd)

**A, B.** Relative viabilities of AspC1 (**A**) and Panc1 (**B**) control and PKM2KO cells under 50  $\mu$ M cystine with (+) or without (-) 1 mM glutamine treated with 5  $\mu$ M IKE. **C.** Relative viabilities of AsPC1 control and PKM2KO cells under 50  $\mu$ M (+) and 0  $\mu$ M (-) cystine with (+) or without (-) 1 mM glutamine. **D.** Relative lipid peroxidation in AsPC1 Control and PKM2KO clone #1 under 50  $\mu$ M (+) or 0  $\mu$ M (-) cystine with (+) or without (-) 1 mM glutamine. For **A-D**, significance was assessed by two-way ANOVA. \* $p$ <0.05, \*\* $p$ <0.01, \*\*\* $p$ <0.001. Multiple hypothesis correction by Tukey test. **E, F.** Western blot of xCT and GPX4 expression in AsPC1 (**A**) and Panc1 (**F**) cells under 50  $\mu$ M (+) and 0  $\mu$ M (-) cystine with (+) or without (-) 1 mM glutamine. **G-I.** Relative viabilities of AsPC1 control and PKM2KO clones under 50  $\mu$ M (+) or 0  $\mu$ M (-) cystine with (+) or without (-) 1 mM glutamine supplemented with either 8 mM dimethyl- $\alpha$ -ketoglutarate ( $\alpha$ KG), 8 mM dimethyl-succinate (Suc), or 32 mM dimethyl-malate (Mal). Significance was assessed by one-way ANOVA. \* $p$ <0.05, \*\* $p$ <0.01, \*\*\* $p$ <0.001. Multiple hypothesis correction by Sidak test.

### Malic enzyme 1 enables survival of PKM2KO PDAC under cystine starvation

We next aimed to identify the metabolic pathway that the PKM2KO cells rely on to alter glutamine metabolism and promote defense against ferroptosis. KRAS mutant PDAC upregulates several metabolic enzymes, including glutamate oxaloacetate transaminase 1 (GOT1), glutamate oxaloacetate transaminase 2 (GOT2), and malic enzyme 1 (ME1), to alter glutamine metabolism and promote defense against ferroptosis.<sup>77</sup> Additionally, inhibition of GOT1 promotes ferroptosis in PDAC.<sup>289</sup> The fact that malate promotes increased survival of cystine starvation and that our U-<sup>13</sup>C<sub>5</sub>-

glutamine labeling data demonstrates high levels of glutamine flux into malate and aspartate led us to hypothesize that malic enzyme and the malate aspartate shuttle are important for providing the metabolic advantage in PKM2KO cells under cystine starvation. To address this possibility, we evaluated the expression of ME1 in the AsPC1 and Panc1 PKM2KO. Surprisingly, the PKM2KO clones demonstrate elevated ME1 expression compared to their respective controls; however, expression was minimally impacted by the presence or absence of cystine (Fig. 3.6A-B). We next attempted to block ME1 using malic enzyme inhibitor (ME1i) to test whether this would influence ferroptosis. We found that inhibition of ME1 significantly decreases viability of control and PKM2KO cells under cystine starvation (Figs. 3.6C-G & B.8A-B). Co-treatment with ferrostatin-1 was able to significantly restore viability in the Panc1 cells (Fig. 3.6C-E). In AsPC1 cells, only N-acetylcysteine (NAC), an antioxidant, was able to rescue this effect consistently (Figs. 3.6F-G & B.8A-B). This indicates that the decrease in viability induced by cystine starvation and ME1 inhibition in AsPC1 cells is likely specific to oxidative stress but may not be entirely explained by ferroptosis and speaks to the metabolic heterogeneity that has been observed in PDAC.<sup>4</sup> We further demonstrate that supplementation with malate in addition to ME1 inhibition ablates the viability advantage that malate supplementation alone provides in AsPC1 cells (Figs. 3.6H-I & B.8C-G). Because ME1 is important for generating the antioxidant NADPH, we next evaluated NADPH levels in the PKM2KO cells. We observe that NADPH levels are consistently higher in the PKM2KO cells under 0  $\mu$ M cystine, consistent with increased defense against ferroptosis (Fig. 3.6J-K). Based on these results, we have developed a model in which PK influences the expression of ME1 and that under low PKM2 activity, PDAC cells increase glutamine metabolism and

utilization of ME1 to promote NADPH production and defense against ferroptosis (Fig. 3.6L). Furthermore, activation of PKM2 increases glycolysis and de-emphasizes utilization of glutamine for NADPH generation and promotes metabolic conditions more susceptible to ferroptosis (Fig. 3.6M).

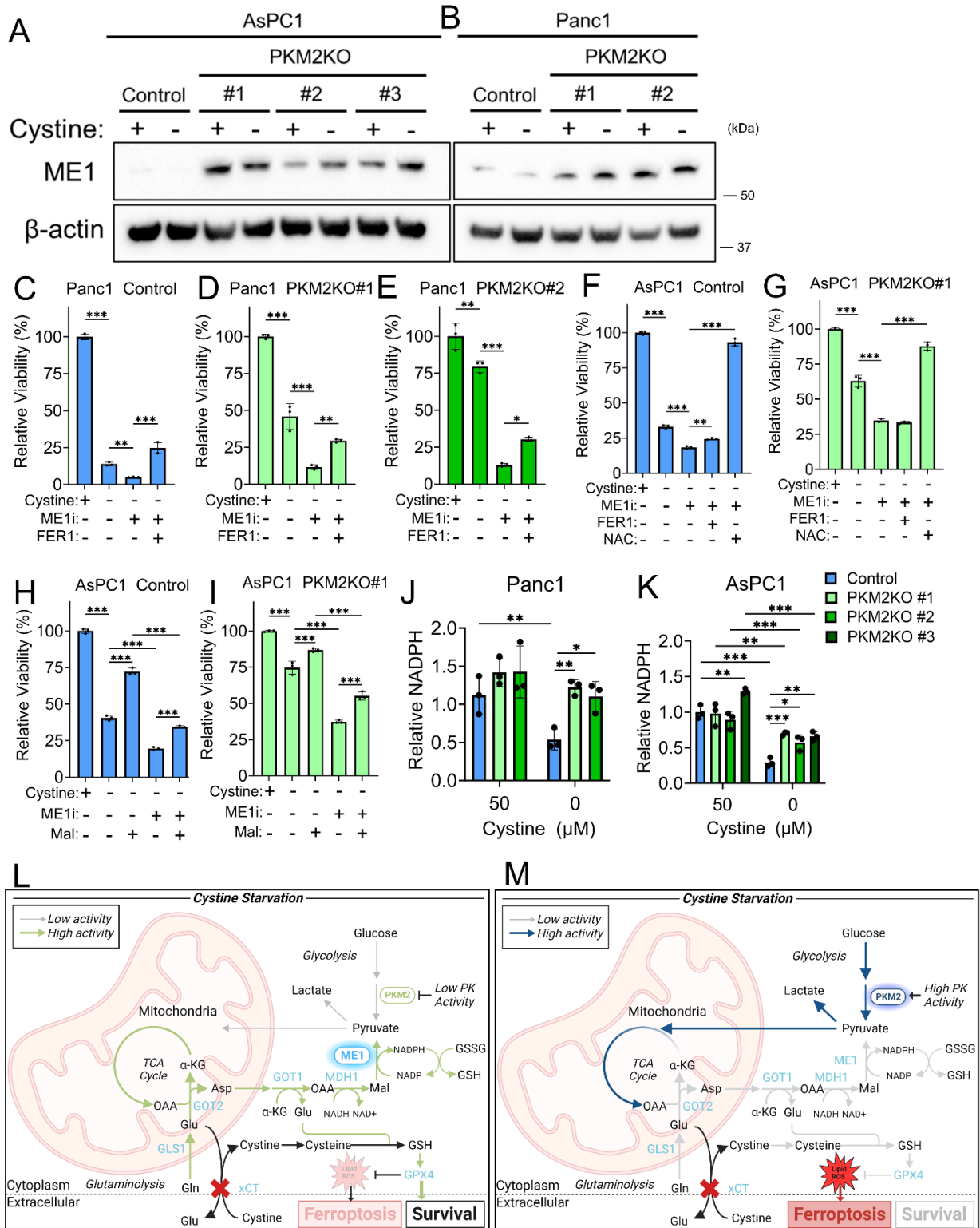


**Figure 3.6 Malic enzyme 1 enables survival of PKM2KO PDAC cells under cystine starvation.**

### Figure 3.6 (cont'd)

**A, B.** Western blot of malic enzyme 1 (ME1) expression in AsPC1 (**A**) and Panc1 (**B**) control cells and PKM2KO clones under 50  $\mu\text{M}$  (+) or 0  $\mu\text{M}$  (-) cystine conditions. **C-G.** Relative viabilities of Panc1 control cells (**C**), Panc1 PKM2KO #1 (**D**), Panc1 PKM2KO #2 (**E**), AsPC1 control (**F**), and AsPC1 PKM2KO clone #1 (**G**) under 0  $\mu\text{M}$  cystine treated with (+) or without (-) 50  $\mu\text{M}$  malic enzyme 1 inhibitor (ME1i) and co-treated with either 5  $\mu\text{M}$  ferrostatin-1 (FER) or 1 mM N-acetylcysteine (NAC). **H, I.** Relative viabilities of AsPC1 control (**H**) and PKM2KO clone #1 (**I**) under 50  $\mu\text{M}$  (+) or 0  $\mu\text{M}$  (-) cystine with (+) or without (-) 50  $\mu\text{M}$  ME1i and 32 mM dimethyl-malate (Mal) supplement. For **C-I**, significance was assessed by one-way ANOVA. \* $p < 0.05$ , \*\* $p < 0.01$ , \*\*\* $p < 0.001$ . Multiple hypothesis correction by Sidak test. **J, K.** Relative NADPH abundance in AsPC1 (**J**) and Panc1 (**K**) control and PKM2KO clones under 50 or 0  $\mu\text{M}$  cystine. For **J-K**, significance was assessed by two-way ANOVA. \* $p < 0.05$ , \*\* $p < 0.01$ , \*\*\* $p < 0.001$ . Multiple hypothesis correction by Tukey test. **L-M.** Proposed model on how PK reprograms metabolism to influence cystine starvation induced ferroptosis under low PK activity (**L**) and high PK activity (**M**).

### **The combination of pyruvate activation and cystine starvation is an efficacious treatment for PDAC *in vivo***

Finally, we tested the impact of increasing pyruvate kinase activity and inhibiting xCT on PDAC growth *in vivo* using NOD scid gamma (NSG) mice injected with Panc1 WT cells. Mice were divided into 4 treatment groups to receive either 50 mg/kg IKE, 30 mg/kg TEPP-46, combination of 50 mg/kg IKE and 30 mg/kg TEPP-46, or vehicle control

(Fig. 3.7A). After 2 weeks of daily intraperitoneal injections, tumor volume was significantly lower in the TEPP-46 and combination treatment groups compared to the vehicle control group (Fig. 3.7B). Tumor weight was also significantly lower in the combination treatment group compared to the control and TEPP-46 treatment groups, with a trend towards decreased weight compared to IKE treatment group (Fig. 3.7C-D). No significant differences in body weight were observed between each of the groups over the duration of the treatment. This provides proof-of-concept that activating pyruvate kinase and inducing cystine starvation is a viable, novel treatment strategy for PDAC.

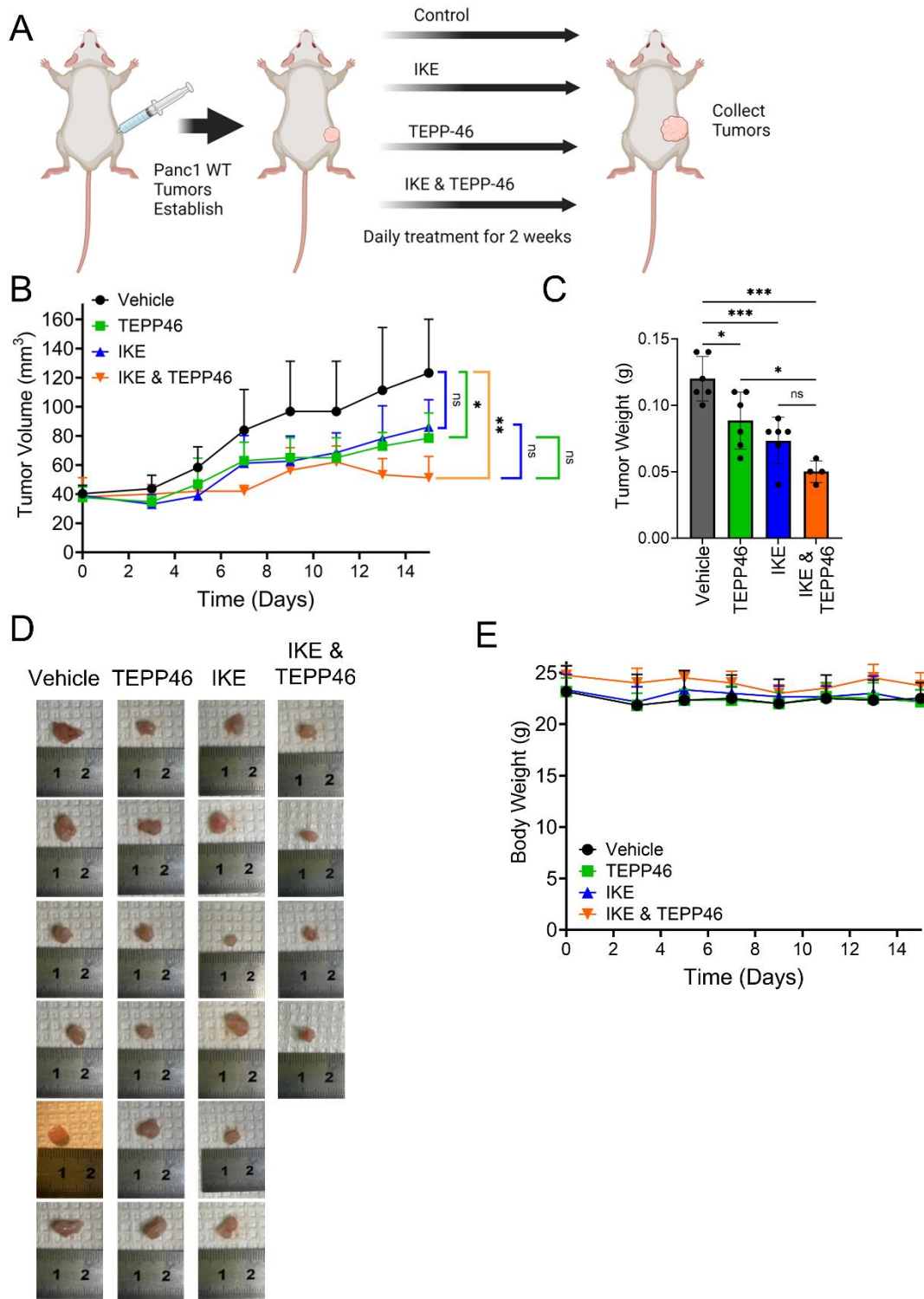


**Figure 3.7** The combination of pyruvate activation and cystine starvation is an efficacious treatment for PDAC in vivo.

### Figure 3.7 (cont'd)

**A.** Treatment schematic for xenograft tumors formed from Panc1 WT cells, treated daily for 2 weeks with vehicle control, IKE, TEPP-46, or IKE and TEPP-46 combined. N=6 for each treatment group, except IKE and TEPP-46 combination with N=4. **B.** Tumor volume of xenograft tumors for each treatment group over time. **C.** Tumor weight at end point for each treatment group. For **B-C**, significance was assessed by one-way ANOVA at end point. \* $p < 0.05$ , \*\* $p < 0.01$ , ns = non-significant. Multiple hypothesis correction by Sidak test. **D.** Images of tumors for each treatment group at end point. **E.** Body weight of treated mice throughout the treatment course.

### Discussion

Pyruvate kinase plays a complex role in the metabolic reprogramming of PDAC cells. Here, we demonstrate for the first time that PKM2KO provides a survival advantage against cystine starvation induced ferroptosis. This survival advantage is mediated by decreased PK activity that leads to reprogrammed glutamine metabolism and activation of ME1 to produce NADPH. Ferroptosis is inherently a consequence of aberrant metabolic conditions and represents an exciting new avenue of targeted metabolic therapy.<sup>4,105</sup> PDAC tumor cells survive under low nutrient conditions and are particularly vulnerable to cystine starvation induced ferroptosis, which has been recently demonstrated *in vivo*.<sup>126</sup> Our study provides evidence that decreasing PK activity is a potential resistance mechanism against cystine starvation induced ferroptosis. While increased PK activity sensitizes cells to oxidative stress, its activity has not yet been connected to ferroptosis.<sup>177,201</sup> Here, we demonstrate for the first time that activation of

PKM2 synergistically enhances cystine starvation induced ferroptosis *in vitro* and suggests a novel strategy for inhibiting survival of PDAC *in vivo*. This newly discovered metabolic vulnerability in PDAC represents a promising opportunity for therapeutic intervention. Further research will identify and optimize potent and selective drugs to target this vulnerability. Interestingly, IKE treatment alone had only a modest effect on PDAC tumor growth in contrast to xenograft tumors from other cancer types.<sup>182,290</sup> Our findings also raise the possibility that cancer cells with low PKM2 expression or low PK activity may provide a pool of persistent cells within a tumor that resist cystine starvation. Thus, the combination of increasing PK activity and inducing cystine starvation presents exciting opportunities for targeting persistent cancer cells.

It has recently been proposed that there is no single unified mechanism for ferroptosis; instead, it exists as a flexible penumbra of regulated defenses.<sup>137</sup> Consistently, we find that decreased PK activity does not universally protect against ferroptosis, but specifically against cystine starvation induced ferroptosis, as inhibition of GPX4 leads to ferroptosis even with low PK activity. Our work also provides further clarity on the role of glutamine metabolism in ferroptosis, which has been somewhat controversial. In other cancer types, removal of glutamine suppressed ferroptosis induced by cystine starvation.<sup>106,153,154</sup> On the other hand, recent observation in pancreatic and hepatocellular cancer cell models show that the removal of glutamine can possibly cause ferroptosis.<sup>156,291</sup> Here, we report that the removal of glutamine eliminates lipid peroxide accumulation and prevents ferroptosis only in PKM2 expressing PDAC cells under cystine starvation. In contrast, removal of glutamine or inhibition of glutaminase decreases survival of PKM2KO cells under cystine starvation. The PKM2KO cells show resistance

to ferroptosis and simultaneously active glutaminolysis through producing TCA cycle intermediates and deriving amino acids from glutamine. This suggests there are metabolic states in which glutamine can be used in either a pro- or anti-ferroptotic manner. We propose that PK plays a key role in coordinating glucose and glutamine metabolism as a potential adaptation response to cystine starvation and resistance to ferroptosis.

Investigating metabolic pathways known to influence antioxidant defense revealed that neither the oxidative pentose phosphate pathway nor glutathione synthesis is the dominant mechanism by which PKM2KO cells defend against ferroptosis. Rather, ME1 and the malate aspartate shuttle are important for providing the metabolic advantage in PKM2KO cells under cystine starvation, as evidenced by malate supplementation promoting survival of cystine starvation, increased malate and aspartate synthesis from glutamine, and elevated ME1 expression in PKM2KO cells. KRAS mutated cancer cells, such as PDAC cells, decouple glucose and glutamine metabolism and upregulate ME1 in addition to GOT1 and GOT2 to facilitate the breakdown of glutamine for anaplerosis and production of NADPH.<sup>76,77,289</sup> ME1 has also been identified as a ferroptosis defense protein in hepatic ischemia/reperfusion injury and synovial sarcoma.<sup>292,293</sup> Our work establishes a novel connection between PK and ME1 as well as their roles in ferroptosis in PDAC. Additionally, our study shows that inhibition of ME1 provides a route to promote ferroptosis and circumvent PDAC metabolic defense strategies for surviving low cystine conditions.

It has been established that the PDAC tumor microenvironment is deficient in many nutrients, including cystine.<sup>66</sup> The mechanism driving this low cystine environment is currently unclear, but possible explanations include changes in tumor cell genetics or

stromal cell composition within the tumor.<sup>66</sup> In our study, we have intentionally used glucose, glutamine, and cystine concentrations reflective of the tumor microenvironment. The low cystine environment has also been shown to influence central carbon metabolism. Specifically, lung cancer cells grown under low cystine conditions have decreased glutamine metabolism and conversely supraphysiologic concentrations of cystine drive enhanced glutaminolysis.<sup>89</sup> The requirement of high cystine to drive glutamine metabolism may explain the lack of robust results in targeting glutamine metabolism in clinical trials.<sup>175,176</sup> The expression of the cystine/glutamate antiporter, xCT, also enhances dependency on glucose as increased glutamate is secreted rather than used in downstream metabolic pathways.<sup>294</sup> Further, high expression levels of xCT increases sensitivity to oxidative stress and alters glutamine metabolism,<sup>295,296</sup> consistent with our observation that PKM2KO cells have decreased xCT expression under cystine starvation.

The precise mechanism by which PKM2 activity changes expression of ME1, xCT, and GPX4 has yet to be determined. Decreased PK activity leads to decreased pyruvate production. As malic enzyme uses malate to produce pyruvate, upregulation of ME1 may serve as a compensatory route for maintaining adequate pyruvate pools. PKM2 mediated reprogramming of metabolism has known effects on nutrient sensing, accumulation of biosynthetic intermediates, and production of antioxidants.<sup>78,201,205,206,275,288,297–299</sup> These changes themselves likely have downstream signaling effects leading to complex changes in metabolic machinery and defense systems against ferroptosis. Additionally, dimeric PKM2 translocates into the nucleus and influences transcription of several genes implicated in cancer progression including Cyclin D1, C-Myc, HIF-1 $\alpha$ , and  $\beta$ -

catenin.<sup>187,219,221</sup> Some of these factors are known to impact ferroptosis; for example,  $\beta$ -catenin is involved in GPX4 synthesis.<sup>300</sup> PKM2 can also inhibit p53, which is known to decrease xCT expression, providing a potential connection between PKM2 and xCT.<sup>301–304</sup> HIF-1 $\alpha$  promotes increased iron uptake and availability suggesting potential connections between iron metabolism and PKM2 which would likely influence ferroptosis.<sup>305–307</sup> However, the fact that we observe resistance to cystine starvation in absence of PKM2 suggests a metabolic mechanism and not PKM2 mediated gene regulation.

In conclusion, our work demonstrates that decreasing PK activity protects PDACs from cystine starvation induced ferroptosis. Additionally, our data show that cancer cells with low PK activity represent a potential pool of resilient cells able to tolerate low nutrient stress and enable tumor persistence. Therefore, this work reveals critical mechanisms by which PDAC cells reprogram their metabolic pathways to support survival when environmental cystine is scarce. Targeted PKM2 activation in combination with cystine metabolism inhibition is a novel strategy against PDAC tumors and represents a promising new path to improve outcomes for PDAC patients.

### **Limitations of This Study**

PDAC has a high degree of metabolic and genetic heterogeneity<sup>4,67–73</sup> which we observe in some differences between PDAC cells evaluated. Further work is still needed to understand the metabolic heterogeneity influencing ferroptosis in PDAC and the role of PK in modulating ferroptosis and its related defense proteins. *In vivo* studies were conducted in heterotopic xenograft models in immunocompromised mice. Future studies will include orthotopic models in immunocompetent mice and optimize drug

selection, doses, pharmacokinetics, and treatment regimen.

### **Acknowledgements**

Support from NIH under award numbers R01CA270136 and R01AI139074 and the Aitch Foundation. Overview schematics were made with BioRender. We thank the MSU Mass spectrometry core facility, MSU campus animal resources, and the additional present and former members of the Lunt lab: Dr. Deanna Broadwater, Amir Roshanzadeh, Dr. Shao Thing Teoh, and Dr. Martin Ogrodzinski for helpful suggestions.

### **Author Contributions**

Conceptualization, E.E. and S.Y.L.; Methodology, E.E. and S.Y.L.; Investigation, E.E., T.J., H.C.D.M., G.T., A.P., L.Y.; Writing – Original Draft, E.E. and S.Y.L.; Writing – Review & Editing, E.E., T.J., H.C.D.M., G.T., A.P., L.Y., S.Y.L.; Funding Acquisition, S.Y.L.; Project Administration, E.E. and S.Y.L.; Supervision, S.Y.L.

### **Declaration of Interests**

Sophia Y. Lunt, Elliot Ensink, Tessa Jordan, and Hyllana C. D. Medeiros hold a provisional patent on the method of treating cancer by manipulating pyruvate kinase activity and inhibiting cysteine metabolism. Sophia Y. Lunt is an advisory board member of the Van Andel Institute Metabolism & Nutrition Program. Remaining authors declare no competing interests.

### **Ethical Approval Statement:**

All animal operations were approved by the Institutional Animal Care and Use Committee of Michigan State University.

## **Inclusion and Diversity**

We support inclusive, diverse, and equitable conduct of research. One or more of the authors of this paper self-identifies as an underrepresented ethnic minority in science. We worked to ensure sex balance in the selection of non-human subjects. We worked to ensure diversity in experimental samples through the selection of the cell lines. While citing references scientifically relevant for this work, we also actively worked to promote gender balance in our reference list.

## **Methods**

### **Cell culture**

The human pancreatic cancer cell lines, AsPC1, Panc1, BxPC3, and MiaPaCa2 were acquired as a gift from Dr. Nouri Neamati at University of Michigan. HEK 293T cells were purchased from ATCC (CRL-3216). Cells were routinely cultured in Dulbecco's modified eagle medium (DMEM) (MT10013CV, Thermo Fisher Scientific,) with sodium pyruvate, supplemented with 10% fetal bovine serum (FBS) (13206C, Sigma-Aldrich), 1% penicillin and streptomycin (P/S) (15140122, Thermo Fisher Scientific), 5 µg/mL plasmocin (ant-mpp, Invivogen), and cultured in a humidified incubator with 5% CO<sub>2</sub> at 37 °C. During experimental procedures cells were incubated in a humidified incubator with 5% CO<sub>2</sub> at 37 °C in DMEM without glucose, glutamine, pyruvate, or cystine (D9815, US Biological) supplemented with 5 mM glucose, 1 mM pyruvate, and varying amounts of glutamine or cystine as indicated, 10% dialyzed FBS (F0392, Sigma-Aldrich), and 1% P/S. Cells were routinely tested for mycoplasma detection with the kit (rep-mysnc-100, Invivogen).

## Gene knockout by lentiviral CRISPR/Cas9 gene editing

CRISPR/Cas9-mediated genome editing was used to achieve PKM2 knockout with lentivirus-mediated gene expression.<sup>265</sup> Guide RNAs targeting exon 10 of the PKM gene (region determinative of PKM2 expression) were designed by CRISPR DESIGN (<http://crispr.mit.edu.proxy1.cl.msu.edu/>) and set just before the protospacer adjacent motif (PAM), a DNA sequence immediately following the Cas9-targeted DNA sequence. A lentiviral vector was used expressing one single guide RNA, caspase 9, and an antibiotic selection marker. The sgRNA sequence for PKM2 knockout plasmid vector is 5'-GTTCTTCAAACAGCTTGCGG-3' along with puromycin resistance. The sequence for scramble control plasmid with puromycin selection maker is 5'-GCACTACCAGAGCTAACTCA-3'. CRISPR gene editing plasmid vectors with gRNA and Cas9 co-expression were a gift from Paul-Joeseph Aspuria. The VSVG plasmid was a gift from Bob Weinberg (Addgene plasmid # 8454; <http://n2t.net/addgene:8454>; RRID: Addgene 8454). The psPAX2 plasmid was a gift from Didier Trono (Addgene plasmid # 12260; <http://n2t.net/addgene:12260>; RRID: Addgene 12260). Vectors were amplified by transforming Stbl3 bacterial cells grown in LB broth under 100 µg/mL ampicillin for antibiotic selection. Plasmids were harvested by Midi-prep (12243, Qiagen). To produce lentivirus, HEK293T cells were seeded in 10-cm plates containing OptiMEM (110580221, Thermo Fisher Scientific) with 4% FBS. When the HEK293T cells reached ~50% confluency, they were transfected using Lipofectamine 3000 (L3000001, Thermo Fisher Scientific) according to the manufacturer's instructions with 10.0 µg lentivirus plasmids, 0.5 µg VSVG, and 5.0 µg psPAX2 plasmids. After 24 hours, fresh DMEM with 15% FBS and 1% P/S was added, and cells were grown for another 48 hours to generate virus. For

transduction with lentivirus, the AsPC1 and Panc1 cells ( $1 \times 10^5$  cells) were seeded in 10-cm plates. The supernatant of transfected HEK293T was collected and passed through 0.45 micron PVDF syringe filter. Five mL of the viral supernatant and 5 ml of fresh media were added to recipient AsPC1 and Panc1 cell plates with polybrene (TR1003G, Thermo Fisher Scientific) at final concentration of 4  $\mu\text{g}/\text{ml}$ . The cells were cultured for 24 hours followed by adding fresh DMEM medium supplemented with 10% FBS and treated for 12 days with 2  $\mu\text{g}/\text{mL}$  puromycin (A1113803, Thermo Fisher Scientific) for selection. The selected cells were then expanded and analyzed for successful gene knockout by sequencing and western blot analysis. Genomic DNA was extracted using DNeasy Blood and Tissue Kit (69506, Qiagen) to check for successful gene editing. PCR primers used to amplify the targeted region around exon 10 of PKM consisted of a forward primer (5'-GCACTTGGTGAAGGACTGGT-3') and reverse primer (5'-AATGGACTGCTCCCAGGAC-3'). A nested primer (5'-GTGACTCTTCCCCTCCCTCT-3') was used for sequencing. Sequencing was completed by ACTG. Individual clones were selected by diluting the population to single cells plated in a 96-well plate and then expanding the population. PKM2 deletion for isolated clones was determined by western blot.

### **PKM1 and PKM2 overexpression**

Overexpression of PKM1 and PKM2 was achieved using a lentiviral gene expression purchased from VectorBuilder. The vector contained the blasticidin resistance gene and either the PKM1 or PKM2 protein coding sequence under the EF1A promoter. Lentivirus was produced and used to transduce target cells in an identical manner as described in the previous section. Transduced cells were selected using 10  $\mu\text{g}/\text{ml}$  blasticidin

(A1113903, Thermo Fisher Scientific). The selected cells were then expanded and analyzed for successful gene knockout by western blot analysis.

### **Protein extraction and western blot analysis**

Cells were plated in 10 cm plates and grown until ~60-70% confluent. Plates were washed twice with PBS w/o calcium or magnesium (D8537, Sigma-Aldrich) and the media was replaced with experimental media. Panc1 cells were incubated for 12 hours, AspC1 were incubated for 24 hours as described above. Cell lysis for protein extract was completed using cell lysis buffer (9803, Cell signaling). Western blot analysis was carried out using standard protocols. Briefly, protein samples were diluted to 1 µg/mL, reduced with 6x Laemmli loading dye, and boiled for 5 minutes. 30 µg of protein was loaded to precast Bolt 10- or 17-well 4-12% polyacrylamide, Bis-Tris, 1.0 mm gels (NW04120BOX, NW04127BOX, Thermo Fisher Scientific,). Gel electrophoresis was carried out in MES running buffer (B000202, Thermo Fisher Scientific) at 200V for 22 minutes. Protein was transferred to nitrocellulose membranes, which were then stained with Ponceau S stain (A40000279, Thermo Scientific) to confirm total protein equivalence between samples and were then cut for appropriate targets of interest. The following dilutions of primary commercial antibodies in 5% BSA in tris buffered saline with 0.1% TWEEN20 (TBST) were used as probes: 1:1000 dilution of anti-PKM1 (7067S, Cell Signaling Technology), 1:1000 dilution of anti-PKM2 (4053S, Cell Signaling Technology), 1:1000 dilution of anti-GPX4 (52455, Cell Signaling Technology), 1:500 dilution of anti xCT (12691, Cell Signaling Technology), 1:1000 dilution of anti-β-actin (4970S, Cell Signaling Technology), 1:1000 dilution of anti-cofilin (5175, Cell Signaling Technology) and 1:1000 dilution of anti-vinculin (13901, Cell Signaling Technology). Primary antibodies were diluted in 5% BSA

in TBST and incubated overnight at 4 °C. HRP-linked secondary anti-rabbit antibodies (7074S, Cell Signaling Technology) were diluted in 5% non-fat milk at a dilution of 1:5000 and incubated at room temperature for 1 h. Clarity Western ECL Substrate Kit (1705060, BioRad) was used for detection. Images were captured on the BioRad ChemiDoc XRS+ imager and Image Lab 5.2.1 was used for image processing.

### **Cell viability and proliferation analysis**

Cells were plated on 96-well plates at 2000 cells/well for Panc1 and 4000 cells/well for all other cell lines under standard conditions described above. Cells were allowed to seed overnight (approximately 18 hours). Media was aspirated and cells were washed twice with phosphate buffered saline (PBS) w/o calcium or magnesium (D8537, Sigma) before adding 100 µL of experimental media containing compounds and nutrients at indicated concentrations to each well. Proliferation was measured using the Incucyte platform (Sartorius). Briefly, images were captured every 2-4 hours and automatically counted using the Incucyte Cell-by-Cell software analysis package. Proliferation counts were normalized to the first cell count obtained immediately after beginning experimental conditions. Viability was assessed at 48 hour time points for AsPC1 and BxPC3 cells and 24 hour timepoints for Panc1 and MiaPaCa2 cells using AlamarBlue (A50100, Thermo Fisher Scientific) according to the manufacturer's instructions. Briefly, 10 µL of AlamarBlue was added to each well containing 100 µL of experimental media. Plates were gently agitated to promote mixing, then incubated under standard conditions for a fixed time interval. Fluorescence was measured using 545 nm excitation and 590 nm emission using a BioTek Synergy H1 fluorescent plate reader. For the trypan blue viability assay, 50,000 cells/well were plated on 6-well plates overnight and switched to

experimental media as described previously. At the indicated time point cells were washed twice with 1 mL of PBS w/o calcium or magnesium (D8537, Sigma-Aldrich) and removed from the plate using 200  $\mu$ L of Trypsin-EDTA (0.25%) (2520056, Thermo Fisher Scientific) incubated for 5 minutes, and quenched with 200  $\mu$ L of cell culture media. The suspended cell solution was mixed with equal parts of trypan blue 0.4% (15250061, Thermo Fisher Scientific) and counted using the Cellometer Auto T4 (Nexcelom Bioscience) for cell counting and viability measurement.

### **Cell culture reagents**

The following is a list of chemical compounds used in cell culture experiments: 1 mM N-acetyl-L-cysteine (A9615, Sigma-Aldrich), 100  $\mu$ M Trolox (238813, Sigma-Aldrich), 100  $\mu$ M deferoxamine (D9533, Sigma-Aldrich), 5  $\mu$ M Ferrostatin-1 (SML0583, Sigma-Aldrich), 50  $\mu$ M Z-VAD-FMK (14463, Cayman Chemical), 10  $\mu$ M Necrostatin-1S (20924, Cayman Chemical), 0.16 – 50  $\mu$ M IKE (27088, Cayman Chemical), 0.16 – 10  $\mu$ M RSL3 (SML2234, Sigma-Aldrich), 25-100  $\mu$ M TEPP-46 (HY-18657, MedChem Express), 10  $\mu$ M compound 3k (36815, Cayman Chemical), 50  $\mu$ M Malic enzyme inhibitor (HY-124861, MedChem Express), 8 and 32 mM DM-Malate (374318, Sigma-Aldrich), 8 mM DM-Succinate (73605, Sigma-Aldrich), 8 mM DM- $\alpha$ -ketoglutarate (28394, Cayman Chemical), 5  $\mu$ M CB-839 (22038, Cayman Chemical), 300  $\mu$ M BSO (14484, Cayman Chemical), 1 mM GSH-EE (14953, Cayman Chemical), and 0.1-0.5%DMSO (D4540, Sigma-Aldrich).

### **Lipid and general ROS quantification**

The cells were seeded 25,000 cells/well in 24 well plates overnight. Cells were then washed with PBS twice and incubated in the experimental media for 24 hours. Cells were then stained for 30 minutes with either 10  $\mu$ M chloromethyl-2', 7'-

dichlorodihydrofluorescein diacetate (CM-H2DCFDA) (C6827, Thermo Fisher Scientific) for general ROS quantification or 10  $\mu$ M C11-BODIPY (D3861, Invitrogen) for lipid peroxidation according to the manufacturers protocol. Cells were also stained for 30 minutes simultaneously with 1  $\mu$ M 2'-[4-ethoxyphenyl]-5-[4-methyl-1-piperazinyl]-2,5'-bi-1H-benzimidazoletrihydrochloride trihydrate (Hoechst) (33342, Thermo Fisher Scientific) for nuclear visualization and cell localization. Cells were then washed two times with PBS and placed in live imaging solution (A14281DJ, Thermo Fisher Scientific) for image capture. Brightfield images and fluorescence were measured using a Leica DMI8 microscope, a PE4000 LED light source, 20x and 40x objective, a DFC9000GT camera, DAPI, GFP, or TexasRed filter set, and LAS X imaging software. 3 images for each fluorescent channel were captured for each well. For image processing and quantification, the images were imported into the Fiji version of ImageJ (<http://fiji.sc>).<sup>308</sup> Cells in each image were selected, background selected and normalized to cell area. Fluorescence of cells for each well was determined by the average fluorescent signal for the 3 images for that well. Relative fluorescence is shown in the figures relative to control media conditions. Images shown are representative of the images captured for each condition.

### **Metabolomic profiling and stable isotope labeling**

To quantify metabolites, each cell line was seeded 200,000 cells/well in triplicate (n=3) in 6-well plates with media as described in the cell culture methodology section until achieving approximately 80% confluency (approximately 24 hours). For stable isotope labeling, media was refreshed on the plates and incubated for 2 hours. Plates were then washed with PBS then switched to labeling media containing either 1 mM  $^{13}\text{C}_5$ -glutamine (CLM-1822-H-PK, Cambridge Isotope Laboratories) or 5 mM  $^{13}\text{C}_{1,2}$ -glucose (CLM-504-

PK, Cambridge Isotope Laboratories) and 10% dialyzed FBS (F0392, Sigma-Aldrich). Samples were collected at 0 minutes (unlabeled control) and 4 hours for  $^{13}\text{C}_{1,2}$ -glucose and  $^{13}\text{C}_5$ -glutamine labeling for the Panc1 cells. AsPC1 samples were collected identically with the exception that  $^{13}\text{C}$ -glutamine labeling was also tested at 24 hours. Metabolite extraction was performed as described previously.<sup>266</sup> Briefly, each well is washed with 0.9% saline (16005–092, VWR), then 500  $\mu\text{L}$  of HPLC grade methanol is added followed by 300  $\mu\text{L}$  of HPLC-grade water containing 0.5  $\mu\text{M}$  camphorsulfonic acid ( ) as an internal control. Cells are scraped from the plate and the solution is transferred to a 1.5 mL Eppendorf tube containing 500  $\mu\text{L}$  of HPLC-grade chloroform. Samples are vortexed for 10 minutes, then centrifuged at 4 °C 16,000 $\times g$  for 15 minutes. The polar layer is then removed and dried by lyophilization. In addition to intracellular metabolites, 100  $\mu\text{L}$  media samples were also taken from each well at the same time points and extracted using the same procedure outline above. Protein extracted from the cells was dissolved in 0.2 M potassium hydroxide aqueous solution overnight and quantified using Pierce BCA Protein Assay Kit (PI23225, Thermo Fisher Scientific). Extracted metabolites are then resuspended in HPLC-grade water containing 5  $\mu\text{M}$  1,4-piperazinediethanesulfonic acid (PIPES; P6757, Sigma-Aldrich) as an internal standard.

LC-MS/MS analysis was performed with ion-pairing reverse phase chromatography using an Ascentis Express column (C18, 5 cm  $\times$  2.1 mm, 2.7  $\mu\text{m}$ , Sigma-Aldrich) for separation and a Waters Xevo TQ-XS triple quadrupole mass spectrometer. Metabolite peak processing was performed in MAVEN.<sup>268,309</sup> Total metabolite abundance (labeled and unlabeled) was scaled by the camphorsulphonic acid internal standard and protein content. The entire dataset for each independent experiment was then normalized

by probabilistic quotient normalization.<sup>310</sup> For isotope labeled samples, the data was corrected for the natural <sup>13</sup>C abundance using IsoCor and reported as the abundance of labeled metabolite relative to the control cell under control media conditions.<sup>269</sup>

### **Pyruvate Kinase Activity Assay**

Cells were plated 200,000 cells/well in 6-well plates and incubated overnight. Plates were washed twice with PBS w/o calcium or magnesium (Sigma, D8537) and the media was replaced with experimental media in triplicate for each condition as indicated. Panc1 cells were incubated for 12 hours, AspC1 were incubated for 24 hours as described above. Pyruvate kinase activity kit (MAK072, Sigma-Aldrich) was used according to the manufacturer's protocol to evaluate pyruvate kinase activity. Briefly cells were lysed and scraped from the plate and centrifuged at 16,000xg for 5 minutes to clear debris. 5  $\mu$ L of supernatant was used for each sample for the assay. The Pierce BCA Protein Assay Kit (PI23225, Thermo Fisher Scientific) was used to quantify protein extracted from the cells to normalize activity. After quantifying PK activity in nmole/min/mL, activity was normalized to the control cell line under normal media conditions to show relative PK activity.

### **NADPH Quantification**

Cells were plated in a white 96-well plate with clear bottoms at 8,000 cells/well for each cell line tested. Cells were allowed to seed overnight before switching the media to experimental conditions for a 24 hour incubation in Panc1 and a 48 hour incubation in AsPC1. The media was aspirated from the wells, the cells were washed twice with PBS, and 50  $\mu$ L of PBS was added to each well. The manufacturer's protocol was then followed for the assay (G9081, Promega). Briefly, 50  $\mu$ L of a 1% DTAB and bicarbonate base

buffer were added to each sample and 50  $\mu\text{L}$  of sample were moved to a new set of empty wells. The plate is then heated at 60°C for 15 minutes. After the plate has been heated, the plate incubates at room temperature for 10 minutes. To the base-treated samples, 50  $\mu\text{L}$  of a solution containing equal parts of 0.4N HCl and Trizma base were added to each well. Luciferase detection reagent was prepared and 100  $\mu\text{L}$  were added to each well. The plate was briefly mixed on a plate shaker and covered in aluminum foil to keep light from entering the reaction. The plate was incubated for 30-60 minutes at room temperature before the luminescence was read on a BioTek Synergy HI plate reader.

### ***In vivo* PDAC xenograft studies**

To inoculate mice and produce xenograft tumors in mice, AsPC1 Control and PKM2KO Clone #1 cells were grown and prepared into a solution of  $5 \times 10^7$  cells/mL in PBS w/o calcium or magnesium (Sigma, D8537). 100  $\mu\text{L}$  of each solution ( $5 \times 10^6$  cells) was injected subcutaneously into the right flank of 8 week old male NOD scid gamma (NSG) mice. 12 mice received the control cells, and 12 mice received the PKM2KO cells. After 1 month the two groups of tumor bearing mice were each divided into 2 groups of 6 mice to receive intraperitoneal injections of either 200  $\mu\text{L}$  of 50 mg/kg IKE (27088, Cayman Chemical), in 65% DW5 (5% Dextrose in water), 5% TWEEN-80 (P1754, Sigma-Aldrich), and 30% PEG-300 (202371, Sigma-Aldrich) or 200  $\mu\text{L}$  of vehicle control. Treatment was delivered 6 days a week for 2 total weeks. Tumor volume and mouse body weight were measured 4 times a week. Tumor volume was estimated by caliper measurement across the long and short axes of the tumor using the equation  $\text{length} * \text{width}^2 * 0.5 = \text{volume (mm}^3\text{)}$ . After two weeks, the mice were euthanized, and tumors were excised.

To evaluate the combination of IKE and TEPP-46 *in vivo*. Panc1 WT cells were grown and prepared into a solution of  $5 \times 10^7$  cells/mL in PBS w/o calcium or magnesium (Sigma, D8537). 100  $\mu$ L of each solution ( $5 \times 10^6$  cells) was injected subcutaneously into the right flank of 6 week old female NSG mice. After ~3 weeks the tumor bearing mice were divided randomly into 4 groups (n=6 for each group except the IKE and TEPP46 combination which had n=4). Mice received daily intraperitoneal injections for 2 weeks of either 50 mg/kg IKE (27088, Cayman Chemical), 30 mg/kg TEPP-46 (HY-18657, MedChem Express), the combination of 50 mg/kg IKE with 30 mg/kg TEPP-46, or vehicle control. IKE treatment was delivered in 200  $\mu$ L volumes and was formulated in 65% DW5 (5% Dextrose in water), 5% TWEEN-80, and 30% PEG-300. TEPP-46 was delivered in 200  $\mu$ L volumes and was formulated in 5% DMSO, 40% PEG-300, 5% TWEEN-80, and 50% saline (0.9%). Tumor volume and mouse body weight were measured 4 times a week. Tumor volume was estimated by caliper measurement across the long and short axes of the tumor using the equation  $\text{length} * \text{width}^2 * 0.5 = \text{volume (mm}^3\text{)}$ . After two weeks, the mice were euthanized, and tumors were excised.

### **Statistical Analysis and Graph Generation.**

All data are expressed as means +/- standard deviation. Each experiment was conducted with three to six replicates and was reproduced in at least two independent experiments unless otherwise indicated. The figures shown are the results of one independent experiment representative of the results reproducible in each independent experiment. Statistical analysis and graphing were performed in Graph Pad v10 using Student's T-Test, one-Way ANOVA, or two-Way ANOVA and corrected for multiple hypothesis testing using the Tukey test or Sidak test where appropriate. A *p*-value of < 0.05 was used as

cutoff for determining significance. In figures \* or # =  $p$ -val  $< 0.05$ , \*\* =  $p$ -val  $< .01$ , \*\*\* =  $p$ -val  $< 0.001$ , \*\*\*\* =  $p$ -val  $< 0.0001$ .

## CHAPTER 4: MEASURING THE NUTRIENT METABOLISM OF ADHERENT CELLS IN CULTURE

### Preface

This chapter is a modified version of a previously published article:

Martin P. Ogrodzinski, Shao Thing Teoh, Lei Yu, Deanna Broadwater, **Elliot Ensink** & Sophia Y. Lunt. Measuring the Nutrient Metabolism of Adherent Cells in Culture. *Methods Mol. Biol.* **1862**, 37–52 (2019).

In this book chapter, I contributed to the methodology and manuscript preparation describing our lab's methodology in measuring the metabolism of cancer cells *in vitro*. The initial methodology was primarily developed by Sophia Lunt, Martin Ogrodzinski, and Shao Thing Teoh. Over the years since the publishing of this paper, I have made several improvements to our methodology. New changes are inserted after particular steps and are italicized for emphasis.

### Introduction

The comprehensive profiling of cellular metabolites has received growing attention in recent years, due in part to the development of increasingly sensitive instrumentation for the detection and quantification of a wide array of metabolites. Metabolomics approaches using cells cultured *in vitro* have several advantages compared to *in vivo* approaches. First, experiments utilizing cells grown in culture are generally less costly and can be performed faster than experiments using animal models. Second, growth conditions *in vitro* can be easily manipulated, which enables substantial control of experimental conditions and reduces certain confounding variables such as relative nutrient availability or concentrations of circulating hormones and growth factors. Third,

the relative ease of handling makes it possible to quickly quench metabolism and extract metabolites, thereby limiting potential metabolite degradation during longer sample collection procedures. Many metabolic processes, such as glycolysis and the tricarboxylic acid (TCA) cycle, have rapid rates of turnover.<sup>311,312</sup> Therefore, quickly quenching metabolism is necessary to ensure metabolites of interest are measured in a biologically relevant state.

This chapter describes in detail a method for metabolite extraction of adherent cells using a cold methanol:chloroform:water extraction protocol (Fig. 4.1). Metabolic quenching can be achieved through the addition of a cold organic solvent, such as methanol, directly to the cell culture dish after washing the cells to remove extracellular metabolites. While the optimal solvent conditions for a given experiment likely depend on the metabolites of interest<sup>313</sup>, the cold methanol:chloroform:water method described here enables the extraction of a wide range of intracellular metabolites, including glycolytic intermediates, TCA cycle metabolites, pentose phosphate pathway intermediates, nucleotide metabolism intermediates, amino acids, and fatty acids<sup>205</sup>. After addition of cold methanol and water, adherent cells can be scraped and collected into a cold polypropylene microcentrifuge tube. The addition of cold chloroform to the extract enables the separation of cellular metabolites by polarity, with polar metabolites accumulating in the less dense methanol/water phase and nonpolar metabolites accumulating in the denser chloroform phase. These phases of the metabolite extract can then be separated and used for downstream metabolomic analyses.

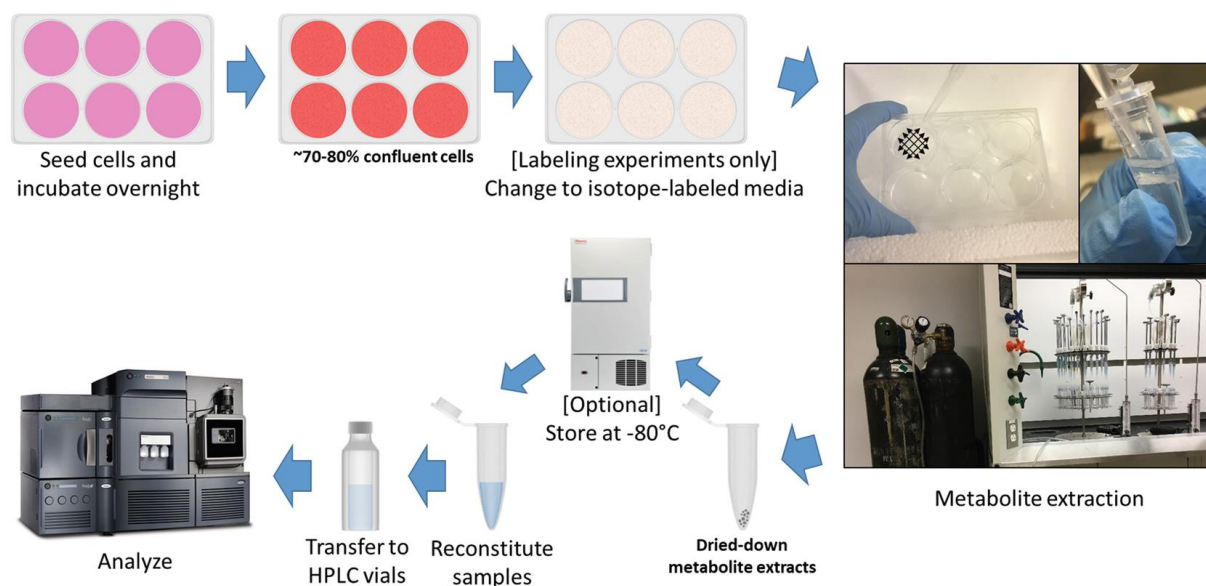


**Figure 4.1 Overview of the metabolite extraction and analysis workflow.**

Cells are prepared for metabolite extraction by seeding on 6-well plates and incubating until they reach ~70–80% confluency. For labeling studies, media is changed to stable isotope labeled media. The metabolite extraction proceeds as detailed in this chapter. Dried-down metabolite extracts may be optionally stored at  $-80\text{ }^{\circ}\text{C}$ . The samples are reconstituted in HPLC-grade water and transferred to HPLC vials for downstream analysis.

Comprehensive, reproducible, and accurate measurement of relative metabolite abundances can facilitate investigation of many biological processes. For example, the activity of the metabolic enzyme, pyruvate kinase, is regulated by several metabolites including fructose-1,6-bisphosphate, phenylalanine, alanine, serine, and oxalate among others.<sup>196,198,203</sup> Metabolomics analyses have been used to determine that metabolic regulation of pyruvate kinase splice isoforms plays an important role in cancer metabolism, tumor growth, and tumorigenesis.<sup>177,186</sup>

In addition to examining the levels of metabolites involved in regulating an enzyme, metabolite pools can also be used to measure the metabolic effects of genetic manipulations in cultured cells. For example, by measuring metabolite pools, it was determined that PKM2 deleted mouse embryonic fibroblasts have depleted nucleotides, leading to proliferation arrest.<sup>205</sup> It is also possible to use stable isotope labeling studies to determine the metabolic flux through various pathways. For example, growing cells in media containing <sup>13</sup>C-labeled glucose and extracting metabolites at various time points enables measurement of glucose carbon incorporation rates into downstream metabolites.<sup>314,315</sup> While labeled glucose is commonly used for this purpose, it is possible to design studies using numerous other isotopically labeled substrates.

Extracted metabolites are commonly analyzed using mass spectrometry. Two chromatographic techniques that are commonly used to improve mass spectrometry are gas chromatography (GC) and liquid chromatography (LC), which enable the separation of compounds by their physical properties. While GC is ideal for analyzing volatile compounds that do not deteriorate when vaporized, LC enables the detection of a wide range of compounds that can deteriorate under the conditions required for GC analysis. These heat-labile compounds include metabolites involved in numerous metabolic pathways including glycolysis, the pentose phosphate pathway, and nucleotide metabolism.<sup>316</sup> Additionally, sample preparation for liquid chromatography-mass spectrometry (LC-MS) is generally simpler and does not require chemical derivatization of metabolites, which is necessary for gas chromatography-mass spectrometry to improve thermal stability and volatility. Derivatization techniques, such as carboxybenzyl derivatization of amino acids, can still be used to further increase the range of compounds

that can be analyzed using a single LC-MS method. This flexibility makes LC-MS a valuable tool for examining cellular metabolism. The metabolite extraction method described in this chapter can be employed to investigate the metabolic state of cultured adherent mammalian cells and gain insight into cellular activity at the molecular level.

## **Materials**

### **Preparation of Adherent Cells**

1. Hemocytometer or alternative cell counting apparatus (see Note 1).
2. 6-well cell culture plates.
3. Cell culture media (see Note 2).
4. Phosphate-buffered saline (PBS), or alternative cell washing buffer.
5. Trypsin or alternative cell dissociation agent.
6. Humidified, temperature-controlled, CO<sub>2</sub> tissue culture incubator.
7. Biological safety cabinet.

### **Optional: Isotope Labeling**

1. 6-well cell culture plates.
2. Cell culture media containing labeled isotopes (see Note 3).
3. Humidified, temperature-controlled, CO<sub>2</sub> tissue culture incubator.
4. Biological safety cabinet.

### **Metabolite Extraction**

1. Camphorsulfonic acid or other primary internal standard (see Notes 4 and 5).  
Prepare high-performance liquid chromatography (HPLC)-grade water containing 0.5  $\mu$ M camphorsulfonic acid as an internal standard by adding 5  $\mu$ L of 1 mM camphorsulfonic acid to 10 mL HPLC-grade water (see Note 6).

2. HPLC-grade methanol kept on dry ice.
3. HPLC-grade chloroform kept on wet ice.
4. Blood bank saline 0.9% (see Note 7).
5. 1.7 mL polypropylene microcentrifuge tubes.
6. Dry ice.
7. Wet ice.
8. Vortexer.
  - *Refrigerated vortexer is optimal*
9. Refrigerated centrifuge.
10. Nitrogen evaporator.
  - *Lyophilizer and vacuum pump can also be used instead see metabolite extraction methods section step 16.*
11. Nitrogen tanks, purity >99.9%.

### **Resuspension of Metabolite Extracts**

1. 1,4-Piperazinediethanesulfonic acid (PIPES) or another secondary internal standard (see Note 8). Prepare 5  $\mu$ M HPLC-grade water containing PIPES internal standard by adding 50  $\mu$ L of 1 mM PIPES internal standard to 10 mL HPLC-grade water.
2. 1.7 mL polypropylene microcentrifuge tubes.
3. HPLC vials.
4. Refrigerated centrifuge.

### **LC-MS Analysis**

1. Solvent A: 10 mM tributylamine and 15 mM acetic acid in 97:3 HPLC-grade

water: HPLC-grade methanol (pH 4.95).

2. Solvent B: HPLC-grade methanol.
3. Ascentis Express column (C18, 5 cm × 2.1 mm, 2.7 μm) or alternative LC column.
4. Acquity UPLC H-Class system or alternative LC system.
5. Waters Xevo TQ-S triple quadrupole mass spectrometer or alternative mass spectrometer.
6. Nitrogen tanks, purity >99.9%.
7. Argon tanks, purity >99.9%.

## **Methods**

### **Preparation of Adherent Cells**

Perform all steps in an appropriate biological safety cabinet.

1. Plate cells in triplicates per experimental condition into 6-well cell culture plates for metabolite extraction. Prepare identical plates for cell counting (Fig.4.2).
  - *There is now no need for a separate plate for a cell count. Using a separate plate introduces potential variation from initial seeding conditions. Protein collection during extraction serves as a valid proxy for cell abundance and comes directly from the extracted cells. In lab experiments confirmed that protein and cell count correlate reasonably well. If cell counts are desired, images of the plate can be captured using the Incucyte and processed for automated cell counting.*

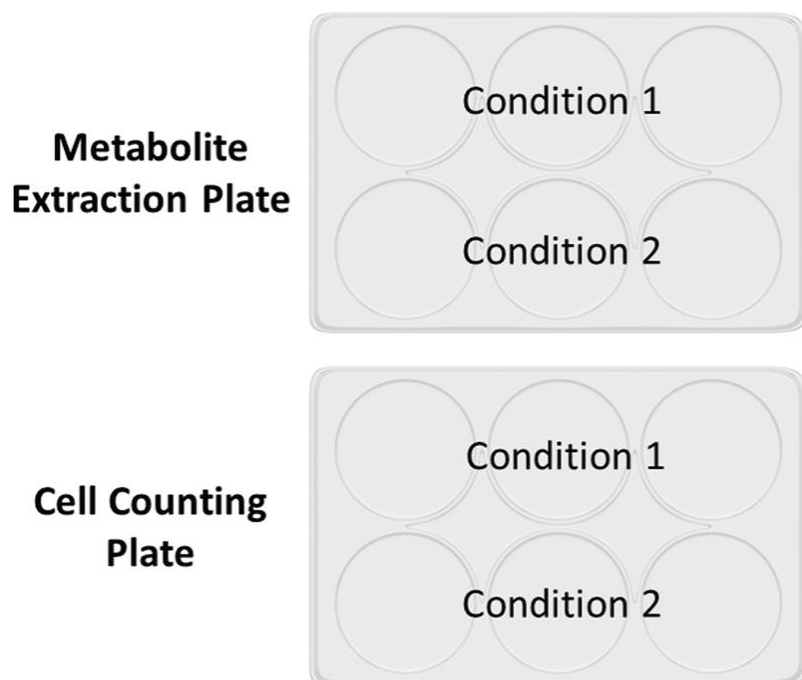


**Figure 4.2 Example layout for cell plating.**

Conditions can vary by experimental design, cell culture conditions, or time points for stable isotope labeling.

2. Culture cells in a humidified, temperature-controlled, CO<sub>2</sub> tissue culture incubator until they reach ~70–80% confluence (see Note 9).
3. Replace the cell culture media with fresh, pre-warmed (37 °C) media 1 h before extraction (see Note 10).
  - *Replace media 2 hours before to ensure equilibrium is reached. When using a new cell line, it would be best practice to establish the time until steady state is reached using <sup>13</sup>C-glucose and <sup>13</sup>C-glutamine tracers. In our experience with adherent breast and pancreatic cancer cells this occurs within a few minutes for glucose but can take 1-2 hours for glutamine.*

### Optional: Isotope Labeling

1. Culture cells in a humidified, temperature-controlled, CO<sub>2</sub> tissue culture incubator to be ~70–80% confluent at the time of extraction (see Note 9).
2. Replace the cell culture media with fresh, pre-warmed (37 °C) unlabeled media 1 h before starting the labeling study (see Note 10).
  - *Replace media 2 hours before starting the labeling study, see step 3 of the preparation of adherent cells section*
3. Aspirate all media from experimental plates.
4. Add 2 mL of pre-warmed (37 °C) labeled media to each experimental well. Do not add labeled media to time 0 plates (see Note 11).
5. Extract metabolites at each extraction time point (see metabolite extraction section and Note 12).

### Metabolite Extraction

Work with one plate at a time, and work as quickly as possible (see Note 13).

1. Keep HPLC-grade water containing 0.5 μM camphorsulfonic acid as an internal standard on wet ice.
2. At room temperature, aspirate media from each well of the remaining 6-well plates.
  - *Media can also be extracted to evaluate secreted metabolites such as lactate or glutamate. Before aspirating media, remove 100 μL of media and transfer it to a prelabeled tube containing 300 μL of HPLC-grade water with internal standards, 500 μL of HPLC-grade methanol, and 500 μL of HPLC-grade chloroform. Downstream processing is the same as*

*cell extracts.*

3. At room temperature, rinse each well once with 2 mL blood bank saline 0.9% (see Note 7).
4. At room temperature, aspirate saline.
5. Place the plate on dry ice and add 500  $\mu$ L HPLC-grade methanol (kept on dry ice) to each well of the plate.
6. Add 200  $\mu$ L of HPLC-grade water containing an internal standard (prepared in Subheading 3.3, step 1) to each well of the plate (see Note 14).
  - *Use 300  $\mu$ L of HPLC-grade water. This ensures more consistent separation between polar and non-polar phases.*
7. Thoroughly scrape the cells from one well of the plate on dry ice using a 1000  $\mu$ L pipette tip. Hold the tip orthogonal to the bottom of the plate and scrape the bottom of the plate in several opposing directions (Fig. 4.3). Wash down the well by pipetting the extraction solvent across the plate while holding the plate at a  $\sim 45^\circ$  angle. Transfer all contents from the well to a prelabeled 1.7 mL polypropylene microcentrifuge tube, then place the tube on dry ice.
  - *Using a tip limits surface area content and consistent scraping. Use of a sterile cell scraper is more effective.*

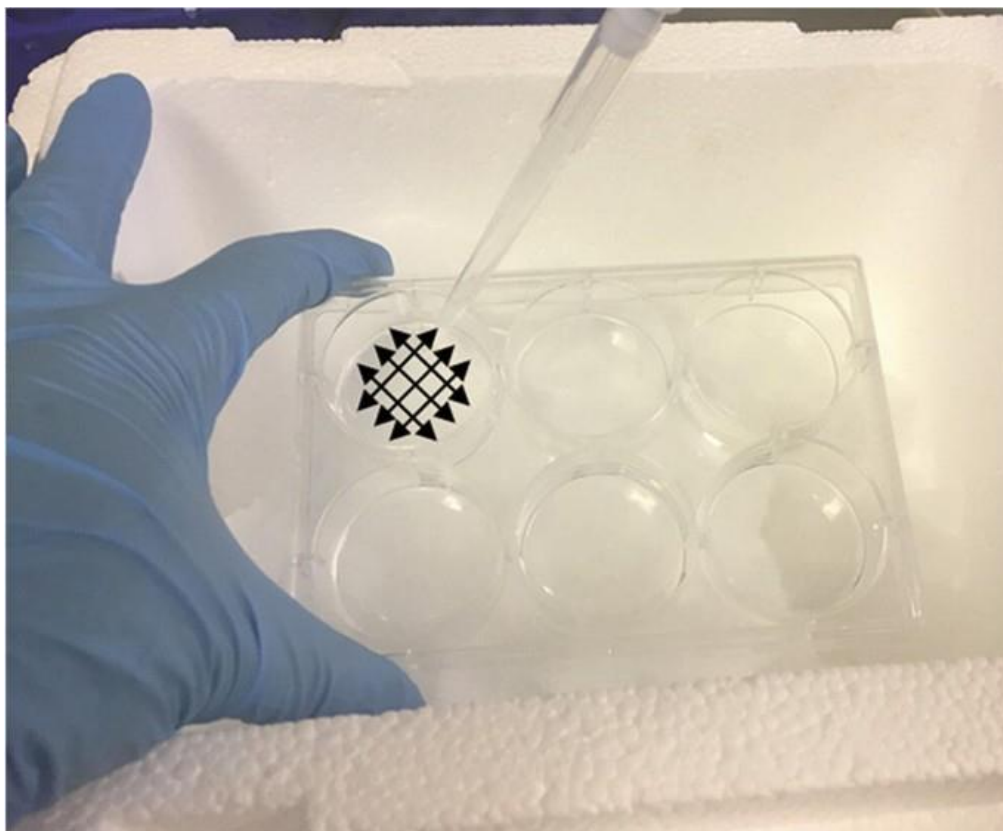


**Figure 4.3 Cell scraping.**

Thoroughly scrape the entire area of the well using a pipette tip. Scrape the plate from several opposing directions to ensure maximum coverage.

8. Repeat step 7 for all remaining wells of the 6-well plate.
9. Add 500  $\mu$ L HPLC-grade chloroform (kept on wet ice) to each tube (see Note 15).
  - *HPLC-grade chloroform can be pre-aliquoted in labeled tubes before beginning the experiment to improve workflow efficiency and speed of extraction.*
10. Vortex each tube by hand for a few seconds.
11. Place tubes on a vortexer for 10 min at 4 °C. After vortexing, the mixed contents

should appear milky white (Fig. 4.4a).

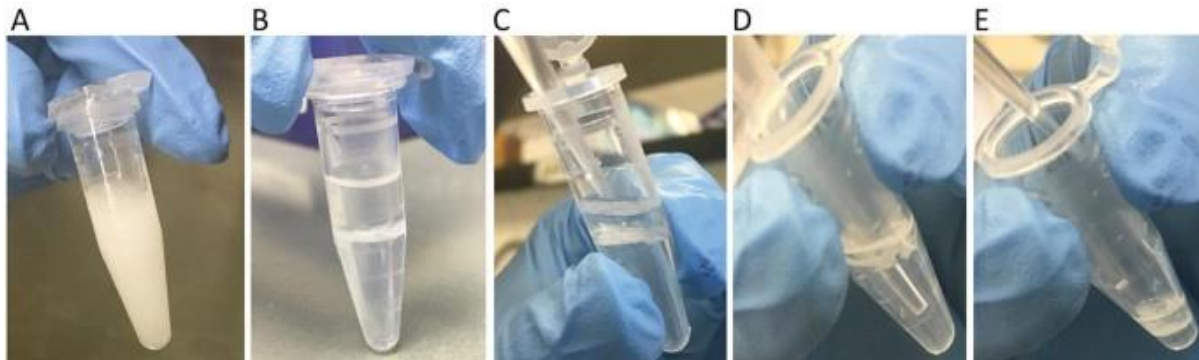


**Figure 4.4 Separation of extraction layers.**

**A.** Metabolite extraction mixture after vortexing. **B.** Separation of upper methanol/water layer and lower chloroform layer after centrifugation. Note the thin white interphase containing macromolecules such as protein and nucleic acids. **C.** Removal of the upper methanol/water layer. **(d)** Removal of the lower chloroform layer. **E.** The small amount of remaining solvent can be left to evaporate overnight, leaving the white interphase.

12. Centrifuge tubes at  $>15,000 \times g$  for 15 min at 4 °C.

13. Carefully remove the tubes from the centrifuge without disrupting the separated layers. There will be two solvent layers, with a thin interphase layer containing macromolecules such as nucleic acids and protein in the middle (Fig. 4.4b): an upper methanol/water layer containing polar metabolites; and a lower chloroform layer containing nonpolar metabolites (e.g., fatty acids).

14. Without touching the interphase that contains proteins, transfer 400  $\mu\text{L}$  of the upper layer containing polar metabolites into a new pre-labeled 1.7 mL polypropylene microcentrifuge tube for each sample (Fig. 4.4c). Keep the tubes on dry ice.

- *We are now using a different approach for drying samples by using lyophilization (freeze drying) rather than nitrogen stream drying. To accomplish this, transfer 400-500  $\mu$ L of upper polar layer to a prelabeled 5 mL polypropylene tube containing 4 mL of HPLC grade water kept on wet ice. This dilution step is necessary to bring the methanol concentration to < 10% to ensure sample remains in the solid phase during lyophilization. 3-5 holes should be poked into the lids of each tube to allow for sublimation, this can be done in preparation beforehand. Store samples in  $-80^{\circ}\text{C}$  until ready for lyophilization.*
15. Without collecting the interphase, transfer 400  $\mu$ L of the lower layer containing nonpolar metabolites into new prelabeled 1.7 mL polypropylene microcentrifuge tubes (Fig. 4.4d; see Note 16). Keep the tubes on wet ice.
- *We do not routinely use the nonpolar phase for lipidomics analysis in our lab and thus have not evaluated whether nitrogen stream drying or lyophilization is the superior approach.*
16. Dry down the samples under a stream of nitrogen until all solvents have evaporated (see Notes 17 and 18). The upper layer should take  $\sim 1.5$  h, and the lower layer should take  $\sim 20$  min. Dried samples can be stored at  $-80^{\circ}\text{C}$  (Fig. 4.5).
- *Use lyophilization instead. To complete this, prepare the lyophilizer by turning on the device and using the automatic settings. Remove samples from the  $-80^{\circ}\text{C}$  freezer and place in liquid nitrogen bath to ensure freezing is complete. Quickly place tubes within the vacuum chamber, seal the*

chamber, and activate the vacuum pump. The more samples used at once the longer it will take, but for a typical experiment of 24-48 samples this will take about 24 hours. Shelf temperature (heat application) and sample layout will influence drying time and should be further optimized. Once drying is complete, samples can be stored in the -80 °C. Samples are stable in this state, but analysis should be completed in a short time frame.

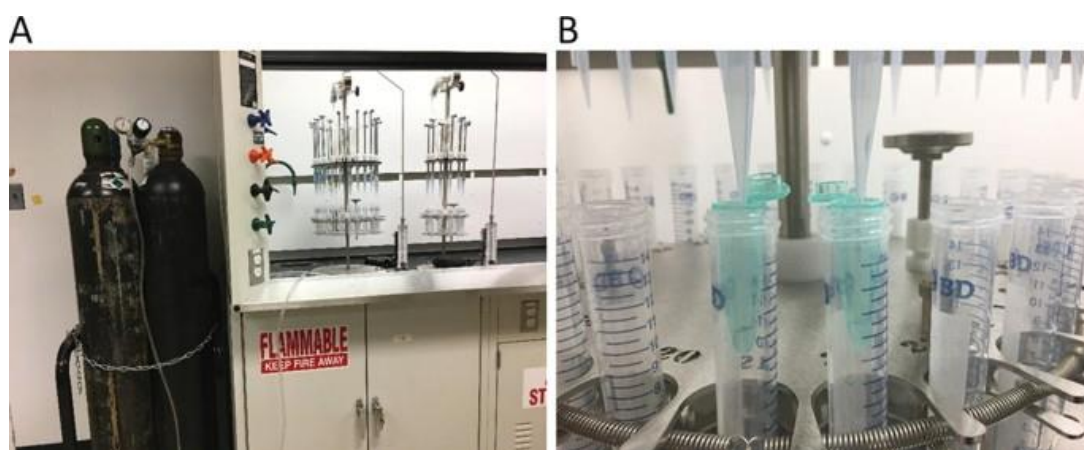


**Figure 4.5 Drying station setup.**

**A.** Nitrogen tanks are attached to a drying apparatus. **B.** Microcentrifuge tubes with polar-phase metabolites are placed under a stream of nitrogen without the tip of the apparatus contacting the solution.

17. OPTIONAL: The interphase containing macromolecules can be dried overnight by leaving the tubes open in a chemical fume hood and used for subsequent analyses (Fig. 4.4e; see Note 19).

- *This is now our preferred normalization approach.*

## Resuspension of Metabolite Extracts

1. Resuspend each sample in 105  $\mu\text{L}$  HPLC-grade water containing 5  $\mu\text{M}$  PIPES internal standard (see Note 8).
  - *Dried samples from lyophilization consist of white powder adherent to the walls of the 5 mL tube. Centrifuge the tube at 2000xg at 4 °C to concentrate then add 100  $\mu\text{L}$  of HPLC-grade water containing the 5  $\mu\text{M}$  PIPES internal standard.*
2. Vortex tubes thoroughly dissolve all metabolites from the sides of the tube.
3. Centrifuge tubes at  $>15,000 \times g$  for 10 min at 4 °C to remove any macromolecules such as proteins that may have precipitated out of solution.
4. Transfer the supernatant only into HPLC vials (see Notes 20 and 21). If amino acids will be derivatized for analysis, only transfer 80  $\mu\text{L}$  of the supernatant to HPLC vials, as 20  $\mu\text{L}$  will be needed for derivatization
  - *Resuspended samples can also be stored in a smaller microcentrifuge tube for later analysis. A minimum of 40  $\mu\text{L}$  can be used for routine LC-MS analysis, 20  $\mu\text{L}$  can be used for amino acid analysis, and 5  $\mu\text{L}$  for 3-Nitrophenylhydrazine derivatization (subheading on 3-Nitrophenylhydrazine derivatization)*
5. Prepare a blank sample containing only the solvents used for resuspending the metabolite extracts.
6. Analyze metabolites using LC-MS (see subhead on LC-MS analysis).

## Carboxybenzyl (CBZ) Derivatization

- *This process is no longer used in our lab due to the toxicity of compounds*

- used and lengthy process. Therefore, I have omitted this section from this thesis. Instead, we use a method developed by the MSU metabolomics core using the Xevo TQS-micro and a 10 mM perfluoroheptanoic acid (PFHA) solvent (see protocol MSMC-002 version 1.1 FREE AMINO ACID EXTRACTION for details). To prepare the samples, add 20  $\mu$ L of sample prepared in section 3.4 to a prelabeled HPLC tube containing 20  $\mu$ L of 20 mM PFHA (final concentration of 10 mM PFHA). If not using isotope labeled tracers, 0.2  $\mu$ M  $^{13}$ C labeled amino acids can be used as internal standards to improve quantification. Keep samples on ice.*
- *For LC-MS Analysis contact the MSU mass spectrometry core to ensure the TQS-micro is set up for amino acid analysis.*
  - *Samples should be run in conjunction with a standard curve consisting of 50, 12.5, 3.13, 0.78, 0.195, 0.049, and 0.012  $\mu$ M amino acids in solution with appropriate internal standards.*

### **3-Nitrophenylhydrazine (3-NPH) Derivatization**

*This derivatization method protects carbonyl and carboxyl groups allowing for improved quantification of important metabolites including pyruvate, lactate, citrate, isocitrate,  $\alpha$ -ketoglutarate, malate, fumarate, and oxaloacetate.*

1. *Mix 5  $\mu$ L of sample prepared in subheading 3.4 with 5  $\mu$ L of 250 mM 3-NPH in methanol, 5  $\mu$ L of 150 mM 1-ethyl-3(3-(dimethylamino) propyl) carbodiimide (EDC) in methanol, and 5  $\mu$ L of 7.5% pyridine in methanol. (Note that the 3NPH, EDC, and pyridine can be prepared in a master mix of appropriate ratios and dispensed together to mix with each sample)*

2. *Incubate samples at 0° C for 2 hours*
3. *To each sample add 4 µL of 2 mg/mL (~9 mM) butylated hydroxytoluene (BHT) in methanol*
4. *Add 56 µL of water to dilute sample. (Note that this can be completed simultaneously with step 3 by first preparing a master mix at an appropriate ratio)*
5. *Vortex samples to mix for 10 seconds*
6. *Centrifuge samples at 15,000xg for 5 minutes at 4 °C*
7. *Transfer sample to prelabeled HPLC tubes and proceed immediately to analysis to ensure optimum quality.*

### **LC-MS Analysis**

1. Use solvent A and solvent B for LC-MS analysis.
  - *Solvent A: 10 mM tributylamine and 15 mM acetic acid in 97:3 HPLC-grade water: HPLC-grade methanol (pH 4.95).*
  - *Solvent B: HPLC-grade methanol.*
2. Prepare the instrument for analysis by installing the Ascentis Express column (C18, 5 cm × 2.1 mm, 2.7 µm), priming the solvents, and verifying the instrument operational parameters (see Note 24).
3. Mass spectra are acquired using negative-mode electrospray ionization operating in multiple reaction monitoring mode.
4. Operate the instrument using the following parameters: capillary voltage, 3000 V; cone voltage, 50 V; autosampler temperature, 5 °C; injection volume, 5 µL; and column temperature, 50 °C. Nitrogen is used as cone gas and desolvation gas, with flow rates of 150 L/h and 600 L/h, respectively. Argon is used as the

collision gas at a manifold pressure of  $4.3 \times 10^{-3}$  mbar. The source temperature is 150 °C, and desolvation temperature is 500 °C.

5. Elution from the column is performed over 12 min with the following solvent gradient: t = 0, 0% solvent B, flow rate 0.4 mL/min; t = 1, 0% solvent B, flow rate 0.4 mL/min; t = 2, 20% solvent B, flow rate 0.3 mL/min; t = 3, 20% solvent B, flow rate 0.25 mL/min; t = 5, 55% solvent B, flow rate 0.15 mL/min; t = 8, 95% solvent B, flow rate 0.15 mL/min; t = 9.5, 95% solvent B, flow rate 0.15 mL/min; t = 10, 0% solvent B, flow rate 0.4 mL/min; t = 12, 0% solvent B, flow rate 0.4 mL/min.
6. Load the blanks and samples prepared previously into the sample manager of the mass spectrometer (see Note 25).
7. Begin the analysis by first injecting the blank, followed by several injections of the quality control sample (see Note 26).
8. Continue the analysis by injecting the samples prepared previously (see Note 27).
9. After all samples have been analyzed, the resulting data can be processed (see Note 28).

## Notes

1. Accurate cell counts enable normalization of the metabolomic data by the number of extracted cells. This helps prevent differences in metabolite abundance that could be attributed to different numbers of extracted cells.
  - *Protein content can also be used instead of cell counts.*
2. Any cell culture media that has been optimized for use with a particular cell line of interest can be used.

- *Careful consideration should be made to utilize media conditions that closely resemble environmental conditions representative of the endogenous environment.*<sup>88</sup>
3. Prepare isotope labeling media using the base cell culture media that is optimized for the cell line of interest but does not contain the unlabeled substrate. For example, Dulbecco's modified eagle medium (DMEM) containing 25 mM glucose and 4 mM glutamine can be used for labeling with these compounds. To prepare <sup>13</sup>C-glucose labeled DMEM, DMEM base without glucose or glutamine is supplemented with 25 mM <sup>13</sup>C -glucose and 4 mM unlabeled glutamine. To prepare <sup>13</sup>C-glutamine labeled DMEM, 25 mM unlabeled glucose and 4 mM <sup>13</sup>C-glutamine is added to the DMEM base. Dialyzed fetal bovine serum that does not contain unlabeled small molecules such as glucose and amino acids should also be used.
- *5 mM glucose and 1 mM glucose should be used routinely to avoid supraphysiologic metabolic conditions.*
4. Internal standards may be added to the initial extraction solvent, and/or the solvent used to reconstitute dried-down metabolite extracts (typically dissolved in HPLC-grade water). By including an internal standard in the initial extraction solvent (primary internal standard), any random or systematic variations in subsequent steps may be corrected. After normalization by the abundance of the internal standard, differences in overall metabolite abundance between the samples still remain. This could then be attributed to differences in the initial amount of sample (i.e., number of cells). Therefore, it is always worthwhile to

strive to harvest each sample at similar, if not identical, cell number or confluence.

5. During sample preparation and analysis, it is possible for random or systematic variation to occur. This includes inaccuracies in volume transfer or resuspension of dried-down metabolites, instrument-specific fluctuations in injected sample volume, and/or drifts in ionization efficiency or detector sensitivity over time. These and other factors may contribute to fluctuations in the final detected peak intensities of the sample. It is therefore important to correct for these inconsistencies by the use of appropriate internal standards. The choice of internal standards is not rigid but should be based on the following three considerations. (1) The internal standard must not be endogenously produced by the cells of interest. If the cells produce this metabolite, the abundance may differ between samples depending on the particular cell line, rendering it impossible to normalize samples based on the internal standard intensity. (2) The internal standard must be stable in solution and not degrade appreciably over the course of the analytical run. To determine stability, it is recommended that a biological sample be spiked with a candidate internal standard compound and be analyzed for variations in peak intensity over the expected time frame of a typical analytical run (e.g., 24 h). (3) The internal standard should possess good chromatographic characteristics (sharp peak with no tailing) and good peak intensity for the analytical system (e.g., chromatographic column, solvent gradient, ionization mode, and mass detector type) used.
6. Low-purity solvents may contain impurities that can lead to contamination,

instrument failures, and complications with resolution during analysis, and/or unforeseen reactions. It is always best to use the highest purity reagents available for sample preparation and analysis.

7. Washing cells with unbuffered saline helps remove residual media, waste products, cell debris, and phosphate salts. While saline does contain sodium and chloride, removing phosphate salts significantly reduces ion suppression during mass spectrometry analysis. Pure water should not be used to wash cells, as this will cause osmotic shock and can rupture cells.
8. It is good practice to reconstitute dried-down samples in volumes corresponding to their measured cell number or protein quantification value (e.g., from performing a Bradford protein assay on the protein-containing interphase). The relationship between metabolite concentration and intensity is not necessarily linear; a metabolite at double abundance may not show twice the peak intensity, and dividing the detected intensity by two will not give a final value reflective of the actual abundance. Resuspending each sample according to cell number or quantified protein ensures that each sample starts at roughly the same overall metabolite intensity, and their metabolite profiles can be compared with more confidence. In this case, it is recommended that the reconstitution solvent be spiked with a different secondary internal standard, since the concentration of the primary internal standard will vary according to the reconstitution volume. Variation in processes after sample reconstitution, such as the injection volume fluctuation or drift in peak intensity, may be corrected for using the secondary internal standard, which should be present at an identical concentration across

all samples. Following normalization using the secondary internal standard, an additional level of normalization may then be performed using the primary internal standard to correct for variability in sample preparation.

9. Performing metabolite extraction when the cells are at ~70–80% confluence ensures that the cells are in a state of active proliferation and not contact inhibited. If metabolites of interest are present at low concentrations, this protocol can be scaled up to larger plate sizes.
10. Replacing the cell culture media 1 h prior to starting the experiment removes waste products and replenishes metabolites that may have become depleted in the spent media. This ensures consistency in the media composition and is particularly important for isotope labeling studies, where a sudden change in nutrient availability can affect labeling patterns.
11. Only add labeled media to experimental plates at time points greater than 0 min. When collecting short time points (e.g., 0, 1, and 5 min), staggering the start of labeling time points is recommended, as extracting metabolites from each time point takes several minutes.
12. When analyzing metabolomic data from isotope labeling studies, it is important to correct the data for the natural isotope abundance.
13. Metabolism must be quenched quickly during extraction, as intracellular metabolite levels can change within seconds. Additionally, keeping samples at low temperatures by using wet or dry ice throughout the extraction process will minimize metabolite degradation or conversion.
14. Be as precise as possible when adding the resuspension solvent containing an

internal standard. Small errors in the addition of internal standards before drying the extracts can have significant consequences in subsequent data analysis and interpretation.

15. Chloroform has low surface tension and will drip out of the pipette tip. Therefore, chloroform must be transferred from the bottle to the sample quickly to avoid dripping. Do not use chloroform with amylenes, as this will significantly increase drying time. Do not use polystyrene pipettes with chloroform, and do not add chloroform directly to polystyrene cell culture dishes, as chloroform will dissolve the polystyrene.

16. Depress the plunger of the pipette slightly when moving the tip through the interphase containing protein. This will prevent accidental collection of protein with the nonpolar layer.

17. Drying the samples improves metabolite stability during storage. Further, dried samples can be resuspended in volumes based on the cell count or quantified protein, improving pre-analysis normalization (see Notes 8 and 19).

18. A stream of air can also be used to dry down extracts; however, this can cause oxidation of metabolites and should be avoided when analyzing metabolites sensitive to oxidation. A vacuum concentrator can also be used to dry down extracts, but care should be taken to avoid sample heating, which can degrade metabolites.

19. The resuspension volume can be normalized by either the cell count or extracted protein concentration. For example, a sample with twice the protein concentration or number of extracted cells will be resuspended in twice the

volume of HPLC-grade water. To quantify the protein in the interphase, add 1 mL of 0.2 M potassium hydroxide to the dried interphase and allow it to dissolve overnight. The resulting solution can be analyzed by Bradford protein assay.

20. After centrifugation, a small macromolecule pellet may be visible at the bottom of the tube. Even if no pellet is visible, care should be taken to avoid touching the bottom of the tube to prevent accidental collection of macromolecules such as proteins, which can clog the LC column during analysis.
21. When preparing multiple extracts, a quality control sample can be created by pooling a small aliquot from every generated sample. This pooled quality control sample can be run periodically during the analysis to ensure that sample quality and signal detection does not change over the course of the LC-MS run.
22. Chemical derivatization, although not required, can be used for LC-MS. Altering the physical properties of molecules by introducing various functional groups can improve separation by liquid chromatography, and/or increase the ionization efficiency and sensitivity in electrospray ionization mass spectrometry. Derivatization can also enable the prediction of specific fragmentation reactions in tandem MS. Two forms of derivatization techniques are applied to chromatographic analysis. One is pre-column derivatization, which involves the reaction before chromatographic separation and detection, and the other is post-column derivatization, which is carried out after separation of sample components. We use a pre-column derivatization method for improved amino acid retention in reverse-phase columns. This derivatization method only requires an aliquot of the resuspended extract and a two-step derivatization

process. Derivatized amino acids can be detected using the same reverse phase LC-MS method we use to analyze many other metabolites, without significantly increasing the difficulty of sample preparation. However, there are numerous alternative methods that are also suitable for amino acid analysis.

23. Separately add triethylamine to raise the pH of the solution prior to adding benzyl chloroformate. Triethylamine acts as a scavenger for the hydrochloric acid that is formed as an intermediate and enables the reaction to proceed to completion.
24. We perform our LC-MS analysis by ion-pairing reverse phase chromatography using an Ascentis Express C18 column for separation, an Acquity UPLC H-Class system for liquid chromatography, and a Waters Xevo TQ-S triple quadrupole mass spectrometer operated in negative mode as the mass detector. Many different columns, solvents, and instrument parameters can be used for LC-MS analysis. Optimization may be necessary to determine the best method for analyzing a particular metabolite of interest.
25. When analyzing un-derivatized and CBZ-derivatized samples together it is recommended to analyze the un-derivatized samples first and analyze the CBZ-derivatized samples second. This is because the CBZ-derivatized amino acids are generally more stable than many metabolites in the un-derivatized samples.
26. Injecting the quality control sample several times enables the user to establish baseline performance, ensure the chromatographic system has reached equilibrium, and identify potential problems in the operation of the instrument, such as aberrant system pressure spikes or issues in the operation of the autosampler.

27. Randomizing the order that samples are injected is recommended to prevent variability due to the run order. The quality control and blank samples should also be reinjected at regular intervals (see Note 21). Data can be analyzed using software supplied by the instrument manufacturer or using open source software.

- *We routinely use MAVEN<sup>309</sup> and QuanLynx (Waters). It is critical to correct for natural isotope abundance when conducting isotope tracer experiments, we recommend using IsoCor.<sup>269</sup> Metaboanalyst<sup>317</sup> is an excellent tool for quickly visualizing and interpreting data sets. For data normalization we recommend normalizing to the internal standard and protein count for each sample, followed by probabilistic quotient normalization to account for potential total concentration differences between cells.<sup>310</sup>*

## CHAPTER 5: APPLICATIONS OF METABOLOMICS TECHNIQUES AND CONTRIBUTIONS TO SCIENCE

### Preface

The following sections contain additional published works related to cancer metabolism and metabolomics techniques completed in projects beyond my main project of this thesis as described in Chapters 2-4. These include collaborative projects outside of and within the Lunt lab. Specific details regarding target genes of interest and preliminary findings have been omitted to protect secrecy while we work to finish these projects and publish the results.

### Tryptophan Metabolism in the Malignant Transformation of Mammary Epithelial

### Cells

This section contains a modified excerpt of a previously published article<sup>318</sup>:

Jonathan D Diedrich, Romina Gonzalez-Pons, Hyllana C D Medeiros, **Elliot Ensink**, Karen T Liby, Elizabeth A Wellberg, Sophia Y Lunt, Jamie J Bernard. Adipocyte-derived kynurenine stimulates malignant transformation of mammary epithelial cells through the aryl hydrocarbon receptor. *Biochem Pharmacol* 115763 (2023) doi:10.1016/j.bcp.2023.115763.

### **Summary**

The Lunt lab has collaborated with the Bernard lab to address the metabolic changes in mammary epithelial cells upon exposure to fat tissue filtrate that leads to tumorigenic potential. The Bernard lab showed that the non-tumorigenic human breast epithelial cell line, MCF-10A are able to form tumors when cultured in factors released from visceral adipose tissue. They demonstrate that this effect is due to aryl hydrocarbon

receptor (AhR) protein and target genes. AhR binds the endogenous tryptophan metabolite, kynurenine. Additionally, the kynurenine to tryptophan ratio is elevated in patients with obesity. This led to the hypothesis that kynurenine secreted from visceral adipose tissue contributes to tumorigenesis. In close work with Hyllana Medeiros, I contributed to the experimental design and methodology to determine whether adipocytes could metabolize tryptophan and release kynurenine. Further we evaluated whether extracellular kynurenine can be metabolized by MCF-10A cells to contribute to their malignant transformation (Fig. 5.1).

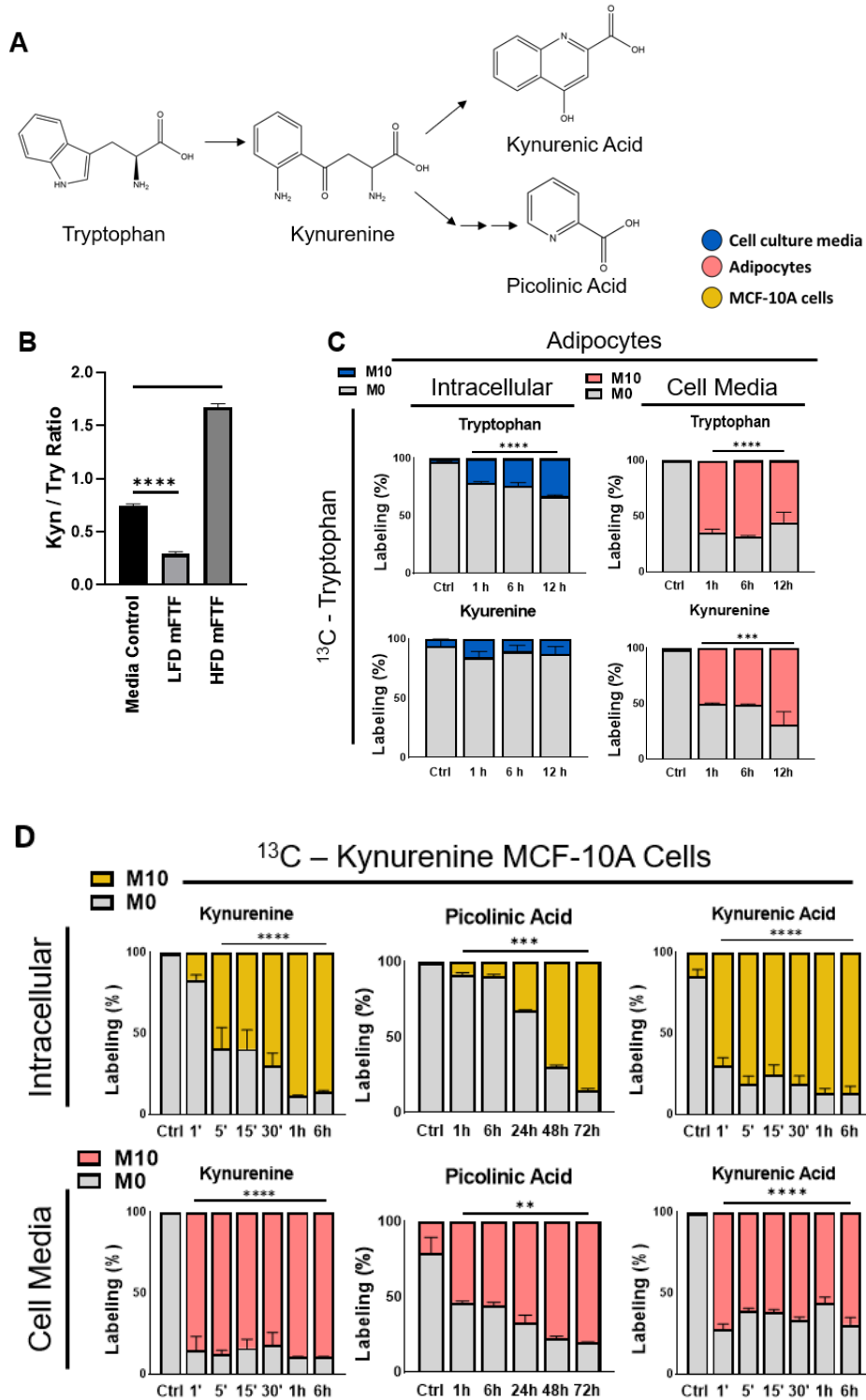


**Figure 5.1 Adipocytes with increased IDO activity excrete endogenous AhR ligand kynurenine, which is internalized and metabolized by mammary cells.**

### Figure 5.1 (cont'd)

**A.** Simplified diagram of the tryptophan metabolism pathway. **B.** Following treatment with HFD (high fat diet), LFD (low fat diet) or cell culture media (Control), mFTF (mouse fat tissue filtrate) was collected for liquid chromatography tandem mass spectrometry (LC-MS/MS) analysis. The kynurenine to tryptophan ratio (Kyn/Trp) was determined using signal intensity to verify indoleamine 2,3- dioxygenase (IDO) activity. **C.** Adipocytes were cultured with  $^{13}\text{C}_{10}$ -tryptophan at 1, 6 and 12 hours. Intracellular metabolites from cells and extracellular metabolites from cell media were extracted for analysis by LC-MS/MS. The graph indicates the percentage of the metabolite labeled fraction (M10) compared to the unlabeled fraction (M0) from adipocytes (blue) and cultured media (red). Unlabeled media and cells cultured in unlabeled media were used as the control (Ctrl). **D.** MCF-10A cells were incubated with  $^{13}\text{C}_{10}$ -kynurenine enriched media ranging from 1 minute to 72 hours to perform isotope labeling experiments. Intracellular metabolites from cells and extracellular metabolites from cell media were extracted and analyzed by LC-MS/MS section to evaluate the cellular uptake of kynurenine and further metabolism by MCF-10A cells. Graphs represent the intracellular labeled fraction (M10) of kynurenine, picolinic acid, and kynurenic acid compared to the unlabeled fraction in MCF-10A cells (yellow) and cultured media (red). Unlabeled media and cells cultured in unlabeled media were used as the control (Ctrl). Data are displayed as means  $\pm$  S.E.M., \*Statistical comparison between the treatment and control groups for unlabeled studies, and between  $^{13}\text{C}$ -labeled control fraction and  $^{13}\text{C}$ -labeled treatment fraction for labeled studies.  $n = 3$ . (Values \*\* $p \leq 0.01$ , \*\*\*\* $p \leq 0.0001$ ).

This project demonstrates that excess visceral adipose tissue promotes malignant transformation through altered tryptophan metabolism and kynurenine signaling. This novel mechanism will be further explored in future studies as well as the role of kynurenine as a biomarker of risk for breast cancer in obese individuals, and the potential for targeting AhR to prevent breast cancer development.

### **Quantification of glutamate released by *S. aureus* Ggt from reduced and oxidized glutathione**

This section is a modified excerpt of a previously published article<sup>319</sup>:

Joshua M. Lensmire, Michael R. Wischer, Cristina Kraemer-Zimpel, Paige J. Kies, Lo Sosinski, **Elliot Ensink**, Jack P. Dodson, John C. Shook, Phillip C. Delekta, Christopher C. Cooper, Daniel H. Havlichek, Jr., Martha H. Mulks, Sophia Y. Lunt, Janani Ravil, Neal D. Hammer. The glutathione import system satisfies the *Staphylococcus aureus* nutrient sulfur requirement and promotes interspecies competition. PLOS Genetics 19, e1010834 (2023).

### **Summary**

The role of metabolomics extends well beyond cancer metabolism. In our collaboration with the Hammer lab, I investigated the ability of *Staphylococcus Aureus* bacterial (*S. aureus*) cells to utilize glutathione as a source of nutrient sulfur. The Hammer lab identified a  $\gamma$ -glutamyl transpeptidase (ggt) that promotes *S. aureus* proliferation in media supplemented with reduced glutathione (GSH) or oxidized glutathione (GSSG) as the sole source of nutrient sulfur. In the process of cleaving the GSH  $\gamma$ -peptide bond, Ggt liberates glutamate. Previous work using glutamate quantification kits was found to be insufficient to adequately detect glutamate release from GSH. Therefore, to contribute to

this project, I used LC-MS/MS to quantify the release of glutamate from GSH and GSSG by Ggt to calculate the enzyme kinetics. This project is a good demonstration of the utility of mass spectrometry based techniques to perform highly sensitive quantification of metabolites. Additionally, the totality of this project shows a novel nutrient sulfur acquisition system that *S. aureus* uses to outcompete other staphylococci.

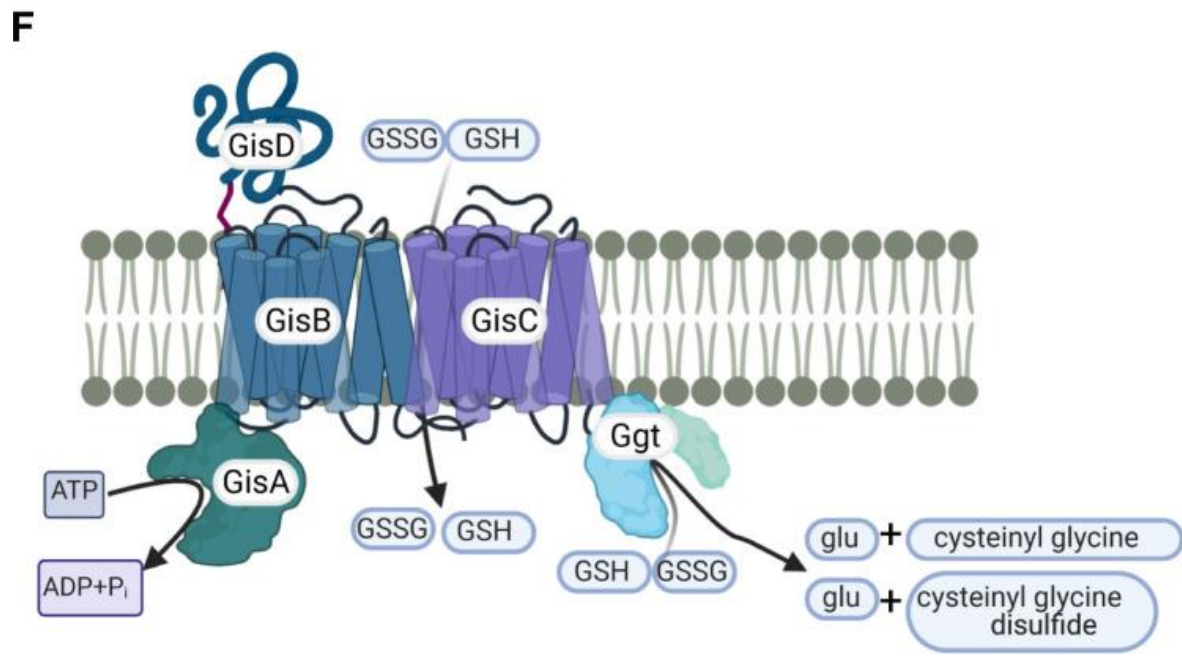
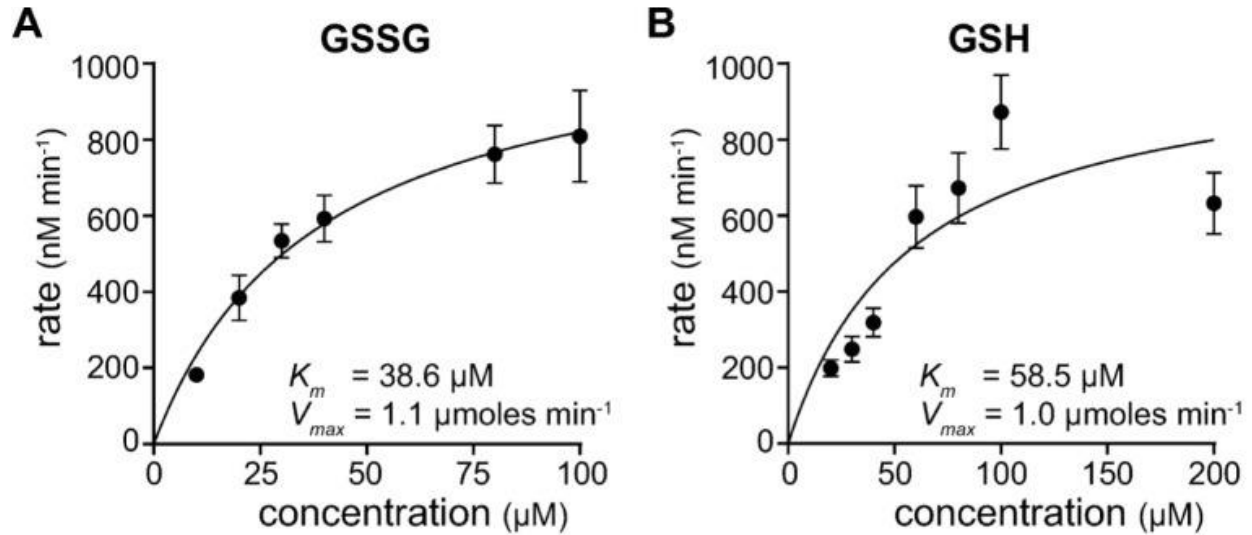


**Figure 5.2 *S. aureus* Ggt liberates glutamate from GSH and GSSG in the cytoplasm.**

## Figure 5.2 (cont'd)

**A** and **B**. Recombinant Ggt was incubated with indicated concentrations of GSSG (**A**) or GSH (**B**). Mean glutamate release per minute was measured using four independent rGgt protein preparations. Glutamate released per minute was calculated and data were fit with the Michaelis Menten equation using GraphPad Prism. Error bars represent  $\pm$  standard error of the mean. **F**. Bioinformatic predictions and experimental evidence support the presented model of *S. aureus* import and catabolism of exogenous GSH and GSSG. The predicted substrate-binding protein, glutathione import system (Gis) D, binds GSH or GSSG in the extracellular milieu, which are transported into the cytoplasm by the transmembrane permease complex, GisBC. GisA hydrolysis of ATP provides energy needed for import. Finally, GSH and GSSG are cleaved in the cytoplasm by Ggt, generating glutamate and cysteinyl-glycine or cysteinyl-glycine disulfide, depending on the substrate. The model illustration was created using BioRender.

## Methods

### Quantitation of Ggt enzyme kinetics.

$\gamma$ -glutamyl transpeptidase reactions contained 5  $\mu$ g recombinant Ggt, reaction buffer (10 mM tris with 150 mM NaCl), and the indicated concentrations of GSH and GSSG dissolved in reaction buffer. Reactions proceeded for 30 min at 37° C after which samples were incubated at 80° C for 5 min to stop the reaction. Samples were dried using a roto-vac speed vacuum and stored at -80° C until they were hydrated via resuspension in water, derivatized with carboxybenzyl (CBZ), and applied to a Waters Xevo TQ-S triple quadrupole mass spectrometer as previously described.<sup>266</sup> Peak processing was performed by MAVEN, and the signal was normalized to a <sup>13</sup>C-glutamine internal

standard<sup>268</sup>. An external glutamate standard curve was generated using the same chromatographic conditions, and the signal was normalized to a <sup>13</sup>C-glutamine internal standard. A fit equation to the standard curve was employed to quantify glutamate within the samples. Glutamate released per min was calculated and data were fit to the Michaelis-Menten equation using GraphPad Prism. Data represents the average of glutamate quantified from four independent protein purifications.

**Other co-authored papers:**

Williams M, Liu X, Zhang Y, Reske J, Bahal D, Gohl TG, Hollern D, **Ensink E**, Kiupel M, Luo R, Das R, Xiao H. NCOA5 deficiency promotes a unique liver protumorigenic microenvironment through p21<sup>WAF1/CIP1</sup> overexpression, which is reversed by metformin. *Oncogene*. 2020 May;39(19):3821-3836. doi: 10.1038/s41388-020-1256-x. Epub 2020 Mar 20. PMID: 32203160; PMCID: PMC7210077.

Contributions: RNA seq experiment design and methodology, manuscript editing.

Medeiros, H. C. D., Yang, C., Herrera, C. K., Broadwater, D., **Ensink, E.**, Bates, M., Lunt, R. R., Lunt, S. Y., *Chem. Eur. J.* 2023, 29, e202202881.

Contributions: experiment design, methodology, *In vivo* experiments, manuscript editing.

## CHAPTER 6: CONCLUSIONS AND FUTURE DIRECTIONS

### Conclusions

PKM2 is a critical metabolic enzyme involved in the metabolic reprogramming of pancreatic cancer. My work, along with my colleagues, described in this thesis demonstrates for the first time that low PK activity mediates a survival advantage against cystine starvation induced ferroptosis in pancreatic cancer. This survival advantage against ferroptosis is mediated by reprogramming of glutamine metabolism and utilization of ME1 to produce NADPH.

Aberrant metabolic conditions in response to oxidative stress lead to ferroptosis in cancer cells and this represents an exciting new avenue of targeted metabolic therapy.<sup>4,105</sup> The evidence in this thesis demonstrates that pharmacologic activation of PK in addition to cystine starvation is a novel synergistic approach for inhibiting survival of pancreatic cancer cells *in vitro*. Preliminary exploration of this process *in vivo* has showed promising initial results and further optimization and exploration of this metabolic vulnerability is currently being investigated.

Finally, our data indicates that cancer cells with low PK activity represent a potential pool of resilient cells able to tolerate low nutrient stress and enable tumor persistence. Therefore, this work reveals critical mechanisms by which PDAC cells reprogram their metabolic pathways to support survival within the TME. Targeted activation of PK in combination with cystine metabolism inhibition represents an exciting new vulnerability in PDAC which should be exploited as a novel therapeutic strategy for intervention in pancreatic cancer and improving outcomes for patients.

## **Future Directions**

The work described in this thesis demonstrates great improvements to our collective understanding of the role of metabolism in pancreatic cancer and beyond. However, there are many exciting and interesting questions that have yet to be answered. In particular, our lab will be focusing on continuing the work described in Chapter 3. The most important next step is to address the potential of utilizing the combination of pyruvate kinase activation with cystine starvation as a novel therapeutic strategy for treating pancreatic cancer. As shown in the appendix of Chapter 3, our preliminary efforts have demonstrated promising successes using TEPP-46 and IKE in combination in decreasing tumor growth. However, the fact that there are differences in response depending on PDAC cell type suggests molecular subgroups should be explored to stratify tumors that will likely respond to this type of metabolic therapy. Further, a safe and effective dosage still needs to be solidified.

We have promising preliminary data for this novel combinational therapy *in vivo* and the underlying *in vitro* data is robust and worth further optimization. I propose the following approaches to optimize our *in vivo* models. First, we are in the process of optimizing the treatment duration for Panc1 subcutaneous tumors as seen in Figure 3.39. Given the signs of toxicity we will utilize more mature mice and test a lower dosage over a longer period of time. Blood chemistry will be collected to evaluate for signs of toxicity (liver toxicity, hemolysis, kidney toxicity, etc.)

Second, orthotopic xenograft models of PDAC should be tested in addition to subcutaneous tumor modules. While orthotopic models will be more challenging to execute and monitor for disease progression, the factors by the endogenous tumor

microenvironment are likely critical. Indeed, orthotopic and heterotopic tumor models present different tumor biology and reactions to chemotherapies.<sup>320</sup> However, some work has shown that the metabolic profile (glycolytic, TCA cycle, and redox intermediate abundance) is relatively similar between orthotopic and heterotopic models, indicating that subcutaneous xenograft models are not an invalid approach to studying PDAC metabolism *in vivo*.<sup>321</sup> Several WT human PDAC cell lines should also be individually examined to capture the heterogeneity observed in PDAC and identify the types of cells that respond well to IKE and TEPP-46 combination therapy.<sup>4,67-73</sup> Collecting associated genetic and histologic characteristics of tumors produced from each cell line will lay the groundwork for molecular subtyping tumors and predicting which patients may respond well to this therapy in the future.

Third, a model of spontaneously arising PDAC tumors, such as the K-ras<sup>LSL.G12D/+</sup>, p53<sup>R172H/+</sup>, PdxCre (KPC) mouse model should be used.<sup>15</sup> The KPC mouse model allows for accelerated development of pancreatic intraepithelial neoplasia and faithfully recapitulates many of the metastatic features, immunohistochemical markers, and genomic alterations observed in human PDAC.<sup>15</sup> Even more importantly, KPC mice are immunocompetent, as opposed to the immunocompromised human xenograft models we have previously used in our *in vivo* experiments. This is especially important when considering recent evidence that suggests ferroptosis plays a role in immune tolerance.<sup>322,323</sup> Using these two *in vivo* models will address potential confounding factors due to changes in the tumor microenvironment.

Beyond optimizing the model system used, the next step to address is the appropriate mechanism by which to induce PKM2 activation and cystine starvation.

Currently two main compounds are used for activation of PKM2, TEPP-46 and DASA-58. We limited our study to TEPP-46 as this is more commonly used *in vivo* due to more favorable characteristics<sup>177</sup>, however other activators should be pursued to ensure optimum PKM2 activation is achieved. Recently a new PKM2 activator, TP-1454, was developed by Sumitomo Dainippon Pharm Oncology and is currently the first PKM2 activator to reach a phase 1 clinical trial.<sup>324,325</sup> The approach to achieving cystine starvation *in vivo* also needs to be optimized. We utilized IKE due to its promising effects *in vitro* and established efficacy in other cancer models.<sup>182</sup> However, other approaches are possible including IKE linked nanoparticles, cysteine free diets, and cyst(e)inase.<sup>126,182,289</sup> Additionally, our evidence suggests that direct inhibition of GPX4 with RSL3 may be more effective at inducing ferroptosis regardless of PKM2 status. Therefore, pursuit of GPX4 inhibition *in vivo* with compounds such as RSL3 and ML162 in combination with PKM2 activation should also be investigated. Biochemical analysis of markers of PKM2 activation, cystine depletion, oxidative stress, metabolic changes, and ferroptosis also need to be completed in *in vivo* dosing optimization studies to properly evaluate biochemical response to these drugs.

While addressing the *in vivo* application of PKM2 activation and cystine starvation is the most clinically relevant next step, there are also open questions regarding the mechanism by which PKM2 mediates the response to ferroptosis. We provide strong evidence that decreased PK activity is responsible for mediating resistance to ferroptosis rather than PKM1 or PKM2 specific isoform changes. The fact that the PKM2KO cells have low PK activity and no PKM2 expression while maintaining resistance to cystine starvation induced ferroptosis makes a strong case that this effect is driven primarily by

metabolic function not PKM2 mediated gene regulation. Nevertheless, establishing changes in gene expressions when PKM2 is inhibited or activated should be evaluated to fully understand the implications of targeting this protein *in vivo* and in human patients. Understanding the genetic changes enabling reprogramming of metabolism to support survival under cystine starvation will yield critical dependencies for future interventions. Additionally, genetic screening will review potential markers to stratify types of cells that may respond strongly to dual activation of PKM2 in combination with cystine starvation.

To address these questions, I propose conducting differential gene expression analysis of control and PKM2KO cells in response to cystine replete or depleted conditions. Additionally, gene expression should be evaluated in WT PDAC cells in response to PK activity modulation with or without the presence of environmental cystine or drug induced cystine starvation. Gene expression evaluation could be completed using RNAseq or a more targeted approach could be completed using a Nanostring nCounter gene expression panel focused on genes pertinent to metabolism, oxidative stress, and ferroptosis. Differential gene expression should subsequently be confirmed by qPCR and western blots. Immunohistochemical evaluation of PK translocation to the nucleus should also be completed in both *in vitro* and *in vivo* models.

The mechanism by which PKM2KO influences ME1 expression should be further explored. It is currently unclear whether PK activity or isoform specific effects are influencing ME1 expression. Experiments are currently underway to evaluate ME1 expression in response to pharmacologic activation and inhibition of PKM2. The gene expression evaluation experiments described above will also likely help in this investigation. It is known that ME1 expression is turned on downstream of activated

antioxidant response signaling pathways such as NRF2 and KRAS<sup>77,326,327</sup>. Additionally PKM2 is activated by NRF2 in astrocytes and PKM2 plays a role in the antioxidant response in cancer cells.<sup>201,328</sup> As such it is conceivable that low PKM2 activity and increased ME1 expression may simply correlate as part of a larger metabolic program. The fact remains that elevated ME1 expression is a means for generating critical NADPH for defense against ferroptosis; further exploration of targeting ME1 in addition to inducing ferroptosis should be conducted.

Our evidence suggests that glutamine metabolism potentiates ferroptosis, yet under a low PK activity state, glutamine anaplerosis and catabolism into pyruvate through ME1 may actually support NADPH production and resist ferroptosis. Targeting glutamine metabolism alone has failed to demonstrate strong efficacy when put to the test in clinical trials.<sup>175,176</sup> Indeed, several lines of evidence show that inhibiting glutamine metabolism in WT cancer cells prevents ferroptosis.<sup>106,153,154</sup> Therefore, careful consideration should be considered when targeting glutamine metabolism is appropriate as well as the precise target involved in the metabolism of glutamine. We demonstrate that cells with low PK activity are particularly dependent on glutamine (in agreement with other previous work<sup>206,288</sup>), therefore it may be worth pursuing the combination of PKM2 and glutamine metabolism inhibition. Experiments are currently ongoing in our lab to characterize the metabolic utilization of glucose and glutamine under cystine starvation and concurrent treatment with PKM2 activators and inhibitors. Additionally, targeting ME1 in combination with PKM2 activation would be another promising start at addressing the complex metabolic changes that support ferroptosis resistance in PDAC.

There are a few additional metabolic questions that remain open for investigation.

Specifically, we have not yet addressed the role of iron metabolism in relation to PKM2 and ferroptosis. PKM2 influences HIF-1 $\alpha$  expression and HIF-1 $\alpha$  promotes increased iron uptake and availability suggesting potential connections between iron metabolism and PKM2 which likely would influence ferroptosis.<sup>305–307</sup> We also have not fully addressed the metabolic fate of cystine in PKM2KO cells. We found no differences in cystine abundance between control and PKM2KO cells, however, this finding alone is insufficient to fully capture differences in cysteine metabolism. <sup>13</sup>C-cystine tracers should be used to identify whether there is differential flux of cystine into pyruvate, GSH, or CoA in PKM2KO cells. Lastly, we have not yet addressed the role of the transsulfuration pathway and the contributions of methionine to cysteine production in PKM2KO cells. Our media contains methionine which should potentially serve as a source of cysteine production, however the availability of methionine fails to change sensitivity to cystine starvation consistent with previous studies.<sup>329</sup> Thus transsulfuration is likely not a major contributor to altered ferroptosis resistance in PKM2KO cells.

Finally, ferroptosis is not a unique process to PDAC. There are applications in many cancer types as well as other physiologic and pathological processes including neurodegeneration, organ injury induced by iron overload, antiviral immunity, and aging.<sup>105</sup> We have begun exploring the role of PKM2 in ferroptosis in prostate cancer as discussed in Chapter 5. Given the importance of KRAS in driving the biology of PDAC, a logical next cancer to focus on would be another RAS driven disease such as lung cancer.

Clearly there are many interesting questions to address regarding PKM2, ferroptosis, and targeted metabolic therapies for cancer. This project initiated from humble beginnings with the very unexpected finding that PKM2 deletion prompted

improved survival under cystine starvation. From this initial experiment stemmed an enormity of questions and experiments thoroughly discussed in this thesis. I along with my colleagues in the Lunt lab have made a promising start to elucidating the role of PKM2 in ferroptosis, and there is ample opportunity for future investigation in the years to come.

## REFERENCES

1. American Cancer Society. Cancer Facts & Figures 2023. *Atlanta: American Cancer Society* (2023).
2. Rahib, L. *et al.* Projecting Cancer Incidence and Deaths to 2030: The Unexpected Burden of Thyroid, Liver, and Pancreas Cancers in the United States. *Cancer Res* **74**, 2913–2921 (2014).
3. Principe, D. R. *et al.* The Current Treatment Paradigm for Pancreatic Ductal Adenocarcinoma and Barriers to Therapeutic Efficacy. *Frontiers in Oncology* **11**, (2021).
4. Halbrook, C. J. & Lyssiotis, C. A. Employing Metabolism to Improve the Diagnosis and Treatment of Pancreatic Cancer. *Cancer Cell* **31**, 5–19 (2017).
5. Hasan, S., Jacob, R., Manne, U. & Paluri, R. Advances in pancreatic cancer biomarkers. *Oncol Rev* **13**, (2019).
6. Yachida, S. *et al.* Distant metastasis occurs late during the genetic evolution of pancreatic cancer. *Nature* **467**, 1114–1117 (2010).
7. Rhim, A. D. *et al.* Stromal Elements Act to Restrain, Rather Than Support, Pancreatic Ductal Adenocarcinoma. *Cancer Cell* **25**, 735–747 (2014).
8. SEER\*Explorer: An interactive website for SEER cancer statistics [Internet]. [https://seer.cancer.gov/statistics-network/explorer/application.html?site=40&data\\_type=1&graph\\_type=2&compareBy=stage&chk\\_stage\\_104=104&chk\\_stage\\_105=105&chk\\_stage\\_106=106&chk\\_stage\\_107=107&hdn\\_rate\\_type=1&sex=1&race=1&age\\_range=1&advopt\\_precision=1&advopt\\_show\\_ci=on&hdn\\_view=0&advopt\\_show\\_apc=on&advopt\\_display=1](https://seer.cancer.gov/statistics-network/explorer/application.html?site=40&data_type=1&graph_type=2&compareBy=stage&chk_stage_104=104&chk_stage_105=105&chk_stage_106=106&chk_stage_107=107&hdn_rate_type=1&sex=1&race=1&age_range=1&advopt_precision=1&advopt_show_ci=on&hdn_view=0&advopt_show_apc=on&advopt_display=1) (2023).
9. Andersson, R., Pereira, C.-F., Bauden, M. & Ansari, D. Is immunotherapy the holy grail for pancreatic cancer? *Immunotherapy* **11**, 1435–1438 (2019).
10. Huang, L. *et al.* Resection of pancreatic cancer in Europe and USA: an international large-scale study highlighting large variations. *Gut* **68**, 130–139 (2019).
11. Wu, Y. H. A. *et al.* Selecting surgical candidates with locally advanced pancreatic cancer: a review for modern pancreatology. *J Gastrointest Oncol* **12**, 2475–2483 (2021).
12. Zeng, S. *et al.* Chemoresistance in Pancreatic Cancer. *Int J Mol Sci* **20**, (2019).
13. Golan, T. *et al.* Maintenance Olaparib for Germline BRCA-Mutated Metastatic Pancreatic Cancer. *N Engl J Med* **381**, 317–327 (2019).

14. Marabelle, A. *et al.* Efficacy of Pembrolizumab in Patients With Noncolorectal High Microsatellite Instability/Mismatch Repair-Deficient Cancer: Results From the Phase II KEYNOTE-158 Study. *J Clin Oncol* **38**, 1–10 (2020).
15. Westphalen, C. B. & Olive, K. P. Genetically Engineered Mouse Models of Pancreatic Cancer. *Cancer J* **18**, 502–510 (2012).
16. Jones, S. *et al.* Core Signaling Pathways in Human Pancreatic Cancers Revealed by Global Genomic Analyses. *Science* **321**, 1801–1806 (2008).
17. Maitra, A. *et al.* Multicomponent analysis of the pancreatic adenocarcinoma progression model using a pancreatic intraepithelial neoplasia tissue microarray. *Mod Pathol* **16**, 902–912 (2003).
18. Huang, L., Guo, Z., Wang, F. & Fu, L. KRAS mutation: from undruggable to druggable in cancer. *Sig Transduct Target Ther* **6**, 1–20 (2021).
19. Hunter, J. C. *et al.* Biochemical and Structural Analysis of Common Cancer-Associated KRAS Mutations. *Mol Cancer Res* **13**, 1325–1335 (2015).
20. Lim, S. M. *et al.* Therapeutic targeting of oncogenic K-Ras by a covalent catalytic site inhibitor. *Angew Chem Int Ed Engl* **53**, 199–204 (2014).
21. Hunter, J. C. *et al.* In situ selectivity profiling and crystal structure of SML-8-73-1, an active site inhibitor of oncogenic K-Ras G12C. *Proc Natl Acad Sci U S A* **111**, 8895–8900 (2014).
22. Janes, M. R. *et al.* Targeting KRAS Mutant Cancers with a Covalent G12C-Specific Inhibitor. *Cell* **172**, 578-589.e17 (2018).
23. Kemp, S. B. *et al.* Efficacy of a Small-Molecule Inhibitor of KrasG12D in Immunocompetent Models of Pancreatic Cancer. *Cancer Discov* **13**, 298–311 (2023).
24. Johnson, B. L. *et al.* Desmoplasia and oncogene driven acinar-to-ductal metaplasia are concurrent events during acinar cell-derived pancreatic cancer initiation in young adult mice. *PLoS One* **14**, e0221810 (2019).
25. Neeße, A. *et al.* Stromal biology and therapy in pancreatic cancer. *Gut* **60**, 861–868 (2011).
26. Tape, C. J. *et al.* Oncogenic KRAS Regulates Tumor Cell Signaling via Stromal Reciprocation. *Cell* **165**, 910–920 (2016).
27. Shields, M. A. *et al.* Snail Cooperates with KrasG12D to Promote Pancreatic Fibrosis. *Molecular Cancer Research* **11**, 1078–1087 (2013).

28. Jacobetz, M. A. *et al.* Hyaluronan impairs vascular function and drug delivery in a mouse model of pancreatic cancer. *Gut* **62**, 112–120 (2013).
29. Cheng, X.-B., Kohi, S., Koga, A., Hirata, K. & Sato, N. Hyaluronan stimulates pancreatic cancer cell motility. *Oncotarget* **7**, 4829–4840 (2015).
30. Whatcott, C. J., Posner, R. G., Von Hoff, D. D. & Han, H. Desmoplasia and chemoresistance in pancreatic cancer. in *Pancreatic Cancer and Tumor Microenvironment* (eds. Grippo, P. J. & Munshi, H. G.) (Transworld Research Network, 2012).
31. Provenzano, P. P. *et al.* Enzymatic targeting of the stroma ablates physical barriers to treatment of pancreatic ductal adenocarcinoma. *Cancer Cell* **21**, 418–429 (2012).
32. Shah, V. M., Sheppard, B. C., Sears, R. C. & Alani, A. WG. Hypoxia: Friend or Foe for drug delivery in Pancreatic Cancer. *Cancer Lett* **492**, 63–70 (2020).
33. Ikenaga, N. *et al.* CD10+ Pancreatic Stellate Cells Enhance the Progression of Pancreatic Cancer. *Gastroenterology* **139**, 1041-1051.e8 (2010).
34. Lonardo, E., Frias-Aldeguer, J., Hermann, P. C. & Heeschen, C. Pancreatic stellate cells form a niche for cancer stem cells and promote their self-renewal and invasiveness. *Cell Cycle* **11**, 1282–1290 (2012).
35. Özdemir, B. C. *et al.* Depletion of Carcinoma-Associated Fibroblasts and Fibrosis Induces Immunosuppression and Accelerates Pancreas Cancer with Reduced Survival. *Cancer Cell* **25**, 719–734 (2014).
36. Karamitopoulou, E. Tumour microenvironment of pancreatic cancer: immune landscape is dictated by molecular and histopathological features. *Br J Cancer* **121**, 5–14 (2019).
37. Ene-Obong, A. *et al.* Activated Pancreatic Stellate Cells Sequester CD8+ T-Cells to Reduce Their Infiltration of the Juxtatumoral Compartment of Pancreatic Ductal Adenocarcinoma. *Gastroenterology* **145**, 1121–1132 (2013).
38. Huber, M. *et al.* The Immune Microenvironment in Pancreatic Cancer. *Int J Mol Sci* **21**, 7307 (2020).
39. Ullman, N. A., Burchard, P. R., Dunne, R. F. & Linehan, D. C. Immunologic Strategies in Pancreatic Cancer: Making Cold Tumors Hot. *J Clin Oncol* **40**, 2789–2805 (2022).
40. Cancer Facts & Figures 2013. <https://www.cancer.org/research/cancer-facts-statistics/all-cancer-facts-figures/cancer-facts-figures-2013.html>.
41. Warburg, O. The Metabolism of Carcinoma Cells. *The Journal of Cancer Research* **9**, 148–163 (1925).

42. Warburg, O. On the Origin of Cancer Cells. *Science* **123**, 309–314 (1956).
43. Vander Heiden, M. G., Cantley, L. C. & Thompson, C. B. Understanding the Warburg Effect: The Metabolic Requirements of Cell Proliferation. *Science* **324**, 1029–1033 (2009).
44. Dayton, T. L., Jacks, T. & Vander Heiden, M. G. PKM2, cancer metabolism, and the road ahead. *EMBO Rep* **17**, 1721–1730 (2016).
45. Koppenol, W. H., Bounds, P. L. & Dang, C. V. Otto Warburg's contributions to current concepts of cancer metabolism. *Nat Rev Cancer* **11**, 325–337 (2011).
46. Tan, A. S. *et al.* Mitochondrial Genome Acquisition Restores Respiratory Function and Tumorigenic Potential of Cancer Cells without Mitochondrial DNA. *Cell Metabolism* **21**, 81–94 (2015).
47. Weinberg, F. *et al.* Mitochondrial metabolism and ROS generation are essential for Kras-mediated tumorigenicity. *Proc Natl Acad Sci U S A* **107**, 8788–8793 (2010).
48. Fan, T. W. *et al.* Altered regulation of metabolic pathways in human lung cancer discerned by <sup>13</sup>C stable isotope-resolved metabolomics (SIRM). *Molecular Cancer* **8**, 41 (2009).
49. Maher, E. A. *et al.* Metabolism of [U-<sup>13</sup>C]glucose in human brain tumors in vivo. *NMR in Biomedicine* **25**, 1234–1244 (2012).
50. Larson, S. M. Molecular Imaging: A Tool for Developing Central Nervous System Drugs.
51. Liberti, M. V. & Locasale, J. W. The Warburg Effect: How Does it Benefit Cancer Cells? *Trends Biochem Sci* **41**, 211–218 (2016).
52. Locasale, J. W. & Cantley, L. C. Metabolic flux and the regulation of mammalian cell growth. *Cell Metab* **14**, 443–451 (2011).
53. Shestov, A. A. *et al.* Quantitative determinants of aerobic glycolysis identify flux through the enzyme GAPDH as a limiting step. *eLife* **3**, e03342 (2014).
54. Levine, A. J. & Puzio-Kuter, A. M. The control of the metabolic switch in cancers by oncogenes and tumor suppressor genes. *Science* **330**, 1340–1344 (2010).
55. DeBerardinis, R. J., Lum, J. J., Hatzivassiliou, G. & Thompson, C. B. The biology of cancer: metabolic reprogramming fuels cell growth and proliferation. *Cell Metab.* **7**, 11–20 (2008).
56. Cairns, R. A., Harris, I. S. & Mak, T. W. Regulation of cancer cell metabolism. *Nat Rev Cancer* **11**, 85–95 (2011).

57. Boroughs, L. K. & DeBerardinis, R. J. Metabolic pathways promoting cancer cell survival and growth. *Nat Cell Biol* **17**, 351–359 (2015).
58. Lunt, S. Y. & Vander Heiden, M. G. Aerobic glycolysis: meeting the metabolic requirements of cell proliferation. *Annu. Rev. Cell Dev. Biol.* **27**, 441–464 (2011).
59. Madhukar, N. S., Warmoes, M. O. & Locasale, J. W. Organization of Enzyme Concentration across the Metabolic Network in Cancer Cells. *PLoS One* **10**, e0117131 (2015).
60. DeBerardinis, R. J. & Chandel, N. S. We need to talk about the Warburg effect. *Nat Metab* **2**, 127–129 (2020).
61. Hanahan, D. & Weinberg, R. A. The Hallmarks of Cancer. *Cell* **100**, 57–70 (2000).
62. Hanahan, D. & Weinberg, R. A. Hallmarks of Cancer: The Next Generation. *Cell* **144**, 646–674 (2011).
63. Hanahan, D. Hallmarks of Cancer: New Dimensions. *Cancer Discovery* **12**, 31–46 (2022).
64. Jones, R. G. & Thompson, C. B. Tumor suppressors and cell metabolism: a recipe for cancer growth. *Genes Dev.* **23**, 537–548 (2009).
65. Tsai, P.-Y. *et al.* Adaptation of pancreatic cancer cells to nutrient deprivation is reversible and requires glutamine synthetase stabilization by mTORC1. *Proceedings of the National Academy of Sciences* **118**, e2003014118 (2021).
66. Sullivan, M. R. *et al.* Quantification of microenvironmental metabolites in murine cancers reveals determinants of tumor nutrient availability. *eLife* **8**, (2019).
67. Baek, G. *et al.* MCT4 Defines a Glycolytic Subtype of Pancreatic Cancer with Poor Prognosis and Unique Metabolic Dependencies. *Cell Reports* **9**, 2233–2249 (2014).
68. Boudreau, A. *et al.* Metabolic plasticity underpins innate and acquired resistance to LDHA inhibition. *Nat Chem Biol* **12**, 779–786 (2016).
69. Daemen, A. *et al.* Metabolite profiling stratifies pancreatic ductal adenocarcinomas into subtypes with distinct sensitivities to metabolic inhibitors. *Proc Natl Acad Sci U S A* **112**, E4410–E4417 (2015).
70. Bailey, P. *et al.* Genomic analyses identify molecular subtypes of pancreatic cancer. *Nature* **531**, 47–52 (2016).
71. Collisson, E. A. *et al.* Subtypes of pancreatic ductal adenocarcinoma and their differing responses to therapy. *Nat Med* **17**, 500–503 (2011).

72. Moffitt, R. A. *et al.* Virtual microdissection identifies distinct tumor- and stroma-specific subtypes of pancreatic ductal adenocarcinoma. *Nat Genet* **47**, 1168–1178 (2015).
73. Sancho, P. *et al.* MYC/PGC-1 $\alpha$  Balance Determines the Metabolic Phenotype and Plasticity of Pancreatic Cancer Stem Cells. *Cell Metabolism* **22**, 590–605 (2015).
74. Lau, A. N. *et al.* Dissecting cell-type-specific metabolism in pancreatic ductal adenocarcinoma. *eLife* **9**, e56782 (2020).
75. Ying, H. *et al.* Oncogenic Kras Maintains Pancreatic Tumors through Regulation of Anabolic Glucose Metabolism. *Cell* **149**, 656–670 (2012).
76. Gaglio, D. *et al.* Oncogenic K-Ras decouples glucose and glutamine metabolism to support cancer cell growth. *Mol Syst Biol* **7**, 523 (2011).
77. Son, J. *et al.* Glutamine supports pancreatic cancer growth through a Kras-regulated metabolic pathway. *Nature* **496**, 101–105 (2013).
78. DeBerardinis, R. J. *et al.* Beyond aerobic glycolysis: Transformed cells can engage in glutamine metabolism that exceeds the requirement for protein and nucleotide synthesis. *Proc Natl Acad Sci U S A* **104**, 19345–19350 (2007).
79. Ju, H.-Q., Lin, J.-F., Tian, T., Xie, D. & Xu, R.-H. NADPH homeostasis in cancer: functions, mechanisms and therapeutic implications. *Sig Transduct Target Ther* **5**, 1–12 (2020).
80. DeNicola, G. M. *et al.* Oncogene-induced Nrf2 transcription promotes ROS detoxification and tumorigenesis. *Nature* **475**, 106–109 (2011).
81. Chio, I. I. C. *et al.* NRF2 Promotes Tumor Maintenance by Modulating mRNA Translation in Pancreatic Cancer. *Cell* **166**, 963–976 (2016).
82. DeNicola, G. M. *et al.* NRF2 regulates serine biosynthesis in non-small cell lung cancer. *Nat Genet* **47**, 1475–1481 (2015).
83. Mitsuishi, Y. *et al.* Nrf2 Redirects Glucose and Glutamine into Anabolic Pathways in Metabolic Reprogramming. *Cancer Cell* **22**, 66–79 (2012).
84. Lien, E. C. *et al.* Glutathione biosynthesis is a metabolic vulnerability in PI(3)K/Akt-driven breast cancer. *Nat Cell Biol* **18**, 572–578 (2016).
85. Lim, J. K. M. *et al.* Cystine/glutamate antiporter xCT (SLC7A11) facilitates oncogenic RAS transformation by preserving intracellular redox balance. *PNAS* **116**, 9433–9442 (2019).
86. Davidson, S. M. *et al.* Environment Impacts the Metabolic Dependencies of Ras-Driven Non-Small Cell Lung Cancer. *Cell Metabolism* **23**, 517–528 (2016).

87. Schug, Z. T., Vande Voorde, J. & Gottlieb, E. The Nurture of Tumors Can Drive Their Metabolic Phenotype. *Cell Metabolism* **23**, 391–392 (2016).
88. Lagziel, S., Gottlieb, E. & Shlomi, T. Mind your media. *Nat Metab* **2**, 1369–1372 (2020).
89. Muir, A. *et al.* Environmental cystine drives glutamine anaplerosis and sensitizes cancer cells to glutaminase inhibition. *eLife* **6**, (2017).
90. Kimmelman, A. C. The dynamic nature of autophagy in cancer. *Genes Dev.* **25**, 1999–2010 (2011).
91. Yang, S. *et al.* Pancreatic cancers require autophagy for tumor growth. *Genes Dev.* **25**, 717–729 (2011).
92. Li, J. *et al.* Regulation and function of autophagy in pancreatic cancer. *Autophagy* **17**, 3275–3296 (2020).
93. Commisso, C. *et al.* Macropinocytosis of protein is an amino acid supply route in Ras-transformed cells. *Nature* **497**, 633–637 (2013).
94. Kamphorst, J. J. *et al.* Human Pancreatic Cancer Tumors Are Nutrient Poor and Tumor Cells Actively Scavenge Extracellular Protein. *Cancer Res* **75**, 544–553 (2015).
95. Palm, W. *et al.* The Utilization of Extracellular Proteins as Nutrients Is Suppressed by mTORC1. *Cell* **162**, 259–270 (2015).
96. Sousa, C. M. *et al.* Pancreatic stellate cells support tumour metabolism through autophagic alanine secretion. *Nature* **536**, 479–483 (2016).
97. Magni, G., Amici, A., Emanuelli, M., Raffaelli, N. & Ruggieri, S. Enzymology of NAD<sup>+</sup> synthesis. *Adv Enzymol Relat Areas Mol Biol* **73**, 135–182, xi (1999).
98. Ju, H.-Q. *et al.* Regulation of the Nampt-mediated NAD salvage pathway and its therapeutic implications in pancreatic cancer. *Cancer Letters* **379**, 1–11 (2016).
99. Nwosu, Z. C. *et al.* Uridine-derived ribose fuels glucose-restricted pancreatic cancer. *Nature* **618**, 151–158 (2023).
100. Stockwell, B. R. *et al.* Ferroptosis: a regulated cell death nexus linking metabolism, redox biology, and disease. *Cell* **171**, 273–285 (2017).
101. Zheng, J. & Conrad, M. The Metabolic Underpinnings of Ferroptosis. *Cell Metabolism* **32**, 920–937 (2020).
102. Li, J. *et al.* Ferroptosis: past, present and future. *Cell Death Dis* **11**, 1–13 (2020).

103. Chen, X., Comish, P. B., Tang, D. & Kang, R. Characteristics and Biomarkers of Ferroptosis. *Frontiers in Cell and Developmental Biology* **9**, (2021).
104. Ide, K. & Souma, T. IN VIVO ASSESSMENT OF FERROPTOSIS AND FERROPTOTIC STRESS IN MICE. *Curr Protoc* **2**, e413 (2022).
105. Stockwell, B. R. Ferroptosis turns 10: Emerging mechanisms, physiological functions, and therapeutic applications. *Cell* **185**, 2401–2421 (2022).
106. Dixon, S. J. *et al.* Ferroptosis: an iron-dependent form of nonapoptotic cell death. *Cell* **149**, 1060–1072 (2012).
107. Eagle, H. The specific amino acid requirements of a human carcinoma cell (Stain HeLa) in tissue culture. *The Journal of experimental medicine* **102**, 37–48 (1955).
108. Eagle, H. Amino Acid Metabolism in Mammalian Cell Cultures. *Science* **130**, 432–437 (1959).
109. Bannai, S., Tsukeda, H. & Okumura, H. Effect of antioxidants on cultured human diploid fibroblasts exposed to cystine-free medium. *Biochem Biophys Res Commun* **74**, 1582–1588 (1977).
110. Schwarz, K. Production of Dietary Necrotic Liver Degeneration Using American Torula Yeast. *Proceedings of the Society for Experimental Biology and Medicine* **77**, 818–823 (1951).
111. Schwarz, K. & Foltz, C. M. Factor 3 Activity of Selenium Compounds. *Journal of Biological Chemistry* **233**, 245–251 (1958).
112. Ursini, F., Maiorino, M., Valente, M., Ferri, L. & Gregolin, C. Purification from pig liver of a protein which protects liposomes and biomembranes from peroxidative degradation and exhibits glutathione peroxidase activity on phosphatidylcholine hydroperoxides. *Biochimica et Biophysica Acta (BBA) - Lipids and Lipid Metabolism* **710**, 197–211 (1982).
113. Golberg, L. & Smith, J. P. Changes Associated with the Accumulation of Excessive Amounts of Iron in Certain Organs of the Rat. *Br J Exp Pathol* **39**, 59–73 (1958).
114. Dolma, S., Lessnick, S. L., Hahn, W. C. & Stockwell, B. R. Identification of genotype-selective antitumor agents using synthetic lethal chemical screening in engineered human tumor cells. *Cancer Cell* **3**, 285–296 (2003).
115. Yang, W. S. & Stockwell, B. R. Synthetic lethal screening identifies compounds activating iron-dependent, nonapoptotic cell death in oncogenic-RAS-harboring cancer cells. *Chem Biol* **15**, 234–245 (2008).

116. Yagoda, N. *et al.* RAS-RAF-MEK-dependent oxidative cell death involving voltage-dependent anion channels. *Nature* **447**, 864–868 (2007).
117. Sato, H., Tamba, M., Ishii, T. & Bannai, S. Cloning and expression of a plasma membrane cystine/glutamate exchange transporter composed of two distinct proteins. *J Biol Chem* **274**, 11455–11458 (1999).
118. Dixon, S. J. & Stockwell, B. R. The Hallmarks of Ferroptosis. *Annu. Rev. Cancer Biol.* **3**, 35–54 (2019).
119. Choi, D. W. Glutamate neurotoxicity and diseases of the nervous system. *Neuron* **1**, 623–634 (1988).
120. Murphy, T. H., Miyamoto, M., Sastre, A., Schnaar, R. L. & Coyle, J. T. Glutamate toxicity in a neuronal cell line involves inhibition of cystine transport leading to oxidative stress. *Neuron* **2**, 1547–1558 (1989).
121. Ishii, T., Bannai, S. & Sugita, Y. Mechanism of growth stimulation of L1210 cells by 2-mercaptoethanol in vitro. Role of the mixed disulfide of 2-mercaptoethanol and cysteine. *J Biol Chem* **256**, 12387–12392 (1981).
122. Banjac, A. *et al.* The cystine/cysteine cycle: a redox cycle regulating susceptibility versus resistance to cell death. *Oncogene* **27**, 1618–1628 (2008).
123. Dixon, S. J. *et al.* Pharmacological inhibition of cystine–glutamate exchange induces endoplasmic reticulum stress and ferroptosis. *eLife* **3**, e02523 (2014).
124. Seiler, A. *et al.* Glutathione peroxidase 4 senses and translates oxidative stress into 12/15-lipoxygenase dependent- and AIF-mediated cell death. *Cell Metab* **8**, 237–248 (2008).
125. Yang, W. S. *et al.* Regulation of ferroptotic cancer cell death by GPX4. *Cell* **156**, 317–331 (2014).
126. Badgley, M. A. *et al.* Cysteine depletion induces pancreatic tumor ferroptosis in mice. *Science* **368**, 85–89 (2020).
127. Harris, I. S. *et al.* Deubiquitinases maintain protein homeostasis and survival of cancer cells upon glutathione depletion. *Cell Metab* **29**, 1166-1181.e6 (2019).
128. Conrad, M. & Pratt, D. A. The chemical basis of ferroptosis. *Nat Chem Biol* **15**, 1137–1147 (2019).
129. Wang, Y., Yu, L., Ding, J. & Chen, Y. Iron Metabolism in Cancer. *Int J Mol Sci* **20**, 95 (2018).

130. Cao, H., Schroeder, B., Chen, J., Schott, M. B. & McNiven, M. A. The Endocytic Fate of the Transferrin Receptor Is Regulated by c-Abl Kinase. *J Biol Chem* **291**, 16424–16437 (2016).
131. Yambire, K. F. *et al.* Impaired lysosomal acidification triggers iron deficiency and inflammation in vivo. *eLife* **8**, e51031 (2019).
132. Tang, M., Chen, Z., Wu, D. & Chen, L. Ferritinophagy/ferroptosis: Iron-related newcomers in human diseases. *J Cell Physiol* **233**, 9179–9190 (2018).
133. Ryu, M.-S., Duck, K. A. & Philpott, C. C. Ferritin Iron Regulators, PCBP1 and NCOA4, Respond to Cellular Iron Status in Developing Red Cells. *Blood Cells Mol Dis* **69**, 75–81 (2018).
134. Huang, T. *et al.* Growth Inhibition of a Novel Iron Chelator, DpdtC, against Hepatoma Carcinoma Cell Lines Partly Attributed to Ferritinophagy-Mediated Lysosomal ROS Generation. *Oxid Med Cell Longev* **2018**, 4928703 (2018).
135. Winterbourn, C. C. & Hampton, M. B. Thiol chemistry and specificity in redox signaling. *Free Radical Biology and Medicine* **45**, 549–561 (2008).
136. Ayala, A., Muñoz, M. F. & Argüelles, S. Lipid Peroxidation: Production, Metabolism, and Signaling Mechanisms of Malondialdehyde and 4-Hydroxy-2-Nonenal. *Oxid Med Cell Longev* **2014**, 360438 (2014).
137. Dixon, S. J. & Pratt, D. A. Ferroptosis: A flexible constellation of related biochemical mechanisms. *Molecular Cell* **83**, 1030–1042 (2023).
138. Gaschler, M. M. *et al.* Determination of the Subcellular Localization and Mechanism of Action of Ferrostatins in Suppressing Ferroptosis. *ACS Chem Biol* **13**, 1013–1020 (2018).
139. Doll, S. *et al.* FSP1 is a glutathione-independent ferroptosis suppressor. *Nature* **575**, 693–698 (2019).
140. Shimada, K. *et al.* Global survey of cell death mechanisms reveals metabolic regulation of ferroptosis. *Nat Chem Biol* **12**, 497–503 (2016).
141. Bersuker, K. *et al.* The CoQ oxidoreductase FSP1 acts parallel to GPX4 to inhibit ferroptosis. *Nature* **575**, 688–692 (2019).
142. Kraft, V. A. N. *et al.* GTP Cyclohydrolase 1/Tetrahydrobiopterin Counteract Ferroptosis through Lipid Remodeling. *ACS Cent Sci* **6**, 41–53 (2020).
143. Soula, M. *et al.* Metabolic determinants of cancer cell sensitivity to canonical ferroptosis inducers. *Nat Chem Biol* **16**, 1351–1360 (2020).

144. Mao, C. *et al.* DHODH-mediated ferroptosis defence is a targetable vulnerability in cancer. *Nature* **593**, 586–590 (2021).
145. Yang, W. S. & Stockwell, B. R. Ferroptosis: Death by Lipid Peroxidation. *Trends Cell Biol* **26**, 165–176 (2016).
146. Kagan, V. E. *et al.* Oxidized arachidonic and adrenic PEs navigate cells to ferroptosis. *Nat Chem Biol* **13**, 81–90 (2017).
147. Dixon, S. J. *et al.* Human Haploid Cell Genetics Reveals Roles for Lipid Metabolism Genes in Nonapoptotic Cell Death. *ACS Chem Biol* **10**, 1604–1609 (2015).
148. Doll, S. *et al.* ACSL4 dictates ferroptosis sensitivity by shaping cellular lipid composition. *Nat Chem Biol* **13**, 91–98 (2017).
149. Shah, R., Shchepinov, M. S. & Pratt, D. A. Resolving the Role of Lipoxygenases in the Initiation and Execution of Ferroptosis. *ACS Cent Sci* **4**, 387–396 (2018).
150. Kamata, T. Roles of Nox1 and other Nox isoforms in cancer development. *Cancer Sci* **100**, 1382–1388 (2009).
151. Shimada, K., Hayano, M., Pagano, N. C. & Stockwell, B. R. Cell-Line Selectivity Improves the Predictive Power of Pharmacogenomic Analyses and Helps Identify NADPH as Biomarker for Ferroptosis Sensitivity. *Cell Chem Biol* **23**, 225–235 (2016).
152. Ding, C.-K. C. *et al.* MESH1 is a cytosolic NADPH phosphatase that regulates ferroptosis. *Nat Metab* **2**, 270–277 (2020).
153. Gao, M. *et al.* Role of Mitochondria in Ferroptosis. *Mol Cell* **73**, 354-363.e3 (2019).
154. Gao, M., Monian, P., Quadri, N., Ramasamy, R. & Jiang, X. Glutaminolysis and Transferrin Regulate Ferroptosis. *Mol Cell* **59**, 298–308 (2015).
155. Gan, B. Mitochondrial regulation of ferroptosis. *J Cell Biol* **220**, e202105043 (2021).
156. Xiao, Z. *et al.* Glutamine deprivation induces ferroptosis in pancreatic cancer cells. *Acta Biochim Biophys Sin (Shanghai)* (2023) doi:10.3724/abbs.2023029.
157. Magtanong, L. *et al.* Context-dependent regulation of ferroptosis sensitivity. *Cell Chemical Biology* **29**, 1409-1418.e6 (2022).
158. Yan, B. *et al.* Membrane Damage during Ferroptosis Is Caused by Oxidation of Phospholipids Catalyzed by the Oxidoreductases POR and CYB5R1. *Molecular Cell* **81**, 355-369.e10 (2021).

159. Zou, Y. *et al.* Cytochrome P450 oxidoreductase contributes to phospholipid peroxidation in ferroptosis. *Nat Chem Biol* **16**, 302–309 (2020).
160. Yang, W.-H. *et al.* The Hippo Pathway Effector TAZ Regulates Ferroptosis in Renal Cell Carcinoma. *Cell Reports* **28**, 2501-2508.e4 (2019).
161. Kang, R. & Tang, D. Autophagy and Ferroptosis - What's the Connection? *Curr Pathobiol Rep* **5**, 153–159 (2017).
162. Gao, M. *et al.* Ferroptosis is an autophagic cell death process. *Cell Res* **26**, 1021–1032 (2016).
163. Hou, W. *et al.* Autophagy promotes ferroptosis by degradation of ferritin. *Autophagy* **12**, 1425–1428 (2016).
164. Torii, S. *et al.* An essential role for functional lysosomes in ferroptosis of cancer cells. *Biochemical Journal* **473**, 769–777 (2016).
165. Armenta, D. A. *et al.* Ferroptosis inhibition by lysosome-dependent catabolism of extracellular protein. *Cell Chemical Biology* **29**, 1588-1600.e7 (2022).
166. Zhang, Y. *et al.* mTORC1 couples cyst(e)ine availability with GPX4 protein synthesis and ferroptosis regulation. *Nat Commun* **12**, 1589 (2021).
167. Conlon, M. *et al.* A compendium of kinetic modulatory profiles identifies ferroptosis regulators. *Nat Chem Biol* **17**, 665–674 (2021).
168. Chu, B. *et al.* ALOX12 is required for p53-mediated tumour suppression through a distinct ferroptosis pathway. *Nat Cell Biol* **21**, 579–591 (2019).
169. Jiang, L. *et al.* Ferroptosis as a p53-mediated activity during tumour suppression. *Nature* **520**, 57–62 (2015).
170. Tarangelo, A. *et al.* Nucleotide biosynthesis links glutathione metabolism to ferroptosis sensitivity. *Life Science Alliance* **5**, (2022).
171. Tarangelo, A. *et al.* p53 Suppresses Metabolic Stress-Induced Ferroptosis in Cancer Cells. *Cell Rep* **22**, 569–575 (2018).
172. Xie, Y. *et al.* The Tumor Suppressor p53 Limits Ferroptosis by Blocking DPP4 Activity. *Cell Reports* **20**, 1692–1704 (2017).
173. Farber, S. & Diamond, L. K. Temporary remissions in acute leukemia in children produced by folic acid antagonist, 4-aminopteroyl-glutamic acid. *N Engl J Med* **238**, 787–793 (1948).
174. Luengo, A., Gui, D. Y. & Vander Heiden, M. G. Targeting Metabolism for Cancer Therapy. *Cell Chem Biol* **24**, 1161–1180 (2017).

175. Tannir, N. M. *et al.* Efficacy and Safety of Telaglenastat Plus Cabozantinib vs Placebo Plus Cabozantinib in Patients With Advanced Renal Cell Carcinoma: The CANTATA Randomized Clinical Trial. *JAMA Oncol* **8**, 1411–1418 (2022).
176. Halama, A. & Suhre, K. Advancing Cancer Treatment by Targeting Glutamine Metabolism—A Roadmap. *Cancers (Basel)* **14**, 553 (2022).
177. Anastasiou, D. *et al.* Pyruvate kinase M2 activators promote tetramer formation and suppress tumorigenesis. *Nat Chem Biol* **8**, 839–847 (2012).
178. Yacovan, A. *et al.* 1-(sulfonyl)-5-(arylsulfonyl)indoline as activators of the tumor cell specific M2 isoform of pyruvate kinase. *Bioorganic & Medicinal Chemistry Letters* **22**, 6460–6468 (2012).
179. Su, Q. *et al.* The role of pyruvate kinase M2 in anticancer therapeutic treatments. *Oncol Lett* **18**, 5663–5672 (2019).
180. Park, J. H. *et al.* Specific Pyruvate Kinase M2 Inhibitor, Compound 3K, Induces Autophagic Cell Death through Disruption of the Glycolysis Pathway in Ovarian Cancer Cells. *Int J Biol Sci* **17**, 1895–1908 (2021).
181. Mohammad, G. H. *et al.* Targeting Pyruvate Kinase M2 and Lactate Dehydrogenase A Is an Effective Combination Strategy for the Treatment of Pancreatic Cancer. *Cancers (Basel)* **11**, 1372 (2019).
182. Zhang, Y. *et al.* Imidazole ketone erastin induces ferroptosis and slows tumor growth in a mouse lymphoma model. *Cell Chem Biol* **26**, 623-633.e9 (2019).
183. Takenaka, M. *et al.* Alternative splicing of the pyruvate kinase M gene in a minigene system. *Eur J Biochem* **235**, 366–371 (1996).
184. Mazurek, S. Pyruvate kinase type M2: A key regulator of the metabolic budget system in tumor cells. *The International Journal of Biochemistry & Cell Biology* **43**, 969–980 (2011).
185. Garnett, M. E., Dyson, R. D. & Dost, F. N. Pyruvate kinase isozyme changes in parenchymal cells of regenerating rat liver. *J Biol Chem* **249**, 5222–5226 (1974).
186. Christofk, H. R. *et al.* The M2 splice isoform of pyruvate kinase is important for cancer metabolism and tumour growth. *Nature* **452**, 230–233 (2008).
187. Zhang, Z. *et al.* PKM2, function and expression and regulation. *Cell & Bioscience* **9**, 52 (2019).
188. David, C. J., Chen, M., Assanah, M., Canoll, P. & Manley, J. L. HnRNP proteins controlled by c-Myc deregulate pyruvate kinase mRNA splicing in cancer. *Nature* **463**, 364–368 (2010).

189. Taniguchi, K. *et al.* Organ-specific PTB1-associated microRNAs determine expression of pyruvate kinase isoforms. *Sci Rep* **5**, 8647 (2015).
190. Parasido, E. *et al.* The Sustained Induction of c-MYC Drives Nab-Paclitaxel Resistance in Primary Pancreatic Ductal Carcinoma Cells. *Mol Cancer Res* **17**, 1815–1827 (2019).
191. Ala, M. Target c-Myc to treat pancreatic cancer. *Cancer Biol Ther* **23**, 34–50 (2022).
192. Noguchi, T., Inoue, H. & Tanaka, T. The M1- and M2-type isozymes of rat pyruvate kinase are produced from the same gene by alternative RNA splicing. *J. Biol. Chem.* **261**, 13807–13812 (1986).
193. Dombrauckas, J. D., Santarsiero, B. D. & Mesecar, A. D. Structural basis for tumor pyruvate kinase M2 allosteric regulation and catalysis. *Biochemistry* **44**, 9417–9429 (2005).
194. Ashizawa, K., Willingham, M. C., Liang, C. M. & Cheng, S. Y. In vivo regulation of monomer-tetramer conversion of pyruvate kinase subtype M2 by glucose is mediated via fructose 1,6-bisphosphate. *Journal of Biological Chemistry* **266**, 16842–16846 (1991).
195. Yan, M. *et al.* Succinyl-5-aminoimidazole-4-carboxamide-1-ribose 5'-Phosphate (SAICAR) Activates Pyruvate Kinase Isoform M2 (PKM2) in Its Dimeric Form. *Biochemistry* **55**, 4731–4736 (2016).
196. Chaneton, B. *et al.* Serine is a natural ligand and allosteric activator of pyruvate kinase M2. *Nature* **491**, 458–462 (2012).
197. Yuan, M. *et al.* An allostatic mechanism for M2 pyruvate kinase as an amino-acid sensor. *Biochemical Journal* **475**, 1821–1837 (2018).
198. Morgan, H. P. *et al.* M2 pyruvate kinase provides a mechanism for nutrient sensing and regulation of cell proliferation. *Proceedings of the National Academy of Sciences* **110**, 5881–5886 (2013).
199. Schulz, J., Sparmann, G. & Hofmann, E. Alanine-mediated reversible inactivation of tumour pyruvate kinase caused by a tetramer-dimer transition. *FEBS Lett* **50**, 346–350 (1975).
200. Srivastava, D., Nandi, S. & Dey, M. Mechanistic and Structural Insights into Cysteine-Mediated Inhibition of Pyruvate Kinase Muscle Isoform 2. *Biochemistry* **58**, 3669–3682 (2019).
201. Anastasiou, D. *et al.* Inhibition of pyruvate kinase M2 by reactive oxygen species contributes to cellular antioxidant responses. *Science* **334**, 1278–1283 (2011).

202. Hitosugi, T. *et al.* Tyrosine Phosphorylation Inhibits PKM2 to Promote the Warburg Effect and Tumor Growth. *Sci. Signal.* **2**, ra73–ra73 (2009).
203. Israelsen, W. J. & Vander Heiden, M. G. Pyruvate kinase: Function, regulation and role in cancer. *Semin. Cell Dev. Biol.* **43**, 43–51 (2015).
204. Eigenbrodt, E., Reinacher, M., Scheefers-Borchel, U., Scheefers, H. & Friis, R. Double role for pyruvate kinase type M2 in the expansion of phosphometabolite pools found in tumor cells. *Crit Rev Oncog* **3**, 91–115 (1992).
205. Lunt, S. Y. *et al.* Pyruvate kinase isoform expression alters nucleotide synthesis to impact cell proliferation. *Mol. Cell* **57**, 95–107 (2015).
206. Li, X. *et al.* The responsively decreased PKM2 facilitates the survival of pancreatic cancer cells in hypoglycose. *Cell Death Dis* **9**, (2018).
207. Israelsen, W. J. *et al.* PKM2 isoform-specific deletion reveals a differential requirement for pyruvate kinase in tumor cells. *Cell* **155**, 397–409 (2013).
208. Davidson, S. M. *et al.* Pyruvate Kinase M1 Suppresses Development and Progression of Prostate Adenocarcinoma. *Cancer Research* **82**, 2403–2416 (2022).
209. Dayton, T. L. *et al.* Germline loss of PKM2 promotes metabolic distress and hepatocellular carcinoma. *Genes Dev.* **30**, 1020–1033 (2016).
210. Hillis, A. L. *et al.* PKM2 is not required for pancreatic ductal adenocarcinoma. *Cancer Metab* **6**, (2018).
211. Lau, A. N. *et al.* PKM2 is not required for colon cancer initiated by APC loss. *Cancer Metab* **5**, 10 (2017).
212. Cortés-Cros, M. *et al.* M2 isoform of pyruvate kinase is dispensable for tumor maintenance and growth. *Proceedings of the National Academy of Sciences of the United States of America* **110**, 489 (2013).
213. Morita, M. *et al.* PKM1 Confers Metabolic Advantages and Promotes Cell-Autonomous Tumor Cell Growth. *Cancer Cell* **33**, 355-367.e7 (2018).
214. Sonveaux, P. *et al.* Targeting lactate-fueled respiration selectively kills hypoxic tumor cells in mice. *J Clin Invest* **118**, 3930–3942 (2008).
215. Hui, S. *et al.* Glucose feeds the TCA cycle via circulating lactate. *Nature* **551**, 115–118 (2017).
216. Faubert, B. *et al.* Lactate metabolism in human lung tumors. *Cell* **171**, 358-371.e9 (2017).

217. Payen, V. L., Mina, E., Van Hée, V. F., Porporato, P. E. & Sonveaux, P. Monocarboxylate transporters in cancer. *Mol Metab* **33**, 48–66 (2019).
218. Yang, W. *et al.* ERK1/2-dependent phosphorylation and nuclear translocation of PKM2 promotes the Warburg effect. *Nat Cell Biol* **14**, 1295–1304 (2012).
219. Yang, W. *et al.* Nuclear PKM2 regulates  $\beta$ -catenin transactivation upon EGFR activation. *Nature* **480**, 118–122 (2011).
220. Yang, W. & Lu, Z. Nuclear PKM2 regulates the Warburg effect. *Cell Cycle* **12**, 3154–3158 (2013).
221. Luo, W. *et al.* Pyruvate Kinase M2 is a PHD3-stimulated Coactivator for Hypoxia-Inducible Factor 1. *Cell* **145**, 732–744 (2011).
222. Wang, H.-J. *et al.* JMJD5 regulates PKM2 nuclear translocation and reprograms HIF-1 $\alpha$ -mediated glucose metabolism. *Proc Natl Acad Sci U S A* **111**, 279–284 (2014).
223. Gao, X., Wang, H., Jenny, J. Y., Liu, X. & Liu, Z.-R. Pyruvate Kinase M2 Regulates Gene Transcription by Acting as A Protein Kinase. *Mol Cell* **45**, 598–609 (2012).
224. Gao, X. *et al.* Reciprocal Regulation of Protein Kinase and Pyruvate Kinase Activities of Pyruvate Kinase M2 by Growth Signals. *J Biol Chem* **288**, 15971–15979 (2013).
225. Wang, Y.-H. *et al.* Cell state-specific metabolic dependency in hematopoiesis and leukemogenesis. *Cell* **158**, 1309–1323 (2014).
226. Hosios, A. M., Fiske, B. P., Gui, D. Y. & Vander Heiden, M. G. Lack of evidence for PKM2 protein kinase activity. *Mol Cell* **59**, 850–857 (2015).
227. Cancer Facts & Figures 2014. <https://www.cancer.org/research/cancer-facts-statistics/all-cancer-facts-figures/cancer-facts-figures-2014.html>.
228. Siegel, R. L., Miller, K. D. & Jemal, A. Cancer Statistics, 2017. *CA Cancer J Clin* **67**, 7–30 (2017).
229. Conroy, T. *et al.* Current standards and new innovative approaches for treatment of pancreatic cancer. *Eur J Cancer* **57**, 10–22 (2016).
230. Kleeff, J. *et al.* Pancreatic cancer. *Nat Rev Dis Primers* **2**, 16022 (2016).
231. Falasca, M., Kim, M. & Casari, I. Pancreatic cancer: Current research and future directions. *Biochim Biophys Acta* **1865**, 123–132 (2016).

232. Perera, R. M. & Bardeesy, N. Pancreatic Cancer Metabolism - Breaking it down to build it back up. *Cancer Discov* **5**, 1247–1261 (2015).
233. Cohen, R. *et al.* Targeting cancer cell metabolism in pancreatic adenocarcinoma. *Oncotarget* **6**, 16832–16847 (2015).
234. Hosein, A. N. & Beg, M. S. Pancreatic Cancer Metabolism: Molecular Mechanisms and Clinical Applications. *Curr Oncol Rep* **20**, 56 (2018).
235. Jurica, M. S. *et al.* The allosteric regulation of pyruvate kinase by fructose-1,6-bisphosphate. *Structure* **6**, 195–210 (1998).
236. Osterman, J. & Fritz, P. J. Pyruvate kinase isozymes: a comparative study in tissues of various mammalian species. *Comp Biochem Physiol B* **44**, 1077–1085 (1973).
237. Marie, J., Levin, M. J., Simon, M. P. & Kahn, A. Genetic and epigenetic control of the pyruvate kinase isozymes in mammals. *Isozymes Curr Top Biol Med Res* **7**, 221–240 (1983).
238. Sato, T., Morita, M., Nomura, M. & Tanuma, N. Revisiting glucose metabolism in cancer: lessons from a PKM knock-in model. *Mol Cell Oncol* **5**, e1472054 (2018).
239. Bandara, I. A., Baltatzis, M., Sanyal, S. & Siriwardena, A. K. Evaluation of tumor M2-pyruvate kinase (Tumor M2-PK) as a biomarker for pancreatic cancer. *World J Surg Oncol* **16**, 56 (2018).
240. Li, C., Zhao, Z., Zhou, Z. & Liu, R. PKM2 Promotes Cell Survival and Invasion Under Metabolic Stress by Enhancing Warburg Effect in Pancreatic Ductal Adenocarcinoma. *Dig Dis Sci* **61**, 767–773 (2016).
241. Azoitei, N. *et al.* PKM2 promotes tumor angiogenesis by regulating HIF-1 $\alpha$  through NF- $\kappa$ B activation. *Molecular Cancer* **15**, 3 (2016).
242. Feng, J. *et al.* PKM2 gene regulates the behavior of pancreatic cancer cells via mitogen-activated protein kinase pathways. *Molecular Medicine Reports* **11**, 2111–2117 (2015).
243. Ogawa, H. *et al.* The combination of the expression of hexokinase 2 and pyruvate kinase M2 is a prognostic marker in patients with pancreatic cancer. *Molecular and Clinical Oncology* **3**, 563–571 (2015).
244. Mohammad, G. H., Olde Damink, S. W. M., Malago, M., Dhar, D. K. & Pereira, S. P. Pyruvate Kinase M2 and Lactate Dehydrogenase A Are Overexpressed in Pancreatic Cancer and Correlate with Poor Outcome. *PLoS One* **11**, e0151635 (2016).

245. Lockney, N. A. *et al.* Pyruvate Kinase Muscle Isoenzyme 2 (PKM2) Expression Is Associated with Overall Survival in Pancreatic Ductal Adenocarcinoma. *J Gastrointest Cancer* **46**, 390–398 (2015).
246. Zhu, H. *et al.* Pyruvate kinase M2 (PKM2) expression correlates with prognosis in solid cancers: a meta-analysis. *Oncotarget* **8**, 1628–1640 (2017).
247. Wu, J. *et al.* Pyruvate kinase M2 overexpression and poor prognosis in solid tumors of digestive system: evidence from 16 cohort studies. *Onco Targets Ther* **9**, 4277–4288 (2016).
248. Gidekel Friedlander, S. Y. *et al.* Context-Dependent Transformation of Adult Pancreatic Cells by Oncogenic K-Ras. *Cancer Cell* **16**, 379–389 (2009).
249. Rowsell, E. V., Carnie, J. A., Wahbi, S. D., Al-Tai, A. H. & Rowsell, K. V. L-serine dehydratase and L-serine-pyruvate aminotransferase activities in different animal species. *Comp Biochem Physiol B* **63**, 543–555 (1979).
250. Yamada, T. *et al.* Crystal structure of serine dehydratase from rat liver. *Biochemistry* **42**, 12854–12865 (2003).
251. Zogg, C. K. Phosphoglycerate Dehydrogenase: Potential Therapeutic Target and Putative Metabolic Oncogene. *J Oncol* **2014**, 524101 (2014).
252. Yoshino, H. *et al.* PHGDH as a key enzyme for serine biosynthesis in HIF2 $\alpha$ -targeting therapy for renal cell carcinoma. *Cancer Res* **77**, 6321–6329 (2017).
253. Zhang, B. *et al.* PHGDH Defines a Metabolic Subtype in Lung Adenocarcinomas with Poor Prognosis. *Cell Rep* **19**, 2289–2303 (2017).
254. Comb, D. G. & Roseman, S. The sialic acids. I. The structure and enzymatic synthesis of N-acetylneuraminic acid. *J Biol Chem* **235**, 2529–2537 (1960).
255. Ji, W. *et al.* Characterization of a novel N-acetylneuraminic acid lyase favoring N-acetylneuraminic acid synthesis. *Sci Rep* **5**, 9341 (2015).
256. Schirch, L. & Gross, T. Serine transhydroxymethylase. Identification as the threonine and allothreonine aldolases. *J Biol Chem* **243**, 5651–5655 (1968).
257. Lima, S., Khristoforov, R., Momany, C. & Phillips, R. S. Crystal structure of Homo sapiens kynureninase. *Biochemistry* **46**, 2735–2744 (2007).
258. Stipanuk, M. H. Sulfur amino acid metabolism: pathways for production and removal of homocysteine and cysteine. *Annu. Rev. Nutr.* **24**, 539–577 (2004).
259. Yokoyama, M. *et al.* Pyruvate kinase type M2 contributes to the development of pancreatic ductal adenocarcinoma by regulating the production of metabolites and reactive oxygen species. *International Journal of Oncology* **52**, 881–891 (2018).

260. Ma, E. H. *et al.* Serine Is an Essential Metabolite for Effector T Cell Expansion. *Cell Metab* **25**, 345–357 (2017).
261. Locasale, J. W. *et al.* Phosphoglycerate dehydrogenase diverts glycolytic flux and contributes to oncogenesis. *Nat Genet* **43**, 869–874 (2011).
262. Kohl, J. B., Mellis, A. & Schwarz, G. Homeostatic impact of sulfite and hydrogen sulfide on cysteine catabolism. *Br J Pharmacol* **176**, 554–570 (2019).
263. Yao, W. *et al.* Syndecan 1 is a critical mediator of macropinocytosis in pancreatic cancer. *Nature* **568**, 410–414 (2019).
264. Muzumdar, M. D. *et al.* Survival of pancreatic cancer cells lacking KRAS function. *Nat Commun* **8**, 1090 (2017).
265. Ran, F. A. *et al.* Genome engineering using the CRISPR-Cas9 system. *Nat Protoc* **8**, 2281–2308 (2013).
266. Ogrodzinski, M. P. *et al.* Measuring the Nutrient Metabolism of Adherent Cells in Culture. *Methods Mol. Biol.* **1862**, 37–52 (2019).
267. Han, J., Gagnon, S., Eckle, T. & Borchers, C. H. Metabolomic Analysis of Key Central Carbon Metabolism Carboxylic Acids as Their 3-Nitrophenylhydrazones by UPLC/ESI-MS. *Electrophoresis* **34**, 2891 (2013).
268. Melamud, E., Vastag, L. & Rabinowitz, J. D. Metabolomic Analysis and Visualization Engine for LC–MS Data. *Anal Chem* **82**, 9818–9826 (2010).
269. Millard, P., Letisse, F., Sokol, S. & Portais, J.-C. IsoCor: correcting MS data in isotope labeling experiments. *Bioinformatics* **28**, 1294–1296 (2012).
270. Saldanha, A. J. Java Treeview--extensible visualization of microarray data. *Bioinformatics* **20**, 3246–3248 (2004).
271. de Hoon, M. J. L., Imoto, S., Nolan, J. & Miyano, S. Open source clustering software. *Bioinformatics* **20**, 1453–1454 (2004).
272. Wood, L. D., Canto, M. I., Jaffee, E. M. & Simeone, D. M. Pancreatic Cancer: Pathogenesis, Screening, Diagnosis, and Treatment. *Gastroenterology* **163**, 386-402.e1 (2022).
273. Pavlova, N. N. & Thompson, C. B. THE EMERGING HALLMARKS OF CANCER METABOLISM. *Cell Metab* **23**, 27–47 (2016).
274. Encarnación-Rosado, J. & Kimmelman, A. C. Harnessing metabolic dependencies in pancreatic cancers. *Nat Rev Gastroenterol Hepatol* **18**, 482–492 (2021).

275. Liu, M. *et al.* PKM2 promotes reductive glutamine metabolism. *Cancer Biol Med* **15**, 389–399 (2018).
276. Bott, A. J. *et al.* Glutamine Anabolism Plays a Critical Role in Pancreatic Cancer by Coupling Carbon and Nitrogen Metabolism. *Cell Rep* **29**, 1287-1298.e6 (2019).
277. Cramer, S. L. *et al.* Systemic depletion of serum l-Cyst(e)ine with an engineered human enzyme induces production of reactive oxygen species and suppresses tumor growth in mice. *Nat Med* **23**, 120–127 (2017).
278. Combs, J. A. & DeNicola, G. M. The Non-Essential Amino Acid Cysteine Becomes Essential for Tumor Proliferation and Survival. *Cancers (Basel)* **11**, (2019).
279. Larraufie, M.-H. *et al.* Incorporation of metabolically stable ketones into a small molecule probe to increase potency and water solubility. *Bioorg Med Chem Lett* **25**, 4787–4792 (2015).
280. Daher, B., Vučetić, M. & Pouysségur, J. Cysteine Depletion, a Key Action to Challenge Cancer Cells to Ferroptotic Cell Death. *Front Oncol* **10**, (2020).
281. Liu, X. *et al.* Cystine transporter regulation of pentose phosphate pathway dependency and disulfide stress exposes a targetable metabolic vulnerability in cancer. *Nat Cell Biol* **22**, 476–486 (2020).
282. Yu, L. *et al.* Cysteine catabolism and the serine biosynthesis pathway support pyruvate production during pyruvate kinase knockdown in pancreatic cancer cells. *Cancer & Metabolism* **7**, 13 (2019).
283. Ferguson, E. C. & Rathmell, J. C. New roles for pyruvate kinase M2: working out the Warburg effect. *Trends Biochem Sci* **33**, 359–362 (2008).
284. Irokawa, H. *et al.* Comprehensive analyses of the cysteine thiol oxidation of PKM2 reveal the effects of multiple oxidation on cellular oxidative stress response. *Biochemical Journal* **478**, 1453–1470 (2021).
285. Hensley, C. T., Wasti, A. T. & DeBerardinis, R. J. Glutamine and cancer: cell biology, physiology, and clinical opportunities. *J Clin Invest* **123**, 3678–3684 (2013).
286. Gross, M. I. *et al.* Antitumor activity of the glutaminase inhibitor CB-839 in triple-negative breast cancer. *Mol. Cancer Ther.* **13**, 890–901 (2014).
287. Hamada, S. *et al.* Nrf2 Activation Sensitizes K-Ras Mutant Pancreatic Cancer Cells to Glutaminase Inhibition. *Int J Mol Sci* **22**, 1870 (2021).
288. Li, L. *et al.* Pyruvate Kinase M2 Coordinates Metabolism Switch between Glycolysis and Glutaminolysis in Cancer Cells. *iScience* **23**, 101684 (2020).

289. Kremer, D. M. *et al.* GOT1 inhibition promotes pancreatic cancer cell death by ferroptosis. *Nat Commun* **12**, 4860 (2021).
290. Alborzinia, H. *et al.* MYCN mediates cysteine addiction and sensitizes neuroblastoma to ferroptosis. *Nat Cancer* **3**, 471–485 (2022).
291. Zhao, Y., Wang, Y., Miao, Z., Liu, Y. & Yang, Q. c-Myc protects hepatocellular carcinoma cell from ferroptosis induced by glutamine deprivation via upregulating GOT1 and Nrf2. *Mol Biol Rep* (2023) doi:10.1007/s11033-023-08495-1.
292. Brashears, C. B. *et al.* Malic Enzyme 1 Absence in Synovial Sarcoma Shifts Antioxidant System Dependence and Increases Sensitivity to Ferroptosis Induction with ACXT3102. *Clin Cancer Res clincanres.0470.2022* (2022) doi:10.1158/1078-0432.CCR-22-0470.
293. Fang, X. *et al.* Malic Enzyme 1 as a Novel Anti-Ferroptotic Regulator in Hepatic Ischemia/Reperfusion Injury. *Adv Sci (Weinh)* **10**, e2205436 (2023).
294. Koppula, P., Zhang, Y., Shi, J., Li, W. & Gan, B. The glutamate/cystine antiporter SLC7A11/xCT enhances cancer cell dependency on glucose by exporting glutamate. *J Biol Chem* **292**, 14240–14249 (2017).
295. Yan, Y. *et al.* SLC7A11 expression level dictates differential responses to oxidative stress in cancer cells. *Nat Commun* **14**, 3673 (2023).
296. Shin, C.-S. *et al.* The glutamate/cystine xCT antiporter antagonizes glutamine metabolism and reduces nutrient flexibility. *Nat Commun* **8**, 15074 (2017).
297. Xiaoyu, H. *et al.* The mTOR Pathway Regulates PKM2 to Affect Glycolysis in Esophageal Squamous Cell Carcinoma. *Technol Cancer Res Treat* **17**, 1533033818780063 (2018).
298. He, C.-L. *et al.* Pyruvate Kinase M2 Activates mTORC1 by Phosphorylating AKT1S1. *Sci Rep* **6**, 21524 (2016).
299. Sun, Q. *et al.* Mammalian target of rapamycin up-regulation of pyruvate kinase isoenzyme type M2 is critical for aerobic glycolysis and tumor growth. *Proc Natl Acad Sci U S A* **108**, 4129–4134 (2011).
300. Wang, Y. *et al.* Wnt/beta-catenin signaling confers ferroptosis resistance by targeting GPX4 in gastric cancer. *Cell Death Differ* **29**, 2190–2202 (2022).
301. Sun, Q. *et al.* Rho family GTPase 1 (RND1), a novel regulator of p53, enhances ferroptosis in glioblastoma. *Cell Biosci* **12**, 53 (2022).
302. Koppula, P., Zhuang, L. & Gan, B. Cystine transporter SLC7A11/xCT in cancer: ferroptosis, nutrient dependency, and cancer therapy. *Protein Cell* **12**, 599–620 (2021).

303. Kim, B. *et al.* Endothelial pyruvate kinase M2 maintains vascular integrity. *J Clin Invest* **128**, 4543–4556 (2018).
304. Saleme, B. *et al.* Tissue-specific regulation of p53 by PKM2 is redox dependent and provides a therapeutic target for anthracycline-induced cardiotoxicity. *Science Translational Medicine* **11**, eaau8866 (2019).
305. Peyssonnaud, C., Nizet, V. & Johnson, R. S. Role of the hypoxia inducible factors HIF in iron metabolism. *Cell Cycle* **7**, 28–32 (2008).
306. Matte, A. *et al.* The pyruvate kinase activator mitapivat reduces hemolysis and improves anemia in a  $\beta$ -thalassemia mouse model. *J Clin Invest* **131**, e144206 (2021).
307. Shah, Y. M. & Xie, L. Hypoxia-Inducible Factors Link Iron Homeostasis and Erythropoiesis. *Gastroenterology* **146**, 630–642 (2014).
308. Schindelin, J. *et al.* Fiji: an open-source platform for biological-image analysis. *Nat Methods* **9**, 676–682 (2012).
309. Clasquin, M. F., Melamud, E. & Rabinowitz, J. D. LC-MS Data Processing with MAVEN: A Metabolomic Analysis and Visualization Engine. *Curr Protoc Bioinformatics* **0 14**, Unit14.11 (2012).
310. Dieterle, F., Ross, A., Schlotterbeck, G. & Senn, H. Probabilistic Quotient Normalization as Robust Method to Account for Dilution of Complex Biological Mixtures. Application in <sup>1</sup>H NMR Metabonomics. *Anal. Chem.* **78**, 4281–4290 (2006).
311. Weibel, K. E., Mor, J. R. & Fiechter, A. Rapid sampling of yeast cells and automated assays of adenylate, citrate, pyruvate and glucose-6-phosphate pools. *Anal Biochem* **58**, 208–216 (1974).
312. Koning, W. de & Dam, K. van. A method for the determination of changes of glycolytic metabolites in yeast on a subsecond time scale using extraction at neutral pH. *Analytical Biochemistry* **204**, 118–123 (1992).
313. Sellick, C. A. *et al.* Evaluation of extraction processes for intracellular metabolite profiling of mammalian cells: matching extraction approaches to cell type and metabolite targets. *Metabolomics* **6**, 427–438 (2010).
314. Metallo, C. M., Walther, J. L. & Stephanopoulos, G. Evaluation of <sup>13</sup>C isotopic tracers for metabolic flux analysis in mammalian cells. *J Biotechnol* **144**, 167–174 (2009).
315. Buescher, J. M. *et al.* A roadmap for interpreting <sup>13</sup>C metabolite labeling patterns from cells. *Curr Opin Biotechnol* **34**, 189–201 (2015).

316. Fang, M. *et al.* Thermal Degradation of Small Molecules: A Global Metabolomic Investigation. *Anal Chem* **87**, 10935–10941 (2015).
317. Pang, Z. *et al.* Using MetaboAnalyst 5.0 for LC–HRMS spectra processing, multi-omics integration and covariate adjustment of global metabolomics data. *Nat Protoc* **17**, 1735–1761 (2022).
318. Diedrich, J. D. *et al.* Adipocyte-derived kynurenine stimulates malignant transformation of mammary epithelial cells through the aryl hydrocarbon receptor. *Biochem Pharmacol* 115763 (2023) doi:10.1016/j.bcp.2023.115763.
319. Lensmire, J. M. *et al.* The glutathione import system satisfies the *Staphylococcus aureus* nutrient sulfur requirement and promotes interspecies competition. *PLOS Genetics* **19**, e1010834 (2023).
320. Erstad, D. J. *et al.* Orthotopic and heterotopic murine models of pancreatic cancer and their different responses to FOLFIRINOX chemotherapy. *Dis Model Mech* **11**, (2018).
321. Jun, E. *et al.* Genetic and metabolic comparison of orthotopic and heterotopic patient-derived pancreatic-cancer xenografts to the original patient tumors. *Oncotarget* **9**, 7867–7881 (2017).
322. Dang, Q. *et al.* Ferroptosis: a double-edged sword mediating immune tolerance of cancer. *Cell Death Dis* **13**, 1–16 (2022).
323. Gong, C. *et al.* Ferroptosis in tumor immunity and therapy. *J Cell Mol Med* **26**, 5565–5579 (2022).
324. Patel, S. *et al.* Novel imidazopyrimidines-based molecules induce tetramerization of tumor pyruvate kinase M2 and exhibit potent antiproliferative profile. *European Journal of Pharmaceutical Sciences* **170**, 106112 (2022).
325. Sumitomo Pharma Oncology, Inc. *A Phase I, First-in-human, Open-label, Dose Escalation, Safety, Pharmacokinetic, and Pharmacodynamic Study of Oral TP 1454.* <https://clinicaltrials.gov/study/NCT04328740> (2023).
326. Chakrabarti, G. Mutant KRAS associated malic enzyme 1 expression is a predictive marker for radiation therapy response in non-small cell lung cancer. *Radiat Oncol* **10**, 145 (2015).
327. Holmström, K. M., Kostov, R. V. & Dinkova-Kostova, A. T. The multifaceted role of Nrf2 in mitochondrial function. *Curr Opin Toxicol* **1**, 80–91 (2016).
328. Wei, Y. *et al.* Pyridoxine induces glutathione synthesis via PKM2-mediated Nrf2 transactivation and confers neuroprotection. *Nat Commun* **11**, 941 (2020).

329. Zhang, T. *et al.* Polyamine pathway activity promotes cysteine essentiality in cancer cells. *Nat Metab* **2**, 1062–1076 (2020).

## APPENDIX A: SUPPLEMENTARY DATA IN SUPPORT OF CHAPTER 2

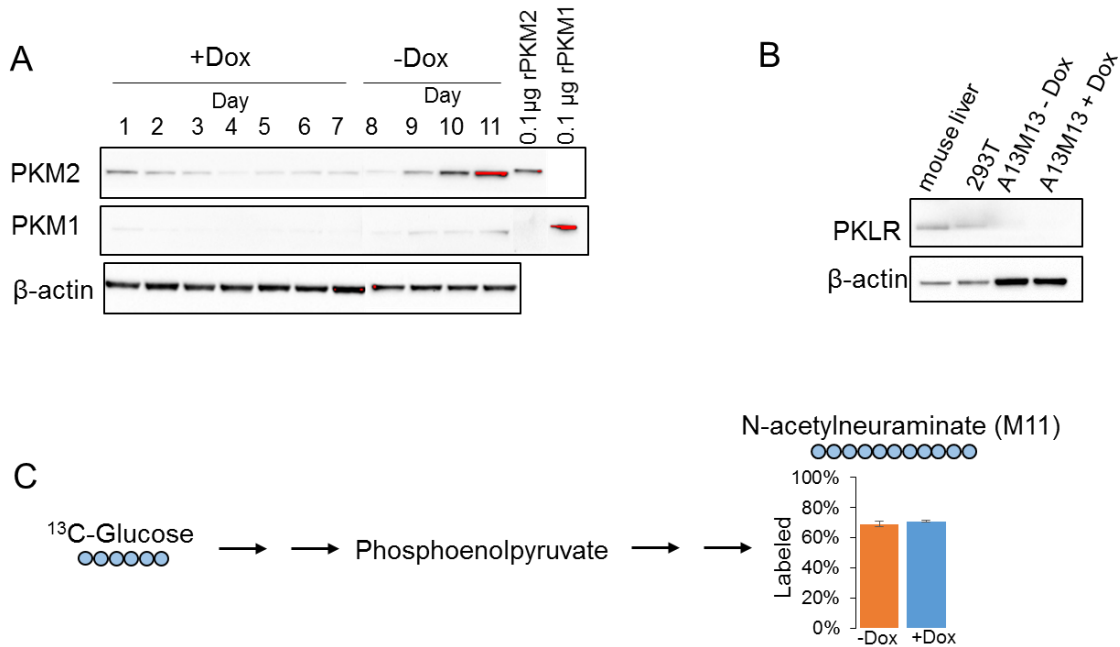


**Figure A.1 Supplementary in support of figure 2.1.**

(A) The effect of doxycycline (Dox) treatment on pyruvate kinase isoform expression in pancreatic cancer cells (PDACs) was assessed by western blot analysis. Cells were treated with 1  $\mu$ g/ml doxycycline (+Dox) or vehicle (-Dox) for the indicated number of days. Recombinant PKM1 or PKM2 lysate were included as control samples that express only PKM1 or PKM2. (B) No PKL/R is expressed in A13M13 cells. (C)  $^{13}\text{C}$ - glucose labeling of intracellular N-acetylneuraminic acid in PDAC cells with vehicle (-Dox) or PKM1/2 knockdown (+Dox). The y-axis for all graphs is the percent labeling of indicated  $^{13}\text{C}$ -isotopologue.

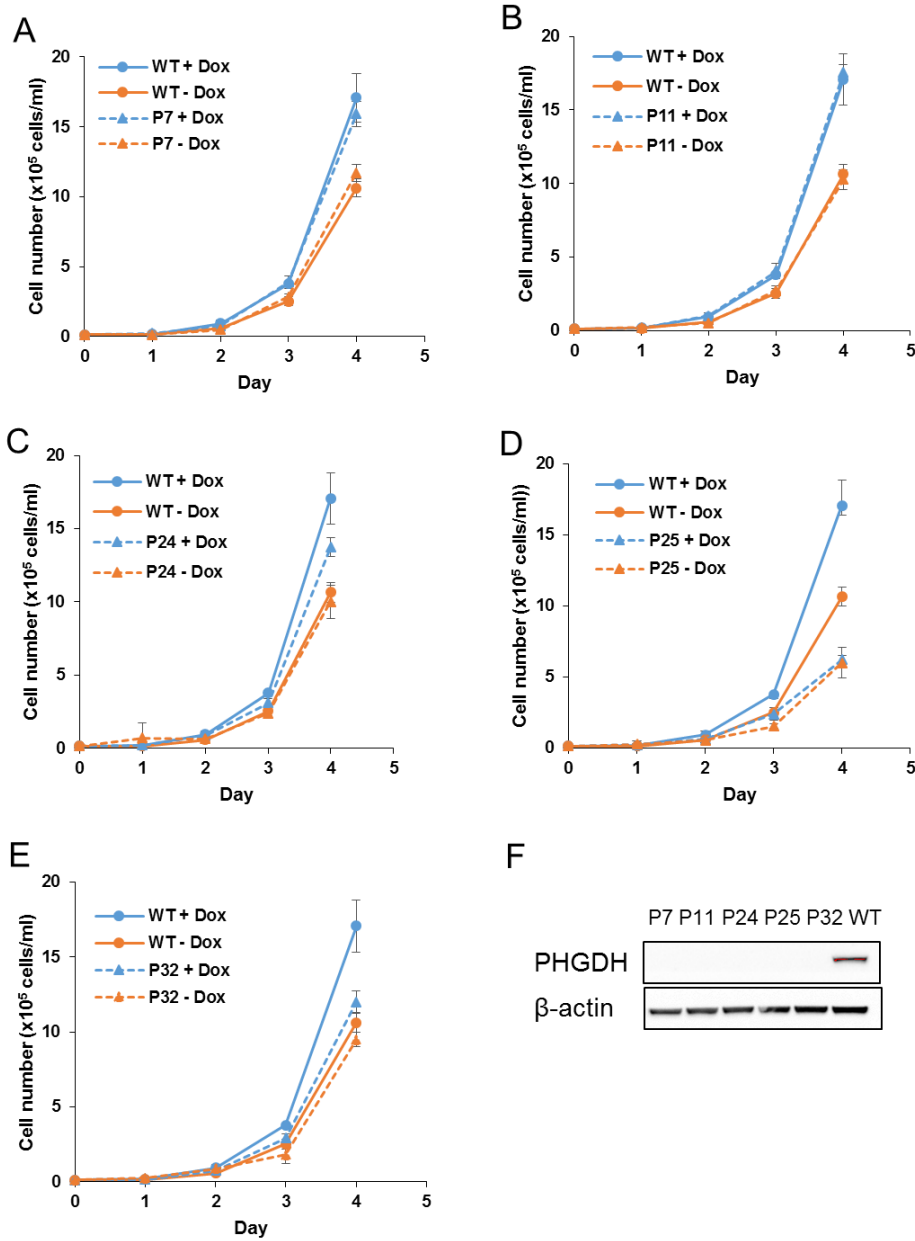


**Figure A.2 Supplementary data in support of figure 2.3.**

**A-E** Proliferation rates of PHGDH CRISPR knockouts of PDAC cell lines with vehicle (-Dox) or PKM1/2 knockdown (+Dox). P7, P11, P24, P25 and P32 are PHGDH knockout clones. WT is wild type PDAC cells. Cell counts were measured daily (n = 3). **F**. Western blot results for wild type and PHGDH knockout PDACs. Protein extraction is performed after cells were treated with doxycycline or vehicle for 7 days.

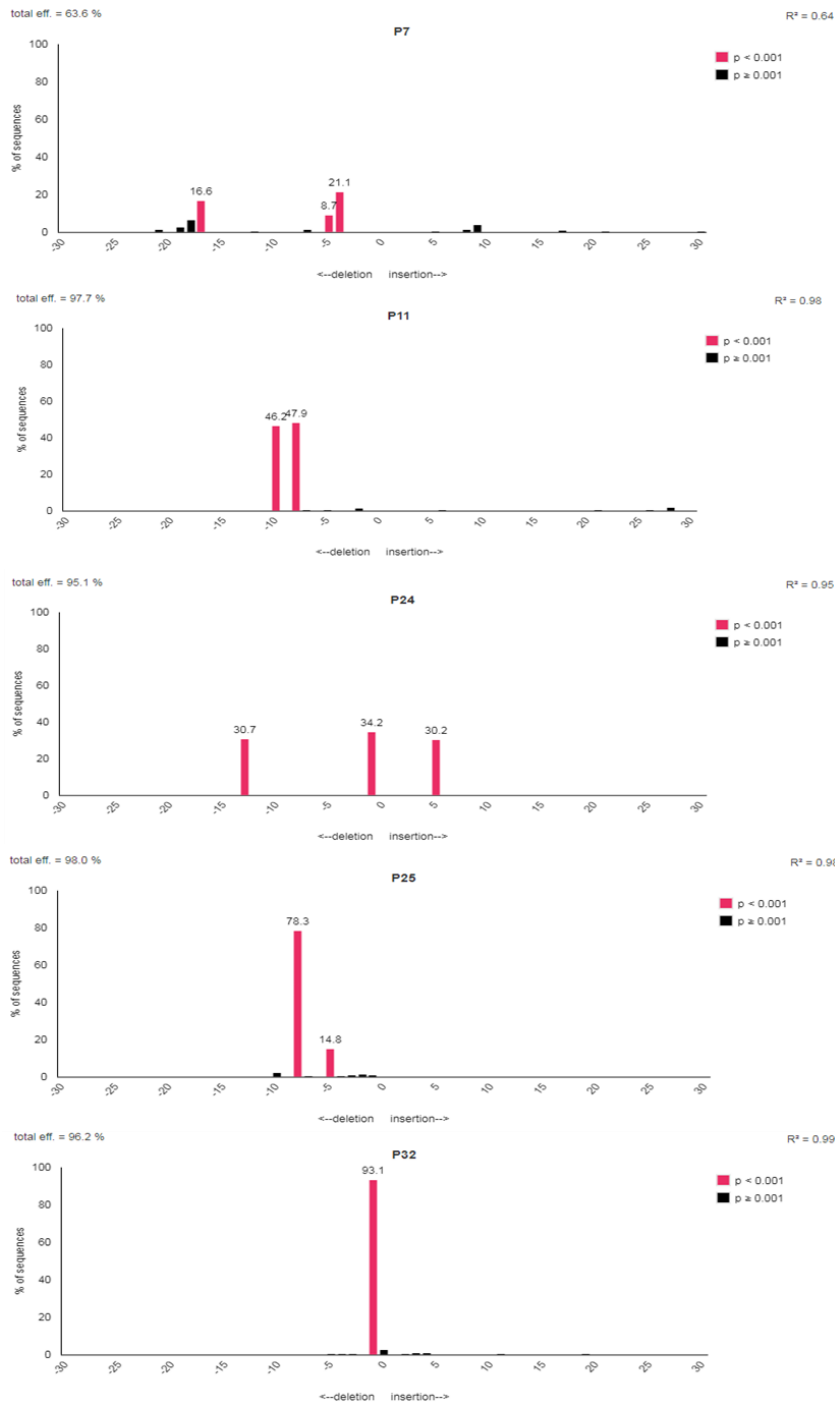


**Figure A.3 Supplementary data in support of figure 2.3.**

Sequencing confirmation of PHGDH knockout clones. About 800bp region enclosing the CRISPR target site was sequenced and analyzed with TIDE (Tracking of Indels by Decomposition) (<http://tide.nki.nl/>). TIDE generates indel spectra showing the predicted

**Figure A.3 (cont'd)**

indels in a mixed population of sequences, as well as the proportion of each sequence. The  $R^2$  value indicates the total proportion of sequences that were successfully analyzed. p-values are calculated for each indel to indicate confidence in the existence of that indel, and indels with high confidence (p-value < 0.001) are highlighted in red.

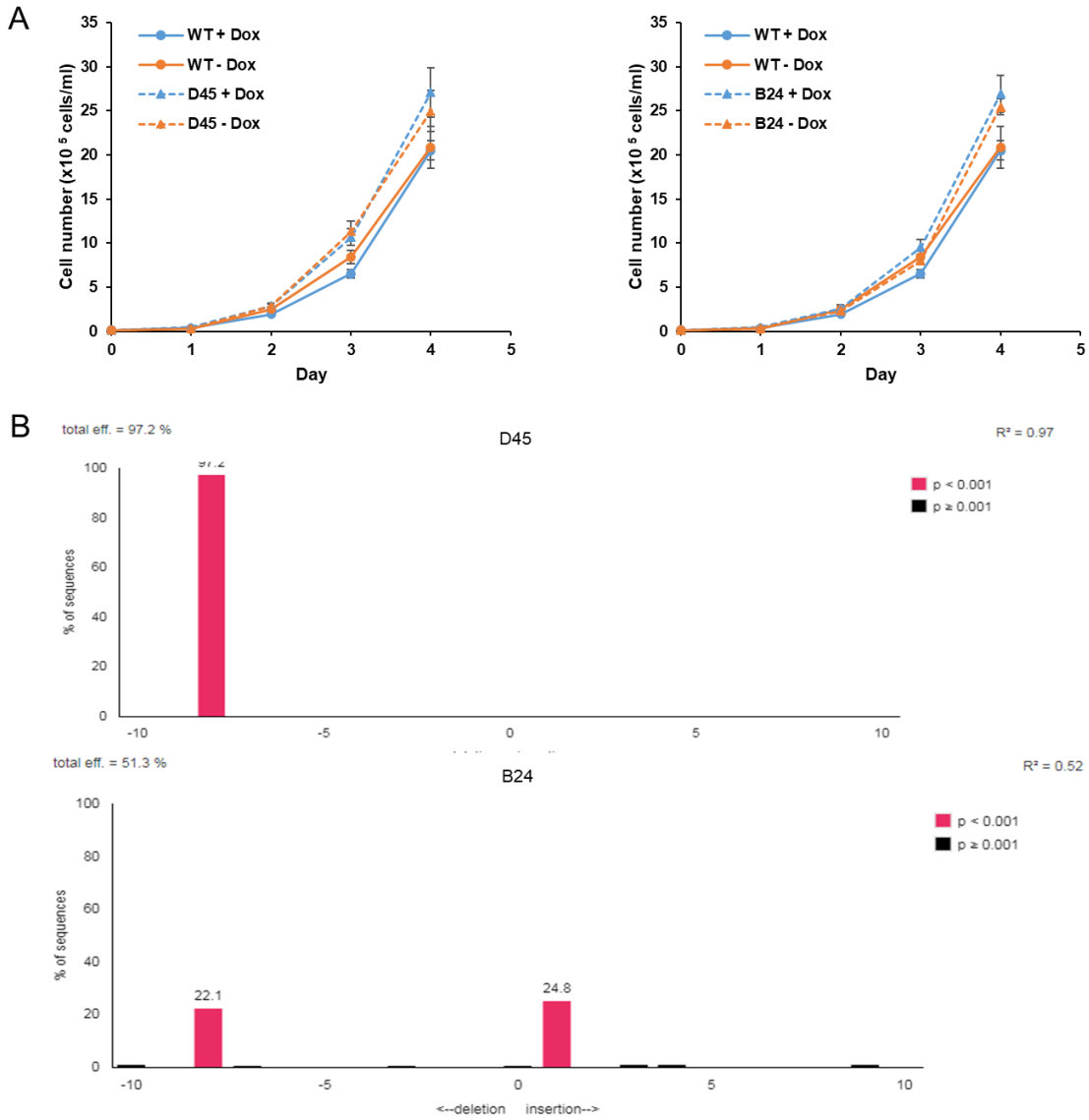


**Figure A.4 Supplementary data in support of figure 2.4.**

Proliferation rates (**A**) and sequence data (**B**) of NPL knockout clones D45 and B24 were performed as described above.

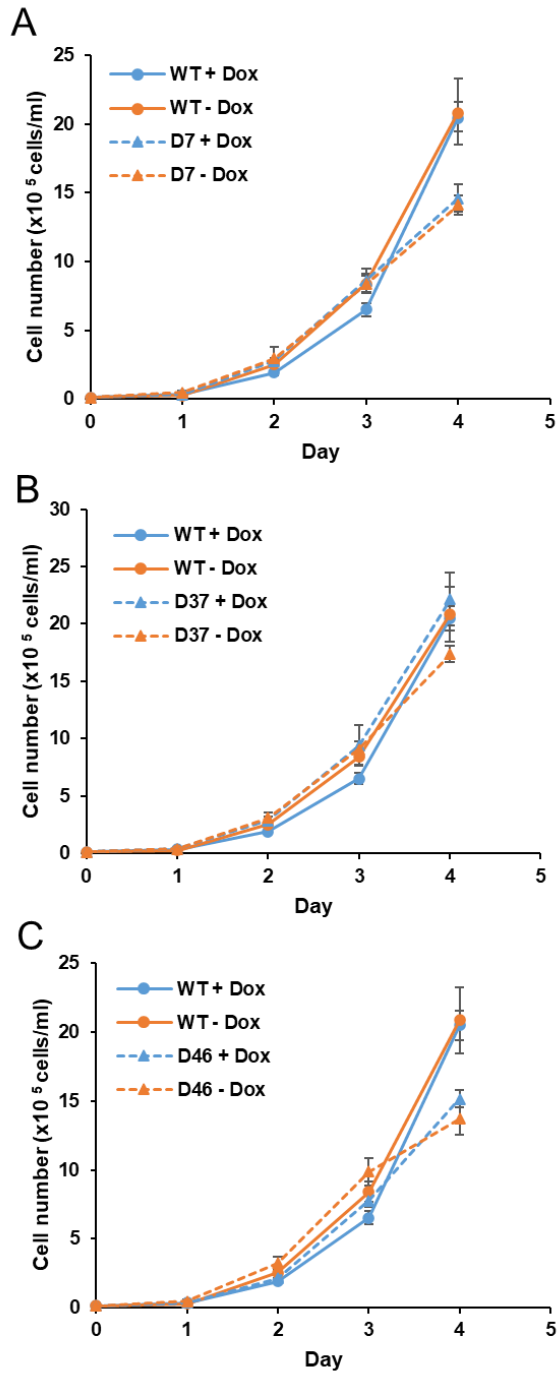


**Figure A.5 Supplementary data in support of figure 2.4.**

**A-C** Proliferation rates of PHGDH/NPL dual knockouts of PDAC cell lines with vehicle (-Dox) or PKM1/2 knockdown (+Dox). Cell counts were measured daily (n = 3).

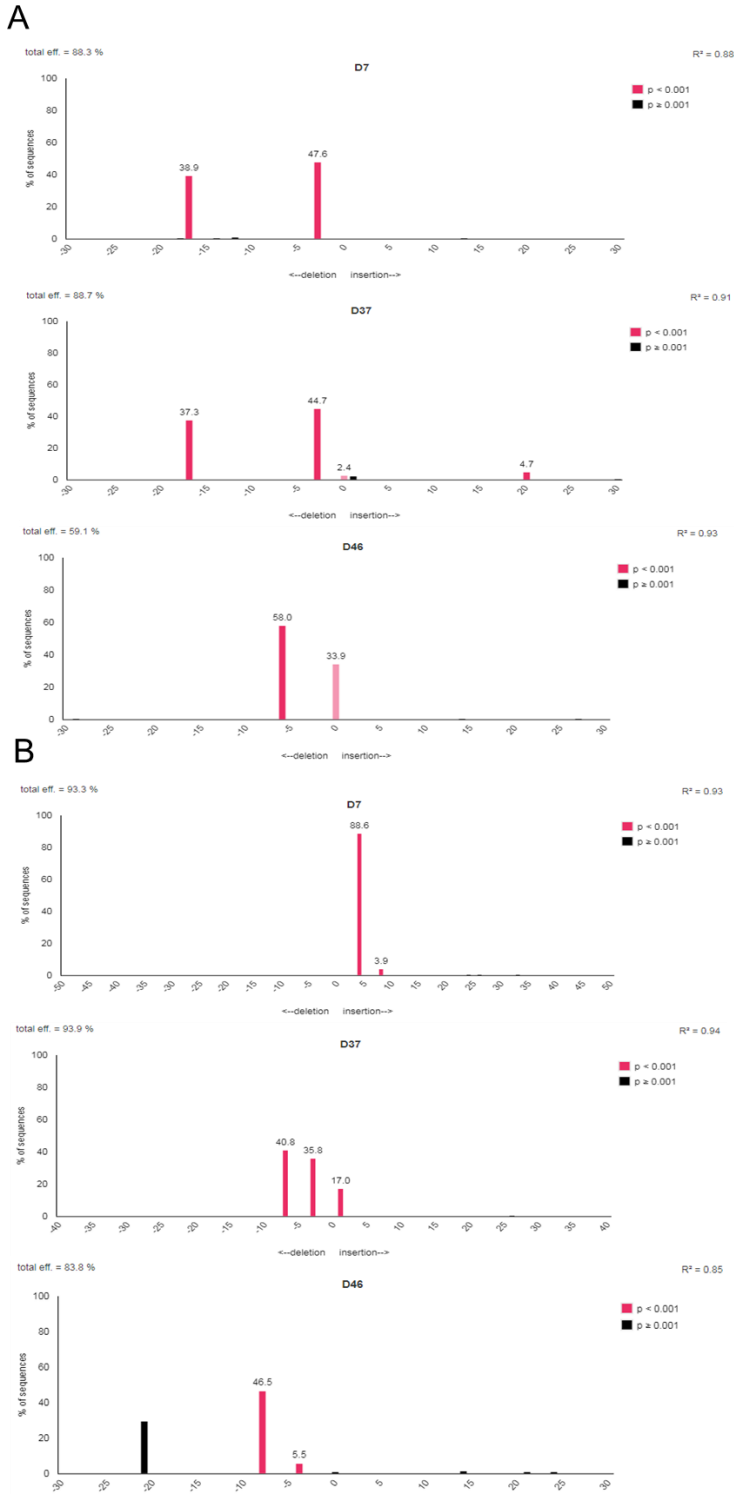


**Figure A.6 Supplementary data in support of figure 2.4.**

Sequencing confirmation of PHGDH/NPL dual knockout clones. **(A)** NPL knockout confirmation, **(B)** PHGDH knockout confirmation.

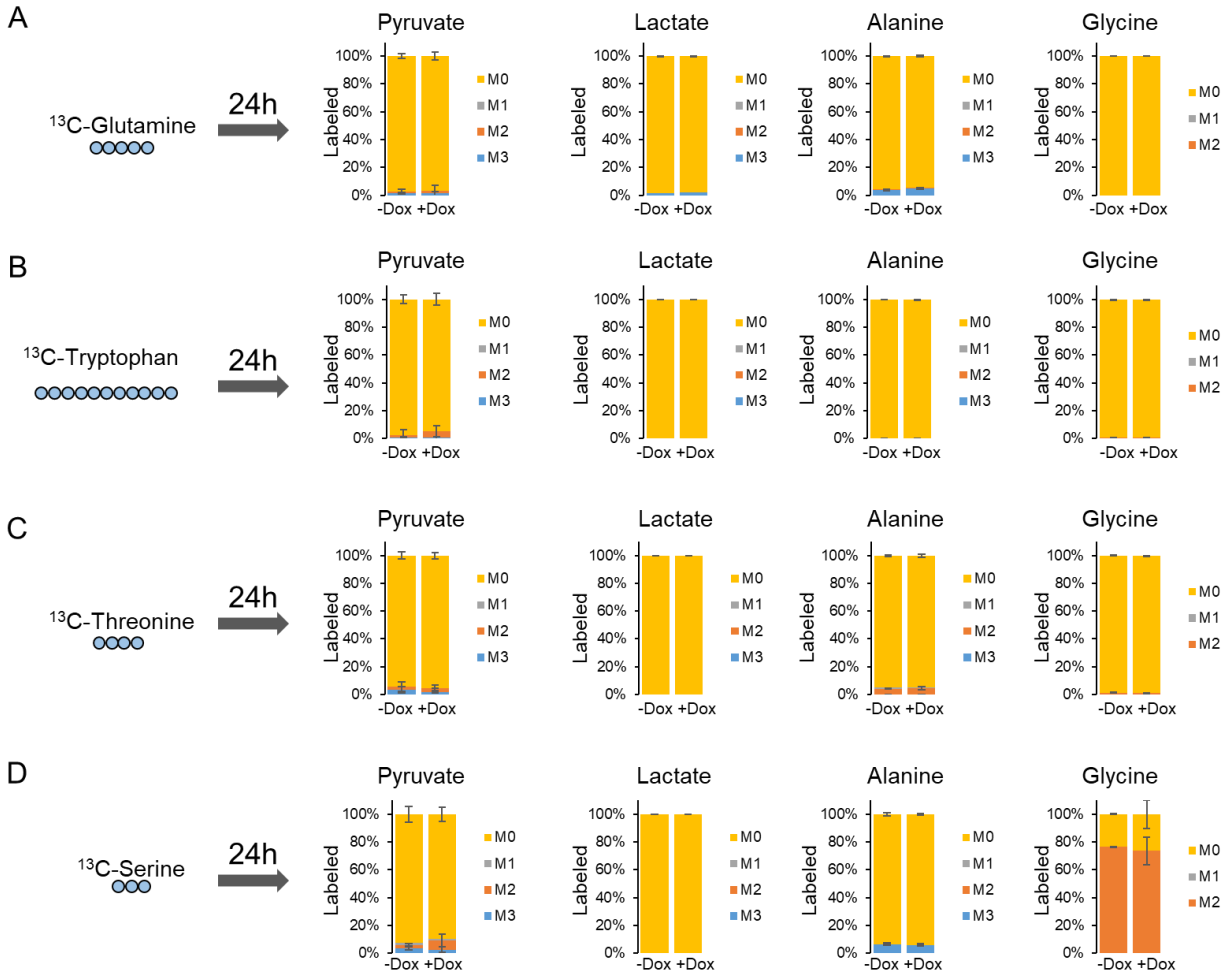


**Figure A.7 Supplementary data in support figure 2.5.**

**A.** U- $^{13}\text{C}$ -glutamine, **B.** U- $^{13}\text{C}$ -tryptophan, **C.** U- $^{13}\text{C}$ -threonine, and **D.** U- $^{13}\text{C}$ -serine labeling of intracellular metabolites in PHGDH/NPL dual KO D7 PDAC cells with vehicle (-Dox) or PKM1/2 knockdown (+Dox). The y-axis for all graphs is the percent labeling of indicated  $^{13}\text{C}$ -isotopologue. All data are displayed as means of triplicates.

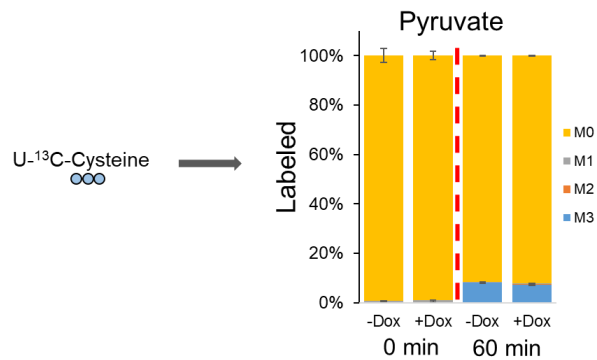


**Figure A.8 Supplementary data in support of figure 2.6.**

Labeling with  $^{13}\text{C}$ -Cysteine generates ~10% labeling of pyruvate in PDAC cells following vehicle (-Dox) or PKM1/2 knockdown (+Dox). The y-axis is the percent labeling of indicated  $^{13}\text{C}$ -isotopologue. Experiments were performed in triplicates, and all data are displayed as the mean values  $\pm$  standard error.

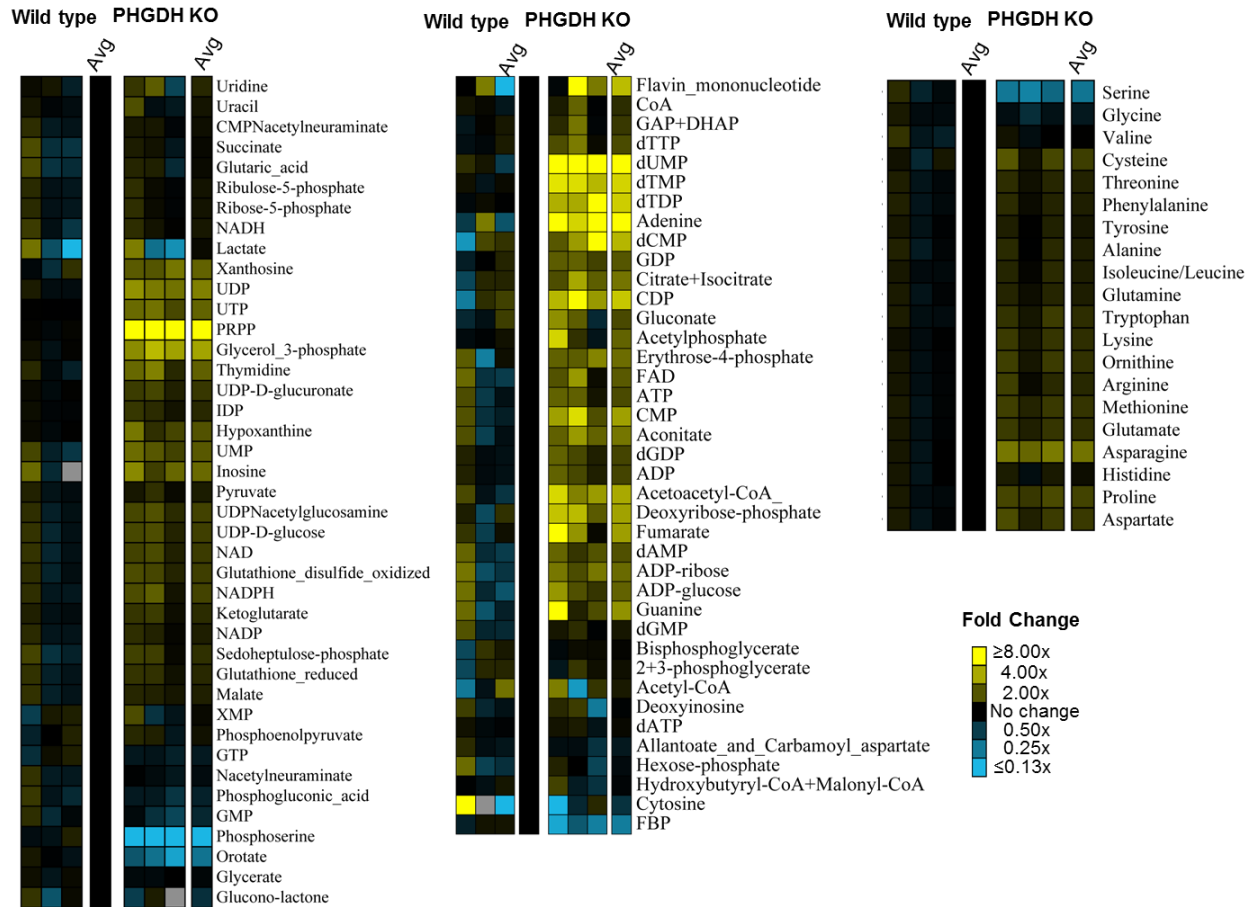


**Figure A.9 Supplementary data in support of figure 2.3.**

Intracellular metabolites in wild type and PHGDH knockout PDAC populations with PKM1/2 knockdown were measured using UPLC-MS/MS.

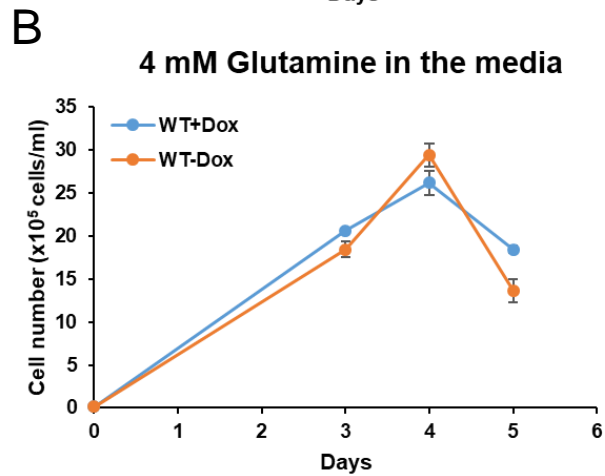
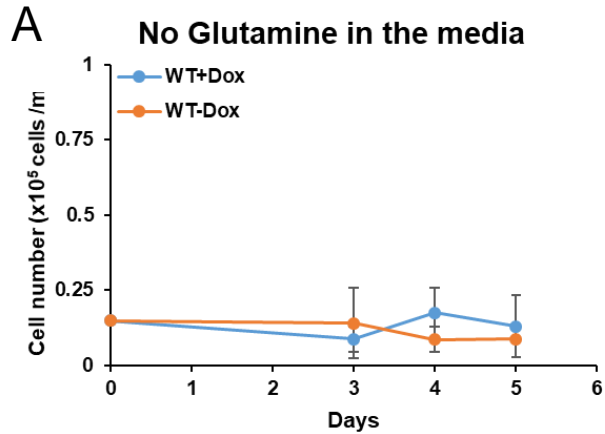


**Figure A.10 PDACs require glutamine for cell proliferation.**

Proliferation rates of A13M13 PDAC cells without (A) or with 4 mM glutamine (B) with vehicle (-Dox) or PKM1/2 knockdown (+Dox). All data are displayed as means of triplicates.

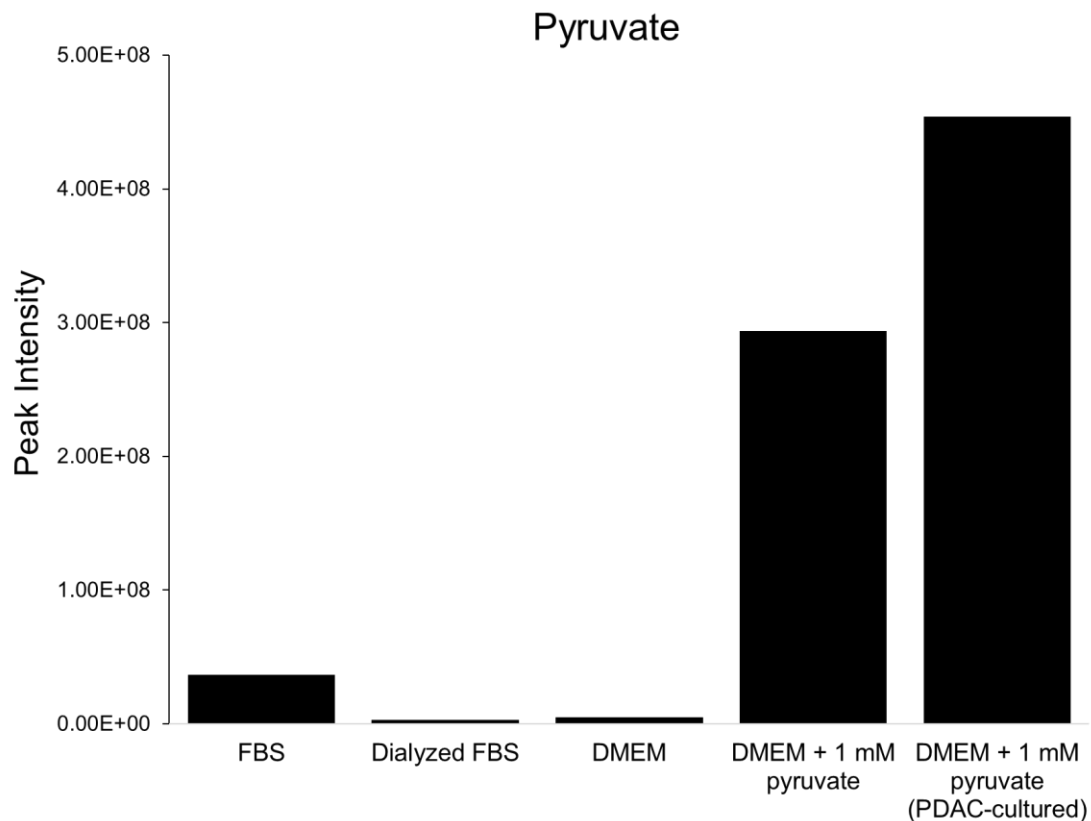


**Figure A.11 Abundance of pyruvate in serum and media.**

FBS (fetal bovine serum), dialyzed FBS (Sigma, F0392), DMEM (Fisher Scientific, MT10017CV), DMEM + 1 mM pyruvate (Fisher Scientific, MT10013CV). WT A13M13 PDAC cells were incubated in DMEM + 1 mM pyruvate on 3 separate plates. Media was collected from each plate and pooled together for analysis.

The observation that cysteine contributes to up to 20% of pyruvate production in pancreatic cancer cells was a novel finding and suggested a new level of importance for this amino acid. However, at the conclusion of this project there remained several critical open questions including: how critical is cysteine availability to cells under PKM2 KD? Would this effect be even more prominent under complete PKM2 KO? Is this effect applicable in human cancer cells? What environmental factors are necessary for cells to rely on cysteine for pyruvate production? To address these questions, I developed specific aims focusing on the role of cysteine metabolism in PKM2 depleted human cells. In particular, I was curious whether the presence of PKM2 would influence the tolerance of environments with low to no cysteine available and what metabolic or environmental factors may contribute to the reliance on cysteine. To my surprise, the loss of PKM2 actually prompted a remarkable increased tolerance of low cysteine conditions (see Chapter 3). This initial discovery brought to my attention a rapidly emerging excitement around a new form of cell death known as ferroptosis. As discussed previously, this form of cell death is characterized by unchecked lipid peroxidation propagated by iron and can be induced by cysteine starvation. No connection between PKM2 and ferroptosis had ever been identified and I immediately began excitedly exploring this novel finding. Originally, I had hypothesized that PKM2-mediated metabolic reprogramming commits glutamine and cysteine metabolism to energy production and biosynthesis needed for proliferation at the expense of glutathione production, limiting pancreatic cancer cell survival under low cysteine conditions. This turned out only to be partially correct and we find surprising connections between the activity of PKM2, ferroptosis, glutamine metabolism, and ME1. My observations on this novel phenomenon will be discussed extensively in Chapter 3.

**APPENDIX B: SUPPLEMENTARY DATA IN SUPPORT OF CHAPTER 3**

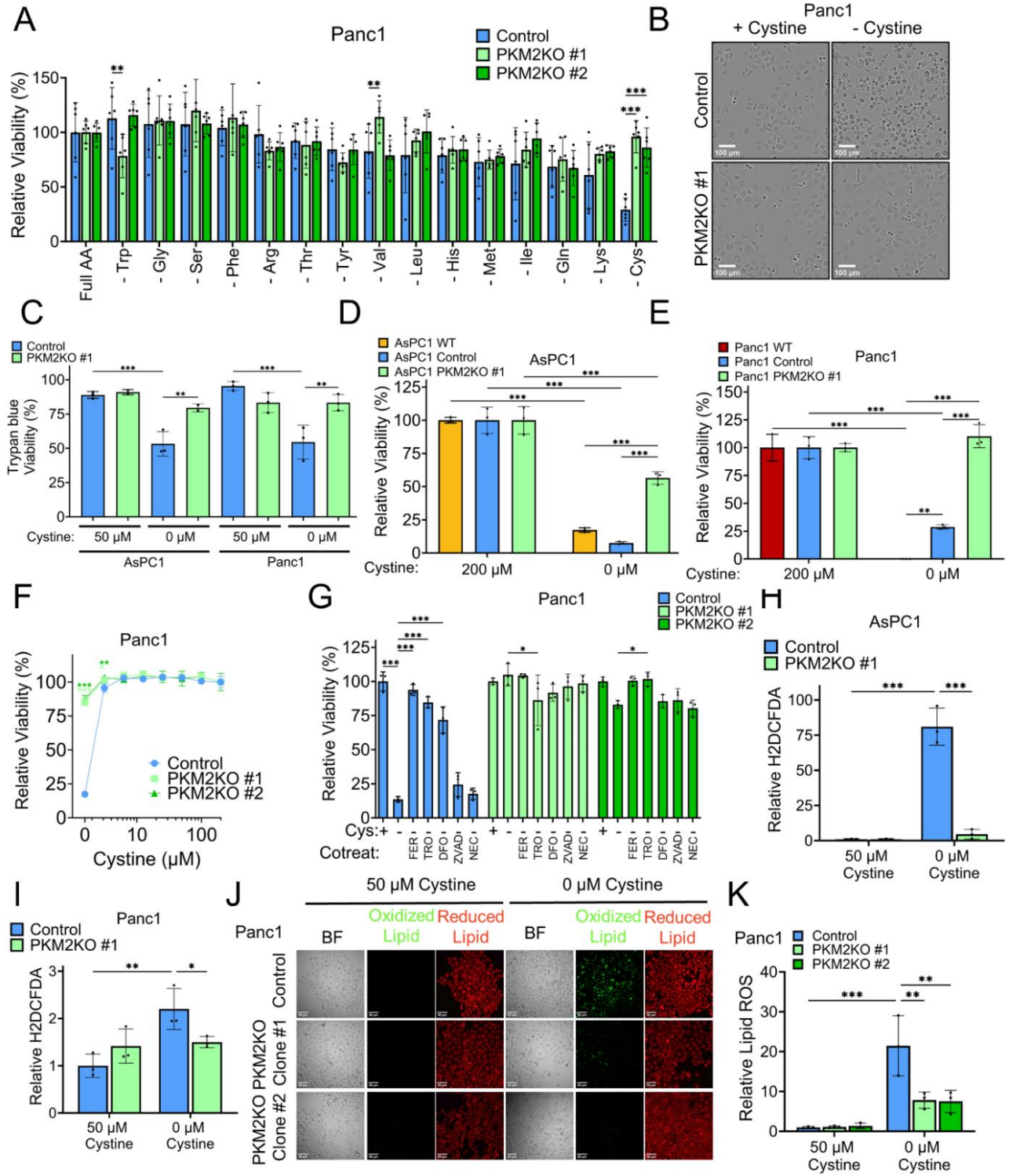


**Figure B.1 Additional data supporting Figure 3.1.**

## Figure B.1 (cont'd)

**A.** Relative viabilities of Panc1 control and respective PKM2KO clones in DMEM without each individual amino acid as shown. Significance was assessed by two-way ANOVA.

\*\* $p < 0.01$ , \*\*\* $p < 0.001$ . Multiple hypothesis correction by Tukey test. **B.** Brightfield

microscopy images of Panc1 Control and PKM2KO cells under either 200 or 0  $\mu\text{M}$  cystine conditions. Scale bar = 100  $\mu\text{m}$ . **C.** Relative viabilities of AsPC1 and Panc1 control and

PKM2KO cells under 50  $\mu\text{M}$  and 0  $\mu\text{M}$  cystine determined using trypan blue. Significance was assessed by two-way ANOVA. \* $p < 0.05$ , \*\* $p < 0.01$ , \*\*\* $p < 0.001$ . Multiple hypothesis

correction by Tukey test. **D-E.** Relative viabilities of AsPC1 (**D**) and Panc1 (**E**) WT,

control, and PKM2KO cells under 200 and 0  $\mu\text{M}$  cystine. Significance was assessed by two-way ANOVA. \* $p < 0.05$ , \*\* $p < 0.01$ , \*\*\* $p < 0.001$ . Multiple hypothesis correction by Tukey

test. **F.** Relative viabilities of Panc1 control and PKM2KO clones under a range of cystine concentrations from 200-0  $\mu\text{M}$ . Significance was assessed by two-way ANOVA. \* $p < 0.05$ ,

\*\* $p < 0.01$ , \*\*\* $p < 0.001$ . Multiple hypothesis correction by Dunnett test. **G.** Relative viabilities

of Panc1 control and PKM2KO cells under 50  $\mu\text{M}$  cystine (+) and 0  $\mu\text{M}$  cystine (-) co-treated with 5  $\mu\text{M}$  ferrostatin-1 (FER), 100  $\mu\text{M}$  trolox (TRO), 100  $\mu\text{M}$  deferoxamine (DFO),

50  $\mu\text{M}$  Z-VAD-FMK (ZVAD), or 10  $\mu\text{M}$  necrostatin-1S (NEC). Significance by two-way ANOVA. \* $p < 0.05$ , \*\*\* $p < 0.001$ . Multiple hypothesis correction by Tukey test. **H-I.** Relative

general ROS production measured by H2DCFDA in AsPC1 (**H**) and Panc1 (**I**) control and PKM2KO cells under 50 and 0  $\mu\text{M}$  cystine. Significance was assessed by two-way

ANOVA. \* $p < 0.05$ , \*\* $p < 0.01$ , \*\*\* $p < 0.001$ . Multiple hypothesis correction by Tukey test. **J.**

Representative brightfield and fluorescent images of Panc1 control and PKM2KO cell lipid peroxidation quantified in panel **K**. Scale bar = 50  $\mu\text{m}$ . **K.** Relative lipid peroxidation of

**Figure B.1 (cont'd)**

Panc1 control and PKM2KO cells under 50  $\mu$ M cystine and 0  $\mu$ M cystine, visualized by C11-BODIPY. Significance was assessed by two-way ANOVA. \*\* $p$ <0.01, \*\*\* $p$ <0.001. Multiple hypothesis correction by Tukey test.

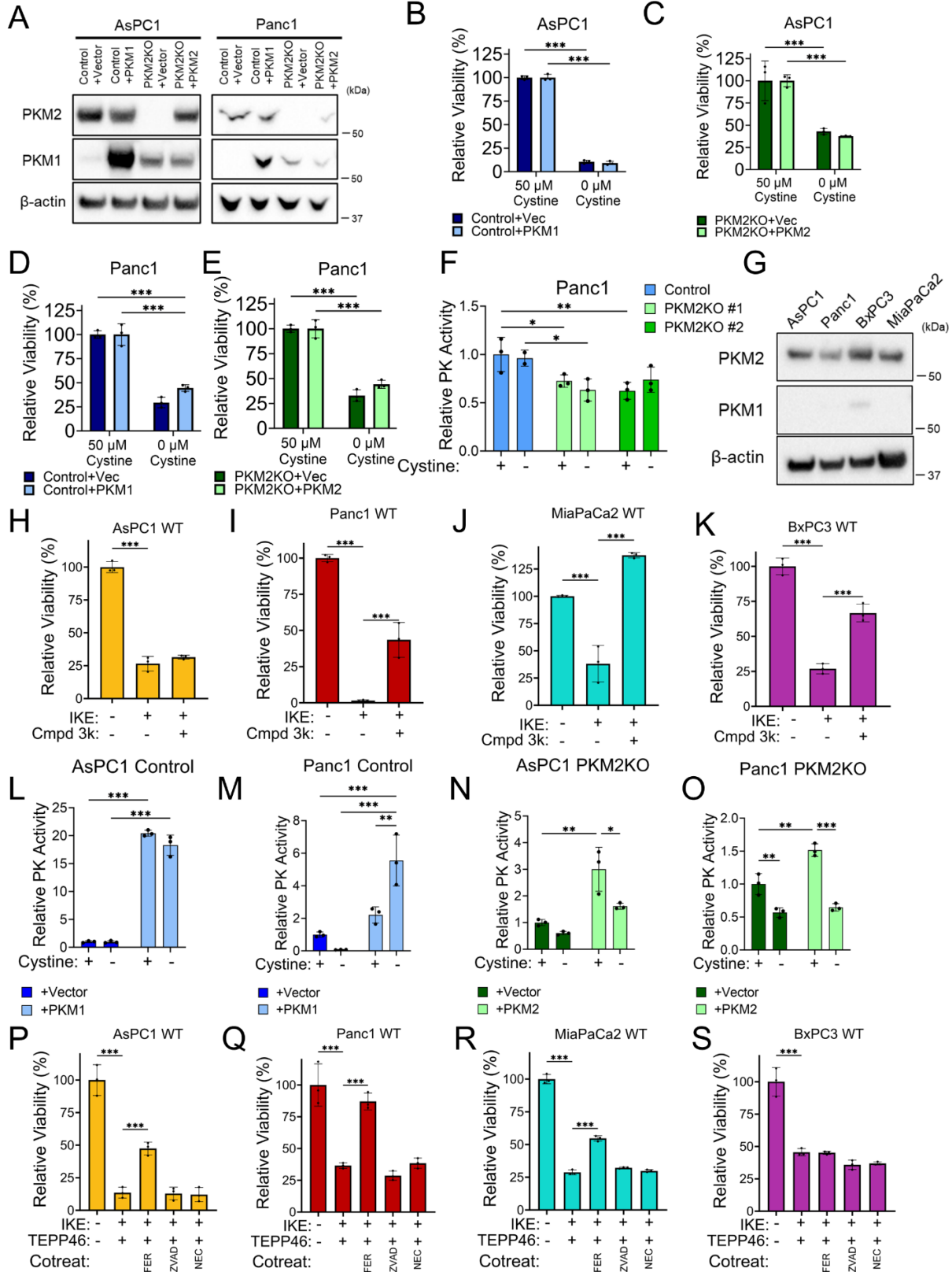


**Figure B.2 Additional data in support of figure 3.2.**

## Figure B.2 (cont'd)

**A.** Western blot of PKM2 and PKM1 expression in AsPC1 and PKM2 control + vector, control + PKM1, PKM2KO + vector, and PKM2KO + PKM2. **B.** Relative viabilities of AsPC1 control + vector and control + PKM1 cells under 50  $\mu\text{M}$  and 0  $\mu\text{M}$  cystine. **C.** Relative viabilities of AsPC1 PKM2KO + vector and PKM2KO + PKM2 cells under 50  $\mu\text{M}$  and 0  $\mu\text{M}$  cystine. **D.** Relative viabilities of Panc1 control + vector and control + PKM1 cells under 50  $\mu\text{M}$  and 0  $\mu\text{M}$  cystine. **E.** Relative viabilities of Panc1 PKM2KO + vector and PKM2KO + PKM2 cells under 50  $\mu\text{M}$  and 0  $\mu\text{M}$  cystine. For **B-E**, significance was assessed by two-way ANOVA. \*\*\* $p < 0.001$ . Multiple hypothesis correction by Tukey test. **F.** Relative pyruvate kinase activity in Panc1 control and PKM2KO cells under 50 and 0  $\mu\text{M}$  cystine. Significance was assessed by two-way ANOVA. \* $p < 0.05$ , \*\* $p < 0.01$ . Multiple hypothesis correction by Tukey test. **G.** Western blot of PKM1 and PKM2 expression in AsPC1, Panc1, BxPC3, and MiaPaCa2 WT cells. **H.** Relative viability of AsPC1 WT cells treated with (+) or without (-) 2.5  $\mu\text{M}$  compound 3k and 5  $\mu\text{M}$  IKE. **I.** Relative viability of Panc1 WT cells treated with (+) or without (-) 10  $\mu\text{M}$  compound 3k and 10  $\mu\text{M}$  IKE. **J.** Relative viability of MiaPaCa2 WT cells treated with (+) or without (-) 10  $\mu\text{M}$  compound 3k and 5  $\mu\text{M}$  IKE. **K.** Relative viability of BxPC3 WT cells treated with (+) or without (-) 2.5  $\mu\text{M}$  compound 3k and 5  $\mu\text{M}$  IKE. For **H-K**, significance was assessed by two-way ANOVA. \* $p < 0.05$ , \*\* $p < 0.01$ , \*\*\* $p < 0.001$ . Multiple hypothesis correction by Tukey test. **L.** Relative pyruvate kinase activity of AsPC1 control + vector and control + PKM1 cells under 50  $\mu\text{M}$  (+) and 0  $\mu\text{M}$  (-) cystine. **M.** Relative pyruvate kinase activity of Panc1 control + vector and control + PKM1 cells under 50  $\mu\text{M}$  (+) and 0  $\mu\text{M}$  (-) cystine. **N.** Relative pyruvate kinase activity of AsPC1 PKM2KO + vector and PKM2KO + PKM2 cells under 50  $\mu\text{M}$  (+)

### Figure B.2 (cont'd)

and 0  $\mu\text{M}$  (-) cystine. **O**. Relative pyruvate kinase activity of Panc1 PKM2KO + vector and PKM2KO + PKM2 cells under 50  $\mu\text{M}$  (+) and 0  $\mu\text{M}$  (-) cystine. For **L-O**, Significance was assessed by two-way ANOVA. \* $p < 0.05$ , \*\* $p < 0.01$ , \*\*\* $p < 0.001$ . Multiple hypothesis correction by Tukey test. **P-S**. Relative viabilities of AsPC1 WT cells (**P**) and BxPC3 WT cells (**S**) treated with (+) or without (-) 10  $\mu\text{M}$  IKE and 50  $\mu\text{M}$  TEPP-46, and Panc1 WT cells (**Q**) and MiaPaCa2 WT cells (**R**) treated with (+) or without (-) 10  $\mu\text{M}$  IKE and 50  $\mu\text{M}$  TEPP-46. In **P-S** cells each were co-treated with 5  $\mu\text{M}$  ferrostatin-1 (FER), 50  $\mu\text{M}$  Z-VAD-FMK (ZVAD), 10  $\mu\text{M}$  necrostatin-1S (NEC). For **P-S**, significance was assessed by two-way ANOVA. \* $p < 0.05$ , \*\* $p < 0.01$ , \*\*\* $p < 0.001$ . Multiple hypothesis correction by Tukey test.

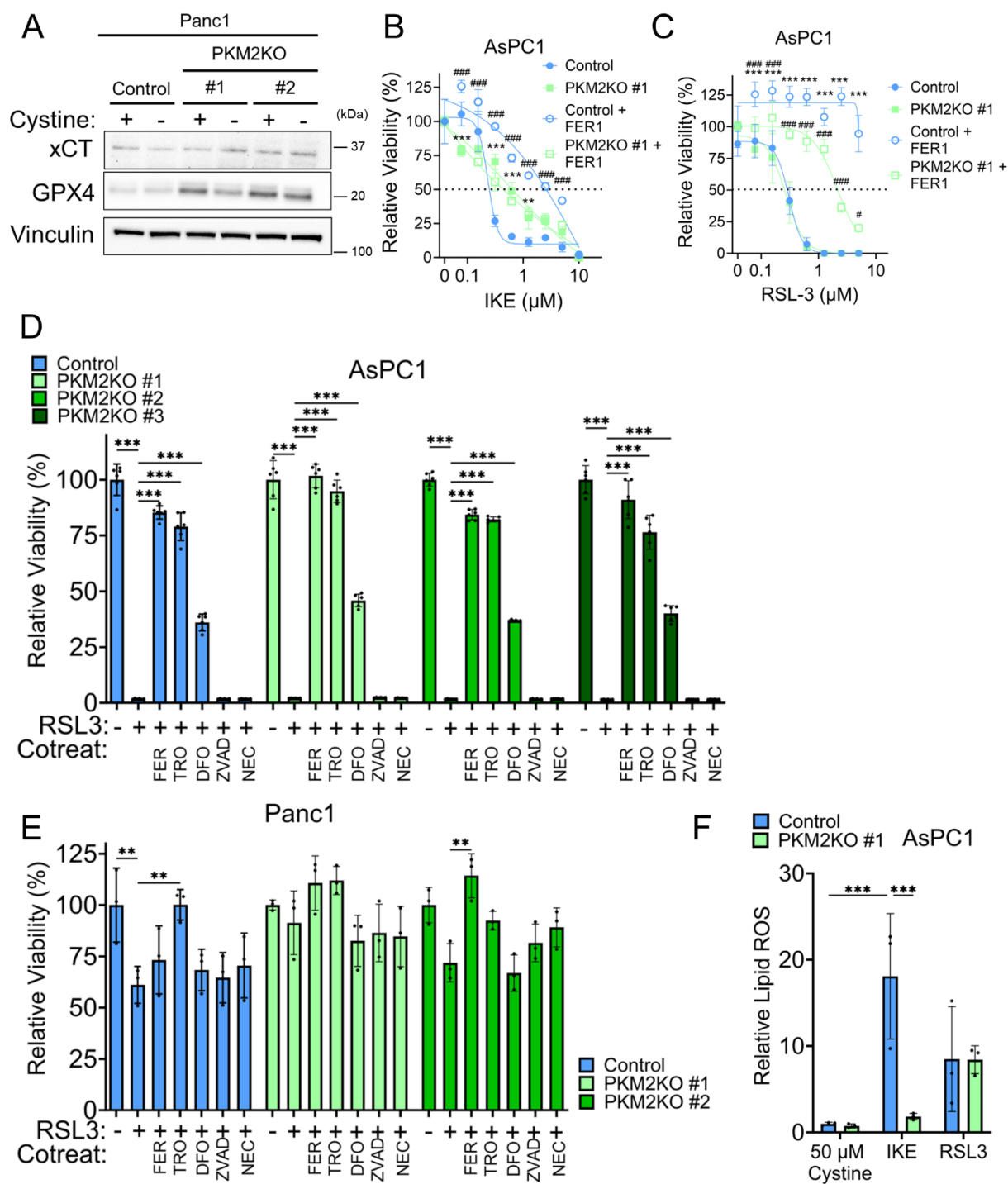
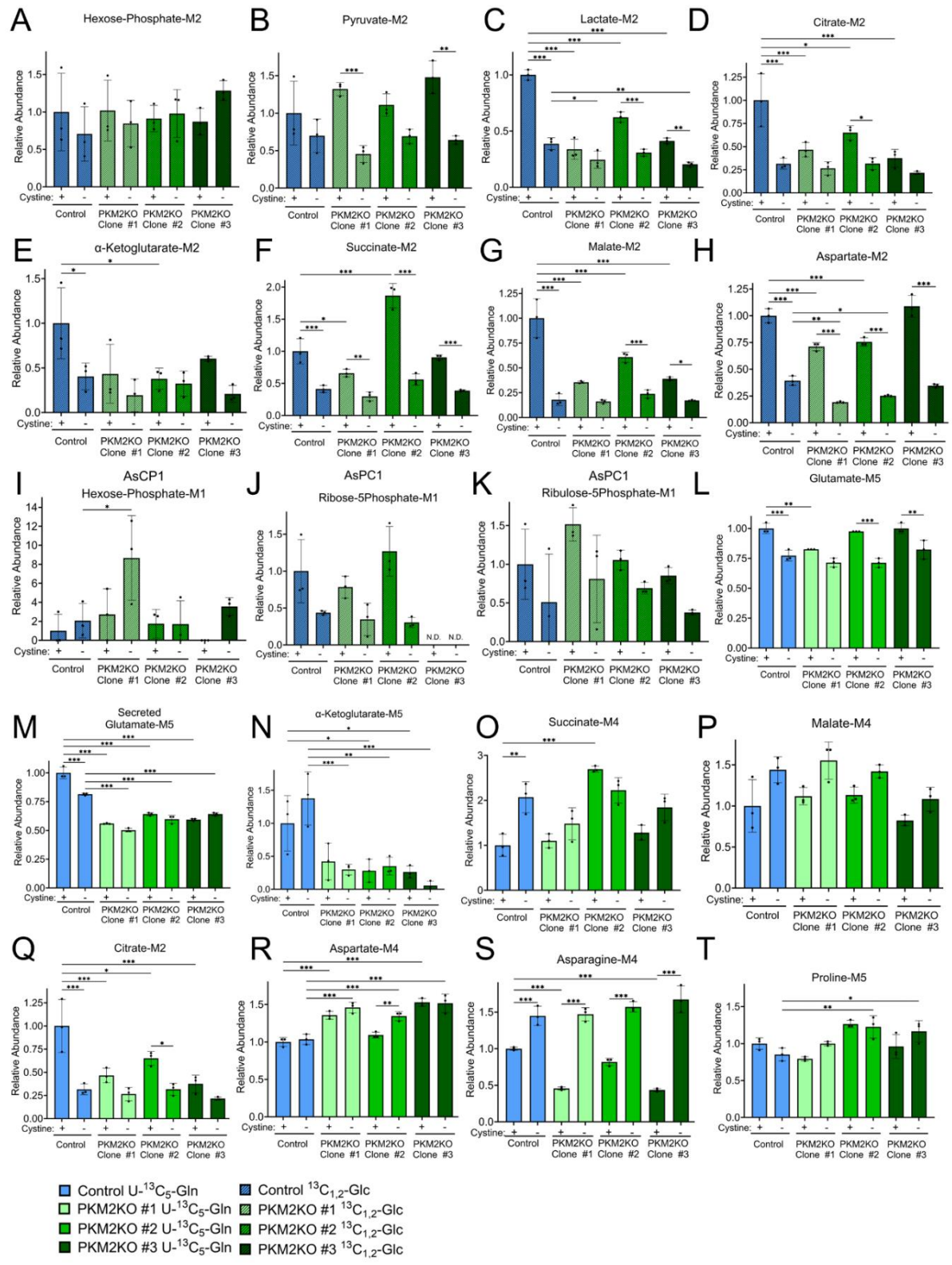


**Figure B.3 Additional data in support of figure 3.3.**

**A.** Western blot of xCT and GPX4 expression in Panc1 control and PKM2KO cells under 50  $\mu$ M (+) and 0  $\mu$ M (-) cystine. **B.** Concentration dependent viability responses of AsPC1

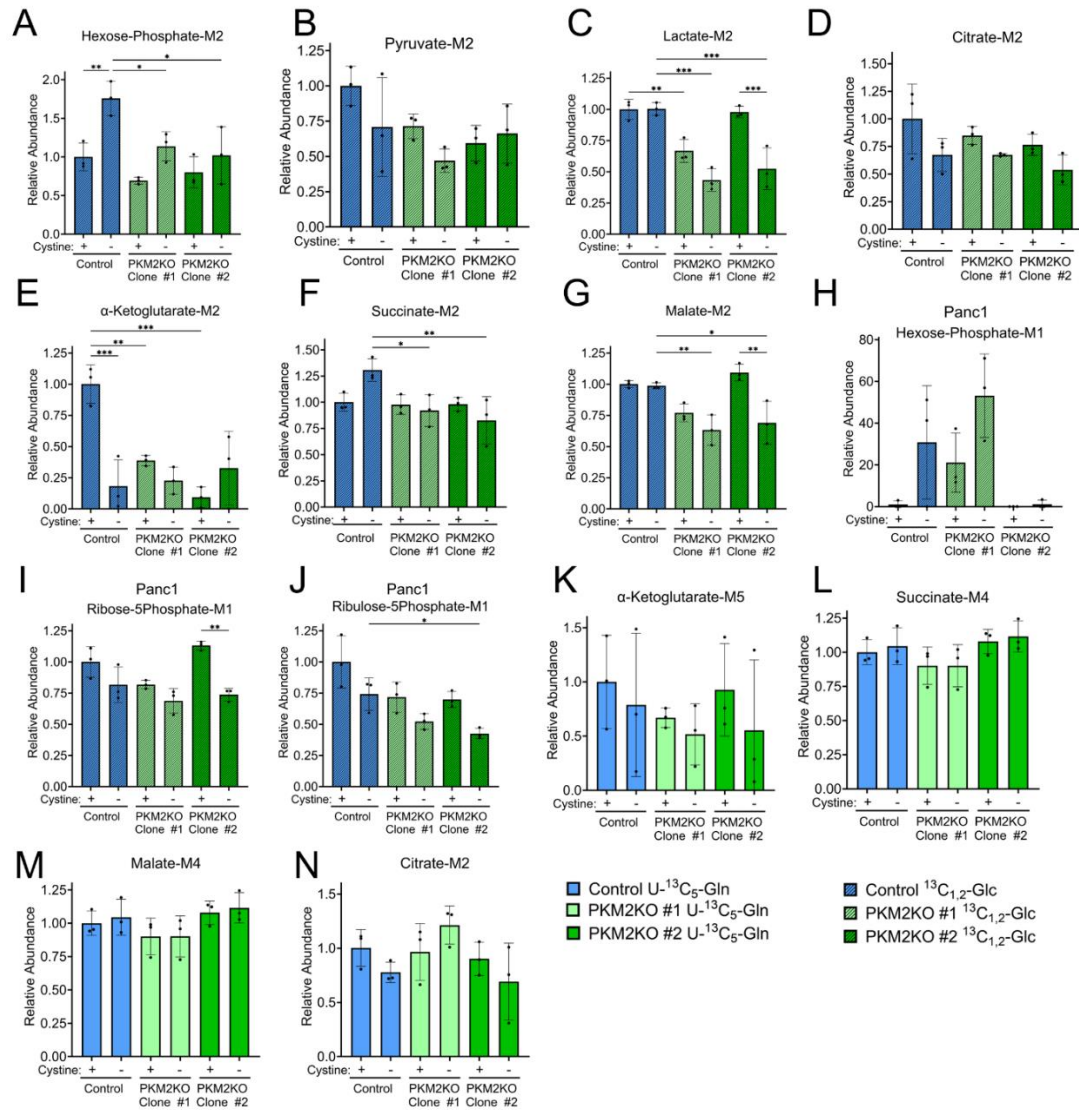
### Figure B.3 (cont'd)

control and PKM2KO clone #1 to a range of IKE concentrations from 10-0  $\mu\text{M}$  and co-treated with 5  $\mu\text{M}$  ferrostatin-1 (FER1). Significance was assessed by two-way ANOVA. Between control and PKM2KO without FER1,  $**p<0.01$ ,  $***p<0.001$ . Between control and control with FER1,  $###p<0.001$ . Multiple hypothesis correction by Tukey test. **C.** Concentration dependent viability responses of AsPC1 control and PKM2KO clone #1 to a range of RSL3 concentrations from 5-0  $\mu\text{M}$  and co-treated with 5  $\mu\text{M}$  Ferrostatin-1 (FER). Significance was assessed by two-way ANOVA. Between control and control with FER1,  $***p<0.001$ . Between PKM2KO and PKM2KO with FER1,  $\#p<0.05$ ,  $###p<0.001$ . Multiple hypothesis correction by Tukey test. **D, E.** Relative viabilities of AsPC1 (**D**) and Panc1 (**E**) control and PKM2KO cells under 50  $\mu\text{M}$  cystine and 5  $\mu\text{M}$  RSL3 co-treated with 5  $\mu\text{M}$  ferrostatin-1 (FER), 100  $\mu\text{M}$  trolox (TRO), 100  $\mu\text{M}$  deferoxamine (DFO), 50  $\mu\text{M}$  Z-VAD-FMK (ZVAD), 10  $\mu\text{M}$  necrostatin-1S (NEC). Significance was assessed by two-way ANOVA.  $*p<0.05$ ,  $**p<0.01$ ,  $***p<0.001$ . Multiple hypothesis correction by Tukey test. **F.** Relative lipid peroxidation of AsPC1 control and PKM2KO #1 under 50  $\mu\text{M}$  cystine, 5  $\mu\text{M}$  IKE, and 5  $\mu\text{M}$  RSL3 treatment visualized by C11-BODIPY. Significance was assessed by two-way ANOVA.  $*p<0.05$ ,  $**p<0.01$ ,  $***p<0.001$ . Multiple hypothesis correction by Tukey test.



#### **Figure B.4 (cont'd)**

**A-K.** Relative abundance of indicated metabolites from stable isotope tracing of  $^{13}\text{C}_{1,2}$ -glucose under 50  $\mu\text{M}$  (+) and 0  $\mu\text{M}$  (-) cystine for 4 hours in AsPC1 control and all PKM2KO clones. **L-T.** Relative abundance of indicated metabolites from stable isotope tracing of U- $^{13}\text{C}_5$ -glutamine under 50 (+) and 0  $\mu\text{M}$  (-) cystine for 24 hours in AsPC1 control and all PKM2KO clones. For **A-T**, significance was assessed by two-way ANOVA. \* $p < 0.05$ , \*\* $p < 0.01$ , \*\*\* $p < 0.001$ . Multiple hypothesis correction by Tukey test. N.D. = No data.



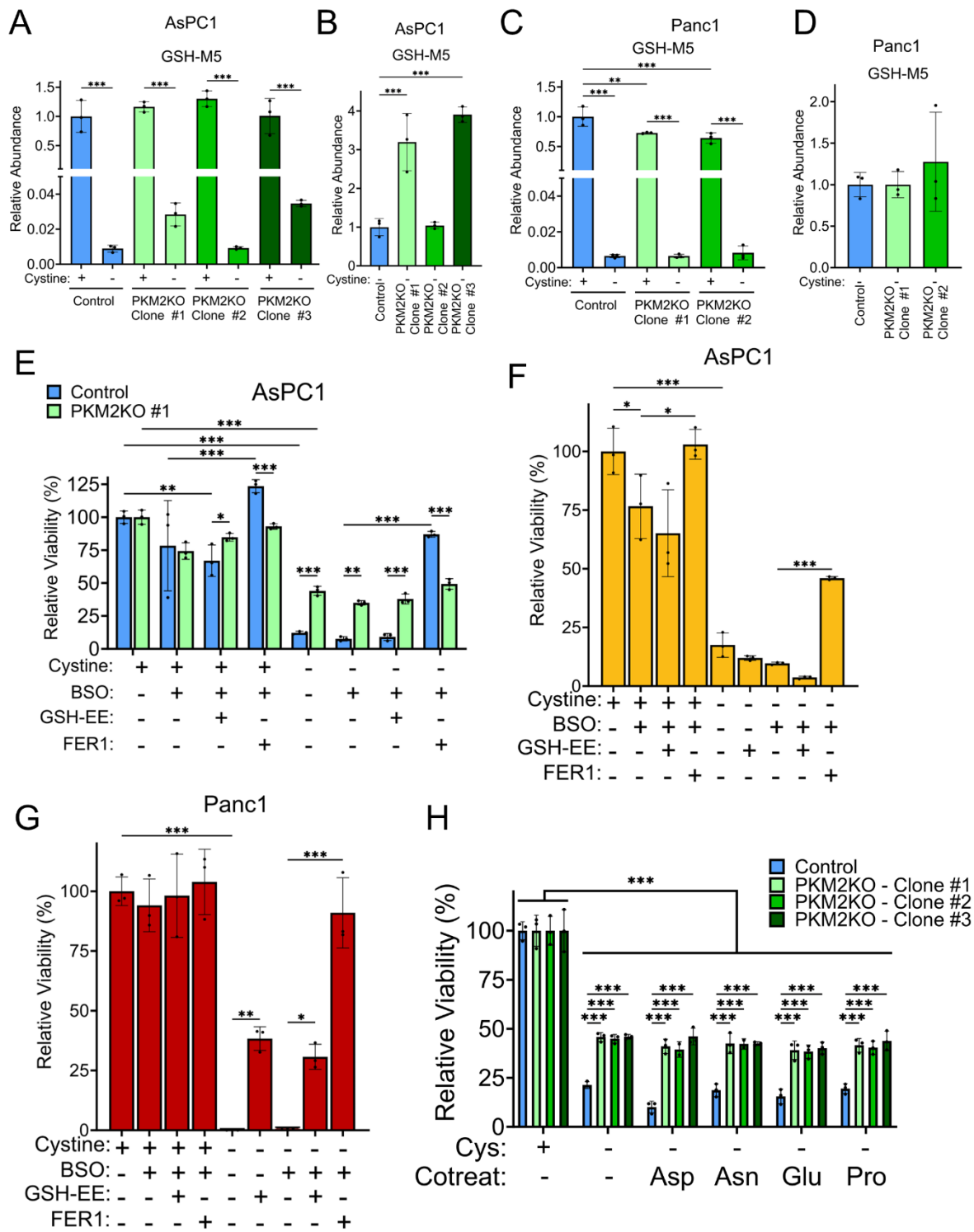


Figure B.6 Additional data in support of Figure 3.4.

### Figure B.6 (cont'd)

**A-B.** Stable isotope tracing of U-<sup>13</sup>C<sub>5</sub>-glutamine under 50 μM (+) and 0 μM (-) cystine for 24 hours in AsPC1 control and all PKM2KO clones to produce M+5 labeled glutathione.

**C.-D.** Stable isotope tracing of U-<sup>13</sup>C<sub>5</sub>-glutamine under 50 μM (+) and 0 μM (-) cystine for 4 hours in Panc1 control and all PKM2KO clones to produce M+5 labeled glutathione. **E-**

**G.** Relative viabilities of AsPC1 control and PKM2KO cells (**E**), AsPC1 WT cells (**F**), and Panc1 WT cells (**G**) under 50 μM (+) or 0 μM (-) cystine co-treated with 300 μM buthionine-sulfoximine (BSO), 1 mM glutathione-ethyl ester (GSH-EE), and/or 5 μM ferrostatin-1 (FER). Significance was assessed by two-way ANOVA. \* $p < 0.05$ , \*\* $p < 0.01$ , \*\*\* $p < 0.001$ .

Multiple hypothesis correction by Tukey test. **H.** Relative viabilities of AsPC1 control and PKM2KO cells under 50 μM (+) and 0 μM (-) cystine supplemented with either 6 μM aspartate, 90 μM asparagine, 90 μM glutamate, or 240 μM proline. Significance was assessed by two-way ANOVA. \* $p < 0.05$ , \*\* $p < 0.01$ , \*\*\* $p < 0.001$ . Multiple hypothesis correction by Tukey test.

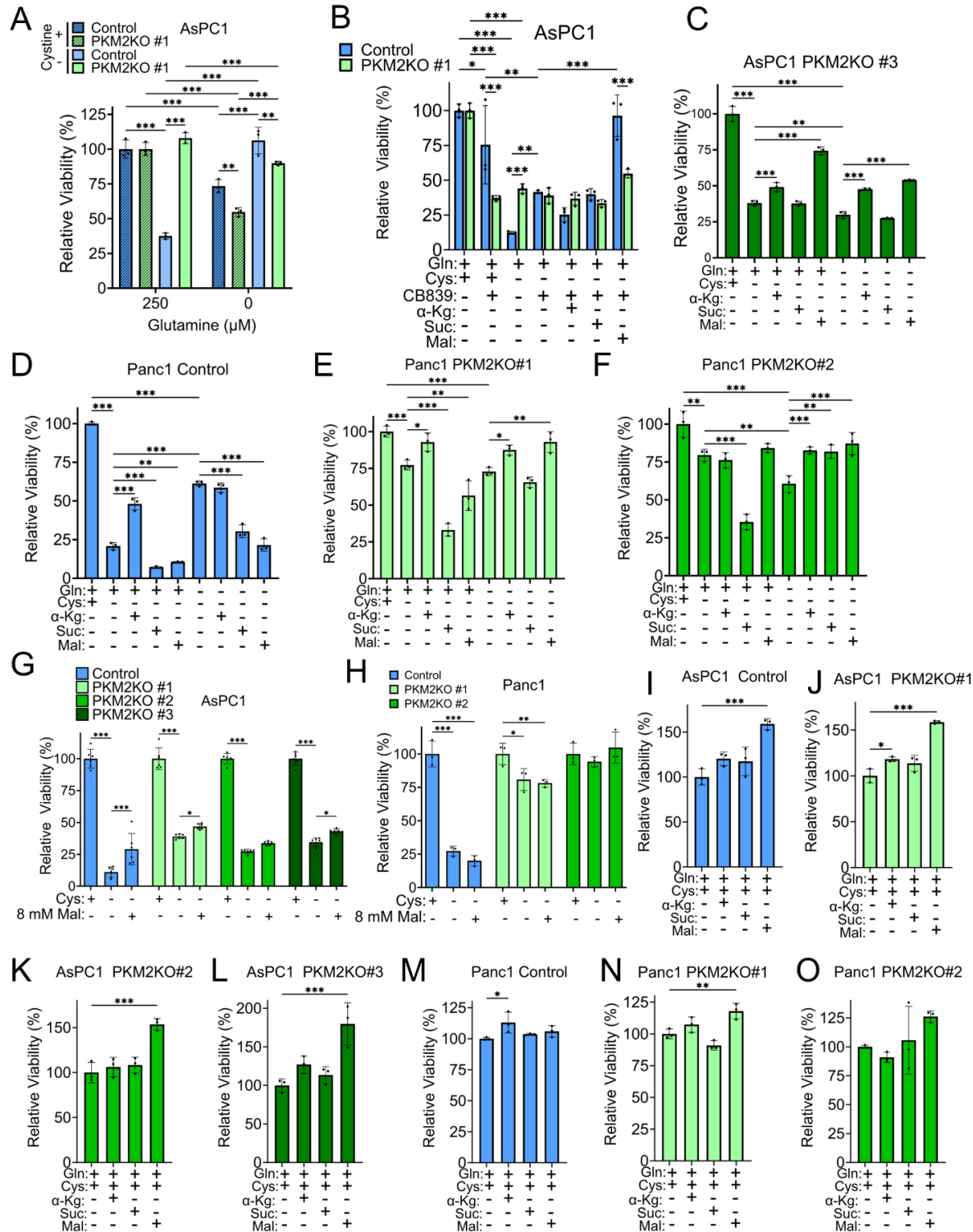
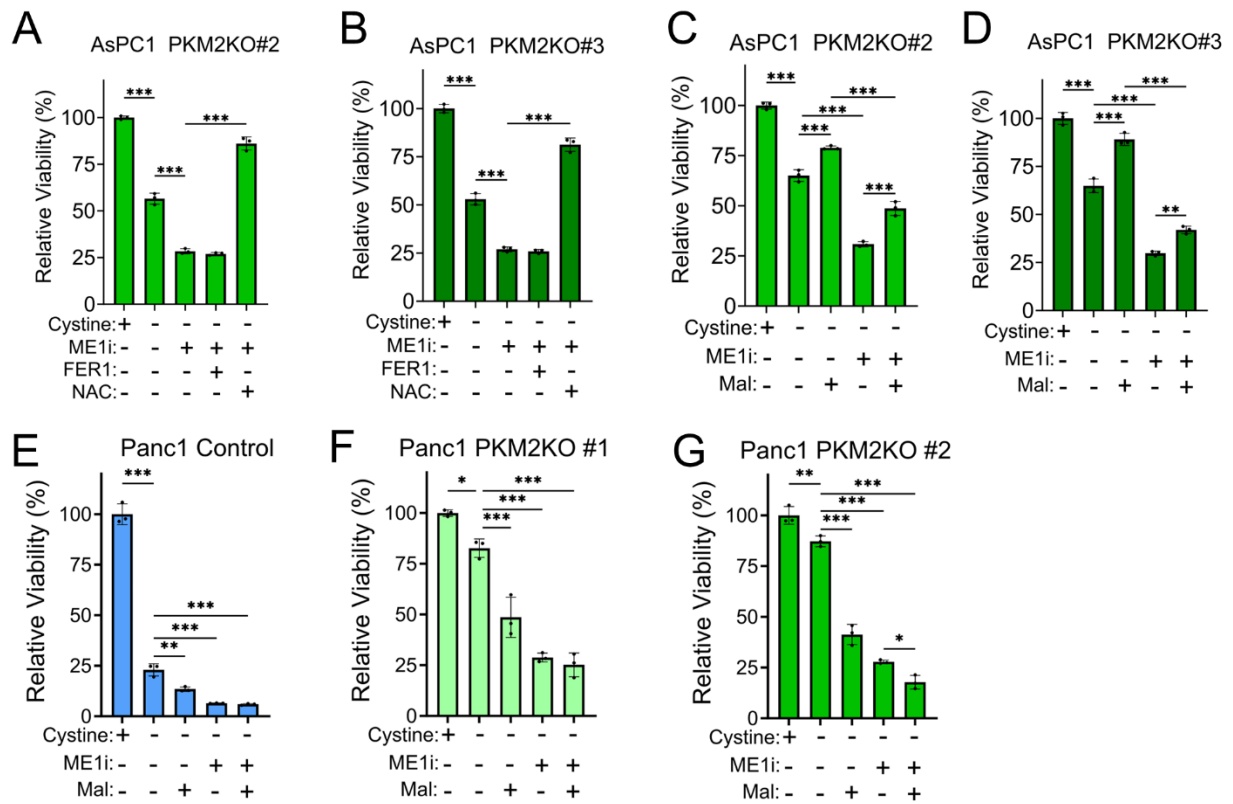


Figure B.7 Data in support of Figure 3.5.

### Figure B.7 (cont'd)

**A.** Relative viabilities of AsPC1 control and PKM2KO#1 under 50  $\mu\text{M}$  (+) and 0  $\mu\text{M}$  (-) cystine with (+) or without (-) 250  $\mu\text{M}$  glutamine. **B.** Relative viabilities of AsPC1 control and PKM2KO #1 under 50  $\mu\text{M}$  (+) or 0  $\mu\text{M}$  (-) cystine treated with 5  $\mu\text{M}$  CB-839 (glutaminase inhibitor), supplemented with either 8 mM dimethyl- $\alpha$ -ketoglutarate ( $\alpha$ -Kg), 8 mM dimethyl-succinate (Suc), or 32 mM dimethyl-malate (Mal). For **A-B**, significance was assessed by two-way ANOVA. \* $p < 0.05$ , \*\* $p < 0.01$ , \*\*\* $p < 0.001$ . Multiple hypothesis correction by Tukey test. **C.** Relative viability of AsPC1 PKM2KO #3 under 50  $\mu\text{M}$  (+) or 0  $\mu\text{M}$  (-) cystine with (+) or without (-) 1 mM glutamine supplemented with either 8 mM dimethyl- $\alpha$ -ketoglutarate ( $\alpha$ -Kg), 8 mM dimethyl-succinate (Suc), or 32 mM dimethyl-malate (Mal). **D-F.** Relative viabilities of Panc1 control (**D**), PKM2KO #1 (**E**), and PKM2KO #2 under 50  $\mu\text{M}$  (+) or 0  $\mu\text{M}$  (-) cystine with (+) or without (-) 1 mM glutamine supplemented with either 8 mM DM- $\alpha$ kg, 8 mM DM-Suc, or 32 mM DM-Mal. For **C-F**, significance was assessed by one-way ANOVA. \* $p < 0.05$ , \*\* $p < 0.01$ , \*\*\* $p < 0.001$ . Multiple hypothesis correction by Sidak test. **G-H.** Relative viabilities of AsPC1 (**A**) and Panc1 (**H**) control and PKM2KO clones under 50  $\mu\text{M}$  (+) or 0  $\mu\text{M}$  (-) cystine supplemented with 8 mM dimethyl-malate (Mal). Significance was assessed by two-way ANOVA. \* $p < 0.05$ , \*\* $p < 0.01$ , \*\*\* $p < 0.001$ . Multiple hypothesis correction by Tukey test. **I-O.** Relative viabilities of AsPC1 control (**I**), AsPC1 PKM2KO #1 (**J**), AsPC1 PKM2KO #2 (**K**), AsPC1 PKM2KO #3 (**L**), Panc1 control (**M**), Panc1 PKM2KO #1 (**N**), and PKM2KO #2 (**O**) under 50  $\mu\text{M}$  cystine supplemented with either 8 mM DM- $\alpha$ kg, 8 mM DM-Suc, or 32 mM DM-Mal. Significance was assessed by one-way ANOVA. \* $p < 0.05$ , \*\* $p < 0.01$ , \*\*\* $p < 0.001$ . Multiple hypothesis correction by Sidak test.



**Figure B.8 Additional data in support of figure 3.6.**

**A-B.** Relative viabilities of AsPC1 PKM2KO #2 (**A**) and AsPC1 PKM2KO #3 (**B**) under 0  $\mu$ M cystine treated with (+) or without (-) 50  $\mu$ M malic enzyme 1 inhibitor (ME1i) and co-treated with either 5  $\mu$ M ferrostatin-1 (FER) or 1 mM N-acetylcysteine (NAC). **C-G.** Relative viabilities of AsPC1 PKM2KO clone #2 (**C**), AsPC1 PKM2KO #3 (**D**), Panc1 control (**E**), Panc1 PKM2KO #1 (**F**), and PKM2KO #2 (**G**) under 50  $\mu$ M (+) or 0  $\mu$ M (-) cystine with or without 50  $\mu$ M ME1i and 32 mM dimethyl-malate (Mal). For **A-G**, significance was assessed by one-way ANOVA. \* $p$ <0.05, \*\* $p$ <0.01, \*\*\* $p$ <0.001. Multiple hypothesis correction by Sidak test.